PAPER-BASED POTENTIOMETRIC PLATAFORMS FOR ESCENTRALISED CHEMICAL ANALYSIS.

Marta Novell Recasens

Dipòsit Legal: T 1462-2015

PAPER-BASED POTENTIOMETRIC PLATFORMS FOR DECENTRALISED CHEMICAL ANALYSIS

DOCTORAL THESIS

Marta Novell Recasens

Tarragona, 2015

UNIVERSITAT ROVIRA I VIRGILI

UNIVERSITAT ROVIRA I VIRGILI
PAPER-BASED POTENTIOMETRIC PLATAFORMS FOR ESCENTRALISED CHEMICAL ANALYSIS.
Marta Novell Recasens
Dipòsit Legal: T 1462-2015

UNIVERSITAT ROVIRA I VIRGILI
PAPER-BASED POTENTIOMETRIC PLATAFORMS FOR ESCENTRALISED CHEMICAL ANALYSIS.
Marta Novell Recasens
Dipòsit Legal: T 1462-2015

Novell Recasens

Paper-based potentiometric platforms for decentralised chemical analysis

Doctoral Thesis

Supervised by Dr. Francisco J. Andrade

Department of Analytical Chemistry and Organic Chemistry

UNIVERSITAT ROVIRA I VIRGILI

Tarragona, 2015

UNIVERSITAT ROVIRA I VIRGILI
PAPER-BASED POTENTIOMETRIC PLATAFORMS FOR ESCENTRALISED CHEMICAL ANALYSIS.
Marta Novell Recasens
Dipòsit Legal: T 1462-2015

UNIVERSITAT ROVIRA I VIRGILI
PAPER-BASED POTENTIOMETRIC PLATAFORMS FOR ESCENTRALISED CHEMICAL ANALYSIS.
Marta Novell Recasens
Dipòsit Legal: T 1462-2015

Paper-based potentiometric platforms for decentralised chemical analysis

Tribunal members:

Prof. Dermot Diamond (Dublin City University)

Prof. Agustín Costa García (Universidad de Oviedo)

Prof. Francesc Xavier Rius Ferrús (Universitat Rovira i Virgili)

External examiners:

Prof Johan Bobacka (Åbo Akademi University)

Prof. Mabel Tudino (Universidad de Buenos Aires)

Tarragona, 2015

UNIVERSITAT ROVIRA I VIRGILI

UNIVERSITAT ROVIRA I VIRGILI
PAPER-BASED POTENTIOMETRIC PLATAFORMS FOR ESCENTRALISED CHEMICAL ANALYSIS.
Marta Novell Recasens
Dipòsit Legal: T 1462-2015

UNIVERSITAT ROVIRA I VIRGILI

DEPARTAMENT DE QUÍMICA ANALÍTICA I
QUÍMICA ORGÀNICA
Campus Sescelades
Carrer Marcel·lí Domingo 1
43007 Tarragona

Dr. FRANCISCO ANDRADE, Ramón y Cajal researcher at the Department of Analytical Chemistry and Organic Chemistry at the Universitat Rovira i Virgili

CERTIFIES:

That the Doctoral Thesis entitled: "Paper-based potentiometric platforms for decentralised chemical analysis" submitted by Marta Novell Recasens in order to achieve the Degree of Doctor, has been carried out under my supervision, at the Department of Analytical Chemistry and Organic Chemistry at the Universitat Rovira i Virgili.

Tarragona, July 10th, 2015

Dr. Francisco J. Andrade

UNIVERSITAT ROVIRA I VIRGILI
PAPER-BASED POTENTIOMETRIC PLATAFORMS FOR ESCENTRALISED CHEMICAL ANALYSIS.
Marta Novell Recasens
Dipòsit Legal: T 1462-2015

Acknowledgements

First, I would like to thank Prof. F. Xavier Rius to give me the opportunity to undertake my PhD studies in his research group. Thanks for convincing me to carry out the master in Nanoscience and Nanotechnology and later on for trusting on me to carry out a PhD, and thanks for all your scientific and personal support.

Secondly, to Francisco Andrade, I would like to thank his trust on me, which helped me to go ahead and believe in myself. Thanks for always seeing the positive part of everything, for believing on the people and for creating a human group that goes beyond mere research. Thanks for all the scientific discussions and for arising in me new curiosities. And finally, I would like to thank him for the support and encouragement received along these years that made me grow personally and scientifically.

Thirdly, I would like to thank my parents: Joan and Anna, for always trusting on me. For helping me always and in everything and for making me believe that I can achieve everything that I wish.

I also want to thank all the colleagues from the Nanosensors group. To the seniors, Jordi Riu for always sharing his joy, to Santiago Macho, for his support in the resolution of any kind of problem and to Pascal Blondeau, for his unconditional help in everything. Also to the colleges that helped me at the begging and that have sought new paths in life, Gastón Crespo, Enrique Parra and Xavi Rius. To the ones that have shared most of the path with me, Patricia Llorente, Marc Parrilla, Jordi Ferré, Jad Sabek and Azizur Rahman, thanks for making it easier and funnier. To the ones that have arrived later or have been sporadically in the group, Rocío Cánovas, Rafael Hoekstra, Leonor Guadarrama and María Cuartero, thanks for having brought the best of each one of you. To all the masters that have been and are in the group. And especially to Tomàs Guinovart, we started the master together and we will finish the PhD together. Thanks for always giving me support and for being

beside me in the best and worst moments. I also want to remember Maarten Fokker, one of the happiest and motivated person I have ever know, because there will always be a part of his spirit on me. Thanks also to the members of the Innovation Hub, Pär and Mº José, for all the happy memories shared. To all, thanks for all the moments lived along these five years.

I would like to thank Prof. Bobacka for having allowed my stay in his group at Åbo Akademi University in Finland. Thanks for his help and guidance. Thanks also to all the members of the Analytical Chemistry Laboratory for making me feel like at home, especially to Ulriika Vanamo, the happiest person ever, thanks for having helped me in everything and for passing on me her happiness.

I would also like to thank all my friends, the ones from the school: Anton, Carles, Elies, Fisco, Ketcu, Marcos, Nacho, Paula, Sai, Uri and Uli, because you are always there, for all the dinners, parties and great moments of fun and happiness. The ones from the university: Anna, Cerra, Emma, Esther, Glòria, Gomes, Joan Carles, Laura, Marc, Porras and Racio, because we share more than our passion for chemistry and because I just remember good moments together. And especially to Brigi and Lidia, because you have always helped me in the best possible way, because we share all our memories and because you know me more than myself. Also to Jonathan, for staying next to me and helping me in everything during the last four years, for having made me really happy and for the trust and friendship that will always be there.

And finally I would like to thank the rest of my family the support and love received along these years, to my uncle Xavier, my aunt Guillermina, Xavi and Eva, to my grandmothers Maria and Maria Teresa, and to my grandfather Albert and my godfather Joan, which will always be present.

Agraïments

En primer lloc, voldria agrair al Prof. F. Xavier Rius l'oportunitat de realitzar el doctorat al seu grup d'investigació. Gràcies per haver-me convençut per fer el màster de Nanociència i Nanotecnologia i per després confiar en mi per fer un doctorat, i gràcies per tot el recolzament científic i també personal.

En segon a Francisco Andrade, li vull agrair la confiança depositada en mi, que m'ha ajudat a seguir sempre endavant i a creure en mi. Gràcies per veure sempre la part positiva de les coses, per creure en les persones i crear un grup humà que va més enllà de la mera investigació científica. Gràcies per totes les discussions científiques i per haver fet créixer en mi noves inquietuds. I finalment, li vull agrair el suport i els ànims rebuts al llarg d'aquests cinc anys, que m'han fet créixer personal i científicament.

En tercer lloc vull agrair als meus pares: Joan i Anna, per haver confiat sempre en mi. Per haver-me ajudat sempre en tot i haver-me fet creure que podia aconseguir tot el que em proposés.

Vull agrair també a tots els companys del grup de Nanosensors el suport rebut. Als sèniors, a Jordi Riu per encomanar sempre la seva alegria, a Santiago Macho, pel seu suport en la resolució de qualsevol problema i a Pascal Blondeau pel seu ajut incondicional en tot. També als companys que em van ajudar al principi i que ja han buscat nous camins a la vida, Gastón Crespo, Enrique Parra i Xavi Rius. Als que han compartit amb mi bona part d'aquest camí, Patricia Llorente, Marc Parrilla, Jordi Ferré, Jad Sabek i Azizur Rahman, gràcies per haver-ho fet tot més fàcil i divertit. Als que han arribat més tard o han estat esporàdicament al grup, Rocío Cánovas, Rafael Hoekstra, Leonor Guadarrama i María Cuartero, gràcies per haver aportat el millor de cada un de vosaltres. I a tots els màsters que han passat i estan al grup. I en especial a Tomàs Guinovart, vam començar el màster junts i acabarem junts el doctorat. Gràcies per haver-me donat sempre suport i per haver estat al meu

costat en els millors i pitjors moments. Vull també recordar a Maarten Fokker, de les persones més felices i motivades que mai he conegut, perquè sempre hi haurà una miqueta del seu esperit en mi. També agrair als membres del Innovation Hub, Pär i Mª José, tots els moments d'alergia compartits. A tots, gràcies per tots els moments viscuts al llarg d'aquests cinc anys.

Li voldria agrair al Prof. Johan Bobacka haver-me permès realitzar una estada al seu grup a la Universitat Åbo Akademi de Finlàndia. Gràcies per la seva ajuda i guia científica. Gràcies també a tots els membres del Laboratori de Química Analítica per haver-me fet sentir com a casa i en especial a Ulriika Vanamo, la persona més alegre que mai he conegut, gràcies per haver-me ajudat en tot i per encomanar-me la teva felicitat.

M'agradaria agrair també a tots els meus amics, als del "cole": Anton, Carles, Elies, Fisco, Ketcu, Marcos, Nacho, Paula, Sai, Uri i Uli, perquè sempre esteu allí, pel tots els sopars, les fetes i els grans moments de diversió i felicitat. Als de la uni: Anna, Cerra, Emma, Esther, Glòria, Gomes, Joan Carles, Laura, Marc, Porras i Racio, perquè compartim molt més la passió per la química i perquè al vostre costat només recordo moments d'alegria. I sobretot a la Brigi i la Lidia, perquè sempre m'heu ajudat de la millor manera possible, perquè compartim tots els records i perquè em coneixeu més que jo mateixa. També al Jonathan, per haver-me acompanyat i ajudat en tot durant els últims quatre anys, per haver-me fet molt feliç i per la confiança i amistat que sempre duraran.

I finalment vull agrair a la resta de la família el suport i estima rebuts durant tots aquests anys, al tiet Xavier i la tieta Guillermina, al Xavi i a l'Eva, a les àvies Maria i Maria Teresa, i a l'avi Albert i al padrí Joan, que sempre estaran presents.

UNIVERSITAT ROVIRA I VIRGILI
PAPER-BASED POTENTIOMETRIC PLATAFORMS FOR ESCENTRALISED CHEMICAL ANALYSIS.
Marta Novell Recasens
Dipòsit Legal: T 1462-2015

UNIVERSITAT ROVIRA I VIRGILI
PAPER-BASED POTENTIOMETRIC PLATAFORMS FOR ESCENTRALISED CHEMICAL ANALYSIS.
Marta Novell Recasens
Dipòsit Legal: T 1462-2015

Table of contents

UNIVERSITAT ROVIRA I VIRGILI
PAPER-BASED POTENTIOMETRIC PLATAFORMS FOR ESCENTRALISED CHEMICAL ANALYSIS.
Marta Novell Recasens
Dipòsit Legal: T 1462-2015

UNIVERSITAT ROVIRA I VIRGILI
PAPER-BASED POTENTIOMETRIC PLATAFORMS FOR ESCENTRALISED CHEMICAL ANALYSIS.
Marta Novell Recasens
Dipòsit Legal: T 1462-2015

UNIVERSITAT ROVIRA I VIRGILI
PAPER-BASED POTENTIOMETRIC PLATAFORMS FOR ESCENTRALISED CHEMICAL ANALYSIS.
Marta Novell Recasens
Dipòsit Legal: T 1462-2015

Summary

The aim of this doctoral thesis is to develop novel analytical tools for decentralised measurements, by using paper modified with carbon nanotubes as a substrate, and potentiometry as detection approach.

The motivation for this work arises from the deep social and technological changes that we have undergone during the last decades. The present world is heading towards a division where some parts of the countries are becoming richer and technologically very advanced, whereas the others are falling behind, with very poor economies. To this scenario, which calls for an urgent change, analytical chemistry should give also an answer. The development of tools for performing measurements out of the lab in a robust, simple and cost-effective way will be of great help to generate, for example, affordable diagnostic tools. This solution will be useful for poor countries –which cannot afford current technologies- but at the same time it may provide an alternative model for the richer countries -where decentralized analysis will introduce a completely different management approach in many areas, especially in the healthcare system-.

The low cost and wide availability of paper in combination with the use of carbon nanotubes (CNTs) -to make conductive substrates- together with the use of ion-selective membranes (ISM) and potentiometric detection has led to the development of ultra-low-cost paper-potentiometric platforms. Ideally, these sensors will meet the necessary requirements for the decentralized analysis.

For this reason, the main goal of this thesis is the development of paper-based ion-selective potentiometric sensors, establishing at the same time a procedure to build a versatile paper-based platform that can be used for the detection of different analytes and with different techniques. The thesis has been structured in different chapters, each one containing the following information:

Chapter 1 provides an overview of the context in which the thesis is framed, in particular, of the emerging trends of decentralised analysis and the existing and emerging needs. Alternative approaches to develop analytical tools to address these needs are reviewed and the general and specific objectives are summarized.

Chapter 2 reports the scientific and technical foundations of potentiometric sensors that will be used throughout this work. Definitions about the principal components of a potentiometric system, the working mechanism of potentiometric sensors and the analytical parameters used for the characterisation are discussed in detail.

Chapter 3 corresponds to the experimental section, where the main reagents, procedures and instrumentation common to all the chapters are described. Information to understand the characterisation techniques is also included.

Chapter 4 provides the first insights and proof of principle to use carbon nanotubes to make conductive papers with ion-to-electron transduction capability. The development of the procedures, the proof of the transduction ability, the advantages of this methodology and the comparison with other materials is presented and discussed.

Chapter 5 describes the development of paper-based potentiometric ion-selective electrodes (ISEs). Analytical performance and characterisation of these electrodes is presented and discussed.

Chapter 6 is a further extension of the previous chapter, where the development of a complete paper cell –reference and working electrodes- for the determination of lithium in blood is presented.

Chapter 7 address the issue of the detection and transmission of the signal, using a novel miniaturized radio frequency identification (RFID) potentiometer tag that can be used in combination with ion-selective electrodes.

Chapter 8 describes the limitations of the paper-ISEs and reports different proposals to overcome them.

Chapter 9 is composed of two sections reporting different analytical directions for analytical applications of the conductive papers. In the first section, a chemiresistor for the detection of human immunoglobulin G is presented. In the second section, a proof of principle for the development of enzymatic-paper electrodes is illustrated through the construction of a glucose electrode.

Chapter 10 outlines the conclusions of the thesis. In addition, future prospects are suggested.

Finally, some appendices have been added with additional information.

UNIVERSITAT ROVIRA I VIRGILI
PAPER-BASED POTENTIOMETRIC PLATAFORMS FOR ESCENTRALISED CHEMICAL ANALYSIS.
Marta Novell Recasens
Dipòsit Legal: T 1462-2015

Resum

L'objectiu d'aquesta tesis doctoral és el desenvolupament de noves eines analítiques per a mesures descentralitzades, fent ús de paper modificat amb nanotubs de carboni com a substrat, i de la potenciometria com a tècnica de detecció.

La motivació d'aquest treball sorgeix dels profunds canvis socials i tecnològics que s'han produït en les darreres dècades. El món actual s'encamina a una divisió on alguns països veuen augmentada la seva riquesa i el seu desenvolupament tecnològic, mentre que d'altres s'estan quedant endarrere amb economies molt empobrides. A aquest escenari, que demana un canvi urgent, la química analítica ha de donar-hi resposta. El desenvolupament d'eines per a realitzar mesures fora del laboratori de manera robusta, simple i econòmica, ajudaria molt a generar, per exemple, eines de diagnòstic assequibles. Aquesta solució seria molt útil pels països pobres –que no es poden permetre les tecnologies actuals-, però al mateix temps proporcionaria un model alternatiu pels països més rics –on els anàlisis descentralitzats introduirien un enfoc diferent en la gestió de varies àrees, especialment en el sistema sanitari-.

El baix cost i l'àmplia disponibilitat del paper en combinació amb l'ús dels nanotubs de carboni –per fer substrats conductors- i juntament amb l'ús de les membranes de ions selectius i la detecció potenciomètrica ha donat lloc al desenvolupament de plataformes potenciomètriques d'ultra-baix cost. Idealment, aquests sensors satisfan els requeriments necessaris pels anàlisis descentralitzats.

Per aquesta raó, el principal objectiu d'aquesta tesis és el desenvolupament de sensors potenciomètrics de ions selectius sobre substrat de paper, establint al mateix temps un procediment per a construir una plataforma de paper versàtil, que pugui ser usada per la detecció de diferents analits i amb diferents tècniques. La

tesis s'ha estructurat en diferents capítols, cada un dels quals conté la següent informació:

El **capítol 1** proporciona una visió general del context en el que s'emmarca la tesis, en concret, de les tendències emergents de l'anàlisi descentralitzat i de les necessitats existents i emergents. També revisa enfocs alternatius per al desenvolupament d'eines analítiques per afrontar aquestes necessitats, i finalment presenta els objectius generals i específics de la tesis.

El **capítol 2** conté les bases científiques i tècniques dels sensors potenciomètrics que s'usaran al llarg d'aquest treball. Així com, la discussió en detall dels principals components d'un sistema potenciomètric, el mecanisme de funcionament dels sensors potenciomètrics i els paràmetres analítics utilitzats per la caracterització d'aquests.

El **capítol 3** descriu la part experimental, on els principals reactius, procediments i instruments comuns en tots els capítols queden recollits. També conté informació per entendre les tècniques de caracterització.

El **capítol 4** proporciona les primeres idees i la prova de principi de l'ús de nanotubs de carboni per fer papers conductors amb capacitat per a la transducció ió-a-electró. També presenta i discuteix el desenvolupament de procediments, la prova de la capacitat de transducció i els avantatges i inconvenients d'aquesta metodologia en comparació amb altres materials.

El **capítol 5** descriu el desenvolupament d'elèctrodes de ions selectius sobre substrat de paper. També presenta i discuteix els paràmetres analítics i la caracterització d'aquests elèctrodes.

El **capítol 6** és una extensió de l'anterior capítol, i presenta el desenvolupament d'una cel·la potenciomètrica complerta –elèctrode de treball i elèctrode de referència- per a la determinació de liti en sang.

El **capítol 7** aborda la qüestió de la detecció i transmissió de la senyal, a través de l'ús d'un potenciòmetre miniaturitzat d'identificació per radiofreqüència en combinació amb els elèctrodes selectius de ions.

El **capítol 8** descriu les limitacions dels elèctrodes de ions selectius sobre substrat de paper i reporta diferents propostes per solucionar-los.

El **capítol 9** està compost per dues seccions que presenten dues propostes analítiques diferents per a l'aplicació dels papers conductors. A la primera secció, es presenta un quimiresistor per a la detecció d'immunoglobulina G. A la segona secció, es presenta la prova de principi per al desenvolupament d'elèctrodes enzimàtics sobre substrat de paper a través de la construcció d'un elèctrode de glucosa.

El **capítol 10** recull les conclusions de la tesis i suggereix futurs treballs en aquesta àrea.

Finalment, s'han afegits algun apèndixs amb informació addicional.

UNIVERSITAT ROVIRA I VIRGILI
PAPER-BASED POTENTIOMETRIC PLATAFORMS FOR ESCENTRALISED CHEMICAL ANALYSIS.
Marta Novell Recasens
Dipòsit Legal: T 1462-2015

CHAPTER

1

INTRODUCTION

UNIVERSITAT ROVIRA I VIRGILI
PAPER-BASED POTENTIOMETRIC PLATAFORMS FOR ESCENTRALISED CHEMICAL ANALYSIS.
Marta Novell Recasens
Dipòsit Legal: T 1462-2015

1.1 Analytical chemistry adapting to the new challenges

During the second half of the 20th century, several changes affected the society and the way in which we face the future. The digital revolution was followed by the expansion and increasing availability of internet and mobile phones to the vast majority of the population. For example, during the last ten years, American population having access to internet has doubled. By the end of 2014 almost 3 billion of people –nearly 40% of the world's population- were using internet[1,2]. The introduction, wide acceptance and use of the global connectivity network through computers, mobile phones, etc., have led to an economy largely based on information and computerization. Cloud computing –understood as the applications delivered as services over the Internet and the hardware and systems software in the data centres that provide those services[3]- will become one of the most powerful tools for business in the near future. The changes are so radical that this period of history is now being known as the "*information age*": a time when large amounts of information are widely available to many people, largely through computer technology.

For this reason, the sales of smartphones, tablets, computers and televisions with internet are still growing year after year, and devices suitable to be worn –the so-called wearable electronic devices- and cars or other objects connected to internet (what is now known as the internet of things) are starting to become daily-life items[4]. Nowadays, we are able to transmit data from almost any point of the world to another almost instantaneously. Data can be sent and stored in the cloud and from there it can be accessed, modified, analysed and downloaded by anyone connected to this network. This has broken the barriers of space and time in generating and sharing information. This information is now accessible to anyone, everywhere and in real time. Our present is still partially digital. The future is fully digital.

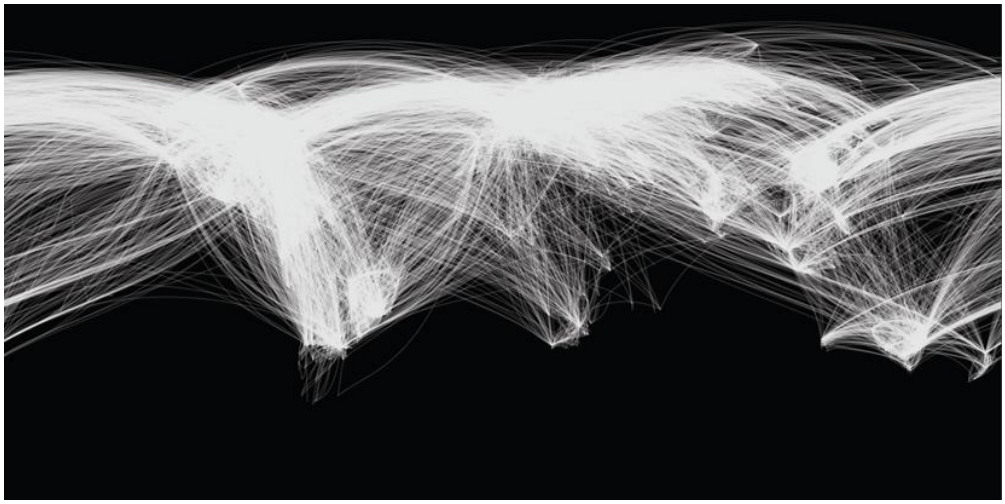

Figure 1.1. Map showing internet connection across the globe. Data from 2011. Picture elaborated by Chris Harrison, from Carnegie Mellon University.

In this new scenario, it is fair to ask what is the role of analytical chemistry. Without any doubt, there will be many new challenges, and one of them will be to help to fill the growing gap between the physical and the digital world[5]. Analytical chemistry is essentially a science that produces information, identifies what substances are present on a sample and in which amount. Traditionally, this activity has been carried out in centralized facilities –the analytical laboratory-. However, as the network of information spreads in a scattered way around the planet, there is an increasing need to generate chemical information everywhere, at any time. Sensors –analytical tools that can be used for identification and quantification of substances outside the laboratory- are becoming an ideal tool to connect the digital and the "real" (physical) world. In that sense, sensors must adapt to this new digital world, providing real-time information for anyone.

The communication network for transmitting the data provided by these sensors is already well stablished and widely used. In fact, a "data-hungry" network with ability to transmit and process a massive amount of information is waiting for inputs and applications. Therefore, a real challenge is to develop sensors that can be plug into these systems, creating what is known as sensing networks[6] and, now

even more popular, wireless sensing networks (WSN). These wireless sensing networks find use across a plethora of different fields. Their use to determine several parameters in urban areas has been captured in the concept of "smart cities"[7]. Having interconnected sensors that can provide localization of buses, free parking spaces, amounts of waste, gas, electricity or water consumption –among others- will enable a totally different management of the resources, making cities much more socially and energetically efficient. In the same way, water and food quality control, environmental analysis[8] or security will experience significant improvements when sensing networks can be implemented. The introduction of these concepts in analytical chemistry was pioneered and popularized by Diamond[5,6,9] and co-workers, who had early nurtured the vision of combining digital communications with analytical chemistry -and more specifically, sensors- during the last fifteen years. These sensing networks, which at some point evolved into wireless sensing networks (WSN) have lately –with the emergence of bendable and wearable electronics- become truly wireless body sensing networks (WBSN)[10]. Clearly, streaming chemical and biochemical data directly from the human body, which has already began with the incorporation of physical sensors, is one of the next big steps. All in all, analytical chemistry has the great opportunity to take advantage of the communication networks already existing for mobile and internet connections and feed them with chemical information of the physical world through a widespread network of sensors.

In order to integrate chemical sensors into this digital world, analytical chemistry must undergo some changes and move from the traditional lab-centred approach to delocalized, scattered autonomous sensors. Traditionally, analytical chemistry has centred almost all of its efforts on making more sensitive, selective and accurate sensors. A race to reduce the limits of detection of the analytical techniques has produced drastic improvements[11]. All these improvements have resulted in very sophisticated instruments, which are usually big, expensive and require considerable expertise to be used. In order to have decentralized analysis,

the efforts must go in the direction of developing simple, compact and portable devicess[5,12]. This change has already started and sensors that can be used to solve countless problems in a decentralized way are being widely developed[9].

A big area that is already undergoing a revolution through these decentralized measurements is the medical area. One of the best examples of these decentralized sensors in the medical field is the glucometer. Since the first glucose enzyme electrode was developed back in 1962[13] and the first commercial device for measuring glucose –the Dextrostix- appeared in 1963[14], massive improvements have been achieved in the management of diabetes. Nowadays, in the developed world, many patients with diabetes can have their own glucometer and control their sugar blood levels several times per day. The personal management of the diabetes has significantly improved the standard of living of the patients, who do not need to go to the hospital for the controls, and have reduced their emergency visits in the hospital and the occurrence and severity of secondary clinical conditions derived from wrong sugar levels[15]. It has been also proved that the cost of the diabetes for the healthcare system has been reduced due to a better management of the disease, thanks to the glucometer[16].

The glucometer is just an example of the upcoming similar devices that will soon become daily objects[17]. Cheap, robust and portable systems like the glucometer are gaining interest as the fields of point-of-care (POC)[18] and telemedicine are growing. POC is the delivery of healthcare products and services at the instant time needed by the patient, by the use of point-of-care tests (POCT) performed by non-laboratory staff –mainly doctors and nurses- outside the main laboratory –at or near the patient's bedside-. The success of the personalized glucose management has been also a great incentive for the development of telemedicine, an approach that aims to use electronic communication tools to generate and exchange clinical information, in order to provide healthcare remotely. Both fields require tests that can be carried out at the patient's bedside. The fast and reliable testing allows the

physicians to take rapid decisions while having a continuous or more frequent control over their patients. Patients, at the same time, have a better management of their health conditions[19]. These rapid decisions decrease the time that the patients need to wait for a diagnostic and improves the whole healthcare delivery. While it all sounds ideal, to expand these POC and telemedicine analysis tools, the development of portable, affordable and simple devices that can be used not just by healthcare professionals but also directly by patients is necessary.

Figure 1.2. Several POC testing devices already in the market[21].

The proliferation of POC devices has already started and it is predicted that in the upcoming years POC diagnostic tools will take over routine analysis, as the healthcare system will change its focus from the curative to preventive care. These technologies will just grow due to the fact that the increased world population and the effort to democratize the progress with new advanced treatments will increase

the healthcare cost to prohibitive levels for most of the population, making necessary a deep change in the healthcare model[20].

Moreover, these devices will not only become a "must" for the developed countries, but also are a primary need for the poor regions of the planet. Truly low-cost diagnostic tools are needed because of the impossibility to afford the cost of the conventional medical system[22]. In the developing countries, people living in rural areas do not have access to laboratory-based tests and the transport of the samples from the patient's home to the central laboratory is expensive and time-consuming. In that areas, sensors that are affordable, sensitive, specific, user-friendly, rapid and robust, equipment free and deliverable to end users (ASSURED tests[22]) are an urgent need[23]. Furthermore, if the information obtained from the sensors can be send through internet, these patients can then be connected to a specialist in the field, who can be in any part of the world, providing them with real time and specialized attention.

Considering all these needs, there is a clear opportunity for the development of low-cost decentralised analytical platforms, sensors that can provide meaningful medical, environmental and social information for this quickly growing interconnected world.

1.2 Paper-based potentiometric sensors: part of the solution

Paper displays some characteristics that make it an ideal candidate to be used as support for decentralized sensors. Paper has been already widely used in analytical and clinical chemistry, in applications ranging from paper-based chromatography to dipsticks or lateral flow immunoassays[24,25]. Paper is inexpensive and widely available; it is thin, light and flexible; it allows passive liquid transport through capillarity; and, being made out of cellulose, it is easy to modify and compatible with biological samples[23,26]. Therefore, providing that no big modifications are

required, sensors made out of paper will be affordable, simple, portable and disposable. Consequently, they would be ideal for decentralized applications.

Bioactive papers, pioneered recently by Pelton and co-workers [27–30], is an extension of the lateral flow assays that aims to address some of those needs. Bioactive papers are defined as "'*paper-like products, cardboard, fabrics and their combinations, etc., with active recognition and/or functional material capabilities*"[30]. They have found a large number of applications. For example, the filtering property of the paper makes it an excellent tool to entrap bacteria and therefore concentrate the sample; also, the lateral flow allows chromatographic separation while the surface chemistry allows easy immobilization of biological elements, etc.

Due to all these promising characteristics, the field of paper-based sensors has experienced an explosive growth during the lasts years (See Figure 1.3 A and B). Paper-based sensors that can detect a huge variety of analytes have been reported; there are several different techniques used to fabricate these sensors -photolithography, inkjet printing, paper cutting, screen printing, etc.- and many techniques used for the detection of analytes [31,32].

Most of the paper-based sensors yield a qualitative "yes/no" answer or provide a semi-quantitative tool based on colorimetric detection. These sensors are usually made by immobilizing a component that will selectively interact with the target analyte producing a change of colour that can be correlated with the analyte concentration in the sample. In that way, sensors to detect glucose and protein in the physiological relevant ranges[33] or the presence of bacteria such as salmonella[34] have been developed. However, qualitative or semi-quantitative information is usually not enough in the medical area, since a diagnostic tool to support medical decisions requires higher levels of accuracy. Therefore, the development of optical sensors that can give quantitative information is also becoming huge focus of research. In order to produce quantitative information, approaches aiming to

replace the visual detection by modern CCD technology are being developed. For example, medical relevant analytes such as glucose[35], enzymatic markers of liver function and protein[35] have been measured using a camera mobile phone[35–37]. Mobile phones have also been used for the determination of copper[38], pH and nitrite[39], and even for blood typing[40] and DNA identification[41]. Cadmium has been quantified in drinking waters with a colour intensity portable reader[42]. And quantification of prostate-specific antigen (PSA)[43], nitrite and uric acid[44] or ELISA immunoassays[45] have been performed using scanners as colour detectors.

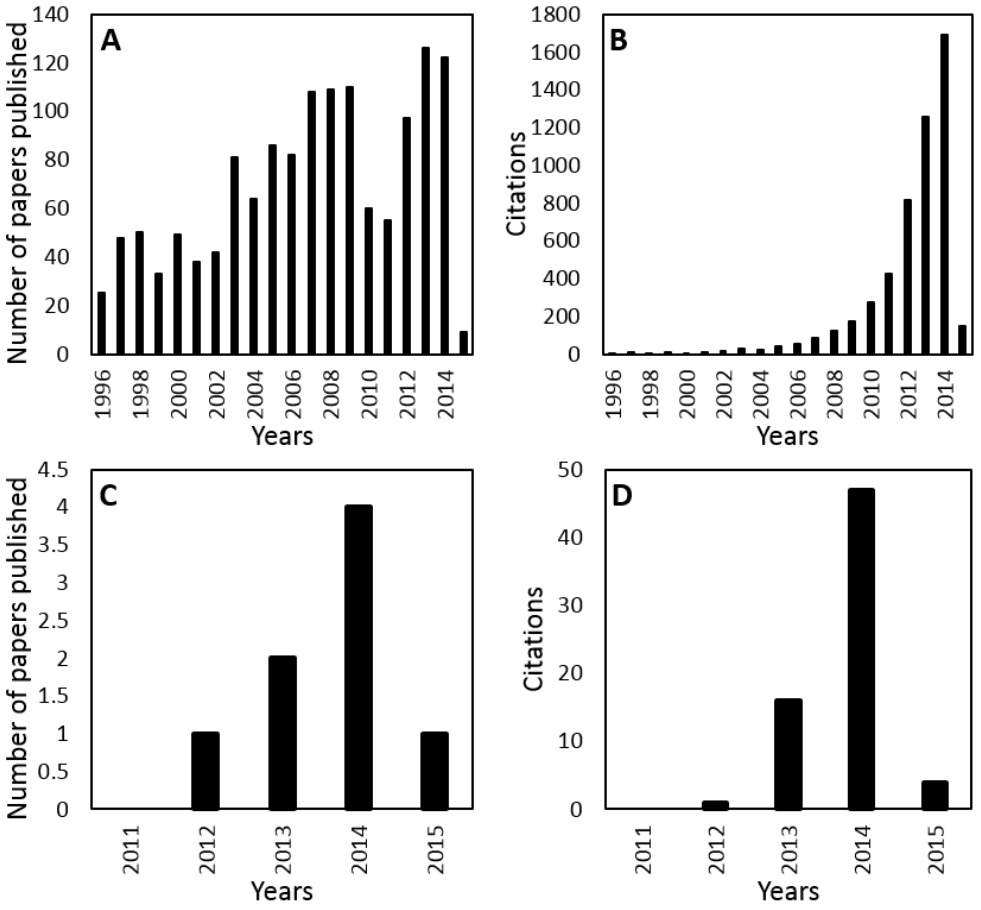

Figure 1.3. Papers published (A and C) and citations (B and D) within the topics of paper-based and sensors (A and B) and paper-based, sensors and potentiometry (C and D) (Accessed 20th of February of 2015 via Web of knowledge).

The group of Whitesides has been the pioneer in the development of these optical paper sensors. The concept of paper-optical sensors was demonstrated back in 2007[33] and since then, this group have published a plethora of articles in this field[23,35,37,45]. These devices are not only optical paper sensors, but also a platform able to perform the whole analytical procedure. In this regard, the term "microfluidic paper-based analytical devices" (µPADs) has been proposed for this paper platforms that emulate all the analytical process, such as sample pre-treatment, reaction and the detection. All this is possible due to the capillary properties of the paper that allow direct sampling through the microfluidic channels[46] patterned on the paper, which can distribute and separate the components of the sample. Their philosophy is to make the analytical procedure as cheap and simple as possible without losing performance and function. Furthermore, they are inspired by a vision where scientific curiosity is, at least in part, focused on providing effective solutions[12]. Driven by this concern, Whitesides and his group have moved forward these µPADs and optical paper sensors, up to the point to create a non-profit company for the free distribution of their sensors in the developing countries[47].

Colorimetric paper-based sensors have the advantages of being portable, affordable and simple, which make them very attractive to be used as POC tests. Moreover, the use of mobile phones, portable readers and scanners that can take an image of the sensor and process it with the use of a suitable software, allows obtaining accurate qualitative information[35,37,39]. The cameras of mobile phones are improving year after year and the access to smartphones is rapidly increasing worldwide. Therefore, they are becoming a powerful tool for detection in optical POC tests. However, in some situations the interpretation of the results may require expertise or advance image analysis, which might not be available in all the situations –patient's home, remote areas, etc.-, moreover interferences from the colour of the sample -especially blood-, the presence of contaminants or inconsistences in lighting may confuse the interpretation of the results. Thus,

colorimetric paper sensor are a very good tool for POC tests but also have some limitations depending on the situation[48].

Some of these limitations can be overcome by the use of electrochemical detection techniques. The measurement of electrical properties –such as current or voltage- is insensitive to light or colour change, very sensitive and easily transformed into a number by simple and inexpensive electronic devices. Moreover, electrochemical devices are being miniaturized and becoming increasingly cheaper while maintaining very low power requirements, thus adapting to the challenges for point of care and decentralized devices[49].

Electrochemical paper sensors are usually constructed sputtering a layer of a conductive material over the paper and then modifying it with a recognition layer. The interaction of the analyte with the recognition layer will produce an electrical signal that will be related to the analyte concentration. Within electrochemistry, different types of voltammetric detections are among the most used ones for paper-based sensors; gold[50] has been quantified with square wave voltammetry; differential pulse voltammetry has been reported for the detection of glucose[51] and cancer biomarkers[52]; NADH and nitrite[53] have been determined using cyclic voltammetry and chronoamperometry has been used for the detection of antibiotics[54], cysteine[55], mycrocystin-LR[56], glucose[57–59], lactate and uric acid[60]. More recently, potentiometric sensors have been also reported for the determination of silver[61], potassium[62], pH and calcium[63]. However, at the beginning of this doctoral thesis in 2011, there were no potentiometric paper sensors reported in the literature (see Figure 1.3 C and D).

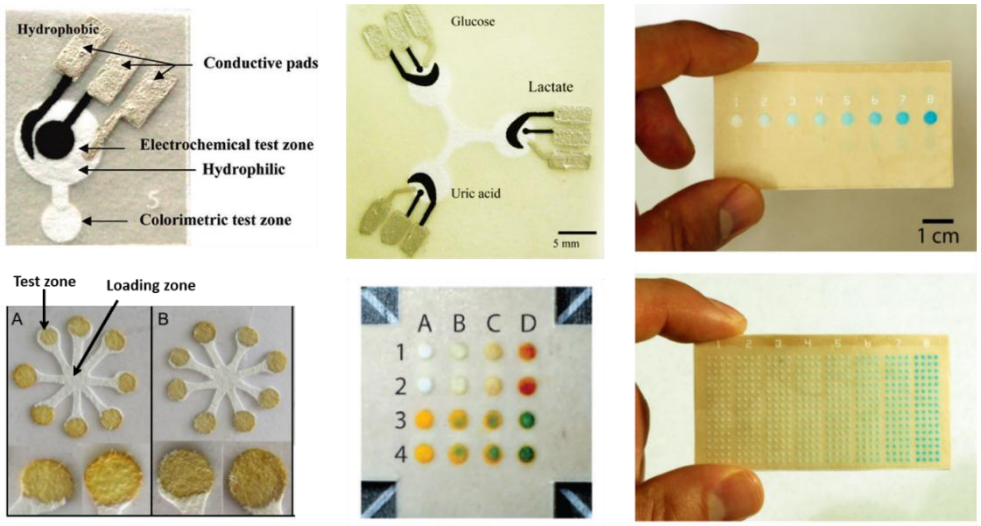

Figure 1.4. Examples of optical and electrochemical paper-based sensor[38,46,50,60].

Among all the analytical techniques, potentiometry offers very attractive features for decentralized analysis. Potentiometric devices are really simple in instrumentation and operation and show very low energy requirements; therefore they can be also easily miniaturised and relatively low-cost compared to other devices. Potentiometric tools –specially potentiometry with ion-selective electrodes (ISEs)- are routinely used for the determination of blood electrolytes[64]. Moreover, with the development of solid-contact technology, potentiometry went through a truly "silent revolution"[64]. During the last three decades, limits of detection and selectivity coefficients have been drastically improved, making them suitable for new applications. The development of solid contact electrodes allowed the miniaturization of such sensors. All in all, the advantages offered in the present potentiometry field make potentiometric sensors an ideal tool for building cheap, simple, easy to use, portable and disposable sensors.

Regarding the forthcoming needs for decentralised analysis in several areas, especially in the area of diagnostics –either for POC analysis or telemedicine in the developed countries or almost zero cost diagnostics for the poor regions of the planet- potentiometric paper sensors arise as very promising candidates for

addressing these needs. Indeed, potentiometric paper sensors fulfil the requirements of simplicity, low-cost, miniaturization, portability and easiness to use necessary for this type of analysis.

1.3 Objectives

The general objective of this doctoral thesis is the development of low-cost paper-based potentiometric platforms for decentralized analysis, *i.e.* for performing measurements out of the lab in a robust, simple and cost-effective way.

This general objective is divided in the following specific objectives:

- Explore the possibility to develop paper-based ion-selective potentiometric sensors and evaluate their analytical performance in comparison to existing solid-contact electrodes.
- Explore the development of a paper-based reference sensor that allows building a whole paper-based potentiometric cell and demonstrate its value through the application to the analysis of real samples.
- Explore the instrumental approaches to develop wireless potentiometers as the detection system for the potentiometric paper cell.
- Evaluate the limitations of the paper sensor in real scenarios and optimize their construction to fulfil real applications.
- Explore alternative applications of the paper platform.

The main added value of this thesis is the fabrication of paper-based potentiometric sensors which have the same performance as conventional ones but with considerable lower cost, and that meet the necessary requirements for “real world” applications. This thesis demonstrates for the first time the possibility to perform routine analysis with paper sensors with the same accuracy as classical sensors, thus opening the possibility to completely change and rethink the healthcare system and providing a useful tool for the personalised healthcare management.

1.4 References

(1) The Nielsen Company. *State of the media: U.S digital consumer report*; 2011.

(2) International Telecommunication Union. *The World in 2014*; 2014.

(3) Armbrust, M.; Stoica, I.; Zaharia, M.; Fox, A.; Griffith, R.; Joseph, A. D.; Katz, R.; Konwinski, A.; Lee, G.; Patterson, D.; Rabkin, A. *Commun. ACM* **2010**, *53*, 50–58.

(4) BI Intelligence. *The future of digital: 2014*; 2014.

(5) Diamond, D. *Anal. Chem.* **2004**, *76*, 279–286.

(6) Byrne, R.; Diamond, D. *Nat. Mater.* **2006**, *5*, 421–424.

(7) Hancke, G. P.; Silva, B. D. E.; Hancke, G. P. *Sensors* **2013**, *13*, 393–425.

(8) Murray, R. *Anal. Chem.* **2010**, *82*, 1569.

(9) Diamond, D.; Coyle, S.; Scarmagnani, S.; Hayes, J. *Chem. Rev.* **2008**, *108*, 652–679.

(10) Vincenzini, P.; Diamond, D. *Wearable/Wireless Body Sensor Networks for Healthcare Applications*; Ltd., Trans Tech Publications: Switzerland, 2013.

(11) Karayannis, M. I.; Efstathiou, C. E. *Talanta* **2012**, *102*, 7–15.

(12) Whitesides, G. M. *Lab Chip* **2013**, *13*, 11–13.

(13) Clark, L.; Lyons, C. *Ann. N. Y. Acad. Sci.* **1962**, *102*, 29–45.

(14) Hellman, R. *Diabetes Spectr.* **2012**, *25*, 135–140.

(15) Clarke, S. F.; Foster, J. R. *Br. J. Biomed. Sci.* **2012**, *69*, 83–93.

(16) Sidorov, J.; Shull, R.; Tomcavage, J.; Girolami, S.; Lawton, N.; Harris, R. *Diabetes Care* **2002**, *25*, 684–689.

(17) Lee, T. M. H. *Sensors* **2008**, *8*, 5535–5559.

(18) Price, C. P. *Clin. Rev.* **2001**, *322*, 1285–1288.

(19) Giljohann, D. A.; Mirkin, C. A. *Nature* **2009**, *462*, 461–464.

(20) IMS Institute for Healthcare Informatics. *Global Outlook for Medicines Through 2018 Introduction*; 2014.

(21) www.healthworkscollective.com.

(22) Mabey, D.; Peeling, R. W.; Ustianowski, A.; Perkins, M. D. *Nat. Rev. Microbiol.* **2004**, *2*, 231–240.

(23) Martinez, A. W.; Phillips, S. T.; Whitesides, G. M.; Carrilho, E. *Anal. Chem.* **2010**, *82*, 3–10.

(24) Fu, E.; Liang, T.; Houghtaling, J.; Ramachandran, S.; Ramsey, S. A.; Lutz, B. *Anal. Chem.* **2011**, *83*, 7941–7946.

(25) Delaney, J. L.; Hogan, C. F.; Tian, J.; Shen, W. *Anal. Chem.* **2011**, *83*, 1300–1306.

(26) Yetisen, A. K.; Akram, M. S.; Lowe, C. R. *Lab Chip* **2013**, *13*, 2210–2251.

(27) Jahanshahi-Anbuhi, S.; Henry, A.; Leung, V.; Sicard, C.; Pennings, K.; Pelton, R.; Brennan, J. D.; Filipe, C. D. M. *Lab Chip* **2014**, *14*, 229–236.

(28) Zhang, Z.; Wang, J.; Ng, R.; Li, Y.; Wu, Z.; Leung, V.; Imbrogno, S.; Pelton, R.; Brennan, J. D.; Filipe, C. D. M. *Analyst* **2014**, *139*, 4775–4778.

(29) Wang, J.; Yiu, B.; Obermeyer, J.; Filipe, C. D. M.; Brennan, J. D.; Pelton, R. *Biomacromolecules* **2012**, *13*, 559–564.

(30) Pelton, R. *TrAC, Trends Anal. Chem.* **2009**, *28*, 925–942.

(31) Liana, D. D.; Raguse, B.; Gooding, J. J.; Chow, E. *Sensors* **2012**, *12*, 11505–11526.

(32) Hu, J.; Wang, S.; Wang, L.; Li, F.; Pingguan-Murphy, B.; Lu, T. J.; Xu, F. *Biosens. Bioelectron.* **2014**, *54*, 585–597.

(33) Martinez, A. W.; Phillips, S. T.; Butte, M. J.; Whitesides, G. M. *Angew. Chem. Int. Ed.* **2007**, *46*, 1318–1320.

(34) Preechakasedkit, P.; Pinwattana, K.; Dungchai, W.; Siangproh, W.; Chaicumpa, W.; Tongtawe, P.; Chailapakul, O. *Biosens. Bioelectron.* **2012**, *31*, 562–566.

(35) Martinez, A. W.; Phillips, S. T.; Carrilho, E.; Thomas, S. W.; Sindi, H.; Whitesides, G. M. *Anal. Chem.* **2008**, *80*, 3699–3707.

(36) Songjaroen, T.; Dungchai, W.; Chailapakul, O.; Henry, C. S.; Laiwattanapaisal, W. *Lab Chip* **2012**, *12*, 3392–3398.

(37) Vella, S. J.; Beattie, P.; Cademartiri, R.; Laromaine, A.; Martinez, A. W.; Phillips, S. T.; Mirica, K. A.; Whitesides, G. M. *Anal. Chem.* **2012**, *84*, 2883–2891.

(38) Ratnarathorn, N.; Chailapakul, O.; Henry, C. S.; Dungchai, W. *Talanta* **2012**, *99*, 552–557.

(39) Lopez-Ruiz, N.; Curto, V. F.; Erenas, M. M.; Benito-Lopez, F.; Diamond, D.; Palma, A. J.; Capitan-Vallvey, L. F. *Anal. Chem.* **2014**, *86*, 9554–9562.

(40) Guan, L.; Tian, J.; Cao, R.; Li, M.; Cai, Z.; Shen, W. *Anal. Chem.* **2014**, *86*, 11362–11367.

(41) Song, Y.; Gyarmati, P.; Araújo, A. C.; Lundeberg, J.; Brumer, H.; Ståhl, P. L. *Anal. Chem.* **2014**, *86*, 1575–1582.

(42) López Marzo, A. M.; Pons, J.; Blake, D. A.; Merkoçi, A. *Anal. Chem.* **2013**, *85*, 3532–3538.

(43) Zhou, M.; Yang, M.; Zhou, F. *Biosens. Bioelectron.* **2014**, *55*, 39–43.

(44) Li, X.; Tian, J.; Shen, W. *Anal. Bioanal. Chem.* **2010**, *396*, 495–501.

(45) Cheng, C.-M.; Martinez, A. W.; Gong, J.; Mace, C. R.; Phillips, S. T.; Carrilho, E.; Mirica, K. A.; Whitesides, G. M. *Angew. Chemie Int. Ed.* **2010**, *49*, 4771–4774.

(46) Martinez, A. W.; Phillips, S. T.; Whitesides, G. M. *PNAS* **2008**, *105*, 19606–19611.

(47) www.dfa.org/index.php.

(48) Maxwell, E. J.; Mazzeo, A. D.; Whitesides, G. M. *MRS Bull.* **2013**, *38*, 309–314.

(49) Wang, J. *TrAC, Trends Anal. Chem.* **2002**, *21*, 226–232.

(50) Apilux, A.; Dungchai, W.; Siangproh, W.; Praphairaksit, N.; Henry, C. S.; Chailapakul, O. *Anal. Chem.* **2010**, *82*, 1727–1732.

(51) Kong, F. Y.; Gu, S. X.; Li, W. W.; Chen, T. T.; Xu, Q.; Wang, W. *Biosens. Bioelectron.* **2014**, *56*, 77–82.

(52) Wu, Y.; Xue, P.; Kang, Y.; Hui, K. M. *Anal. Chem.* **2013**, *85*, 8661–8668.

(53) Metters, J. P.; Houssein, S. M.; Kampouris, D. K.; Banks, C. E. *Anal. Methods* **2013**, *5*, 103–110.

(54) Wu, X.; Kuang, H.; Hao, C.; Xing, C.; Wang, L.; Xu, C. *Biosens. Bioelectron.* **2012**, *33*, 309–312.

(55) Santhiago, M.; Wydallis, J. B.; Kubota, L. T.; Henry, C. S. *Anal. Chem.* **2013**, *85*, 5233–5239.

(56) Wang, L.; Chen, W.; Xu, D.; Shim, B. S.; Zhu, Y.; Sun, F.; Liu, L.; Peng, C.; Jin, Z.; Xu, C.; Kotov, N. A. *Nano Lett.* **2009**, *9*, 4147–4152.

(57) Lankelma, J.; Nie, Z.; Carrilho, E.; Whitesides, G. M. *Anal. Chem.* **2012**, *84*, 4147–4152.

(58) Määttänen, A.; Vanamo, U.; Ihalainen, P.; Pulkkinen, P.; Tenhu, H.; Bobacka, J.; Peltonen, J. *Sens. Actuators, B* **2013**, *177*, 153–162.

(59) Nie, Z.; Nijhuis, C. A.; Gong, J.; Chen, X.; Kumachev, A.; Martinez, A. W.; Narovlyansky, M.; Whitesides, G. M. *Lab Chip* **2010**, *10*, 477–483.

(60) Dungchai, W.; Chailapakul, O.; Henry, C. S. *Anal. Chem.* **2009**, *81*, 5821–5826.

(61) Janrungroatsakul, W.; Lertvachirapaiboon, C.; Ngeontae, W.; Aeungmaitrepirom, W.; Chailapakul, O.; Ekgasit, S.; Tuntulani, T. *Analyst* **2013**, *138*, 6786–6792.

(62) Jaworska, E.; Lewandowski, W.; Mieczkowski, J.; Maksymiuk, K.; Michalska, A. *Analyst* **2013**, *138*, 2363–2371.

(63) Ping, J.; Wang, Y.; Fan, K.; Tang, W.; Wu, J.; Ying, Y. *J. Mater. Chem. B* **2013**, *1*, 4781–4791.

(64) Bakker, E.; Pretsch, E. *Angew. Chem. Int. Ed.* **2007**, *46*, 5660–5668.

UNIVERSITAT ROVIRA I VIRGILI
PAPER-BASED POTENTIOMETRIC PLATAFORMS FOR ESCENTRALISED CHEMICAL ANALYSIS.
Marta Novell Recasens
Dipòsit Legal: T 1462-2015

CHAPTER

2

THE FOUNDATIONS OF THE DETECTION AND CHARACTERISATION APPROACHES

UNIVERSITAT ROVIRA I VIRGILI
PAPER-BASED POTENTIOMETRIC PLATAFORMS FOR ESCENTRALISED CHEMICAL ANALYSIS.
Marta Novell Recasens
Dipòsit Legal: T 1462-2015

2.1 Summary

This chapter contains an overview of the working principles of the potentiometric sensors. The goal of this part of the thesis is to provide general definitions and conventions about the main components of the systems used through most of the work. The foundations of potentiometric sensors and the analytical figures of merit used for the characterisation are discussed in detail.

2.2 Chemical sensors

According to IUPAC a chemical sensor is "*a self-contained integrated device, which is capable of providing specific quantitative or semi-quantitative chemical information using a recognition element that is retained in direct spatial contact with a transduction element*"[1]. When the substance of interest interacts with the recognition element, there is a change of physical or chemical properties that the transducer can convert into a signal. Depending on the signal obtained, the sensors can be classified in different groups: optical, electrochemical, thermometric, etc[2]. All the work of this thesis is within the field of electrochemistry, which measures electrical signals generated upon chemical changes. Within electrochemistry, sensors are divided in three major categories depending on their mode of measurement: potentiometric (measurement of voltage), amperometric (measurement of current) and conductimetric (measurement of conductance or resistance)[3]. Since most of the work of this thesis is based on potentiometric tools, this will be the technique herein described in detail.

2.3 Components of a potentiometric sensor

While there are different types of potentiometric sensors, this work is centred in ion-selective and enzyme-based electrodes. These potentiometric sensors have a

common basic architecture, which consists of a metallic conductor, a transducer and a recognition layer (see Figure 2.1).

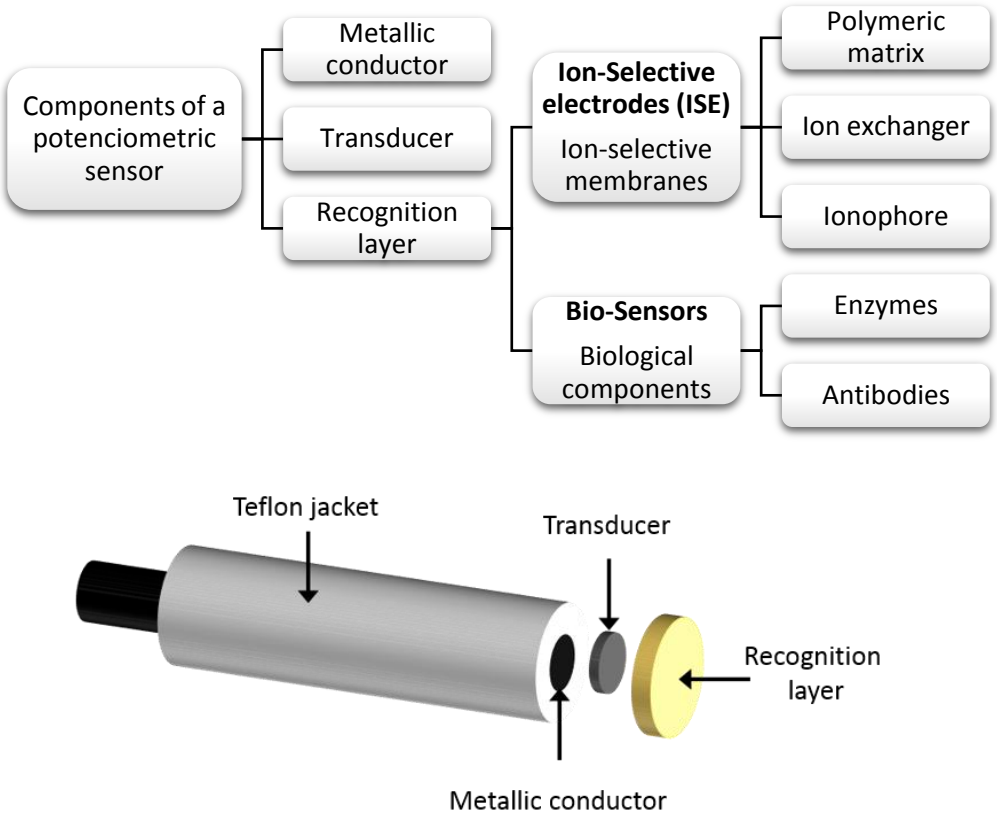

Figure 2.1. Diagram and scheme of the basic components of a sensor. The recognition layer is attached directly over the transducer, and this over the metallic conductor. The Teflon jacket (or other isolators) avoids the contact of the metallic conductor with the sample.

2.3.1 Metallic conductor

The metallic conductor is the support of a sensor and the connection to the measuring device. Most of the other components are usually assembled in direct contact over it. Any kind of good electronic metallic conductor can be used as the sensor support[4], although some materials show superior performance over others. Its role is to carry the electrical signal from the interface to the measurement device.

One of the materials widely used as metallic conductor in potentiometric sensors is glassy carbon (GC). GC is an agranular non-graphitizable carbon material with a very high isotropy of its structural and physical properties and a very low permeability for liquids and gases[5]. The original surfaces and the fracture surfaces have a pseudo-glassy appearance. Their most important properties are high temperature resistance, hardness, low density, low electrical resistance, low friction, low thermal resistance, extreme resistance to chemical attack and impermeability to gases and liquids[6].

2.3.2 Recognition layer

It is the part of the sensor that is involved in a specific interaction with the analyte, either by complex formation, or catalysing a reaction in a selective way. Nature, for example, has evolved a vast array of biomolecules or bio-molecular structures with an exquisite specificity in their molecular recognition properties. The recognition layer usually contains either these natural or synthetic molecules that usually mimic natural recognition elements. Antibodies, enzymes, proteins or DNA are some examples of these natural receptors. Synthetic recognition elements are mainly based in host (molecular receptor) - guest (analyte) interactions, which are usually based in ionic recognition –when the analyte is an ion- and covalent recognition -when the analyte is a neutral specie-. Crown ethers, cryptands, spherands, calixarenes, cavitands and cryptophanes are some examples of these ionic and molecular recognition elements[7].

In this thesis different recognition layers have been used. Ion-selective membranes, for example, were used as the recognition layer for ion-selective electrodes. Enzymes were used to catalyse a reaction in enzyme-based sensors and antibodies were used to selectively interact with a protein in a chemiresistor sensor.

2.3.2.1 Ion-selective membranes

Ion-selective membranes are the recognition layer of ion-selective electrodes. They are usually made with three main components, namely: a) a polymeric matrix, b) a liphophilic ion-exchanger and c) a receptor molecule or ionophore.

a) The polymeric matrix. This is the mechanical support for all the other components. This matrix is composed of lipophilic compounds dissolved in an organic solvent, which forms a stable membrane upon the evaporation of the solvent. In order to preserve this stability, the membrane usually has a hydrophobic character. Therefore, its components are inert and insoluble in water. Usually, polymeric matrices are made of poly-vinyl chloride (PVC)[8], although other membranes made of silicon rubbers[9] or polyacrylic materials[10] are also used. PVC membranes require the use of plasticisers, which give them special structural properties such as flexibility and increased ionic mobility. Although they show some disadvantages, such as the small percolation of water through the membrane (which gives way to some analytical problems) the use of these membranes is still the most common approach. For this reason, they are the main type of membranes used in this thesis.

b) Lipophilic ion-exchangers. These are molecules composed by a large lipophilic anion and a small cation or vice-versa depending if they are cationic or anionic ion exchangers respectively (see Figure 2.2). Because of the lipophilicity, the bigger ion is retained in the membrane while allowing an exchange of the small counter-ion. Ion-exchangers are an essential component to obtain a Nernstian response and guarantee the permselectivity of the membrane[11]. To maintain the permselectivity, no significant amount of counter ions must enter the membrane. The presence of the ion exchange regulates this process and this guarantees the constant concentration of primary ions inside the membrane.

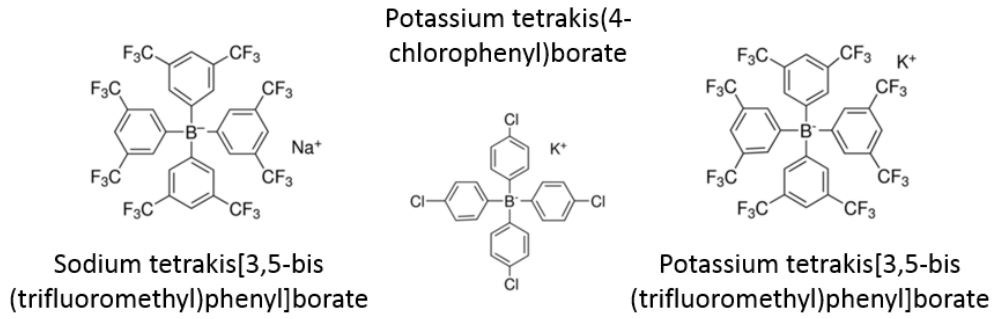

Figure 2.2. Some examples of cation exchangers.

c) The ionophore. This is the component that displays high affinity with the target ion and therefore the main responsible for the membrane selectivity and sensitivity. Ionophores are specifically synthetized for each ion depending on their charge, size and shape. Ionopohores can reversibly bind ions due to the ability to form supramolecular interactions (host-guest) by hydrogen bonding, metal coordination and hydrophobic/lipophilic interactions.

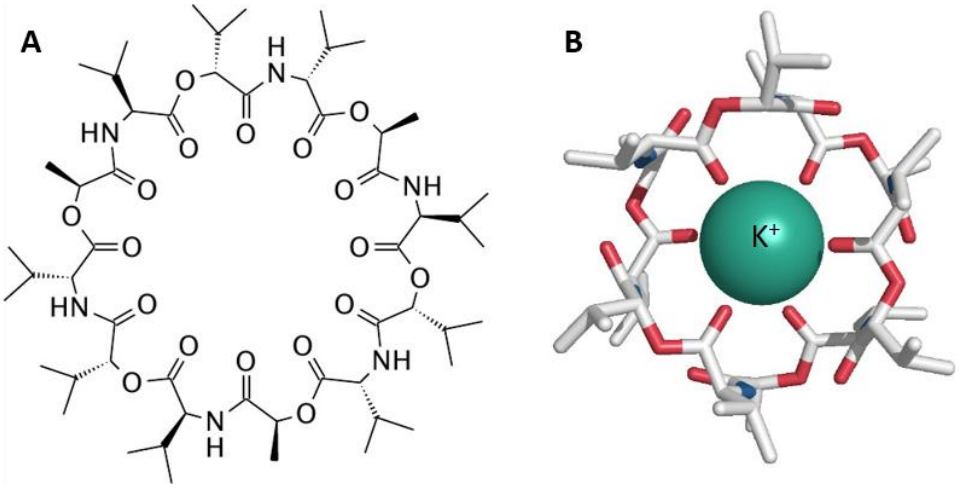

Figure 2.3. A) Valinomycin (potassium ionophore) structure. B) 3-D structure of the complex formed between the potassium ion and the valinomycin[12]. Oxygen atoms are shown in red and ammonium ones in blue. The octahedral coordination between the potassium and the 6 carbonyls can be seen.

For example, valinomycin (potassium ionophore) is a cyclic molecule with a central cavity lined with oxygen atoms that is highly selective for K^+. This selectivity towards potassium comes from its shape and size. K^+ ions show octahedral coordination in a square bipyramid geometry by 6 carbonyl bonds from valinomycin (see Figure 2.3).

2.3.2.2 Biological components

Other recognition elements used in potentiometric sensors are biological components. In this thesis enzymes and antibodies have also been used. Enzymes are macromolecules that act as biocatalysts by increasing the speed of a reaction. In general, enzymes catalyse only one reaction on one substrate, thus providing reaction and substrate specificity respectively. Antibodies are proteins produced by the immune system in response to an exposure to a foreign molecule (antigen) and characterised by its specific binding to a site of that molecule[13]. Therefore, both enzymes and antibodies can act as recognition elements providing high selectivity to the sensor. These components are usually immobilized in the sensor surface by entrapment behind a permeable membrane, entrapment within a polymeric matrix or a bilayer lipid membrane, covalent bonding to the surface or bulk modification of the entire electrode material[14].

Enzyme-based sensors usually detect one product that results from the interaction between the immobilized enzyme and the analyte. Antibody-based sensors detect direct changes in the transducer output due to the binding event (antibody-antigen) or indirect competitive and displacement reactions similar to immunoassays[15].

2.3.3 Transducer

The transducer is the element that converts the change on a given (physical or chemical) property into a measurable signal. In potentiometry, transducers are responsible for ion-to-electron signal transduction. The first transducers used in

potentiometry were liquids, however due to the revolution of the solid-contact sensors new materials appeared, such as conducting polymers and nanostructured materials[4]. In this thesis carbon nanotubes (CNTs) have been used as transducers.

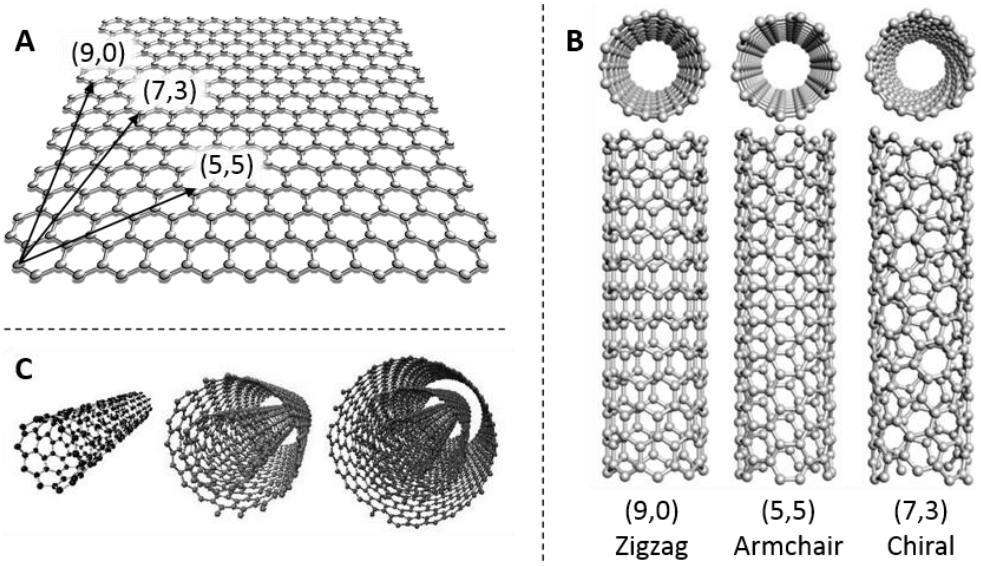

Figure 2.4. CNTs schematic representation. A) Graphene sheet with different folding vectors, resulting in B) different structures. C) Views of SWCNTs or MWCNTs depending on the number of graphene layers rolled up concentrically.

Carbon nanotubes are an allotropic form of carbon, whose structure can be visualized as a cylinder fabricated of rolled up graphene sheets[16] (Figure 2.4). Depending on the number of walls, carbon nanotubes can be classified as single wall carbon nanotubes (SWCNTs) –with just one wall- or multi wall carbon nanotubes (MWCNTs) –made of several coaxial walls-. Because of their excellent electrical, mechanical and optical properties, many potential applications have been proposed, such as their use to make conductive and high-strength composites, energy storage and energy conversion devices, field emission displays, hydrogen storage, probes, nanometer sized semiconductor devices, etc.[17] Regarding the analytical applications, CNTs have been widely used to build gas sensors, enzymatic biosensors, immunosensors or DNA probes, etc. Additionally,

they have been also applied to solid-phase extraction and chromatoghraphy[18]. CNTs are used in sensors in order to increase their sensitivity and chemical stability, to immobilize other components on the sensor or to improve the electron transfer capacity[19]. The ability of carbon nanotubes to act as ion-to-electron transducers in potentiometric sensors has been demonstrated by our research group[20,21].

2.4 Potentiometric sensors

Potentiometry is based on the measurement of the potential generated between two electrodes in a closed circuit and under zero (or near-zero) current conditions (see Figure 2.5). The potential is recorded with a high-impedance voltmeter (a potentiometer) and this potential is referred in terms of electromotive force (EMF). The two electrodes are called reference (RE) and working (WE) electrodes. The role of the reference electrode is to maintain a constant potential that is ideally insensitive to changes of temperature and solution composition. The working electrode must change its potential following a change on the analyte concentration in the solution under analysis. Therefore, the difference of potential between the two electrodes will be related to the concentration of an analyte in solution. There are different kinds of working electrodes, mostly differentiated by its working principle. In this thesis, ion-selective electrodes and enzymatic sensors will be developed.

Potentiometry has a plethora advantages over other electrochemical techniques, particularly when considering field methodologies. First, it displays an unrivalled roughness and simplicity of instrumentation. Second, the response is relatively fast, has a wide dynamic range and is inexpensive and simple to operate when compared to -for example- amperometry. This inherent simplicity stems from the facts that is label free and almost current free, whereas amperometry usually requires some label molecule and needs current for its measurements. However, potentiometry has also some limitations, such as the sometimes limited selectivity,

the relatively poorer limits of detection –when compared against other electrochemical approaches- and the need for calibration of the electrodes (although this last one is a requirement common to all the techniques).

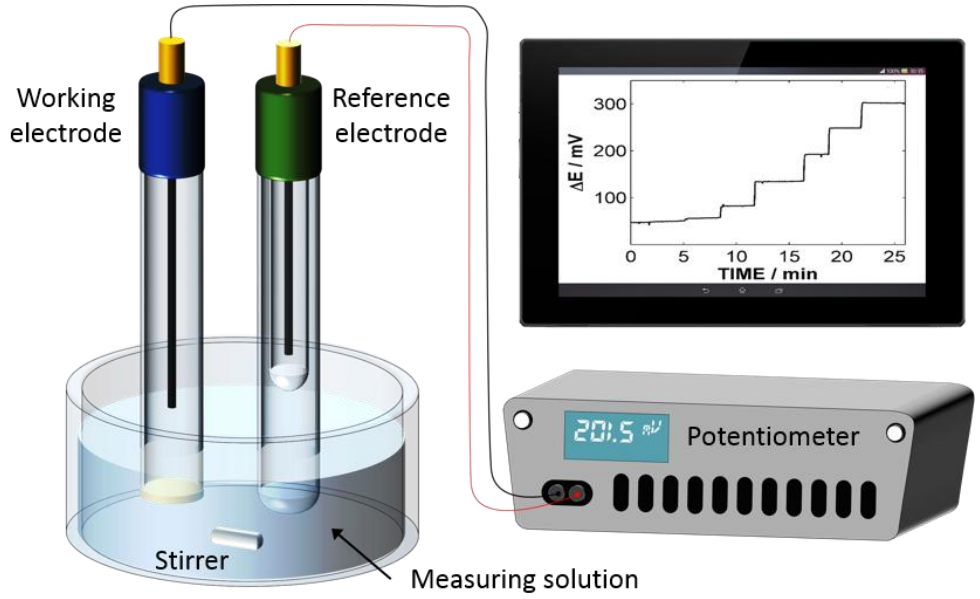

Figure 2.5. Scheme of a potentiometric cell.

2.4.1 Ion-selective electrodes

The most common potentiometric sensors are the ion-selective electrodes (ISEs). The first type of these electrodes was the glass electrode, reported back in 1909[22], and now widely used for the measurement of pH. Ion-selective electrodes can selectively determine the activity of their primary ion in a solution in the presence of other ions. Evidently, as shown in Figure 2.5, ISEs are only half of a potentiometric cell, since –for analytical purposes- a reference electrode is also needed to close the circuit.

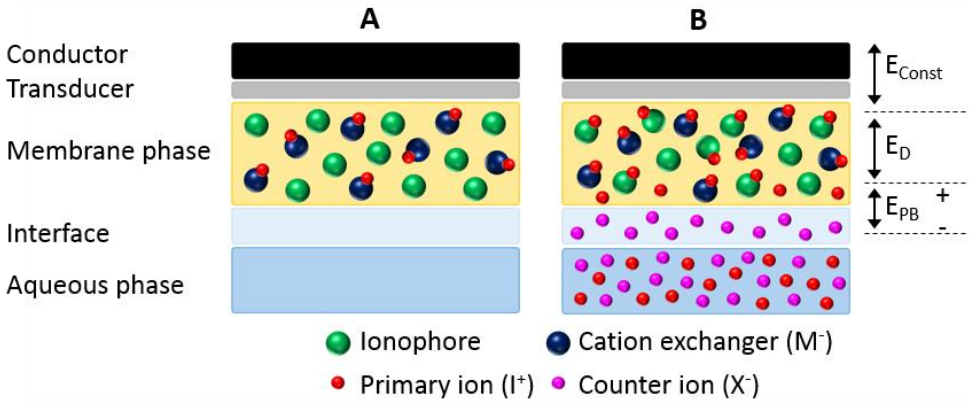

Figure 2.6. Scheme of the phase-boundary potential model. A) Ion-selective electrode in a solution without any ions. B) Ion-selective electrode immersed in an ionic solution. When the organic phase is put in contact with the sample solution, a charge separation occurs and this generates a difference of potential.

Different models to explain the potentiometric response of ISEs have been proposed[23]. Nowadays, the most widely accepted model to explain the working principle of these electrodes is the phase-boundary potential model[23] (see Figure 2.6). This model derives from the classical total-equilibrium models, which consider the EMF measured as a sum of the sample-membrane boundary potential (E_{PB}), the diffusion potential inside the membrane (E_D) and a constant potential generated at the internal interfaces (E_{Const})[4] –membrane-transducer, transducer-metal contact-.

$$EMF = E_{PB} + E_D + E_{Const} \qquad \textit{Equation 2.1}$$

The phase boundary potential model is based in two assumptions[23]:

1. The phase boundary potential at the aqueous-organic interface (E_{PB}) governs the membrane response. Migration effects inside the membrane are ignored, thus making E_D=0 (electroneutrality assumption).

2. The organic phase boundary contacting the sample is in chemical equilibrium with the aqueous sample solution.

In its general form, the phase-boundary potential can be written as follows[23]:

$$E_{PB} = \frac{RT}{z_I F} lnk_I + \frac{R"T}{z_I F} ln \frac{a_I(aq)}{a_I(org)} \qquad \textit{Equation 2.2}$$

where $R^{"}$ is the universal gas constant (8.314 J/K·mol); T the temperature; z_I the charge of the primary ion; F the Faraday constant (96485 C/mol); $a_I(aq)$ the activity of the uncomplexed primary ion in the aqueous sample; $a_I(org)$ the activity of the primary ion in contact with the organic phase boundary and k_I is function of the relative free energies of solvation in both the sample and the membrane phase:

$$k_1 = e^{(\mu_I^0(aq) - \mu_I^0(org))/R"T} \qquad \textit{Equation 2.3}$$

where $\mu_I^0(aq)$ and $\mu_I^0(org)$ are the chemical standard potentials of the ion I^{z_I+} in the respective phase.

The first term of equation 2.2 is ideally constant for a given electrode at a certain point and is called the standard potential E_I^0. The standard potential includes factors affecting the solvation of the ion in the membrane and solution phases and changes on the membrane over time. Therefore, in practical terms, this standard potential changes between experiments and needs to be recalculated often. Moreover, the activity coefficients are assumed to be constant in the membrane phase ($a_I(org)$), thus making the concentration of the primary ion in the membrane independent from the sample. After all these assumptions, equation 2.2 can be re-written in the form of the well-known Nernst equation:

$$E_I = E_I^0 + \frac{R"T}{z_I F} \ln a_I \qquad \textit{Equation 2.4}$$

From equation 2.4, at a temperature of 25°C -and applying a 2.3 factor to change from the natural logarithm (ln) to a 10-based logarithm (log)-, the sensitivity should be 59.2 mV/log a_{I^+} for a singly charged ion and, 29.6 mV/log $a_{I^{2+}}$ for a doubly charged ion. Therefore, the sensitivity for any ion is fixed and can be theoretically predicted. However, in practice not all the ISEs exhibit the theoretical sensitivity,

and values close to the 59.2 are also considered Nernstian. This fixed sensitivity is an advantage from an analytical standpoint, since it simplifies quality assessments or allows, for example, a one-point calibration. Once the sensitivity is known, the potential of one known concentration allows predicting the whole calibration curve. Because of the logarithmic dependence, in general ISEs also exhibit a wide linear range, which means that they can be used to measure ions in many different samples whose analyte concentrations can vary several orders of magnitude. Typical potassium or ammonium electrodes, for example, can measure in concentrations ranging from 10^{-6} M to 10^{-1} M[24,25], *i.e.* they span for more than 5 orders of magnitude. The fixed sensitivity and wide linear range are very attractive features of potentiometry from an analytical standpoint, especially when dealing with decentralized techniques. However, potentiometry also has some weakness. The sensitivity is relatively low if differentiation between closed concentrations is required. For example, potassium concentration in blood ranges between 3.5 mM to 5 mM[26], which in terms of potential is measured as a difference of just of 9.2 mV. Another important drawback is the difficulty to control the standard potential, thus requiring a calibration –at least one point- for each electrode. Several works to improve this problem are now starting to emerge, making more feasible the possibility to have in the near future calibration-free electrodes.

It should be noted that the Nernst equation relates the potential of a half cell with the activity of the solution. Even though at low concentrations, activity and concentration have almost the same value, at high concentration its difference is significant; therefore, in this thesis activity has been always used. The activity has been calculated using the Debye-Hückel approximation[27]. The activity of a solution can be related to its concentration through an activity coefficient following the next equation:

$$a_i = \gamma_i c_i \qquad \textit{Equation 2.5}$$

where a_i is the activity; γ_i the activity coefficient and c_i the concentration of the ion *i*. The activity coefficient can be calculated as follows by using the Debye-Hückel approximation:

$$\log \gamma_{\pm} = 0.5091 z^{+} z^{-} \sqrt{I} \qquad \textit{Equation 2.6}$$

where γ is the activity coefficient, z^+ and z^-, the charges of the cations and anions respectively and *I* the ionic strength of the solution. Which at the same time is calculated following the next equation:

$$I = \frac{1}{2} \sum_{i=1}^{n} c_i z_i^2 \qquad \textit{Equation 2.7}$$

where c_i and z_i are the concentration and charge of a ion *I*, respectively.

2.4.2 Enzyme-based electrodes

Other types of electrodes that are also very popular in other techniques, such as amperometric determinations but not so much in potentiometry are electrodes incorporating an enzyme in the recognition layer to selectively interact with one analyte (schematic representation on Figure 2.7). From these interactions, which involve a chemical reaction, a difference of potential is generated. The first potentiometric enzyme-based electrode was reported back in 1969[28]. It was a urea biosensor that consisted on a urease immobilized over a glass ammonium electrode. The enzyme catalyses the decomposition of urea, which gives ammonium as a product, and this was detected by an ammonium ISE. This working principle is still the most used in potentiometric enzyme electrodes[29]. However, there are other strategies reported with enzyme electrodes: detection of a co-substrate consumption –*e.g.* oxygen-, detection of a product[30] –like on the urea biosensor previously described-, detection of the state of the biocatalyst redox active centre using an immobilized mediator –*e.g.* ferrocene derivates[31,32], Ru or Os

complexes- which reacts sufficiently rapid and is easily detected by the transducer; or direct electron transfer between the active site of a redox enzyme and the electrochemical transducer[14].

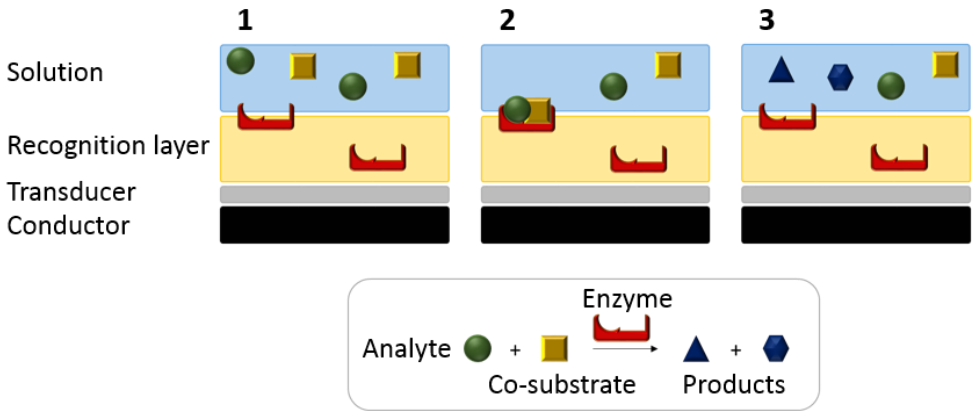

Figure 2.7. Scheme of an enzyme electrode. 1) The electrode is put in contact with a solution containing the analyte that interacts with the enzyme. 2) The analyte and the co-substrate are bind to the enzyme, which catalyses the reaction, 3) producing the final products, which are unbound from the enzyme and diffuse into the solution.

2.4.3 Reference electrode

The reference electrode is a device that shows a stable, reversible and reproducible potential. This means that the electrode potential will not change when the composition of the sample changes; it must return rapidly to its equilibrium value after a small transient perturbation; and –last but not least- will always give the similar potential when the same electrode/solution combination is constructed[3]. There are different types of reference electrodes –standard hydrogen electrode, saturated calomel electrode, silver-silver chloride electrode, etc.- but the most popular, used during this thesis, is the silver-silver chloride electrode.

This electrode consists of three parts: the internal reference element (Ag/AgCl), a reference solution compartment (KCl) and a liquid junction. All this combination is aimed to maintain a constant electrical potential (see Figure 2.8). The requirement

of reversibility is easily satisfied by using a very fast electrochemical reaction with a very high exchange-current density such as de redox couple silver/silver chloride. The stability is maintained by keeping the activity of chloride ions constant. To do so, the Ag/AgCl wire is in contact with a highly concentrated solution of chloride ions (KCl). The electrical contact of this electrode with the sample is done through a liquid junction. In this junction –where two different solution are in contact- a liquid-junction –or diffusion- potential is created. The more concentrated solution will have a tendency to diffuse into the less concentrated one. As anions and cations have a different rate of diffusion –which depends on the electric field and the speed-, its diffusion through time will result in an electrical double layer of positive and negative charges at the junction of the two solutions. This liquid-junction potential cannot be measured but can be estimated following the Henderson equation[3]:

$$E_{Diff} = \frac{\sum_i \frac{|z_i|\mu_i}{z_i}[c_i(\beta) - c_i(\alpha)]}{\sum_i |z_i|\mu_i[c_i(\beta) - c_i(\alpha)]} \frac{R"T}{F} \frac{\sum_i |z_i|\mu_i c_i(\alpha)}{\sum_i |z_i|\,\mu_i c_i(\beta)} \qquad \textit{Equation 2.8}$$

where z_i is the charge, μ_i the mobility and c_i the concentration of an ion *i,* and α and β are the two different solutions.

As mentioned, the junction generates an outflow of the internal reference solution, which helps to stabilize the liquid-junction potential but also contaminates the sample. In order to minimize this problem, double-junction reference electrodes were developed. These electrodes have an extra compartment containing a different electrolyte, which is then in contact with the solution through another junction (Figure 2.8). Usually the initial compartment –filled of KCl- is called inner filling, and the added one, outer filling. This outer filling usually contains lithium acetate as it is the salt that minimizes all the problems that arise from a liquid junction.

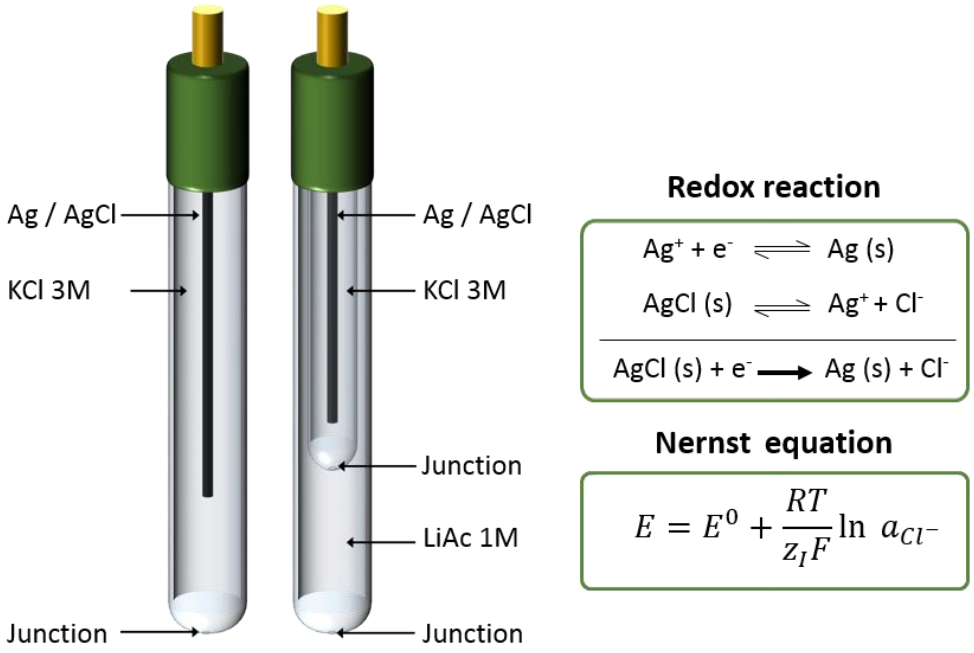

Figure 2.8. Reference electrodes diagram: single junction (left) and double junction (right), with the redox reaction that maintains its potential constant. The potential (as shown by the Nernst equation) just depends on the chloride activity, which is really high, thus not being affected by small changes and keeping the potential constant.

The fact that the reference electrode keeps a constant potential is essential to measure a change in EMF that only depends on the working electrode. However, the use of these inner solutions is not free from drawbacks. Some of these limitations are the difficulty of miniaturization, the fixed working position and the need of periodical maintenance. To overcome all these limitations, reference electrodes are also moving to solid contact approaches. Nevertheless, due to all the requirements, developing solid-contact reference systems has proven more challenging than developing solid-contact working electrodes.

2.4.4 Solid contact potentiometric sensors

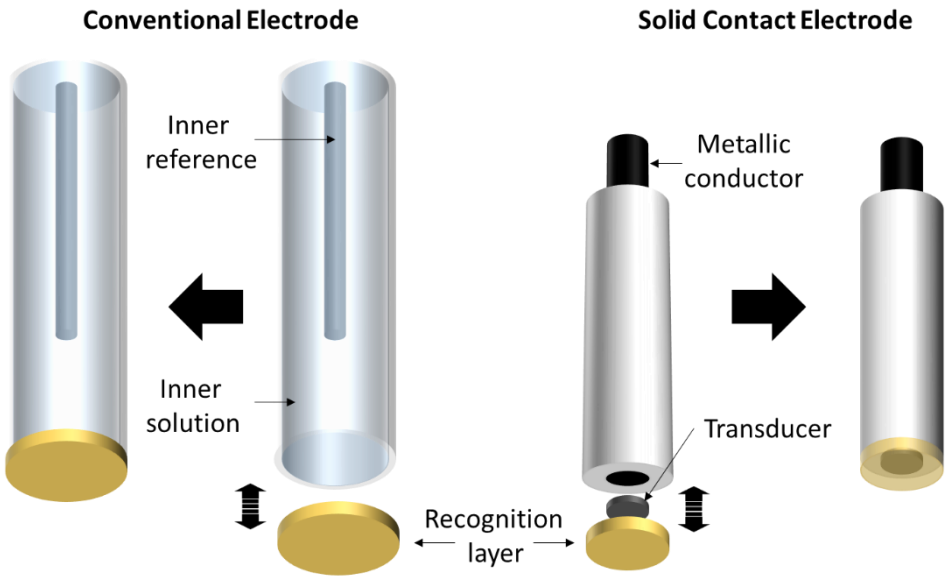

Figure 2.9. Schematic representation of a conventional ion-selective electrode and a solid-contact ion-selective electrode.

Classical potentiometric sensors were built using an internal filling solution as a transducer. Although exhibiting an excellent robustness, potential stability and life time[33], they present several drawbacks inherent to the use of a liquid, such as miniaturization, storage, position of use, etc. However, the wide applicability of potentiometric sensors pushed the field to the development of solid-contact (SC) electrodes (see Figure 2.9). The first progress on this direction was the invention of the "coated wire" electrodes at the beginning of the 1970s. This device consisted of a membrane placed in direct contact with an electrical conductor. While the approach was attractive, these electrodes displayed very poor potential stability. Since then, significant research has been focused on the development of solid materials than can as act as ion-to-electron transducers. The first revolution on this field was achieved through the use of conducting polymers. Later, nanostructured materials[4] have pushed this revolution even farther. Conducting polymers (CPs) are electroactive materials with mixed electronic and ionic conductivity. They were the

first materials to be introduced as solid-contact transducers and are still in use. However, they show some drawbacks such as light and pH sensitivity, redox reactions, sensitivity to CO_2 and O_2, etc. One of the biggest problems of SC-ISE is the presence of a water layer –a thin water film between the membrane and the CP that is formed due to water percolation through the membrane[34]-. This water layer is one of the major sources of signal instability and affects the limits of detection[35]. Nanostructured materials help to overcome many of the problems presented by CPs. Up to the date, several nanostructured materials have been reported to act as excellent ion-to-electron transducers[36].

Solid contact electrodes show many advantages over their liquid-contact analogues, they are simple to fabricate and allow for simple miniaturization; moreover, the elimination of the inner liquid solution eliminates the transport of primary ions from there to the sample –*i.e.* the ion migration across the membrane-. This minimized transmembrane ion flux allows better selectivity and limits of detection[37]. In summary, current solid-contact electrodes match the performance of liquid-contact electrodes, providing advantages in simplicity, cost-effectiveness of fabrication, robustness, reliability, maintenance free and miniaturization[33].

2.5 Analytical performance parameters

There are several parameters to define the analytical performance of a chemical sensor. The most featured ones are defined[38] below and an illustration is shown in Figure 2.10.

- Sensitivity: is the slope of the calibration curve within the linear range. The calibration curve is the curve of the instrumental response – electrical potential- versus the concentration of the analyte. It should be remembered that for ISEs the change in potential is linear with the logarithm of the activity of the analyte, as stated for the Nernst equation (Equation 2.4).

- Limit of detection (LOD): potentiometric sensors can have a lower and upper limit of detection. The lower limit of detection is calculated as the activity –or concentration- of the analyte at the intersection point between the two extrapolated linear segments -the linear range and the low concentration level segment- of the calibration curve. The upper limit of detection could appear when electrodes become insensitive to high ionic activities and is calculated as the activity –or concentration- of the analyte at the intersection point between the two extrapolated segments -the linear range and the high concentration level segment- of the calibration curve. If not stated otherwise, this thesis will refer to the LOD as the lower limit of detection.

- Linear range: is the range of concentrations -or ion activity- where the calibration curve presents Nernstian linearity.

- Selectivity: is the ability of a sensor to detect a particular analyte in a complex mixture without interference from other components in the mixture. The selectivity of a sensor has to be quantified individually for each particular interference and in potentiometry is expressed in terms of selectivity coefficients (K_{IJ}^{pot}) in a logarithmic way. There are several methods to calculate potentiometric selectivity coefficients. In this thesis the two main ones will be used: the fixed interference method (FIM) and the separate-solution method (SSM)[39].

To measure the selectivity coefficients following the FIM, the concentration of the primary analyte is gradually increased in a solution with a fixed concentration of the interfering. The activity of the primary analyte at the LOD is calculated from the calibration curve obtained, and together with the activity of the interfering ion in the background solution is inserted in the following equation:

$$logK_{IJ}^{pot} = \log a_I(DL)/a_J(BG)^{z_I/z_J} \qquad \textit{Equation 2.9}$$

where *K* is the selectivity coefficient; *I* the primary ion; *J* the interfering ion; a_I *(DL)* the activity of the primary ion in the limit of detection; a_J *(BG)* the activity of the

interfering ion in the background solution and z_I and z_J the charge of the primary and interfering ions respectively.

To measure the selectivity coefficients following the SSM, calibration curves with the interfering ions are performed, followed by a calibration curve of the primary analyte. Potential values at 1 M concentration of each interfering ion and the primary analyte are extrapolated from the obtained calibration curves. These values are the inserted in the following equation:

$$logK_{IJ}^{pot} = \left(\frac{E_J^0 - E_I^0}{R"T} z_I F\right) \qquad \textit{Equation 2.10}$$

where *K* is the selectivity coefficient; *I* the primary ion; *J* the interfering ion; E_J^0 and E_I^0 the potential of the interfering and the primary ion at 1 M concentration respectively; *R"* the universal gas constant (8.314 J/K·mol); *T* the temperature; z_I the charge of the primary ion and *F* the Faraday constant (96485 C/mol).

- Response time: is the time required for a sensor response to change from its previous state to a final stable state, which is established according to the experimental conditions. In this thesis the response time will be measured as the time lapse between the moment in which the electrode is put in contact with a new concentration and the moment in which the potential of the cell has reached 90 % of the final value[11].
- Stability: is the ability of the sensor to keep the same signal over time under fixed measuring conditions. Stability is usually quantified as the drift of the electrode, which is the non-random change of signal –potential- over time in a solution of constant composition and temperature. The drift is calculated as the slope of the signal versus the time and is usually given in mV/h or µV/h in potentiometry.

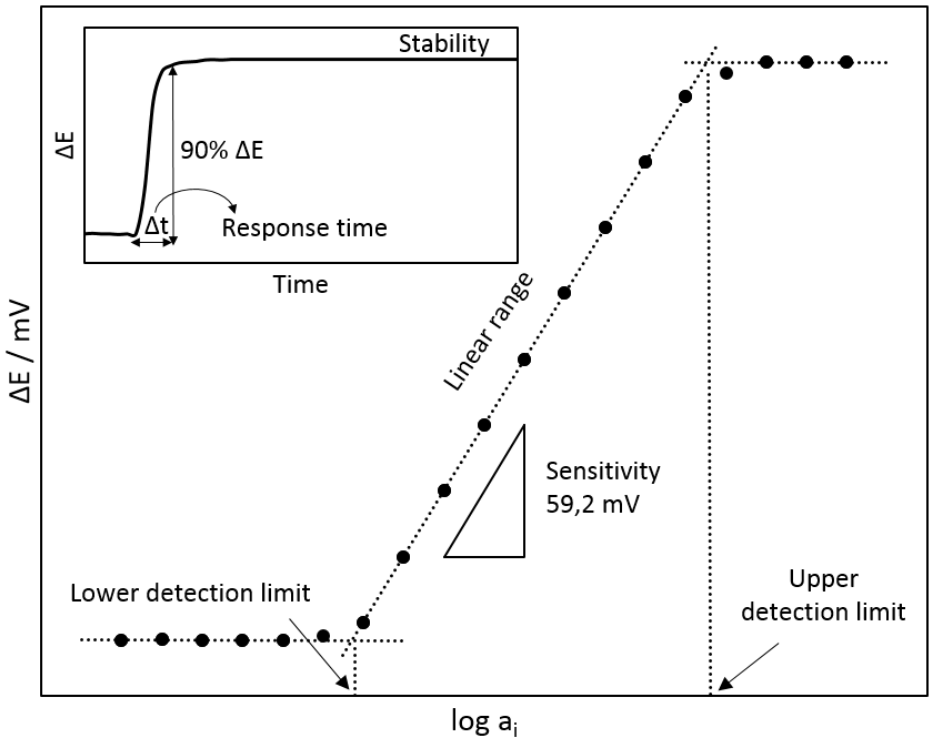

Figure 2.10. Graphical representation of some analytical parameters.

2.6 References

(1) Thevenot, D. R. *Pure Appl. Chem.* **1999**, *71*, 2333–2348.

(2) Hulanicki, A.; Glab, S.; Ingman, F. *Pure Appl. Chem.* **1991**, *63*, 1247–1250.

(3) Janata, J. *Principles of chemical sensors*; Springer: New York, 2009.

(4) Bobacka, J.; Ivaska, A.; Lewenstam, A. *Chem. Rev.* **2008**, *108*, 329–351.

(5) Fitzer, E.; Kochling, K.-H.; Boehm, H. P.; Marsh, H. *Pure Appl. Chem.* **1995**, *67*, 473–506.

(6) Yamada, S.; Sato, H. *Nature* **1962**, *193*, 261–262.

(7) Edmonds, T. E. *Chemical sensors*; Blackie: London, 1988.

(8) Armstrong, R. D.; Horvai, G. *Electrochim. Acta* **1990**, *35*, 1–7.

(9) Malinowska, E.; Oklejas, V.; Hower, R. W.; Brown, R. B.; Meyerhoff, M. E. *Sens. Actuators, B* **1996**, *33*, 161–167.

(10) Mensah, S. T.; Gonzalez, Y.; Calvo-Marzal, P.; Chumbimuni-Torres, K. Y. *Anal. Chem.* **2014**, *86*, 7269–7273.

(11) Bakker, E.; Bühlmann, P.; Pretsch, E. *Chem. Rev.* **1997**, *97*, 3083–3132.

(12) Palmer, M.; Chan, A.; Dieckmann, T.; Honek, J. *Biochemical pharmacology*; John Willey & Sons: New Jersey, 2012.

(13) Nagel, B.; Dellweg, H.; Gierasch, L. M. *Pure Appl. Chem.* **1992**, *64*, 143–168.

(14) Thévenot, D. R.; Toth, K.; Durst, R. A.; Wilson, G. S. *Biosens. Bioelectron.* **2001**, *16*, 121–131.

(15) Taylor, R. F.; Marenchic, I. G.; Spencer, R. H. *Anal. Chim. Acta* **1991,** *249*, 67-70.

(16) Eatemadi, A.; Daraee, H.; Karimkhanloo, H.; Kouhi, M.; Zarghami, N.; Akbarzadeh, A.; Abasi, M.; Hanifehpour, Y.; Joo, S. *Nanoscale Res. Lett.* **2014**, *9*.

(17) Baughman, R. H.; Zakhidov, A. A.; de Heer, W. A. *Science* **2002**, *297*, 787–792.

(18) Trojanowicz, M. *TrAC, Trends Anal. Chem.* **2006**, *25*, 480–489.

(19) Ahammad, A. J. S.; Lee, J.-J.; Rahman, M. A. *Sensors* **2009**, *9*, 2289–2319.

(20) Crespo, G. A.; Macho, S.; Bobacka, J.; Rius, F. X. *Anal. Chem.* **2009**, *81*, 676–681.

(21) Crespo, G. A.; Macho, S.; Rius, F. X. *Anal. Chem.* **2008**, *80*, 1316–1322.

(22) Haber, F.; Klemensiewicz, E. *Z. Phys. Chem.* **1909**, *67*, 385–431.

(23) Bakker, E.; Bühlmann, P.; Pretsch, E. *Talanta* **2004**, *63*, 3–20.

(24) Borchardt, M.; Dumschat, C.; Cammann, K.; Knoll, M. *Sens. Actuators, B* **1995**, *25*, 721–723.

(25) Ghauri, M. S.; Thomas, J. D. *Analyst* **1994**, *119*, 2323–2326.

(26) Merk. *Normal Laboratory Values*; 2011.

(27) Bard, A. J.; Inzelt, G.; Scholz, F. *Electrochemical Dictionary*; Springer: Heidelberg, 2008.

(28) Guilbault, G. G.; Montalvo, J. G. J. *J. Am. Chem. Soc.* **1969**, *91*, 2164–2165.

(29) Perumal, V.; Hashim, U. *J. Econ. Financ. Adm. Sci.* **2013**, *12*, 1–15.

(30) Dungchai, W.; Chailapakul, O.; Henry, C. S. *Anal. Chem.* **2009**, *81*, 5821–5826.

(31) Nie, Z.; Nijhuis, C. A.; Gong, J.; Chen, X.; Kumachev, A.; Martinez, A. W.; Narovlyansky, M.; Whitesides, G. M. *Lab Chip* **2010**, *10*, 477–483.

(32) Nie, Z.; Deiss, F.; Liu, X.; Akbulut, O.; Whitesides, G. M. *Lab Chip* **2010**, *10*, 3163–3169.

(33) Lindner, E.; Gyurcsányi, R. E. *J. Solid State Electrochem.* **2008**, *13*, 51–68.

(34) Fibbioli, M.; Morf, W. E.; Badertscher, M.; de Rooij, N. F.; Pretsch, E. *Electroanal.* **2007**, *12*, 1286–1292.

(35) Lindfors, T. *J. Solid State Electrochem.* **2009**, *13*, 77–89.

(36) Yin, T.; Qin, W. *TrAC, Trends Anal. Chem.* **2013**, *51*, 79–86.

(37) Bakker, E.; Pretsch, E. *Angew. Chem. Int. Ed.* **2007**, *46*, 5660–5668.

(38) Buck, R. P.; Lindner, E. *Pure Appl. Chem.* **1994**, *66*, 2527–2536.

(39) Bakker, E.; Pretsch, E.; Bühlmann, P. *Anal. Chem.* **2000**, *72*, 1127–1133.

UNIVERSITAT ROVIRA I VIRGILI
PAPER-BASED POTENTIOMETRIC PLATAFORMS FOR ESCENTRALISED CHEMICAL ANALYSIS.
Marta Novell Recasens
Dipòsit Legal: T 1462-2015

CHAPTER

3

EXPERIMENTAL PART

UNIVERSITAT ROVIRA I VIRGILI
PAPER-BASED POTENTIOMETRIC PLATAFORMS FOR ESCENTRALISED CHEMICAL ANALYSIS.
Marta Novell Recasens
Dipòsit Legal: T 1462-2015

3.1 Summary

This chapter contains information regarding common materials, procedures and instrumentation that are broadly used during this thesis. It also includes a description and basic information of the techniques most frequently employed for the characterisation of the sensors.

3.2 Reagents

3.2.1 CNTs

Single-wall carbon nanotubes (SWCNTs) of 95 % purity (1–2 nm outer diameter, 5–30 µm length) were purchased from Chengdu Organic Chemicals Co. (Chengdu, Sichuan, China). Multi-wall carbon nanotubes (MWCNTs) of 95 % purity (30–50 nm outer diameter, ~15 µm length) were also purchased from Chengdu Organic Chemicals Co. (Chengdu, Sichuan, China). Both SWCNTs and MWCNTs were used without further purification.

3.2.2 Ion-selective membrane (ISM) components

Ionophores used for each target ion are shown in Table 3.1. All the ionophores were purchased from Sigma-Aldrich.

Table 3.1 Target analyte and corresponding ionophore[1].

Target analyte	Ionophore
Potassium	Valinomycin
Ammonium	Nonactin
Hydrogen	Tridodecylamine
Magnesium	ETH 5506
Sodium	4-tert-Butylcalix[4]arene-tetraacetic acid tetraethyl ester
Calcium	ETH 5234
Lithium	6,6-Dibenzyl-14-crown-4

Lipophilic ion-exchangers. Potassium tetrakis (4-chlorophenyl) borate (KTClPB) with > 98 % purity and sodium tetrakis[3,5-bis(trifluoromethyl)phenyl]borate (NaTFPB) with > 98 % purity and lithium tetrakis(pentafluorophenyl)borate ethyl etherate were acquired from Sigma-Aldrich.

Other components. Bis(2-ethylhexyl)sebacate (DOS) with > 97 % purity, [12-(4-ethylphenyl)dodecyl] 2-nitrophenyl ether (ETH 8045) with > 95 % purity, 2-nitrophenyl octyl ether (NPOE) with > 99 % purity, trioctylphosphine oxide (TOPO), high molecular weight polyvinyl chloride (PVC), silver nitrate, poly(3-octylthiphene) (POT), 3,4-Ethylenedioxythiophene (EDOT), tetradodecylammonium tetrakis(4-chlorophenyl) borate (ETH 500), methyl methacrylate (MMA), n-decyl methacrylate (DMA), tetrahydrofuran (THF) and anhydrous methanol with 99.8 % purity were all purchased from Sigma-Aldrich. $Co(phen)_3(TPFPB)_2$ and $Co(phen)_3(TPFPB)_3$ were synthesized from $[Co(phen)_3](ClO_4)_2$ and $[Co(phen)_3](ClO_4)_3.3H_2O$ respectively[2], which were obtained from Sigma-Aldrich. Polyvinyl butyral (PVB, B-98) was obtained from Quimidroga S.A. (Barcelona, Spain).

3.2.3 Other reagents

Sodium dodecylbenzenesulfonate (SDBS), Poly(sodium 4-styrenesulfonate) (NaPSS), poly(ethylene-co-acrylic acid) (PEAA) with 15 wt % of acrylic acid, poly(vinyl alcohol) with M_w 89000–98000 (PVAL), chitosan medium molecular weight and 78–85 % deacetylated (CHI), glucose oxidase with 228.253 U/g (GOx), tween 20, albumin from bovine serum (BSA), potassium ferricyanide (III) with > 99.99 % purity and potassium ferrocyanide (II) hydrate with > 99.99 % purity were acquired from Sigma-Aldrich.

HIgG (1 mg/ml) and anti-HIgG (1 mg/ml) were obtained from Bethyl Laboratories, Inc.

Analytical-grade chloride salts of ammonium, calcium, lithium, magnesium, potassium, and sodium were purchased from Sigma-Aldrich. Sodium hydrogen

carbonate, potassium hydrogen phosphate, glucose and urea were also purchased from Sigma-Aldrich.

Commercial carbon ink (122-49) was purchased from Creative Materials Inc.

Whatman filter paper nº 5 was purchased from Sigma-Aldrich and a conventional qualitative filter paper (10 cm diameter, 0.01 cm thick paper disk, 10-20 μm fibre thickness) was purchased from Ahlstrom (Barcelona, Spain)

All solutions were prepared using deionized water (18.2 MΩ/cm specific resistance) obtained from Milli-Q PLUS (Millipore Corporation, Bedford, MA; USA).

3.3 Procedures

3.3.1 Membranes preparation

Ion-selective membranes (ISM) were prepared following standard procedures[3–9]. Composition of the membranes in weight % and mmol/kg is shown in Table 3.2.

Table 3.2. ISM composition.

	K^+	NH_4^+	H^+	Ca^{2+}	Mg^{2+}	Na^+	Li^+
Ionophore	2 (18)	1 (13.6)	2 (38.3)	1 (12.5)	1 (9.7)	0.7 (7)	1.5 (39)
KTClPB	0.5 (10)		1 (20.2)	0.3 (6)	0.7 (14)	0.2 (4)	0.5 (10)
PVC	32.8	32.2	33.0	32.9	30	33.0	28.0
DOS	64.7	66.8	65.5				
o-NPOE				65.8		66.1	68.5
ETH 8045					65.3		
TOPO							1.5

All the ISMs were prepared by dissolving 100 mg of the mixture into 1 ml of THF. Membranes with MWCTs were prepared by dissolving 100 mg of the mixture into 1 ml of a solution containing 0.21 wt % of MWCNTs and 5 mg/ml of poly(ethylene-

coacrylic acid)[8] (PEAA). The cocktails were stored at 4 °C and remain stable for about 2 weeks.

The membranes are usually prepared without CNTs, as they are already present in the substrate of the sensor (paper). However, in chapter 7, glassy carbon rods are used for the sensor substrate and CNTs are incorporated on the membrane to avoid complex steps of deposition on the GC.

The reference membrane contains 28 wt % of sodium chloride, 28 wt % of silver nitrate and 44 wt % of PVB. The membrane is prepared by dissolving 178 mg of the mixture in 1 ml of methanol[10].

3.3.2 Pt and gold sputtering

Sputtering of gold and platinum was performed using an ATC Orion 8-HV (AJA International, Inc. MA, U.S.A.) at 200 W, 3 mTorr and magnetron DC sputtering. Both gold and platinum targets have a purity of 99.99 %.

3.3.3 CNT-ink preparation and generation of a CNT conductive paper

The carbon nanotube ink (CNT-ink) was prepared by adding 3 mg/ml of SWCNTs to a 10 mg/ml sodium dodecylbenzenesulfonate (SDBS) aqueous solution, as reported by Cui *et al*.[11] The solution was sonicated using a tip sonicator (Ultrasonic processor UP200S, Hielscher Ultrasonics Gmbh, Teltow, Germany) for two hours (100 W, frequency of 24 kHz, 60 % of amplitude and a cycle of 0.5 s).

To generate the conductive paper, a conventional qualitative filter paper (10 cm diameter, 0.01 cm thick paper disk, 10-20 μm fibre thickness) purchased from Ahlstrom (Barcelona, Spain) was used as initial substrate. The conductive paper is made by painting it with the CNT-ink using a conventional paintbrush. Then the paper was dried, washed and dried again. This process is considered one cycle, and was repeated until the resistance of the dried paper reaches a stable value, usually around 500 Ω/cm^2 –which usually takes 5 to 6 cycles-. All this process is explained in more detail in Chapter 4.

3.4 Characterisation

3.4.1 Microscopic characterisation

Scanning Electron Microscopy (SEM) (JEOL 6400, Japan) was used to characterise the CNTs deposition over the paper substrate. Environmental Scanning Electron Microscopy (ESEM) (FEI Quanta 600, USA) was used for the surface characterisation of CNT and Pt papers. The thickness of the polymeric membranes deposited over paper was also checked with ESEM by cutting the paper for the middle of the membrane. Prior to cut the membrane, the electrodes were frozen with liquid nitrogen and then cut with a sharp cutter.

3.4.2 Electrochemical characterisation

Potentiometric measurements

Electromotive force (EMF) was measured with a high input impedance (10^{15} Ω) EMF16 multichannel data acquisition device (Lawson Laboratories, Inc. Malvern) at room temperature (22 °C) in a stirred distilled water solution without any ionic strength adjuster. A double junction Ag/AgCl/KCl 3 M reference electrode (type 6.0726.100, Methrom AG) containing a 1 M LiAc electrode bridge was used. The working electrode was either a GC rod or a paper electrode. The EMF values were corrected using the Henderson equation for the liquid-junction potential and the activity coefficients calculated by the Debye−Hückel approximation.

Electrochemical Impedance Spectroscopy (EIS)

Electrochemical impedance spectroscopy (EIS) measurements were performed using a potentiostat/galvanostat Autolab PGSTAT128N with a frequency response analyser electrochemical impedance module (FRA2) (AUTOLAB, Eco Chemie, B.V., Utrecht, The Netherlands) fitted with a three electrode electrochemical cell. The paper or glassy carbon electrode was used as the working electrode, a glassy carbon rod with a diameter of 3 mm as the counter electrode, and a Ag/AgCl/KCl

3 M (type 6.0733.100, Methrom AG) single junction electrode as the reference electrode.

Working principles

Electrical resistance is a measurement of how much an object or material opposes the passage of electrons, and is expressed by the well-knowns Ohm's law. However, its use is limited to only one circuit element, the ideal resistor, which accomplish the following requirements: (a) it follows Ohm's Law at all current and voltage levels, (b) its resistance value is independent of frequency and (c) alternating current (AC) and voltage signals through a resistor are in phase with each other. Nevertheless, the real world contains circuit elements that exhibit much more complex behaviour. These elements requires introducing the notion of impedance (*Z*), which is also a measure of the ability of a circuit to resist the flow of electrical current, but unlike resistance, it is not limited by the simplifying properties listed above.

Electrochemical impedance is measured by applying an AC potential to an electrochemical cell and then measuring the current through the cell. The potential applied can be written as:

$$E_t = E_0 \sin(\omega t) \qquad \textit{Equation 3.1}$$

where E_t is the potential at time t, E_0 is the amplitude of the signal, and ω is the radial frequency –which relation with the frequency is expressed as $\omega=2\pi f$-. The current response, I_t, measured in the system is shifted in phase, Φ, and has a different amplitude, I_0:

$$I_t = I_0 \sin(\omega t + \Phi) \qquad \textit{Equation 3.2}$$

Following an analogous expression to Ohm's Law, the impedance of the system can be calculated as:

$$Z = \frac{E_t}{I_t} = \frac{E_0 \sin(\omega t)}{I_0 \sin(\omega t + \Phi)} = Z_0 \frac{\sin(\omega t)}{\sin(\omega t + \Phi)} \qquad \textit{Equation 3.3}$$

The impedance is therefore expressed in terms of a magnitude, Z_0, and a phase shift, Φ. But with Eulers relationship:

$$e^{j\emptyset} = \cos\emptyset + j\sin\emptyset \qquad \textit{Equation 3.4}$$

the impedance can be expressed as a complex number:

$$Z(\omega) = \frac{\mathrm{E}}{I} = \mathrm{Z}_0 e^{j\emptyset} = Z_0(\cos\emptyset + j\sin\emptyset) \qquad \textit{Equation 3.5}$$

Various coordinates can be used for the graphical representation of the impedance, but in this thesis the Nyquist plot (see Figure 3.1) will be the preferred choice.

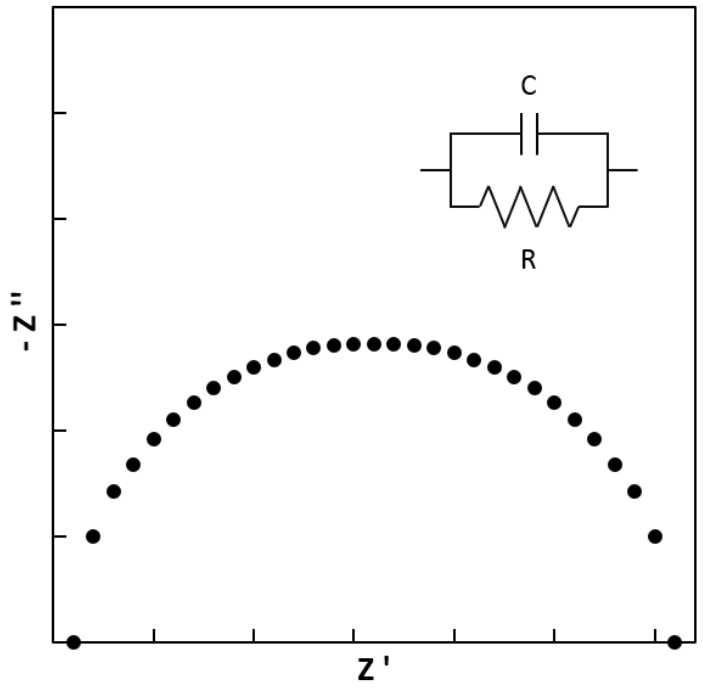

Figure 3.1. Typical Nyquist plot for a circuit with a resistor and a capacitor in parallel.

The expression for Z(ω) is composed of a real and an imaginary part. If the real part is plotted on the X-axis and the imaginary part is plotted on the Y-axis of a chart, the result is a Nyquist Plot, where each point on corresponds to the impedance at one frequency. Low frequency data are on the right side of the plot and higher frequencies are on the left. Under this view, the notion of resistance becomes a particular case of the measurement of impedance (when the imaginary component equals zero).

The interpretation of the data can be performed by comparison with predictions of theoretical models or with an equivalent circuit. The second one will be the employed on this thesis. The electrical circuit is determined from the best fitting of the theoretically calculated plots for this circuit with the ones obtained experimentally. The analysis is done for each set of data measured for different values of external parameters –such as temperature, concentration, etc.- and the equivalent circuit is considered appropriate when the parameters of the elements of the circuit show the expected dependences on the external parameters[12,13]. Figure 3.2 shows some examples of Nyquist plots obtained with their respective equivalent circuits. When an electrical conductor is put in contact with a solution, the resulting equivalent circuit is the one of Figure 3.2 A, where the resistance of the solution is in parallel with a capacitor generated in the interface solution-conductor. The typical Nyquist plot obtained for a SC-ISE is displayed in Figure 3.2 D, R_1 is the solution resistance, R_2 is the resistance of the membrane, C is the capacitor generated in the interface solution-membrane and W is the Warburg impedance, associated with the diffusion through the bulk of the membrane[14].

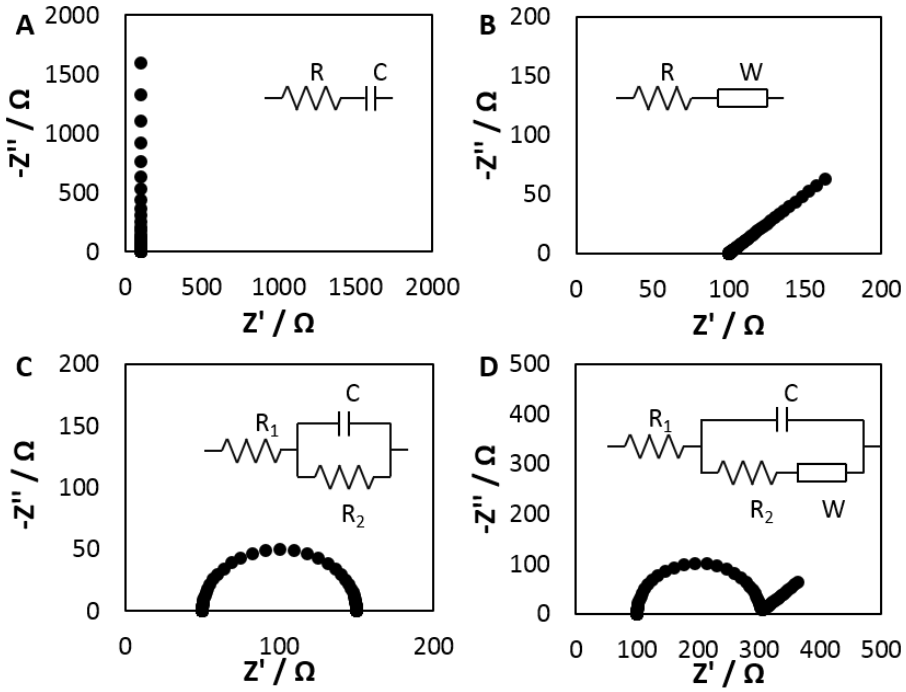

Figure 3.2. Examples of Nyquist plots obtained for the EIS of the circuits inside each plot.

Cyclic Voltammetry (CV)

Cyclic voltammograms were recorded using the same instrument and configuration than EIS spectra.

Working principle

CV measures the current response of an electrode to linearly increasing and decreasing potential cycles. The potential is scanned with a fixed scan rate. The initial potential is set to a potential where no electrode process occurs. The oxidation of an electroactive compound present in the solution at a certain potential produces an anodic current peak, and at the reverse scan it gets reduced producing a cathodic current peak. During the oxidation and reduction, electrons are transferred to the electrode producing the peaks in current (see Figure 3.3). The magnitude of this peaks for a reversible electron transfer is given by the Randles-Sevcik equation[14]:

$$I_p = 0.446nFAc\sqrt{\frac{nFvD}{R"T}} \qquad \textit{Equation 3.6}$$

Where the peak current, I_p, is dependent on *n* (the number of electrons transferred per molecule diffusing to the electrode surface); *F* is the Faraday constant; *A* is the electrode area; *c* is the concentration of analyte in solution; *v* is the scan rate; *D* is the diffusion coefficient; *R"* is the universal gas constant and *T* is the absolute temperature.

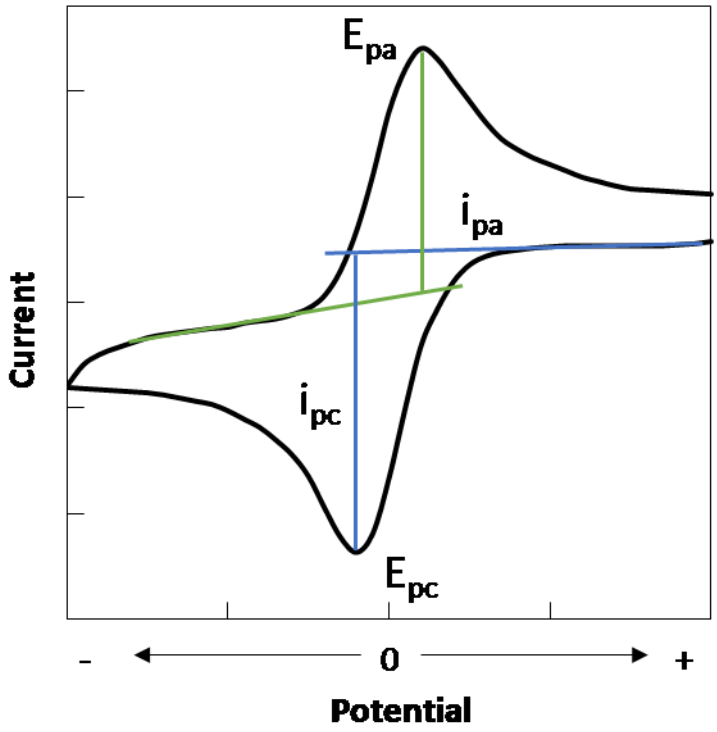

Figure 3.3. Typical CV spectra of a redox couple. Where i_{pa} and i_{pc} are the intensities of the anodic and cathodic peaks respectively and E_{pa} and E_{pc} the potential corresponding to the anodic and cathodic peaks respectively.

This technique can provide information about the potential at which the oxidation or reduction process occurs, the oxidation state of the redox species, the number of electrons involved, the rate of the electron transfer, adsorption effects, etc. In

this thesis is mainly used to provide information about the electrode surface and the electron-transfer process.

3.5 References

(1) Bühlmann, P.; Pretsch, E.; Bakker, E. *Chem. Rev.* **1998**, *98*, 1593–1688.

(2) Zou, X. U.; Cheong, J. H.; Taitt, B. J.; Bühlmann, P. *Anal .Chem.* **2013**, *85*, 9350–9355.

(3) Borchardt, M.; Dumschat, C.; Cammann, K.; Knoll, M. *Sens. Actuators, B* **1995**, *25*, 721–723.

(4) Ghauri, M. S.; Thomas, J. D. *Analyst* **1994**, *119*, 2323–2326.

(5) Oesch, U.; Brzozka, Z.; Xu, A.; Rusterholz, B.; Suter, G.; Pham, H. V.; Welti, D.; Ammann, D.; Pretsch, E.; Simon, W. *Anal. Chem.* **1986**, *58*, 2285–2289.

(6) O'Donnell, J.; Li, H.; Rusterholz, B.; Pedrazza, U.; Simon, W. *Anal. Chim. Acta* **1993**, *281*, 129–134.

(7) Coldur, F.; Andac, M. *Sens. Lett.* **2011**, *9*, 1738–1744.

(8) Zhu, J.; Li, X.; Qin, Y.; Zhang, Y. *Sens. Actuators, B* **2010**, *148*, 166–172.

(9) Cadogan, A. M.; Diamond, D.; Smyth, M. R.; Deasy, M.; Mckervey, M. A.; Harris, S. J. *Analyst* **1989**, *114*, 1551–1554.

(10) Guinovart, T.; Crespo, G. A.; Rius, F. X.; Andrade, F. J. *Anal. Chim. Acta* **2014**, *821*, 72–80.

(11) Hu, L.; Wu, H.; Cui, Y. *Appl. Phys. Lett.* **2010**, *96*, 183502.

(12) Lasia, A. In *Modern Aspects Of Electrochemistry*; Springer: New York, 1999; pp 143–248.

(13) Yuan, X.-Z.; Wang, H.; Song, C.; Zhang, J. *Electrochemical impedance spectroscopy in PEM fuel cells*; Springer: London, 2010.

(14) Bard, A. J.; Inzelt, G.; Scholz, F. *Electrochemical Dictionary*; Springer: Heidelberg, 2008.

UNIVERSITAT ROVIRA I VIRGILI
PAPER-BASED POTENTIOMETRIC PLATAFORMS FOR ESCENTRALISED CHEMICAL ANALYSIS.
Marta Novell Recasens
Dipòsit Legal: T 1462-2015

CHAPTER

4

CONDUCTIVE PAPERS

UNIVERSITAT ROVIRA I VIRGILI
PAPER-BASED POTENTIOMETRIC PLATAFORMS FOR ESCENTRALISED CHEMICAL ANALYSIS.
Marta Novell Recasens
Dipòsit Legal: T 1462-2015

4.1 Summary

In this chapter, the development of conductive papers using carbon nanotubes that display ion-to-electron transduction properties is presented. The description of the procedure, the proof of the transduction properties, the advantages of this approach and the comparison with other materials is presented and discussed. These conductive papers are extensively used throughout this thesis to develop potentiometric sensors. Therefore, they are part of the experimental basis of all the next developments.

4.2 Introduction

Electrochemical sensors require a conductive material to act as the substrate of the sensing interface and, as it was explained in a previous chapter, they also require an ion-to-electron transducer. Usually this support is made with a rod of a metallic conductor –gold, platinum and glassy carbon are the most common choices– or a substrate covered with a metallic layer –either by sputtering or screen printing the material[1–3]-. A layer of a conductive polymer or a nanostructured material deposited or attached over the metallic conductor[4,5] is usually employed as the transducer. Evidently, a merging of both roles can be achieved by a single material if this good electronic conductivity and good transduction of the signal is achieved (see Figure 4.1).

It has been already demonstrated that CNTs combine both properties. From one side, CNTs show outstanding electrical conductivity[6]. From the other, it has been shown that they can act as excellent transducers[7] for the potentiometric signal. Therefore if a material can be impregnated with CNTs, it will become a conductive substrate with ion-to-electron transduction properties.

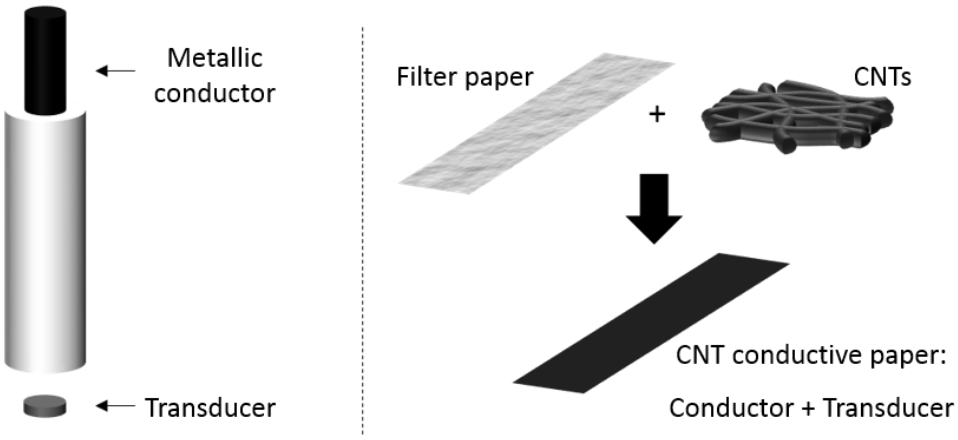

Figure 4.1. Schematic illustration of the merging of the transducer with the conductor.

For many reasons, paper is a good choice as the support material of the sensors. Fortunately, there is also good way in which CNTs can be immobilized onto a cellulose material. It has been shown that if CNTs are dispersed in an aqueous solution, they can be applied through a printing or dying process and remain strongly adsorbed onto the fibres of paper. Unfortunately, CNTs are highly hydrophobic and their suspension in water is not straightforward. To obtain stable aqueous suspensions, a system where the CNT can be dispersed using suitable surfactants or chemical modifications of the nanotubes is required. This system is usually called CNT-ink.

Interestingly, some recent progress in bendable electronics using carbon nanotubes (CNTs) is opening new and attractive avenues in this area. CNTs are well-known for their outstanding electrical and chemical properties, which have been extensively exploited in a plethora of different areas. During the past few years, dispersions of CNTs in aqueous solution have been used to generate conductive papers. CNT-inks can be generated by functionalization of the CNTs (often through oxidation by acid treatment to generate carboxyl groups)[8] or by the use of surfactants[9]. Surfactant-based inks, particularly using sodium dodecylbenzenesulfonate (SDBS), offer better electrical conductivity due to the higher weight fraction of CNTs that can be

suspended[10]. Furthermore, surfactants attach to the CNTs via non-covalent interactions, thus preserving the conjugated π system of the CNTs and their electrical properties. The mechanism of the dispersion is illustrated in Figure 4.2, the surfactant's hydrophobic segment adsorbs into the CNTs, while the hydrophilic segment associates with the water, thus allowing the dispersion of the CNTs[10].

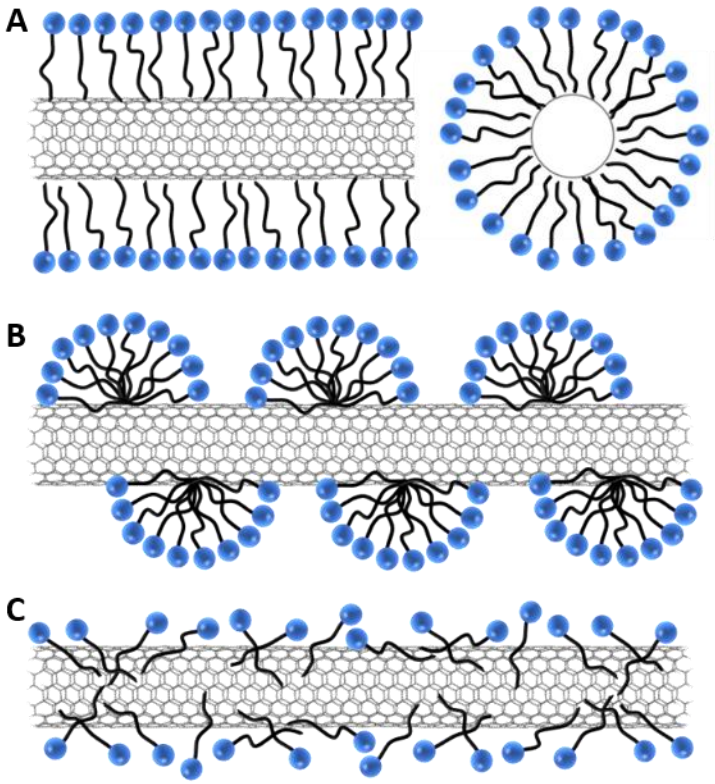

Figure 4.2. Schematic representations of models by which surfactants help disperse SWNTs: A) SWNT encapsulated in a cylindrical surfactant micelle (side view and cross section), B) Hemi micellar adsorption of surfactant molecules on a SWNT and C) Random adsorption of surfactant molecules on a SWNT[11].

Using CNT-inks several groups have produced conductive papers using different technologies. Kordas *et al.*[12] printed a wide range of electrical circuits on a paper using a conventional inkjet printer. Hu *et al.*[13,14] developed paper-based capacitors

using CNT-inks. Remarkably, it has been shown that CNT printed papers present enhanced charge-storage capacity and ability to withstand mechanical work (such as folding or bending) better than metal coated paper. Indeed, because of the strong absorption onto the cellulose fibre, the CNT-conductive paper is in reality a 3D network of conductive fibres, not just a 2D conductive layer. Thus, CNT-conductive papers do not represent simply a replacement but a significant improvement of metal coated papers.

There are several ways to make conductive papers. The most popular are inkjet printing, screen-printing and roll-to-roll printing[15] (see Figure 4.3). Inkjet printing is one of the most versatile methods, since it is rapid and allows high precision, resolution and reproducibility. However, the development of an ink for this approach is not easy, since adjusting the viscosity and surface tension of the ink -critical parameters- usually requires addition of other compounds. Moreover, for printing over paper, the use of already treated papers such as photo paper[16] or coated papers[17] is usually needed to achieve a good printing. Regarding screen-printing, is very robust, simple and has low cost for mass production, there is no other technique as fast and scalable reported to date. However, it requires a screen stencil and produces a film over the material, thus it is hard to make all the paper conductive, just one side. Finally, roll-to-roll process is also fast and reproducible, however low resolutions are obtained and will probably not lead to a whole conductive material if applied to paper, just producing one conductive layer. All in all, inks for direct-printing have less stringent requirements than those for inkjet printing, the dyeing of the paper will result in a whole impregnated material, and the dying process has an unrivalled simplicity.

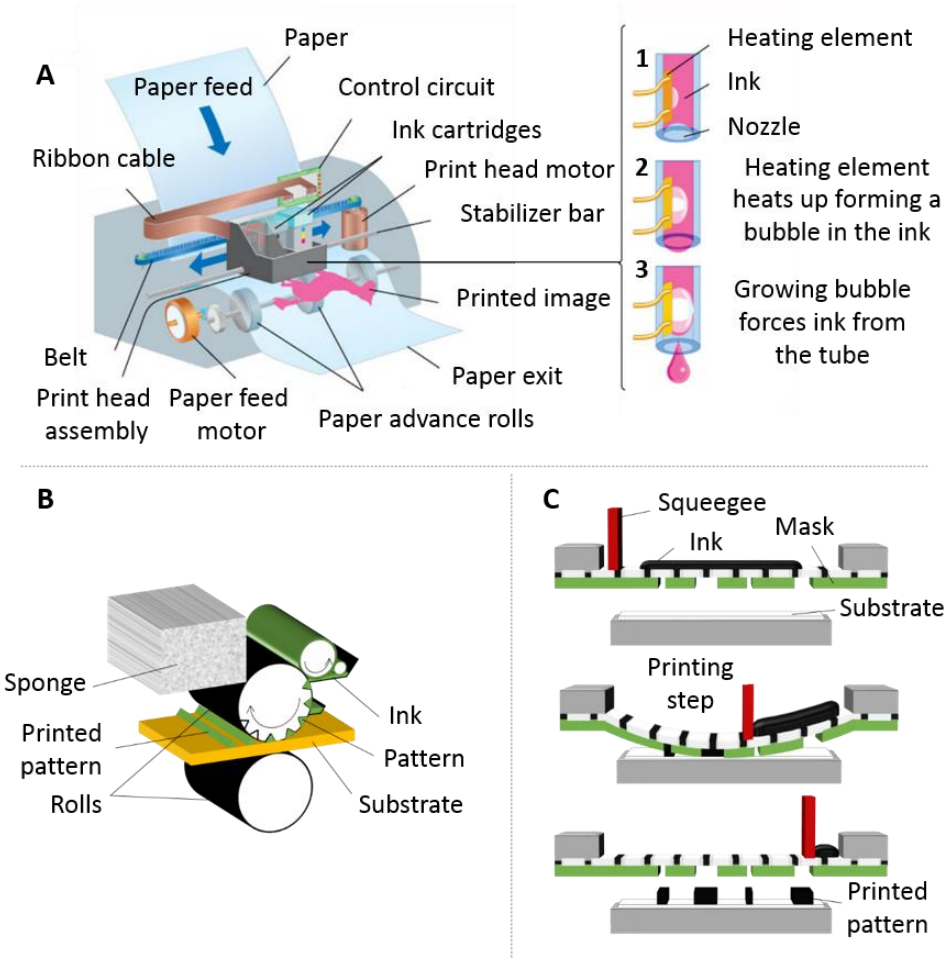

Figure 4.3. Printing techniques: A) Inkjet printing[18], B) Roll-to-roll printing and C) Screen-printing.

This chapter introduces a new methodology to obtain conductive papers through its painting with CNT-ink, and shows the ability of this platform to act as ion-to-electron transducer. A comparison of the advantages of this approach such as the mechanical stability and electric properties, between these CNT-papers and Pt-coated papers is also presented and discussed.

4.3 Experimental part

4.3.1 CNT-ink preparation

The carbon nanotube ink (CNT-ink) was prepared by adding SWCNTs to a 10 mg/ml sodium dodecylbenzenesulfonate (SDBS) aqueous solution, as reported by Cui *et al*.[13] A concentration of 3 mg/ml of SWCNTs was used since it gives optimum ink stability and adherence to the paper. SWCNTs were successfully dispersed using a tip sonicator (Ultrasonic processor UP200S, Hielscher Ultrasonics Gmbh, Teltow, Germany) for two hours (100 W, frequency of 24 kHz, 60 % of amplitude and a cycle of 0.5 s). To avoid overheating and undesirable secondary reactions, the bath was always kept at 4 ºC during the sonication. The CNT-ink, which shows a density of 0.99 g/L, was stored on a fridge at 6 ^{o}C to avoid destabilization. Under these conditions it has been observed that the CNT dispersion can be used for at least three months.

CNTs ink was choose for our purpose because paper absorbs solvents easily and binds with CNTs strongly. Furthermore, the rheology of the paper –different from other substrates, such as glass or plastic– does not demand many requirements for the ink viscosity or surface tension, thus avoiding the need of additives[14].

4.3.2 Generation of CNT-conductive papers

A conventional qualitative filter paper (10 cm diameter, 0.01 cm thick paper disk, 10-20 μm fibre thickness) purchased from Ahlstrom (Barcelona, Spain) was used as initial substrate. The conductive paper was made by painting a 7 cm side square with the CNT-ink using a conventional paintbrush. The ink is readily absorbed by the paper and, after the water evaporates (usually a few minutes), the paper is thoroughly rinsed with water. Some bubbles are observed during the rinsing process showing that -to some extent- the excess of surfactant is being washed out (there is still some controversy on whether this step is really needed[14]). After the rinsing, the paper is dried at room temperature or -to speed up the process-, it can

be placed in an oven at 60 °C for about 5 minutes. At this point the resistance is checked for optimization purposes with a four-point probe. This process of painting, drying, washing out the surfactant and re-drying is considered one cycle. The cycles are repeated until the resistance of the dried paper reaches a stable value, usually around 500 Ω/cm^2. The process is illustrated in Figure 4.4.

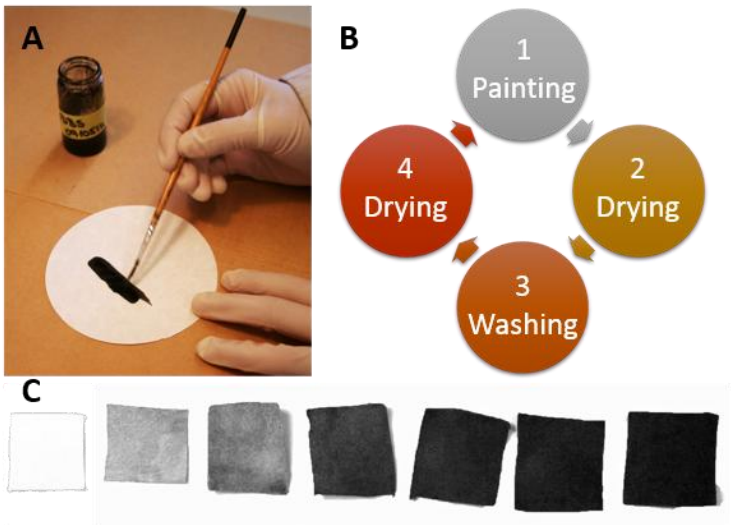

Figure 4.4. Schematic representation of the process: A) Paper painting, B) Steps of one painting cycle and C) Pictures of real paper at increasing painting cycles (from 0 to 6).

A thorough washing of the final paper is done in order to further reduce the amount of SDBS and obtain superhydrophobic CNT-papers. This washing consists on immersing the paper in water for three days, changing the water every 12 hours.

4.3.3 Generation of platinum conductive papers

For this approach, the same conventional filter papers were used. In this case, platinum is sputtered onto the paper using a glow discharge source at low pressure. The process is continued until a final layer of platinum of approximately 50 nm is obtained. The final resistance of the paper (on the Pt layer side) is about 60 Ω/cm^2.

4.3.4 Characterisation of the papers

CNT-conductive papers were characterised using electrochemical impedance spectroscopy (EIS) and cyclic voltammetry (CV). For the characterisation, the CNT-conductive paper was cut into strips of 0.5 cm x 2 cm and partially covered with plastic masks of 1 cm x 1.5 cm on both sides to avoid the contact of the nanotubes with the solution. Therefore, the masks leave one of the ends of the CNT conducting paper uncovered, allowing the electrical contact with the instrument. One of the masks has a circular orifice with an area of 6.2 mm^2 so the area of SWCNT-paper in direct contact with the solution is always the same for all the tested electrodes. In order to avoid that the capillarity of the paper ends up wetting it all and therefore water reaching the contact with the instrument –which will lead to erratic results-, commercial cyanoacrylate adhesive –sold under the brand name of "Superglue"- is applied in between, as showed in Figure 4.5. Tests in the laboratory have shown that the glue stops the capillarity while not affecting the conductivity.

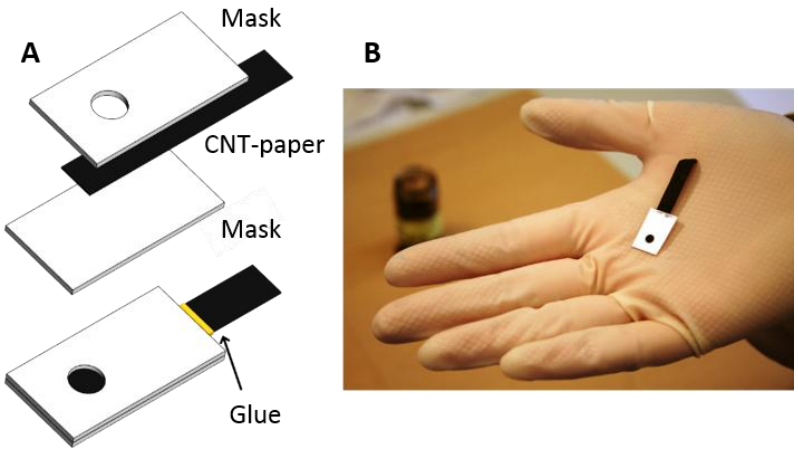

Figure 4.5. A) Scheme of the assembling of the paper for the measurements and B) real image. The masks are auto-adhesive so no glue is necessary to attach them to the paper. However, some glue needs to be added at some point of the paper to avoid the water going up for capillarity and getting in contact with the reading instrument –which will produce erratic results-.

CV measurements were all performed in a solution of 0.1 M KCl as background electrolyte, with or without the presence of $K_3Fe(CN)_6/K_4Fe(CN)_6$ redox couple at different concentrations and different scan rates, but using a constant step potential of 5 mV. Five cycles were always recorded and the 5^{th} is the one display in the figures. EIS spectra were recorded in the frequency range between 0.01 Hz to 100000 Hz, with amplitude of 10 mV, and varying the concentration of the solution and the potential. For both techniques, nitrogen was bubbled into a 0.1 M KCl solution for 30 min to eliminate the oxygen. The stream of nitrogen was stopped during the measurements.

The hydrophobicity of the paper was measured using an automatic video-based optical contact-angle and drop contour analysis system OCA 35 from Dataphysics Instruments. Sessile drop with 2 µl drop was the methodology used and the contact angle was calculated at 47 ms after the drop deposition using an elliptic adjustment with the SCA202 program. The contact angle is used as a measure of the wettability of a solid by a liquid phase. Depending on the contact angle the solids can be classified as hydrophilic, if the contact angle approaches 0^o; hydrophobic, if the contact angle is greater than 90^o; or superhydrophobic, if the contact angle is greater than ~150^o[19].

The bendability of the papers was done in a 180^o angle, where each bends counts for one cycle. After a concrete number of bends, the resistance of the paper is checked using a multimeter by placing the probes in 1 cm distance leaving the bending line in the middle of the electrical path measurement. The procedure is depicted in Figure 4.6Figure *4.6*.

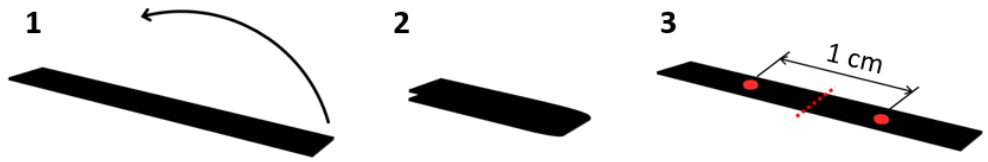

Figure 4.6. Bending procedure: 1. Initial stage; 2. Paper bend at 180^{o} and 3. Measurement of the resistance.

4.4 Results and discussion

4.4.1 Conductive paper

Figure 4.7 shows the result of the conversion of a conventional filter paper into a conductive paper through successive applications of CNT-ink. The initial resistance of the untreated filter paper is extremely high, but it quickly decays with the application of the CNT-ink. Typically, values close to 500 Ω/cm^2 are reached after the 4th-5th cycle. Lower values of electrical resistance can be obtained through further application of the CNT-ink. However, values of a few hundred ohms are considered acceptable taking into account that the paper is intended to be used as the support for an ion-selective electrode and in that system, the overall resistance will be controlled by the resistance of the ion-selective membrane, which is typically one or two orders of magnitude higher[20,21].

The pattern observed in Figure 4.7 is fairly reproducible, so no significant difference is found between the final values of electrical resistance obtained for different papers. These values are also in agreement with those already reported for the generation of CNT conductive papers. Cui *et al.*[14] reported a resistance of 30 Ω/cm^2 using the Meyer rod coating method and one of 300 Ω/cm^2 with the direct pen writing, which is more similar to our methodology. Any comparison, however, is relative, since these authors used Xerox paper, while filter paper has been used for our work.

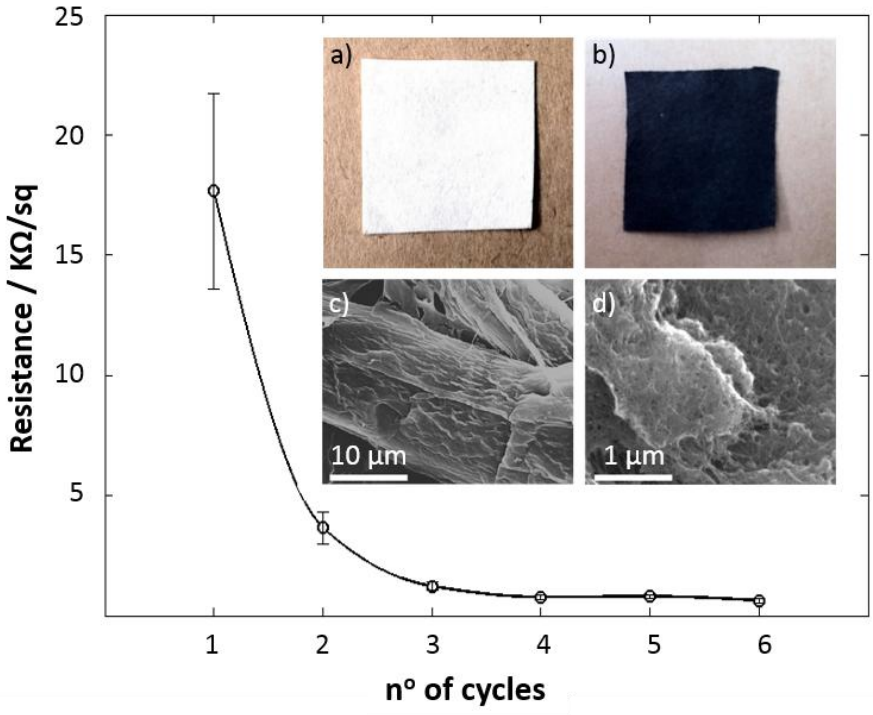

Figure 4.7. Conversion of filter paper into a conductive paper showing the electrical resistance of several filter papers as a function of the number of cycles of CNT-ink: (a) macroscopic image of the filter paper, (b) macroscopic image of conductive paper, (c) SEM image of a filter paper showing the paper fibres and (d) SEM image of filter paper impregnated with CNT-ink.

The role of the surfactant used for the ink on the conductive paper is still a matter of debate. As suggested by Cui *et al.*[14], because of the strong supramolecular interactions between the CNT and the cellulose, the SDBS is rearranged when the CNTs are absorbed onto the paper. These authors reported that there is no significant difference in the conductivity of the paper before and after washing. Some authors have suggested the use of an acid wash as a way to eliminate the surfactant[22]. In our work it is observed that the surfactant is –at least in part- washed during the careful rising of the paper. The leaching of surfactant to the aqueous phase was monitored by absorption spectrophotometry at different times

using either one step or multi washing steps (see additional information of this chapter, Figure A 4.1). The experiment shows that after some rinsing steps SDBS is practically extracted from the paper-CNTs assembly (at least the concentration of SDBS should be lower than 1 µM which is minimum amount that can be determined with this approach). If those rinsing steps are avoided –letting the paper to dry with the surfactant- the value of the electrical resistance obtained is slightly higher, and it can be decreased by proper washing. All in all, if some very low amount of surfactant remains, it seems that it does not seem to produce a significant effect on the resistance, at least for the purpose of this work.

Other type of inks, for example, using different surfactants -such as poly(sodium 4-styrene-sulfonate)- to immobilize CNTs on cellulose have been reported. PSS ink (25 mg/ml of SWCNTs and 50 mg/ml of PSS) was also tested. Nevertheless, this type of ink is very dense and viscous due to the higher molecular weight of the PSS, so its manipulation is more complicated. Following the same methodology here introduced of cycles of painting and washing, the resistance of the paper achieved with SDBS ink is not reached with PSS even after more than 50 cycles. One of the reasons could be that the CNTs show a stronger interaction with the surfactant, thus having more impediments to attach to the cellulose. Therefore, when the paper is being wash, CTNs are washed together with the surfactant. Apparently, using one or another surfactant will not make any difference as the final purpose is to eliminate it. SDBS ink has been used for the rest of the work as it creates a conductive paper with less painting cycles and all the procedure is easier to carry out.

The capillary effects due to the microstructure generated by the cellulose fibre produces a very quick impregnation of the papers with the CNT-ink. The papers acquire a grey-black colour almost instantly, which darkens with successive applications of ink. Figure 4.7 shows an image of the paper before (a) and after (b) the application of the CNT-ink. Apart from the colour change, the conductive paper

does not show any visible sign of the CNT deposition. Scanning electron microscopy images of the untreated (Figure 4.7 c) and CNT covered (Figure 4.7 d) cellulose fibres, show that conductive papers are covered by a widespread a randomly interconnected network of CNT. It is important to stress that CNT-papers form a single system where defined layers are not present. It has been suggested that this structure results from the great stabilization of CNTs on the cellulose fibres by supramolecular interactions, which impedes their detachment when the papers are rinsed with water. This intimate interaction between CNT and cellulose fibres gives conductive CNT-papers a 3D microstructure that is not present in metal covered papers, and that is responsible for two important features. First, the enhanced effective area, which gives good electrical conductivity. This has been exploited for the development of supercapacitors. Second, improved mechanical stability, which allows withstanding bending, folding, etc. without significantly affecting the electrical conductivity[13]. This is a significant advantage when compared to metal-coated papers. It is noteworthy that when the CNT-ink is deposited and dried onto substrates such as glassy carbon or metals, most of the CNT are washed away simply by rinsing with water.

4.4.2 Removal of SDBS: Generation of super-hydrophobic papers

Although no significant amounts of SDBS remain in the CNT-paper with our conventional methodology, it is observed that an additional stronger washing –as described in section 4.3.2- can still decrease the amount of SDBS present in the conductive paper. As it was not possible to monitor the SDBS amount in the washing water, the removal of SDBS was assessed by testing the hydrophobicity of the resulting paper. This hydrophobicity is determined with the measurement of the contact angle between the paper and a drop of water. Clearly, due to the high hydrophobicity of the nanotubes, the conductive paper should be highly hydrophobic. The wettability of the conductive paper may give hints on whether some traces of surfactant remain. As shown in Figure 4.8, there is a clear difference

between the drops of water deposited over the two types of papers. The paper with CNTs –not subjected to an exhaustive washing- is hydrophilic, with a contact angle of $85^{o} \pm 4^{o}$ (n=4), whereas the paper that has been thoroughly washed is almost "superhydrophobic", with a contact angle of $126^{o} \pm 8^{o}$ (n=4). Strictly speaking, only if the contact angle is greater than 150^{o}, the system can be technically considered superhydrophobic. In our case, however, the paper will be referred as superhydrophobic even though it cannot be considered superhydrophobic according to the general classification. As stated in the experimental part, these contact angle measurements were taken at 47 ms, however the drop evolution is also very different in both papers. After 1.5 s the contact angle is around 30^{o} in the first case, while still being higher than 120^{o} in the second, thus confirming the marked different nature of both samples. This can only be explained for the presence of the surfactant, as the substrate and the layers of ink applied are exactly the same. CNTs are a hydrophobic material, but the nature of the final substrate –paper with SWCNTs ink- will be a combination of both materials. Even though most of the SDBS has been washed from the normal paper is evident that not all, and this is why the substrate is still hydrophilic. After applying the harder washing, the substrate become hydrophobic, thus strongly suggesting that more surfactant has been washed out and that CNTs are covering all the cellulose fibres.

This superhydrophobicity of the papers that proves the absence of SDBS is an important feature for the construction of ISEs. It is well known that a hydrophobic material in contact with the membrane will avoid the formation of a water layer[23], which produces instability in the potentiometric signal. In conventional ISEs, surfactant is eliminated through annealing. In the case of these conductive papers annealing cannot be applied, so washing seems the best approach to fully eliminate the surfactant.

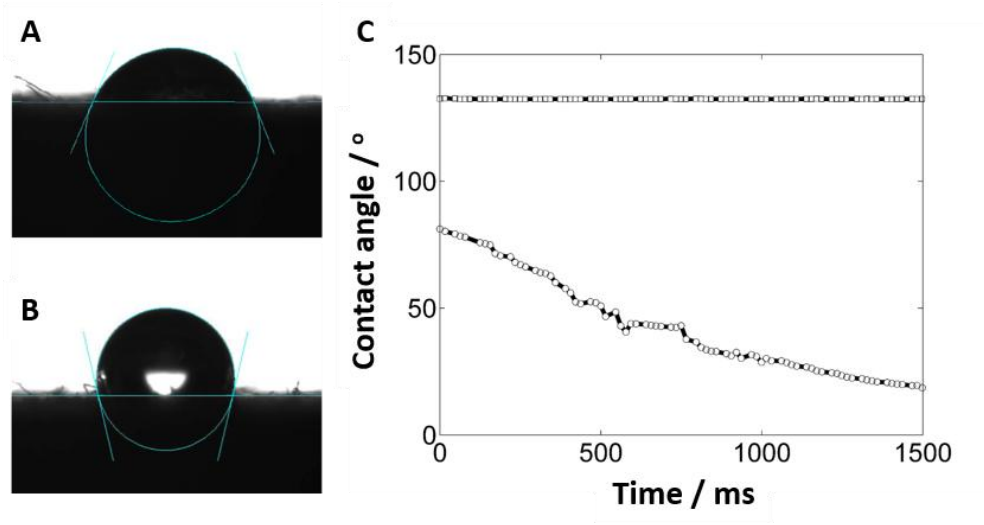

Figure 4.8. Images of the contact angle measurement of (A) CNT-paper and (B) superhydrophobic CNT-paper. (C) Evolution of the contact angle over time for both types of paper: CNT-paper (○) and superhydrophobic CNT-paper (□).

4.4.3 Transduction mechanism of CNT-papers

Carbon nanotubes together with other carbon nanomaterials have been demonstrated to act as good ion-to-electron transducers[7,24]. The main purpose of the development of CNT-papers is their use as the support of ISEs; therefore, the demonstration that CNTs deposited over cellulose through a painting process retain the same ability and performance to act as ion-to-electron transducers is required. The transduction mechanism has been studied using CV and EIS.

Cyclic voltammograms between 0.5 to -0.5 V using a scan rate of 100 mV/s were recorded in the presence and absence of oxygen. The reduction of oxygen occurs in both cases, however, being smaller when a stream of argon had been bubbled into the solution (see Figure A 4.2, in the additional information of this chapter). In any case, this reduction occurs far from the potential value that will be used for the EIS (0.2 V), therefore not affecting those measurements.

The use of the ferri(III)cyanide/ferro(II)cyanide redox couple is widely used to study new electrode surfaces. Cyclic voltammograms with different concentrations of the redox couple –no redox couple, 1, 2, 3, 4 and 5 mM- and different scan rates -20, 50, 100 and 200 mV/s- were recorded. Figure 4.9 (A) shows the cyclic voltammograms of the redox couple at 3 mM concentration obtained by measuring the current during the scan from -0.25 V to 0.75 V at different scan rates.

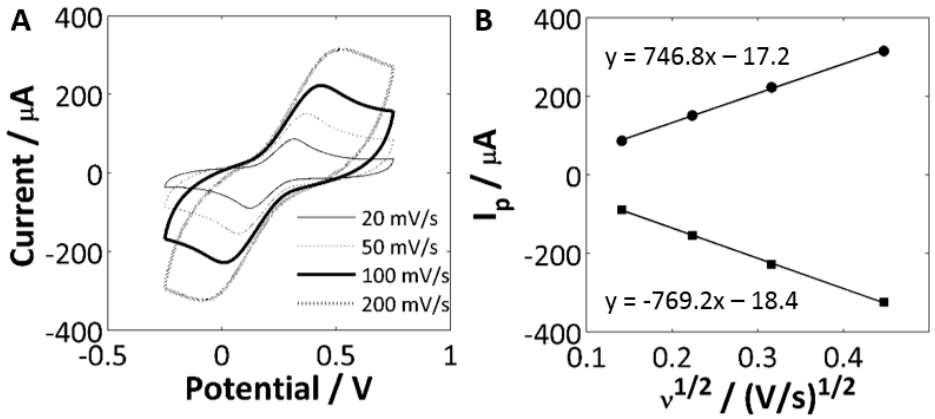

Figure 4.9. (A) Cyclic voltammograms of 3 mM $K_3Fe(CN)_6/K_4Fe(CN)_6$ redox couple in 0.1 M KCl at different scan rates. (B) Variation of the anodic (i_{pa}) and cathodic (i_{pc}) peak currents as function of the square root of the potential scan rate.

As expected, the peak currents increase with the increase of the scan rate, and the magnitude of the peaks is linear with the square root of the potential scan rate (see Figure 4.9 (B). This linearity is typical for a reversible diffusion-controlled reaction and indicative that the reaction is controlled by a semi-infinite linear diffusion[24]. Other parameters of interest extracted from these voltammograms are listed in Table A 4.1 (in the additional information of this chapter). The peak separation is in all the cases much higher than the expected for a one-electron process (59 mV), but this increase may be due to the wettability of the paper –among other factors[25]-.

Electrochemical impedance spectroscopy changing different conditions was used to better understand the system. Spectra were recorded in KCl solutions of 0.1, 0.05 and 0.01 M, with a fixed potential at 0.2 V. The CNT-paper spectra (Figure 4.10) show some deviation from the typical 90° capacitive line obtained for a conductor. At higher frequencies (inset Figure 4.10) this deviation is clearer, as the data can be adjusted to a 45° line, which indicates a lower charge transfer rate. It is also observed that the intersection of the frequency points with the Z' axis depends on the concentration of the ions in the solution, as expected.

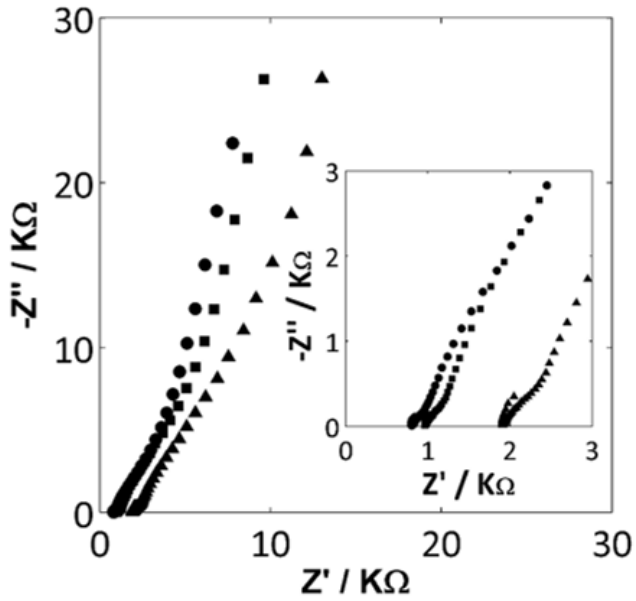

Figure 4.10. Impedance plots for the CNT-paper electrode at different concentrations of KCl: (●) 0.1 M; (■) 0.05 M; and (▲) 0.01 M. The inset shows a magnification of the high frequencies part.

The following equivalent circuit has been proposed to explain the system, and the experimental EIS spectra have been successfully fitted to it. This is the same circuit previously used to describe GC electrodes with a layer of SWCNTs[7] or PEDOT[26] as transducers in aqueous solutions.

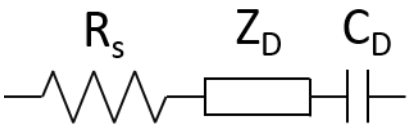

Figure 4.11. Equivalent electrical circuit for the SWCNT-paper. R_s = solution resistance, Z_D = finite-length Warburg diffusion and C_D = bulk capacitance.

Values obtained for these constants are listed in Table 4.1. Evidently, the resistance of the solution is inversely proportional to the concentration of the supporting electrolyte. Although this correlation is clear, the values obtained at the intersection are higher than expected for the resistance of the solution[7], so the CNT-paper itself can be also adding some resistivity to the system. However, attempts to account this resistance and include it in the model were unsatisfactory. Evidently, the system has additional factors that have to be modelled before any calculation can be performed.

Table 4.1. EIS results for the SWCNT-paper electrode obtained by fitting the data to the equivalent circuit shown in Figure 4.11, with a potential of 0.2 V.

[KCl] (M)	R_S (Ω)	Z_D ($Ω/s^{0.5}$)	C_D (mF)
0.01	1692	2878	1.1095
0.05	778	2285	0.9456
0.1	702	1741	1.0569

The influence of the oxygen on the impedance spectra is shown in Figure 4.12. It can be seen that there are no big differences on the spectra for the CNT-paper with and without oxygen, which is in agreement with the voltammograms obtained under the same conditions. The fitting of both spectra to the theoretical model gave capacitance values of 1.06 and 1.02 mF with and without oxygen respectively.

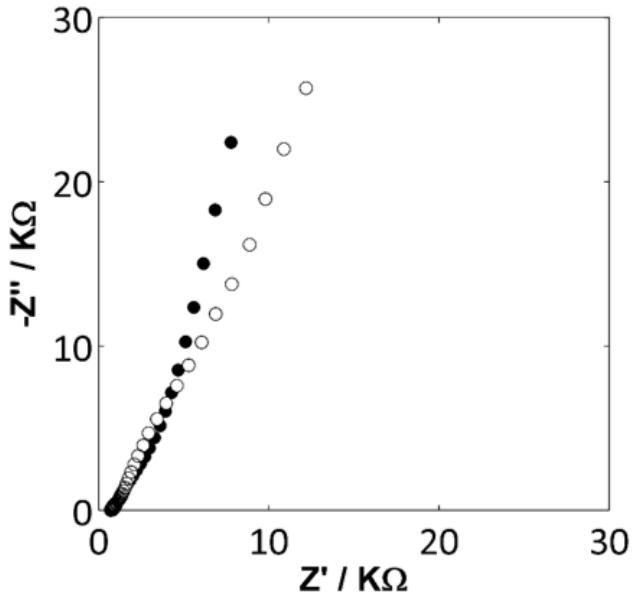

Figure 4.12. Impedance plot of CNT-paper electrode (●) in the presence and (○) absence of oxygen.

For evaluating the effect of the potential, the concentration of the KCl solution was kept constant at 0.1 M and the potential was varied between 0.2, 0 and -0.2 V. The results of this experiment are shown in Figure 4.13. For the CNT-paper there is no much difference between the spectra taken at 0 and 0.2 V, however, the shape of the spectra is very different when it is taken at -0.2 V. It can be seen that at lower frequencies the spectra acquires the shape of a semicircle, indicating a lower charge-transfer rate. This is in agreement with the change in shape observed in the cyclic voltammogram (see Figure A 4.2, in the additional information of this chapter) at this potential. At -0.2 V the peak of the oxygen reduction starts to increase, showing that at this potential the oxygen is affecting the electrode process.

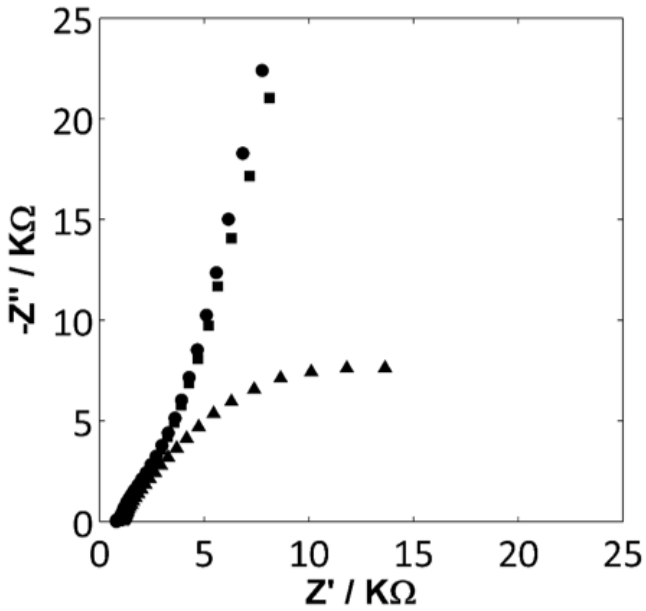

Figure 4.13. Impedance plots for the CNT-paper electrode at (●) 0.2 V; (■) 0 V; and (▲) - 0.2 V

The capacitance obtained for the CNT-papers is very reproducible under different conditions (concentration of background electrolyte and potential) with a value of 1.06 ± 0.8 mF. This value is higher than those reported for CNTs over GC –around 0.45 mF[7]-. When both values are divided by the area of the electrode, the capacitance of the paper electrodes is almost three times higher than it could be expected. It should be stressed, though, that this higher capacitance could be explained by the bigger effective area provided by the paper electrodes due to their 3D structure. While GC have a flat surface, paper is an interweaved network of cellulose fibres, thus providing much higher surface area.

All in all, the results are very comparable to the ones obtained for SWCNTs over a GC surface, thus probing that a new substrate for potentiometric sensors that has similar ion-to-electron transduction ability than conventional metallic electrodes can be developed.

4.4.4 Mechanical tests

Mechanical tests to compare the performance of CNT-papers and Pt-coated papers were carried out. The bendability is an interesting property as it will allow longer lifetime of the sensors and it is an indicator of the ability of the papers to withstand mechanical work. Conducting papers based on CNTs-ink show suitable bendability properties to be used like the substrate of a sensor. Actually, there are not changes in both electrical (resistance) and mechanical properties after bending many times the pieces of papers. In fact, the conductive sheet can be bent as normal – untreated- paper, without being significantly affected the electrical resistance. However, platinum coated papers suffered from a big change in resistance when bended more than 20 times. This difference can be explained by the nature of the papers itself. CNT are all over the filter paper, providing a 3D electrical connection, while Pt coating is just at the superficial part of the paper, actually just a layer of 50 nm is deposited over the paper fibres. Therefore when CNT-papers are subject to bending, some connections between the CNTs will be broken cycle after cycle, but many others will remain due to the interconnection of the CNTs among all the paper, and as it is shown in Figure 4.14, the resistance will slowly increase. However, when bending the Pt paper, the coating may suffer cracks, and when it breaks there is no more connection layer underneath leading to a drastic increase of the resistance. This increase in the electrical resistance due to the breaking of the electrical connection can be observed in Figure 4.14 b and d, where it is clear that CNT-paper has not been very affected, while a clear groove can be seen in the Pt electrode.

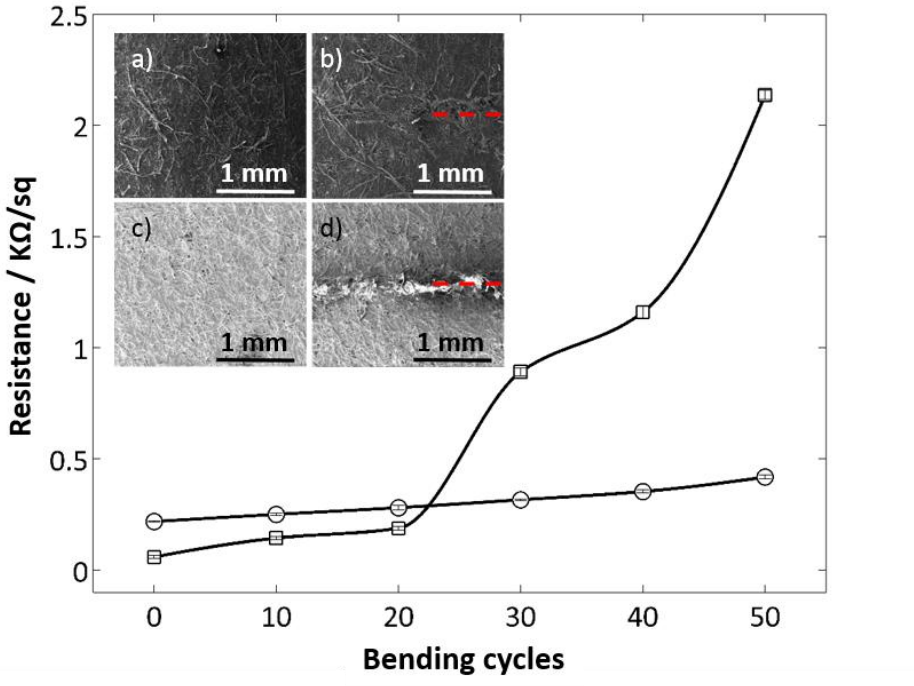

Figure 4.14. Electrical resistance of five CNT and Pt papers as a function of the number of bending cycles, (a) ESEM image of a CNT-paper before bending and (b) ESEM image of a CNT-paper after 50 bends, (c) ESEM image of a Pt-paper before bending and (d) ESEM image of a Pt-paper after 50 bends showing; in red, the bending line.

4.5 Conclusions

A new and extremely simple methodology to convert conventional filter paper into conductive papers by means of a CNT-ink has been introduced. The method allows this conversion in a very few and simple steps, leaving a direct opportunity for scaling up the process. CNT-papers have been proved to maintain the ion-to-electron transduction ability of the CNTs, therefore being excellent candidates for the development of ISEs. These papers have also demonstrated a superior performance in comparison with metal coated papers, showing the ability to withstand mechanical work. All in all, a new and promising platform for the development of potentiometric sensors have been build and characterised.

4.6 Additional information

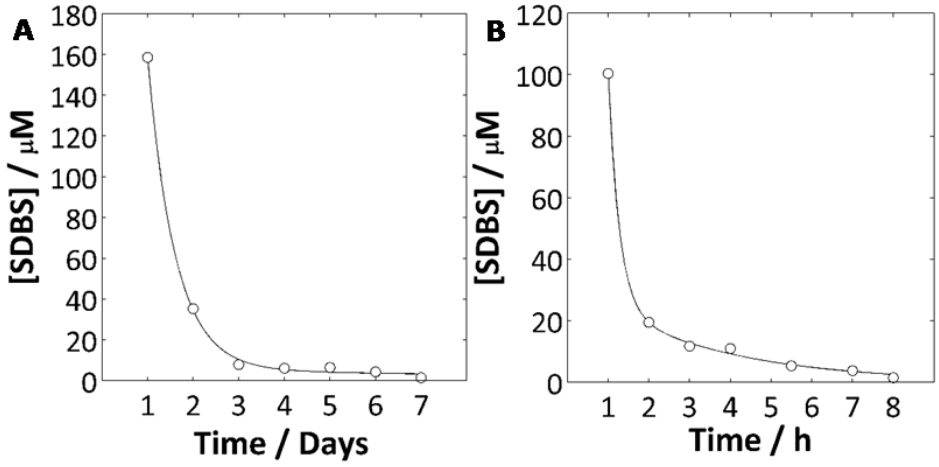

Figure A 4.1. SDBS monitoring experiments. The leaching out of the surfactant to the aqueous phase was evaluated by monitoring the concentration of surfactant in the rinsing water at the final washing step. After the last painting of the paper, this is immersed in 20 ml of distilled water. Then, the water is changed (A) every day and (B) every hour, and the amount of SDBS removed from the paper is quantified by UV absorption spectroscopy.

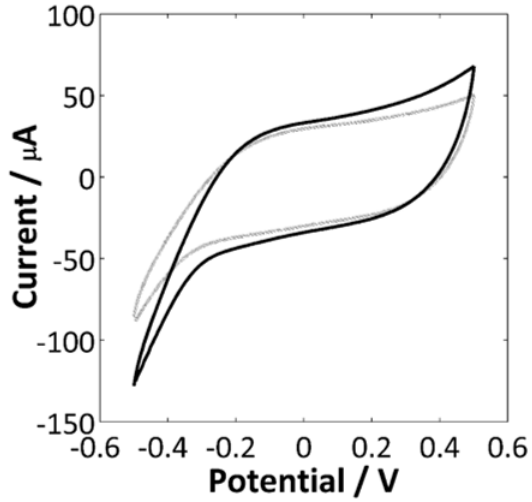

Figure A 4.2. CV for CNT-paper in 0.1 M KCl in the presence (solid line) and absence of oxygen (dashed line).

Table A 4.1. Anodic peak current (i_{pa}), cathodic peak current (i_{pc}), ratio of the peak currents (|ipa/ipc|), anodic peak potential (E_{pa}), cathodic peak potential (E_{pc}), peak separation (ΔEp) and formal reduction potential (E°') obtained from the cyclic voltammograms, measured at different scan rates (v) and analyte concentrations ([xFe(II) + xFe(III)]).

[xFe(II)+xFe(III)] (x mM)	v (mV/s)	i_{pa} (µA)	i_{pc} (µA)	$\lvert i_{pa}/i_{pc} \rvert$	E_{pa} (mV)	E_{pc} (mV)	ΔE_p (mV)	$E^{0'}$ (mV)
0	20	No peaks found						
0	50	No peaks found						
0	100	No peaks found						
0	200	No peaks found						
1	20	44,4	-47,2	0,9	296	143	153	220
1	50	79,6	-82,6	1,0	337	101	236	219
1	100	119,6	-124,0	1,0	399	38	361	219
1	200	178,3	-185,6	1,0	456	-26	482	215
2	20	55,9	-58,2	1,0	300	139	161	220
2	50	100,1	-102,8	1,0	343	95	248	219
2	100	148,0	-152,3	1,0	401	44	357	223
2	200	216,0	-222,7	1,0	496	-61	557	218
3	20	86,2	-89,1	1,0	317	123	194	220
3	50	150,8	-153,7	1,0	371	71	300	221
3	100	222,6	-227,7	1,0	434	10	424	222
3	200	314,5	-323,9	1,0	528	-83	611	223
4	20	116,3	-120,0	1,0	339	101	238	220
4	50	195,6	-199,8	1,0	403	40	363	222
4	100	274,5	-281,4	1,0	468	-26	494	221
4	200	377,2	-391,2	1,0	563	-127	690	218
5	20	162,3	-164,8	1,0	367	79	288	223
5	50	272,0	-276,0	1,0	446	2	444	224
5	100	375,0	-383,8	1,0	520	-75	595	223
5	200	503,2	-524,3	1,0	631	-188	819	222

4.7 References

(1) Fanjul-Bolado, P.; Hernández-Santos, D.; Lamas-Ardisana, P. J.; Martín-Pernía, A.; Costa-García, A. *Electrochim. Acta* **2008**, *53*, 3635–3642.

(2) Rius-Ruiz, F. X.; Crespo, A.; Bejarano-Nosas, D.; Blondeau, P.; Riu, J.; Rius, F. X. *Anal. Chem.* **2011**, *83*, 8810–8815.

(3) Jaworska, E.; Lewandowski, W.; Mieczkowski, J.; Maksymiuk, K.; Michalska, A. *Analyst* **2013**, *138*, 2363–2371.

(4) Privett, B. J.; Shin, J. H.; Schoenfisch, M. H. *Anal. Chem.* **2008**, *80*, 4499–4517.

(5) Tobjörk, D.; Österbacka, R. *Adv. Mater.* **2011**, *23*, 1935–1961.

(6) Ebbesen, T. W., Lezec H. J., Hiura H., Bennett J. W., Ghaemi H. F, T. T. *Nature* **1996**, *382*, 54–56.

(7) Crespo, G. A.; Macho, S.; Bobacka, J.; Rius, F. X. *Anal. Chem.* **2009**, *81*, 676–681.

(8) Dragoman, M.; Dragoman, D.; Ahmad, M. Al; Plana, R.; Flahaut, E. *Nanotechnology* **2009**, *20*, 1–4.

(9) Islam, M. F.; Rojas, E.; Bergey, D. M.; Johnson, A. T.; Yodh, A. G. *Nano Lett.* **2003**, *3*, 269–273.

(10) Blanch, A. J.; Lenehan, C. E.; Quinton, J. S. *J. Phys. Chem. B* **2010**, *114*, 9805–9811.

(11) Yurekli, K.; Mitchell, C. A.; Krishnamoorti, R. *J. Am. Chem. Soc.* **2004**, *126*, 9902–9903.

(12) Kordás, K.; Mustonen, T.; Tóth, G.; Jantunen, H.; Lajunen, M.; Soldano, C.; Talapatra, S.; Kar, S.; Vajtai, R.; Ajayan, P. M. *Small* **2006**, *2*, 1021–1025.

(13) Hu, L.; Wu, H.; Cui, Y. *Appl. Phys. Lett.* **2010**, *96*, 183502.

(14) Hu, L.; Choi, J. W.; Yang, Y.; Jeong, S.; La Mantia, F.; Cui, L. F.; Cui, Y. *PNAS* **2009**, *106*, 21490–21494.

(15) Gonzalez-Macia, L.; Morrin, A.; Smyth, M. R.; Killard, A. J. *Analyst* **2010**, *135*, 845–867.

(16) Mustonen, T.; Kordás, K.; Saukko, S.; Tóth, G.; Penttilä, J. S.; Helistö, P.; Seppä, H.; Jantunen, H. *Phys. Status Solidi B* **2007**, *244*, 4336–4340.

(17) Määttänen, A.; Ihalainen, P.; Pulkkinen, P.; Wang, S.; Tenhu, H.; Peltonen, J. *ACS Appl. Mater. Interfaces* **2012**, *4*, 955–964.

(18) https://yourictclubs.wordpress.com/.

(19) Bard, A. J.; Inzelt, G.; Scholz, F. *Electrochemical Dictionary*; Springer: Heidelberg, 2008.

(20) Crespo, G. A.; Macho, S.; Rius, F. X. *Anal. Chem.* **2008**, *80*, 1316–1322.

(21) Parra, E. J.; Blondeau, P.; Crespo, G. A.; Rius, F. X. *Chem. Commun.* **2011**, *47*, 2438–2440.

(22) Geng, H.-Z.; Kim, K. K.; So, K. P.; Lee, Y. S.; Chang, Y.; Lee, Y. H. *J. Am. Chem. Soc.* **2007**, *129*, 7758–7759.

(23) Michalska, A. *Electroanalysis* **2012**, *24*, 1253–1265.

(24) Tang, L.; Wang, Y.; Li, Y.; Feng, H.; Lu, J.; Li, J. *Adv. Funct. Mater.* **2009**, *19*, 2782–2789.

(25) Kadara, R. O.; Jenkinson, N.; Banks, C. E. *Sens. Actuators, B* **2009**, *138*, 556–562.

(26) Bobacka, J.; Lewenstam, A.; Ivaska, A. *J. Electroanal. Chem.* **2000**, *489*, 17–27.

UNIVERSITAT ROVIRA I VIRGILI
PAPER-BASED POTENTIOMETRIC PLATAFORMS FOR ESCENTRALISED CHEMICAL ANALYSIS.
Marta Novell Recasens
Dipòsit Legal: T 1462-2015

UNIVERSITAT ROVIRA I VIRGILI
PAPER-BASED POTENTIOMETRIC PLATAFORMS FOR ESCENTRALISED CHEMICAL ANALYSIS.
Marta Novell Recasens
Dipòsit Legal: T 1462-2015

CHAPTER

5

DEVELOPMENT OF NOVEL PAPER-BASED POTENTIOMETRIC SENSORS

UNIVERSITAT ROVIRA I VIRGILI
PAPER-BASED POTENTIOMETRIC PLATAFORMS FOR ESCENTRALISED CHEMICAL ANALYSIS.
Marta Novell Recasens
Dipòsit Legal: T 1462-2015

5.1 Summary

This chapter presents the development of potentiometric paper sensors, a new approach to low-cost decentralized sensors. Ion-selective electrodes are constructed over the CNT-paper presented in the previous chapter. The analytical performance of these electrodes is presented and advantages and limitations compared to traditional ion-selective electrodes are discussed.

5.2 Introduction

As mentioned in the introduction, having access to robust, rugged, and low-cost chemical sensors is becoming of paramount importance in a growing number of situations. There are well established needs, such as diagnostic tools for poor regions of the planet[1]. Additionally, the development of chemical sensing networks[2,3] and the increasing role of approaches such as point of care[4–6] and telemedicine[7,8] are pushing the demand for fast access to bio(chemical) information. The term “vanguard analytical approaches”[9] has been proposed by Valcárcel and co-workers to refer to these new platforms that allow low-cost, rapid, on site chemical analysis.

In these new platforms, traditional performance parameters, such as stability, detection limits, etc., must be balanced with the need for speed, cost, and simplicity. A tool that can succeed to reach the final users must have the expected performance, while solving the problems of costs, skills required for the use and access for the specific users. The four parameters must be simultaneously balanced. Therefore, having an excellent analytical device that is expensive, or a very cheap and simple sensor that is not robust enough, is not an option.

Figure 5.1. User's centred approach for analysis requirements.

Under these new lenses, some techniques, such as potentiometry, are regaining new value. Potentiometry has traditionally displayed an unrivalled simplicity of operation and instrumentation[10]. For this reason, it is still one of the workhorses in clinical laboratories and almost the universal approach to measure pH. Ion-selective electrodes have also become the standard procedure for measuring several ions. Furthermore, the development of solid-contact ion-selective electrodes (SC-ISE) during the last few decades has produced a "silent revolution"[11] that has led to drastic improvements of the limits of detection (LOD), increased range of applications, and simplification of the sensor construction, operation, and maintenance. Recent works have also shown the advantages of miniaturization of the electrodes[12], and the development of electrode arrays[13,14] that could be remotely operated. All in all, potentiometric sensors are ideal "vanguard" tools for the remote, out-of-the-lab generation of chemical information.

Some limitations, such as the cost of the sensors, still remain as a challenge when dealing with large scale applications. Despite being among the most affordable instrumental approaches, current potentiometric sensors are still too expensive for data collection at a large scale. Screen-printed electrodes[15,16] have partially addressed this problem, but the need for lower cost sensors still remains a challenge. The searches for new substrates to build electrodes as well as the use of

mass manufacturing techniques are crucial to further reduce the cost of the sensors. Therefore, our work was focused on the exploration of the merge of recent progress on CNT conductive papers and CNT-based potentiometric sensors, which, to the best of our knowledge, had not been explored when this task began.

In this chapter, the development of solid contact ISEs based on conductive papers is presented. Conductive paper made by impregnation of CNT-inks is used as a substrate in combination with a conventional PVC based ion-selective membrane. As a proof of principle, electrodes for the determination of K^+, NH_4^+, and pH were constructed. The resulting paper electrodes show an analytical performance that is comparable to conventional lab made ISEs, opening the way to simple and cost-effective sensors that can be used outside the laboratory. Some limitations and potential future application of these novel sensors in real life scenarios are discussed.

5.3 Experimental part

5.3.1 Paper ion-selective electrode construction

Paper ISEs are constructed by cutting strips of 0.5 cm × 2 cm of CNT-paper and partially covering them with plastic masks of 1 cm × 1.5 cm on both sides. Details of the electrode components (conductive paper, mask, and membrane) and their assembly are schematically shown in Figure 5.2. When glued together, the two plastic masks sandwich the conductive paper, avoiding any direct contact of the carbon nanotubes with the solution. The front mask has a circular orifice with an area of approximately 6.2 mm^2. With this approach, the mask leaves one of the ends of the CNT conducting paper (approximately 0.5 cm long) exposed to make electrical contact with the reading instrument, while the small orifice in front the mask leaves room for casting the membrane. Finally, a volume of 15 µL of the ion-selective membrane cocktail is drop cast onto the paper (onto the orifice left by the plastic mask), in successively amounts of 5 µl. Ion-selective membranes for all the ions are prepared as described in the experimental part (Chapter 3, Section 3.3.1).

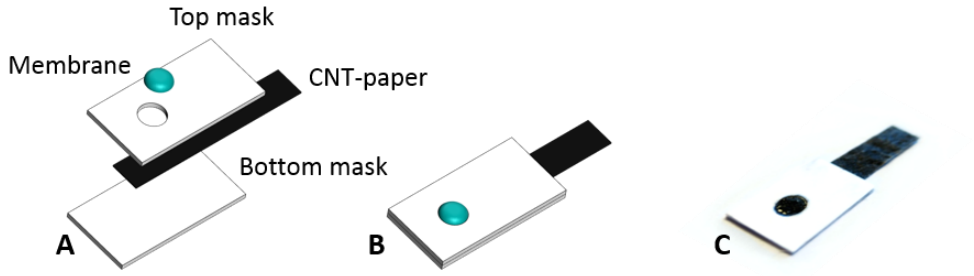

Figure 5.2. A) Scheme of the potentiometric paper-based sensor, B) final sensor view and C) Real image of the sensor.

The membranes usually dry in less than 10 min. The volume of membrane cocktail applied was optimized until maximum (Nernstian) sensitivity was reached. Under optimal conditions, the thickness of the membrane (measured with environmental scanning electron microscopy, ESEM) is approximately 20 µm.

These paper electrodes were used as conventional ion-selective electrodes (assuring that the membrane was always fully immersed into the solution). Electrodes were conditioned in 0.05 M solutions of the primary analyte overnight. Just before using them for the first time, they were preconditioned with a 10^{-4} M solution of the primary analyte for approximately 20 min.

5.3.2 Electrochemical measurements

The paper electrodes are connected to the measuring instrument by means of a small clamp. The membrane is fully covered by the solution but there is no direct contact between the exposed CNT-paper and the solution (see Figure 5.3). The EMF values were corrected using the Henderson equation for the liquid-junction potential and the activity coefficients calculated by the Debye–Hückel approximation. After the measurements, the electrodes were air-dried and stored without using any storage solution. Selectivity coefficients were calculated by the fix interference method (FIM), which is well reported in the literature[17].

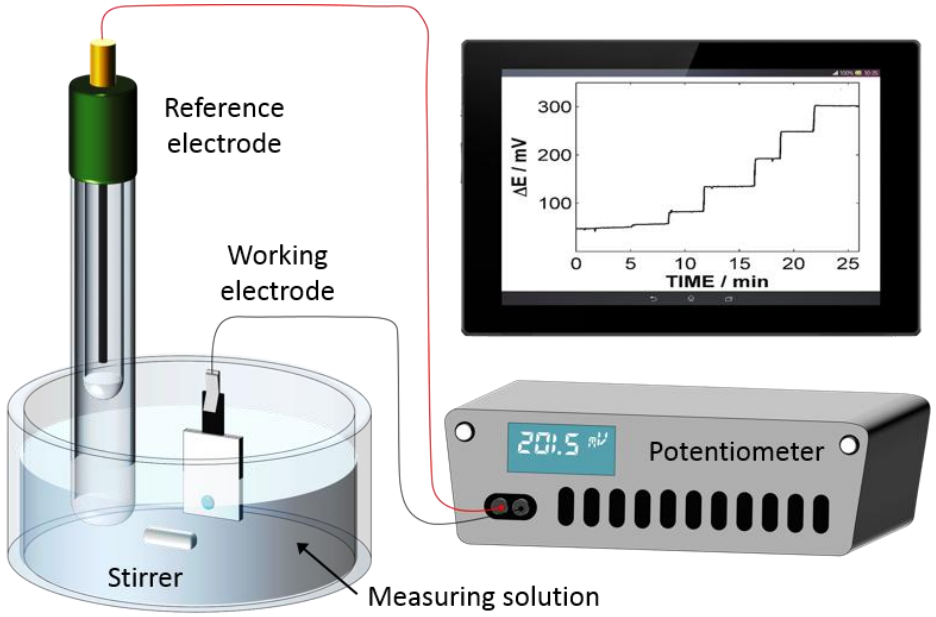

Figure 5.3. Scheme of the working assembly for the potentiometric measurements.

Electrochemical impedance spectroscopy (EIS) measurements were recorded in a frequency range from 100 kHz to 0.01 Hz using an amplitude of excitation of 10 mV in a 0.01 M solution of the target analyte.

5.4 Results and discussion

5.4.1 Paper ISEs analytical performance

Paper-based ion-selective electrodes for three target species, namely, K^+, NH_4^+, and H^+, were prepared and individually tested. Figure 5.4 shows the time trace of the potentiometric response for the three paper SC-ISEs when the activity of the primary analyte is increased. The corresponding calibration plots for each one of the analytes (Figure 5.4) show a Nernstian response from 10^{-5} to 10^{-1} M indicating that the membrane is working as expected. In all cases, error bars cannot be seen in the calibration plots due to the scale. The standard deviation of a single, continuous measurement is well below 1 mV, as with conventional glassy carbon CNT ISE. The reproducibility of several repeated measurements of the same

solution with the same electrode is close to 1 mV. Furthermore, since the slopes are fairly reproducible (1–2 % RSD), the largest source of variability between sensors arises from the "E^0" value (*i.e.* intercept of the calibration plot). Typically, a series of electrodes will show intercepts that will not differ in more than a few millivolts, although it is found that eventually one electrode may show values that differ from the others in as much as 30 mV (while the slope remains Nernstian), thus increasing the uncertainty of this value. The observed intercept value is a function of the individual interface potential between the paper/CNTs layer, CNTs layer/ion-selective membrane, and the rest of the constant potentials along the potentiometric cell (see equations 5.1–5.4 in the section 5.6 additional information of this chapter). It is evident that those potentials will depend intrinsically on the construction of the electrodes (amount of CNTs, homogeneity of CNT-layers, membrane, and CNT-layer thickness, etc). This variability in the intercept indicates that there are some factors in the construction procedure of the electrodes that are not totally under control. However as with many other solid contact ion-selective electrodes manually prepared[18,19] the variability on the intercept values is in the same order of magnitude. Recently, several ways to improve this electrode-to-electrode reproducibility have been reported[20–22]. They are based on the control of the phase-boundary potential at the interface between the conductor and the ISM by controlling the redox capacity of this interface. The implementation of these strategies on paper-ISEs will be presented and discussed in further detail in Chapter 8. In any case, after the intercept has been corrected by proper calibration, the calibration plots overlap well enough so that the error bars cannot be easily seen. Calibration is always necessary since, as it was mentioned before, changes over time occur when electrodes are used intensively (see Figure A 5.1 in the additional information of this chapter). It should be expected that improvements on the electrode manufacturing approach, especially the membrane deposition, will help in the future to overcome this issue. In any case, the results show that the CNT-paper-based electrodes emulate conventional ion-selective electrodes.

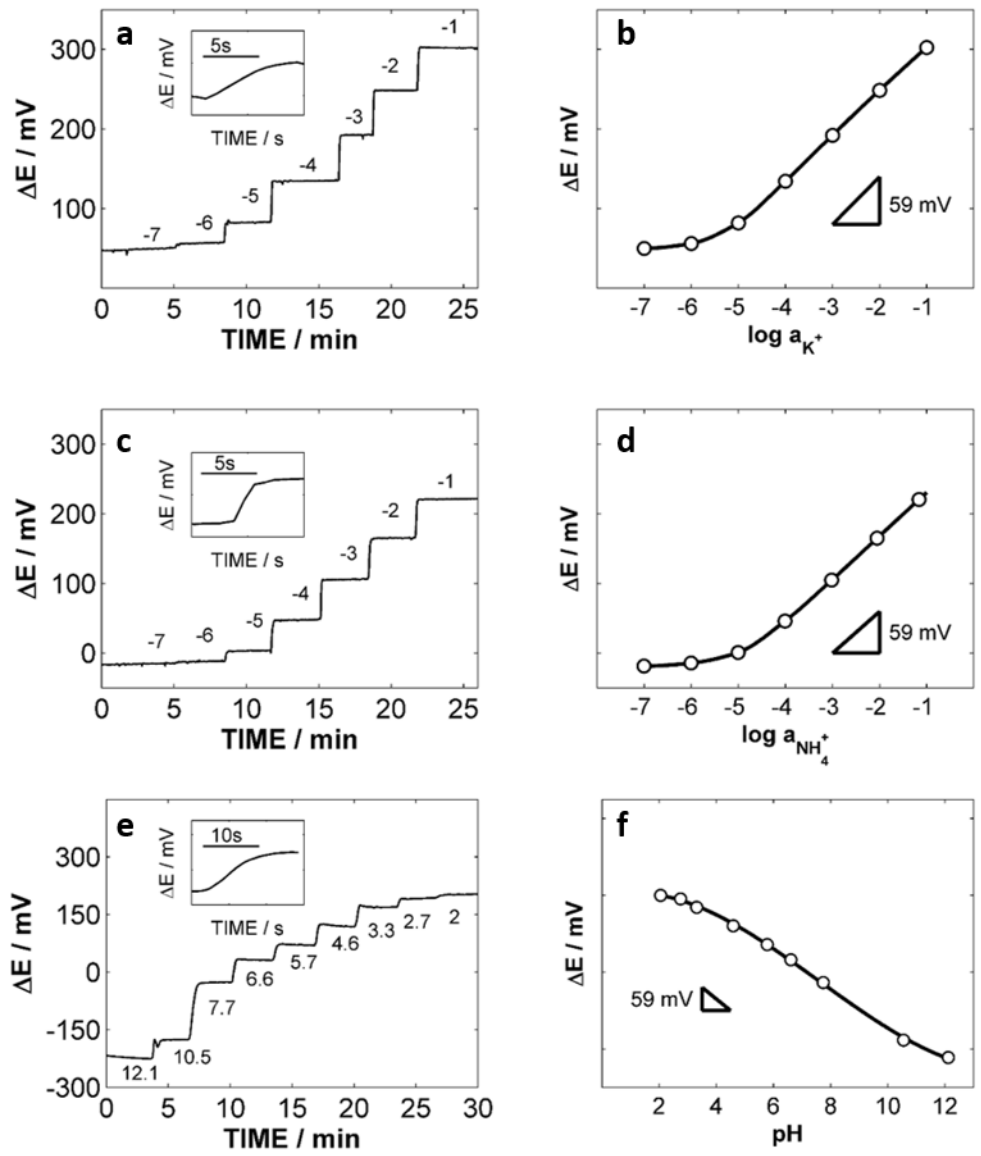

Figure 5.4. Potentiometric response for three different paper ISEs. Time trace (left) and corresponding calibration plots (right) after the addition of the primary analyte for ammonium (a, b), potassium (c, d) and pH (e, f). The inset on the plots a, c, and e shows a detail of the time response for a single addition of the analyte.

Table 5.1 summarizes the most relevant parameters of the analytical performance for the three sensors. Limits of detection (LOD) calculated for K^+ and NH_4^+ are in the micromolar range. These values are satisfactory taking into account the scope of

this work, *i.e.* the development of out-of-the-lab chemical sensing platforms. Indeed, the whole analytical procedure involving handling of sub-micromolar concentrations of these ions in field analysis is not a simple task. Additionally, although some SC-ISE reported in the literature show a significantly lower LOD, this is usually achieved through strict conditioning protocols or using additional approaches to compensate for the undesirable fluxes from the phase boundary membrane to the aqueous solution[23]. These complex procedures require facilities and expertise that fall beyond the expected field of application of these sensors. Thus, these LODs were considered satisfactory for field analysis. Recently, other groups have reported the improvement of the LOD by means of simple modifications, thus, some of these approaches have been also tested to improve these sensors and are discussed in Chapter 8.

Table 5.1. Analytical parameters of the three sensors –ammonium, potassium and pH- (n=3).

	Ammonium	**Potassium**	**pH**
Sensitivity (mV/dec)	56.4 ± 0.8	58.1 ± 0.7	56.6 ± 1.1
Linear range (M)	10^{-5} - 10^{-1}	10^{-5} - 10^{-1}	10^{-4} - 10^{-10}
LOD (M)	$7.2 \cdot 10^{-6}$	$4.1 \cdot 10^{-6}$	----
Response time (s)	10 – 50	10 – 50	50 -100

The selectivity of the electrodes was calculated using the fixed interference method. The selectivity coefficients, log K_{ij} pot ± standard deviation (n = 3) (Table 5.2) are comparable with similar membranes cast on glassy carbon instead of CNT-ink papers[24]. It should be pointed out that differences in the values can be due to the different methodology used for the experimentation. A comparison between these paper-based and glassy carbon (using CNTs as transducers) ISEs shows no differences between the electrodes in terms of the time-response characteristics.

Table 5.2. Selectivity coefficients for potassium ($\log K^{pot}_{Kj}$), ammonium ($\log K^{pot}_{NH_4 j}$) and proton ($\log K^{pot}_{Hj}$) (n=3) compared to the ones reported by other authors[24–26] respectively.

Ion j	K^+- paper-ISE	K^+-ISE[24]
Li^+	-2.7 ± 0.1	-4.4 ± 0.1
Mg^+	-4.1 ± 0.1	-4.9 ± 0.2
Ca^{2+}	-3.9 ± 0.1	-4.7 ± 0.1
Na^+	-2.8 ± 0.1	-3.2 ± 0.2
NH_4^+	-1.9 ± 0.1	-

Ion j	NH_4^+-paper-ISE	NH_4^+-ISE[25]
Mg^+	-3.8 ± 0.5	-4.0
Ca^{2+}	-4.7 ± 0.1	-3.7
Li^+	-4.7 ± 0.1	-3.5
Na^+	-3.0 ± 0.1	-2.4
K^+	-1.2 ± 0.1	-1.0

Ion j	pH-paper-ISE	pH-ISE[26]
K^+	-9.3 ± 0.8	-7.86
NH_4^+	-10.1 ± 0.3	-8.90
Na^+	-10.2 ± 0.1	-8.90
Li^+	-10.1 ± 0.1	-8.90
Ca^{2+}	-10.4 ± 0.1	-8.36
Mg	-9.8 ± 0.1	-9.40

Interestingly, paper-based sensors show good short and medium term stability. In fact, it is observed that the baseline drift is less than 3 mV/h and 5−10 mV/h for potassium and ammonium respectively (based on a continuous 5 h period). Considering that the sensors are expected to be used for short-time readings, these variations of potential can be considered satisfactory. For conventional CNT SC-ISE on glassy carbon, significantly better values, below 230 µV/h, have been reported[27]. It is not yet clear what are the main factors affecting signal stability for these paper electrodes, although it should be expected that both electronic and chemical factors might be playing some role. In the first case, it should be remembered that CNTs are playing a double role, as ion-to-electron transducers and as an electrical conductors. In other words, the body of the electrode, which in conventional

approaches is glassy carbon, is now made by CNT-covered paper. This substrate shows higher resistance (a few hundreds of ohms) than conventional electrodes and it is not shielded, so it might be prone to suffer higher electronic noise. This kind of high frequency noise, however, can be filtered. In a long period of time, more than 1 h, the instability could be related to a parasitic process of the nanostructured interface with a large time constant. This kind of effect is almost neglected in conventional CNT SC-ISEs on glassy carbon and, therefore, the paper-CNT assembly seems to be the cause. On the chemical side, factors affecting the membrane stability (membrane composition variation, adherence (see section 5.4.2), paper degradation, etc.) and its electrical connection to the paper might also be involved. In any case, the stability values obtained seem adequate for the scope of these electrodes.

The ability of the electrodes to withstand long-term storage without affecting the analytical performance will be relevant for the applications in mind. Preliminary tests were conducted by using the electrodes, storing them in a dry place, and re-testing their performance after a given time. The only requisite was to precondition the electrodes for 20 min in a 10^{-4} M primary analyte solution before reusing them. The results show that electrodes can be used, dried, stored, and reused every day for a week without detecting significant changes in the analytical performance (Figure A 5.2 in the additional information of this chapter). The same experiment has been repeated for longer periods of time, and reusing periods of at least 4 weeks have been tested. It has been noticed that after 2 weeks of daily use, the limit of detection may increase up to 1 order of magnitude, while still keeping the Nernstian response (see Figure A 5.1 in the additional information of this chapter). The reasons for this decrease of performance are not yet clear. One possibility is the leaching of the ionophore out of the membrane, a problem that is commonly found with ISE. Approaches such as the immobilization of the ionophore might in this case be a solution[28], since the CNTs are an excellent backbone to link supramolecular receptors. Further work is needed to understand the process of

aging of the membrane on the conductive paper and its analytical implications. In any case, considering the disposable nature of these electrodes, long-term performance is not considered a big problem.

5.4.2 Adherence of the membrane

A topic that deserves a particular discussion is the adherence of the membrane to the conductive papers, since this factor has a large influence on the performance and stability of the sensors. Two sets of experiments were performed to evaluate this point: the well-known water layer test[29] and spectroscopy impedance measurements when the membrane was sequentially torn using a plastic tape. On one hand, the water layer test shows the absence of water between the membrane and the paper-CNT layer (see Figure A 5.3 in the additional information of this chapter) In this case, insignificant changes in the slope are observed when the sensor is subsequently placed in 0.1 M KCl, 0.1 M NaCl, and 0.1 M KCl, the standard procedure to check for a water layer. In contrast, the presence of water is evidenced when glassy carbon/membrane (*i.e.* with a classical coated wire electrode configuration) was used. Therefore, as it has been reported[30], the presence of CNTs helps to avoid the water layer due to their hydrophobic features. On the other hand, the initial impedance measurement shows a well-defined semicircle indicating the absence of holes or channels or inward sample flows (see Figure A 5.4 in the additional information of this chapter). When the membrane is carefully torn, step by step, the total resistance and length of the semicircle decrease from mega-ohms up to a few hundred ohms, holding the membrane a high resistance for at least four torn times. All in all, this suggests that the membrane sticks strongly to the CNT-paper under normal conditions.

5.4.3 Electrical characterisation

Electrical characteristics of the membranes were evaluated by electrochemical impedance spectroscopy (EIS). The results show that the bulk resistances are on

order of 2−2.5 MΩ for the K^+ and NH_4^+ membranes and 3 MΩ for the pH membrane (see Figure A 5.5 in the additional information of this chapter). This confirms the overwhelming contribution of the membrane to the total resistance of the system that makes the contribution of the conductive paper negligible. It should be noticed that these resistances (values 2−3 MΩ) are higher than those reported for solid contact CNT-ISEs on glassy carbon with 10 times thicker PVC membrane (values 150−180 kΩ)[28]. This could be, at least in part, due to the smaller effective area used for the paper electrodes (see Table A 5.1 in the additional information of this chapter, resistivity values) (area 6.2 mm^2) in comparison with the glassy carbon/CNTs/ion-selective membrane classical approach (area 14 mm^2). A higher resistance could also explain the higher susceptibility of these paper electrodes to different sources of noise, thus decreasing their long-term stability, as it was mentioned above. Figure A 5.5 in the additional information of this chapter shows the typical EIS spectra for three membranes, demonstrating that there are not electrical channels between the transducer and the aqueous phase. For the expected application of these sensors, noise has not been seen as a significant problem. However, if noise due to higher impedance values were an issue, different ways to solve it, such as the use of lipophilic salts (such as ETH 500), could be used. Alternatively, working on the electronics of the detection device to achieve very high input impedance is also possible. Therefore, this factor should not be considered a serious issue in the future.

5.4.4 Applicability and extension of the approach

After having deeply characterised these three paper ion-selective electrodes –for potassium, ammonium and pH- the proof of concept is achieved. In order to extend the methodology to other analytes, paper-based ISEs for other cations such as calcium, magnesium and sodium were also constructed. Without further optimization, these electrodes show the expected analytical performance for solid-

contact electrodes (see Table 5.3 and Table 5.4), with Nernstian sensitivities, and linear ranges and LODs similar to those reported in the literature[24].

Table 5.3. Analytical parameters of the three sensors –calcium, magnesium and sodium- (n=3).

	Calcium	**Magnesium**	**Sodium**
Sensitivity (mV/dec)	29.4 ± 0.2	29.3 ± 0.9	53.5 ± 2.4
Linear range (M)	10^{-5} - 10^{-1}	10^{-6} - 10^{-2}	10^{-5} - 10^{-1}
Limit of detection (M)	$1.0 \cdot 10^{-5}$	$2.9 \cdot 10^{-6}$	$2.0 \cdot 10^{-6}$
Response time (s)	10 – 20	20 – 30	10 -100

Table 5.4. Selectivity coefficients for calcium ($\log K^{pot}_{Caj}$), magnesium ($\log K^{pot}_{Mgj}$) and sodium ($\log K^{pot}_{Naj}$) (n=3) compared to the ones reported by other authors[24,31,32] respectively.

Ion j	**Ca^{2+}-paper-ISE**	**Ca^{2+}- ISE[24]**
Li^+	-2.7 ± 0.1	-3.8 ± 0.2
Mg^+	-1.3 ± 0.1	-3.5 ± 0.2
Na^+	-2.0 ± 0.2	-3.5 ± 0.2
NH_4^+	-1.2 ± 0.1	-
K^+	-0.8 ± 0.1	-4.0 ± 0.2

Ion j	**Mg^{2+}-paper-ISE**	**Mg^{2+}- ISE[32]**
Li^+	-3.0 ± 0.2	
Ca^{2+}	-0.7 ± 0.4	-1.9 ± 0.1
Na^+	-3.0 ± 0.1	-3.6 ± 0.1
NH_4^+	-2.8 ± 0.3	
K^+	-2.7 ± 0.3	-2.9 ± 0.1

Ion j	**Na^+-paper-ISE**	**Na^+- ISE[31]**
Li^+	-2.0 ± 0.1	-2.5
Mg^+	-2.7 ± 0.1	>-6
Ca^{2+}	-3.2 ± 0.2	-2.5
NH_4^+	-3.4 ± 0.1	-
K^+	-2.5 ± 0.1	-1.9

Having such a variety of paper ion-selective electrodes opens a whole range of new possibilities. Due to the low cost of the potentiometric platform, performing one or ten measurements will not have a significant difference in cost; therefore measurements with a combination of sensors could provide more information. Just to mention one possible application, these potentiometric paper sensors could be an attractive tool for the fabrication of electronic tongues, as they are cheap and easy to miniaturize[33]. More applications will be presented in the following chapters.

5.4.5 Paper *vs.* Classical ion sensors

Lab-made ISEs were built on glassy carbon to compare the performance of the paper electrodes with these more "conventional" electrodes under similar conditions. The results obtained show similar analytical parameters (see Table 5.5) for paper-based ion sensors and classical electrodes (sensitivity, limit of detection, selectivity, response time, stability) within a range of concentrations relevant for many different field applications (more details are given in chapter 6). Thus, paper-based electrodes might be used instead of conventional ISE as a low-cost, disposable alternative for those applications where conventional electrodes are not affordable.

Table 5.5. Comparison of some analytical performance parameters of a K^+-ISE in paper and in GC[30].

	Paper	**GC**
Sensitivity (mV/dec)	58.1 ± 0.7	58.1 ± 0.4
Linear range (M)	10^{-5} - 10^{-1}	10^{-5} - 10^{-1}
LOD (M)	$4.1 \cdot 10^{-6}$	$3.2 \cdot 10^{-6}$
Response time (s)	10 – 50	~ 10

Some challenges still remain to fully address the problem of affordability and simplicity of operation. In this chapter, the paper electrodes have been used just as a replacement of working electrodes. The following chapter presents the

development of suitable reference systems that allow a simple, integrated potentiometric cell, solving some problems regarding the simplicity of operation.

This has been a pioneer work in the field of potentiometric paper-based sensors. However, in the last years the field has experienced an explosive growth and many other groups have done great advances in the field. Paper has been modified using other inks or transducers[34,35], reference paper electrodes have been developed[36], several ways to improve the standard deviation of the electrodes E^0 have been presented[20–22], etc. Some of these improvements have been progressively incorporated in our system and are presented and discussed in the following chapters. Other works pursuing the same objective of low-cost decentralised chemical analysis have been also developed such as the approach of Rius and co-workers[15] using screen printed CNTs over a plastic substrate for the development of potentiometric cells. These works have been a great inspiration for paper cells. However, the use of paper seems a superior approach, since together with the dyeing methodology it allows to significantly decrease the cost and the system becomes highly versatile.

5.5 Conclusions

In summary, this work has demonstrated that through the combination of recent trends in bendable electronics and carbon nanotubes based potentiometric sensors, a new type of simple, rugged, low-cost sensor with good analytical performance can be built. CNT-papers show excellent performance for making robust field potentiometric sensors, first, because of their excellent electrical properties and second, because of the already demonstrated optimal performance of the CNTs as ion-to-electron signal transducers. Also, the effect of the paper porosity, which provides an increased effective area, may yield additional benefits, such as better conductivity and higher surface area in contact with the membrane. Last but not least, the simplicity of the fabrication should be stressed. The

conductive paper can be simply made by a dyeing process, so the whole electrode can be built using mass manufacturing techniques, which helps to further reduce the costs.

From a technological perspective, there are still many paths to explore, including the development of integrated potentiometric cells (including a reference system), which will be discussed in Chapter 6, and the use of printing technologies to speed up the construction of the sensors and further decrease their cost.

The analytical problem regarding the calibration of the sensor must not be overlooked. There is still considerable work to be done in this area, particularly in factors affecting the reproducibility in the manufacturing process, in order to minimize complex calibration steps. Future perspectives regarding these issues will be further discussed in Chapter 8. In any case, these sensors open new and attractive avenues to merge the analytical science with recent trends in bendable devices, chemical sensing networks, user generated information platforms, telehealth, etc.

5.6 Additional information

Theoretical part:

The electromotive force (emf) measured in ion-selective electrodes can be written as the sum of all interface potential (E_j with j being each interface) across the potentiometric cell (Equation 5.1).

$$EMF = \sum_{j}^{n} E_j \qquad \textit{Equation 5.1}$$

Both in symmetric (inner solution ion-selective electrodes) or asymmetric (solid contact ion-selective electrodes) membranes the only potential which must be analyte dependent is the phase boundary potential (E_{pb}) (Equation 5.2).

$$EMF = \sum_{j=1}^{n-1} E_j + E_{PB} \qquad \textit{Equation 5.2}$$

The phase boundary potential[37] has been always set out as two separate terms according with the permselectivity assumption (Equation 5.3).

$$E_{PB} = E^0(k_i, T, R_T, L, a_i(m), z_i, \beta_{iL}) + \frac{R"T}{z_i F} lna_i(aq) \qquad \textit{Equation 5.3}$$

The first term can be written as a function of the chemical properties of the membrane such as ionic sites (R_T), ionophore concentration (L), formation constant (β_{iL}), *ki* which is the difference between the standard chemical potentials of ion *i* in both phase, activity of ion *i* in the membrane phase ($a_i(m)$), charge (z_i) and temperature (T). The second term is only related to the activity of the primary analyte in the sample phase ($a_i(aq)$) given the well-known Nernstian slope.

Inserting equation 5.3 in 5.2, we obtained equation 5.4. E^0_{exp} is the intercept value obtained from the experimental calibration curve. E^0_{exp} is composed by E^0 and the sum of all interface potential excluding the phase boundary potential.

$$EMF = E^0_{exp}\left(k_i, T, R_T, L, a_i(m), z_i, \beta_{iL}, \sum_{j=1}^{n-1} E_j\right) + \frac{R"T}{z_i F} lna_i(aq) \qquad \textit{Equation 5.4}$$

In our case, the observed intercept value is a function of the individual interface potential between paper/CNTs layer, CNTs layer/ion-selective membrane and the rest of the constants written in equation 5.4. It is evident that those potentials will be depended intrinsically on construction of the electrodes (amount of CNTs, homogeneity of CNTs-layers, membrane and CNT-layer thicknesses, etc). Nonetheless, as we mentioned before, each electrode should be calibrated before use at least with two standard solutions.

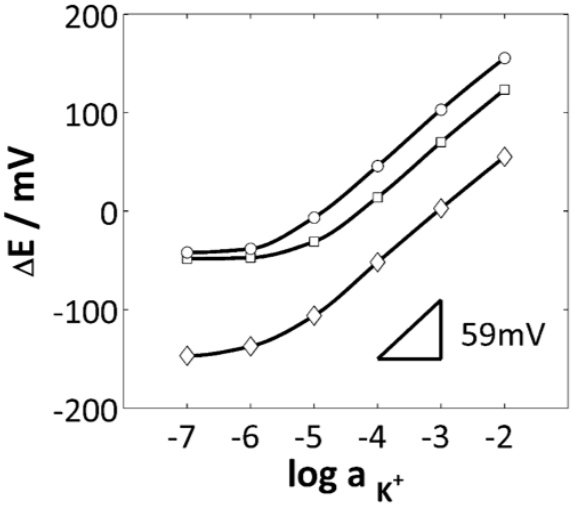

Figure A 5.1. Change over time of the calibration plot for a single K^+ paper-based electrode. Calibration plots after (◊) 1day, (□) 15 days and (o) 1 month of the electrode construction.

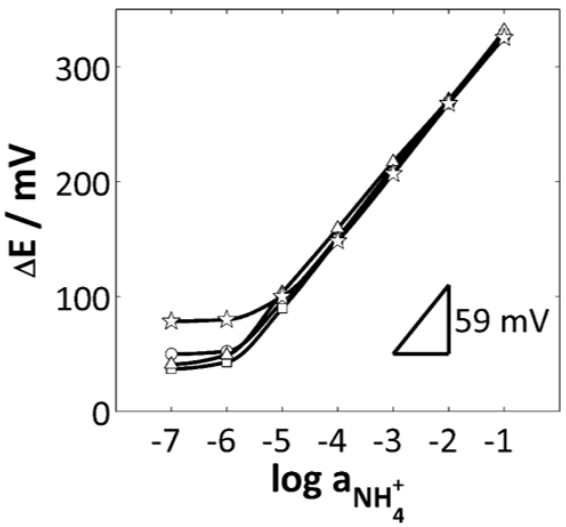

Figure A 5.2. Change over time of the calibration plot for a single NH_4^+ paper-based electrode. Calibration plots after (o) 1 day, (□) 2 days, (△) 3 days and (☆) 6 days of the electrode construction. Is noteworthy to mention that values are not zero-corrected.

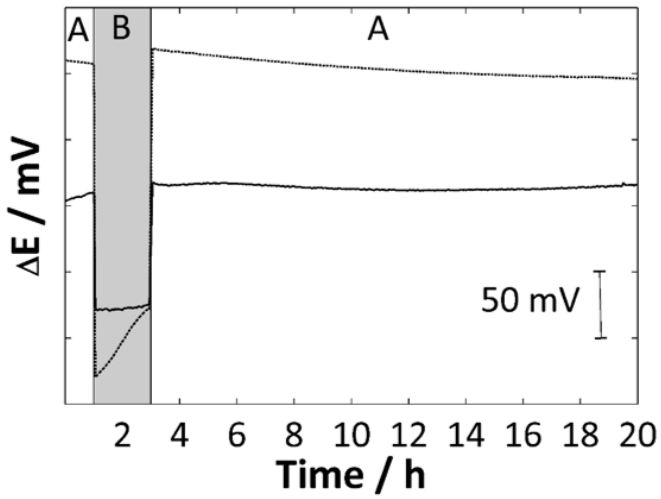

Figure A 5.3. Water-layer test for a K^+-paper SC-ISE (solid line) and a K^+-Glassy Carbon SC-ISE (dashed line). Electrodes are first immersed in (A) 0.1 M KCl and then removed from that solution and immersed in (B) 0.1 M NaCl, finally electrodes are immersed again in (A) 0.1 M KCl.

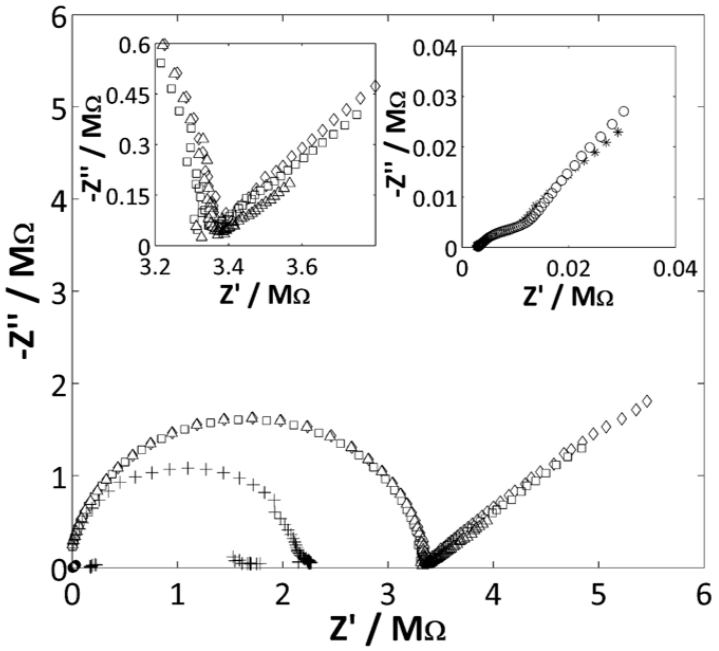

Figure A 5.4. Impedance plots for a sensor after removing (◊) 0, (□) 1, (△) 2, (+) 3, (∗) 4 and (o) 5 layers of tape.

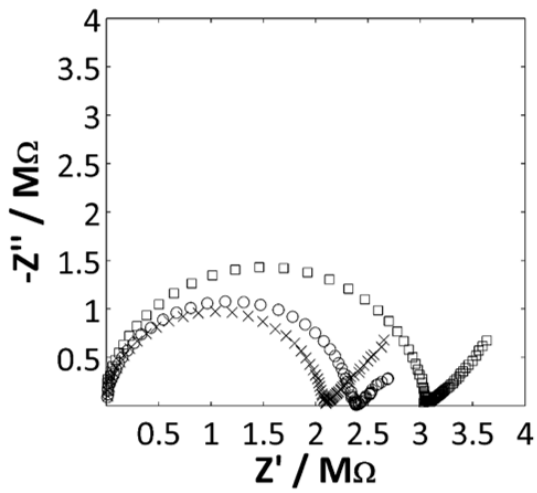

Figure A 5.5. Impedance plots of K^+ (×), NH_4^+ (o) and pH (□) ion-selective papers.

Table A 5.1. Total resistance and resistivity for each membrane.

ISE	R_{ct} (Ω)	Area (m^2)	Thickness (m)	ρ (Ω·m)
K^+	2090000	0,0000028	0,000020 ± 0,000005	691100 ± 244000
NH_4^+	2380000	0,0000028	0,000020 ± 0,000005	787000 ± 278000
pH	3030000	0,0000028	0,000020 ± 0,000005	1001900 ± 354000

5.7 References

(1) Mabey, D.; Peeling, R. W.; Ustianowski, A.; Perkins, M. D. *Nat. Rev. Microbiol.* **2004**, *2*, 231–240.

(2) Diamond, D.; Coyle, S.; Scarmagnani, S.; Hayes, J. *Chem. Rev.* **2008**, *108*, 652–679.

(3) Byrne, R.; Diamond, D. *Nat. Mater.* **2006**, *5*, 421–424.

(4) Yager, P.; Domingo, G. J.; Gerdes, J. *Annu. Rev. Biomed. Eng.* **2008**, *10*, 107–144.

(5) Price, C. P. *Clin. Rev.* **2001**, *322*, 1285–1288.

(6) Aguilera-Herrador, E.; Cruz-Vera, M.; Valcárcel, M. *Analyst* **2010**, *135*, 2220–2232.

(7) Polisena, J.; Coyle, D.; Coyle, K.; McGill, S. *Int. J. Technol. Assess. Health Care* **2009**, *25*, 339–349.

(8) Polisena, J.; Tran, K.; Cimon, K.; Hutton, B.; McGill, S.; Palmer, K. *Diabetes Obes. & Metabol.* **2009**, *11*, 913–930.

(9) Valcárcel, M.; Cárdenas, S. *TrAC, Trends Anal. Chem.* **2005**, *24*, 67–74.

(10) Zoski, C.-E. *Handbook of Electrochemistry*; Elsevier B.V.: Amsterdam, 2007.

(11) Bakker, E.; Pretsch, E. *Angew. Chem. Int. Ed.* **2007**, *46*, 5660–5668.

(12) Wang, J. *TrAC, Trends Anal. Chem.* **2002**, *21*, 226–232.

(13) Anastasova-Ivanova, S.; Mattinen, U.; Radu, A.; Bobacka, J.; Lewenstam, A.; Migdalski, J.; Danielewski, M.; Diamond, D. *Sens. Actuators, B* **2010**, *146*, 199–205.

(14) Forster, R. J.; Diamond, D. *Anal. Proc.* **1991**, *28*, 117–122.

(15) Rius-Ruiz, F. X.; Crespo, A.; Bejarano-Nosas, D.; Blondeau, P.; Riu, J.; Rius, F. X. *Anal. Chem.* **2011**, *83*, 8810–8815.

(16) Wang, J.; Musameh, M. *Analyst* **2004**, *129*, 1–2.

(17) Bakker, E.; Pretsch, E.; Bühlmann, P. *Anal. Chem.* **2000**, *72*, 1127–1133.

(18) Mousavi, Z.; Teter, A.; Lewenstam, A.; Maj-Zurawska, M.; Ivaska, A.; Bobacka, J. *Electroanal.* **2011**, *23*, 1352–1358.

(19) Michalska, A.; Wojciechowski, M.; Bulska, E.; Maksymiuk, K. *Talanta* **2010**, *82*, 151–157.

(20) Vanamo, U.; Bobacka, J. *Electrochim. Acta* **2014**, *122*, 316–321.

(21) Vanamo, U.; Bobacka, J. *Anal .Chem.* **2014**, *86*, 10540–10545.

(22) Zou, X. U.; Cheong, J. H.; Taitt, B. J.; Bühlmann, P. *Anal .Chem.* **2013**, *85*, 9350–9355.

(23) Bakker, E.; Bühlmann, P.; Pretsch, E. *Talanta* **2004**, *63*, 3–20.

(24) Zhu, J.; Li, X.; Qin, Y.; Zhang, Y. *Sens. Actuators, B* **2010**, *148*, 166–172.

(25) Sasaki, S.; Amano, T.; Monma, G.; Otsuka, T.; Iwasawa, N.; Citterio, D.; Hisamoto, H.; Suzuki, K. *Anal. Chem.* **2002**, *74*, 4845–4848.

(26) Crespo, G. A.; Gugsa, D.; Macho, S.; Rius, F. *Anal. Bioanal.Chem.* **2009**, *395*, 2371–2376.

(27) Ampurdanés, J.; Crespo, G. A.; Maroto, A.; Sarmentero, M. A.; Ballester, P.; Rius, F. X. *Biosens. Bioelectron.* **2009**, *25*, 344–349.

(28) Parra, E. J.; Blondeau, P.; Crespo, G. A.; Rius, F. X. *Chem. Commun.* **2011**, *47*, 2438–2440.

(29) Fibbioli, M.; Morf, W. E.; Badertscher, M.; de Rooij, N. F.; Pretsch, E. *Electroanal.* **2007**, *12*, 1286–1292.

(30) Crespo, G. A.; Macho, S.; Rius, F. X. *Anal. Chem.* **2008**, *80*, 1316–1322.

(31) Cadogan, A. M.; Diamond, D.; Smyth, M. R.; Deasy, M.; Mckervey, M. A.; Harris, S. J. *Analyst* **1989**, *114*, 1551–1554.

(32) Zhang, W.; Jenny, L.; Spichiger, U. E. *Anal. Sci.* **2000**, *16*, 11–18.

(33) Ciosek, P.; Wróblewski, W. *Sensors* **2011**, *11*, 4688–4701.

(34) Jaworska, E.; Lewandowski, W.; Mieczkowski, J.; Maksymiuk, K.; Michalska, A. *Analyst* **2013**, *138*, 2363–2371.

(35) Mensah, S. T.; Gonzalez, Y.; Calvo-Marzal, P.; Chumbimuni-Torres, K. Y. *Anal. Chem.* **2014**, *86*, 7269–7273.

(36) Lan, W.-J.; Maxwell, E. J.; Parolo, C.; Bwambok, D. K.; Subramaniam, A. B.; Whitesides, G. M. *Lab Chip* **2013**, *13*, 4103–4108.

(37) Bakker, E. *J. Electroanal. Chem.* **2010**, *639*, 1–7.

UNIVERSITAT ROVIRA I VIRGILI
PAPER-BASED POTENTIOMETRIC PLATAFORMS FOR ESCENTRALISED CHEMICAL ANALYSIS.
Marta Novell Recasens
Dipòsit Legal: T 1462-2015

UNIVERSITAT ROVIRA I VIRGILI
PAPER-BASED POTENTIOMETRIC PLATAFORMS FOR ESCENTRALISED CHEMICAL ANALYSIS.
Marta Novell Recasens
Dipòsit Legal: T 1462-2015

CHAPTER

A PAPER-BASED POTENTIOMETRIC CELL FOR MONITORING LITHIUM LEVELS IN WHOLE BLOOD

UNIVERSITAT ROVIRA I VIRGILI
PAPER-BASED POTENTIOMETRIC PLATAFORMS FOR ESCENTRALISED CHEMICAL ANALYSIS.
Marta Novell Recasens
Dipòsit Legal: T 1462-2015

6.1 Summary

This chapter is aimed to demonstrate the value of the paper sensors when facing an analytical challenge such as a complex and relevant determination. Experimentally, the work is focused on the development of a potentiometric reference electrode and a lithium ISE using the conductive CNT-paper substrate previously described. This allows building a whole paper potentiometric cell, which is used for the determination of lithium in whole blood. The steps to build a novel paper-based reference electrode, the design and construction of the integrated cell and the optimization of the analytical parameters are presented. The integration of both electrodes in a lithium detection cell is the proof of concept of a complete device that is compact, low-cost and extremely simple. Moreover the accurate prediction of lithium in whole blood samples is demonstrated, as an example of the great potential of these systems. The validation of the results obtained against more complex analytical tools, such as atomic emission spectroscopy, demonstrates the power of this approach for the future home-management of chronic conditions.

6.2 Introduction

Up to this point, the feasibility of making paper-ISEs has been demonstrated. Also it has been shown that their analytical performance emulates that of conventional systems. However, for a new technology to be useful –particularly as an analytical tool- its real applicability –in terms of the ability to solve real problems- must be demonstrated. Therefore, this technology needs to answer a crucial question: can it really solve an analytical problem?

Scientists are usually focused on solving complex and difficult problems. It is common to see new tools to detect rare diseases, and it is rarer to see new tools to manage in a better way existing illnesses. However, the paper-based ISEs are not

intended –so far- to replace the sophisticated technologies already existing, but they are rather aimed to facilitate and reduce the cost of routine analysis. Thousands of routine analysis are performed every day -with the cost of personal and resources involved-. Paper-based sensors could be an alternative for this type of situations, helping to completely change the overall approach. If the determinations can be performed in a decentralised way –in a similar fashion than the blood sugar test- this will solve two problems at the same time. From one side it will reduce the routine analysis performed in the laboratories, thus relieving the healthcare system. From the other side, it will allow individuals to make analysis whenever they need it, therefore providing them the control of their life and allowing a personal management of diseases. For this reason, the determination of lithium in a decentralised way has been chosen as a proof of principle.

Lithium is widely known as a mood stabilizer drug. Today, the administration of Li salts is a standard procedure to treat patients with some types of maniac and bipolar disorders and recurrent depression[1]. Despite of this wide utilization, the use of this drug is not free from risks and troubles. From one side, Li has a very narrow effective therapeutic range. For an effective treatment[2,3] the concentration of Li in blood must be adjusted (depending on the type of disorder) to levels in the range of 0.5 to 1.5 mM. Levels below this range are not effective, while levels above it can lead to toxic effects. Chronic toxicity –with kidney, liver or brain function damage- is not a negligible problem, since long term treatments (usually for years or decades) are fairly common. Acute toxicity is an even more worrisome problem, since concentrations in blood in the range of 5 mM may result in permanent damage or even death.

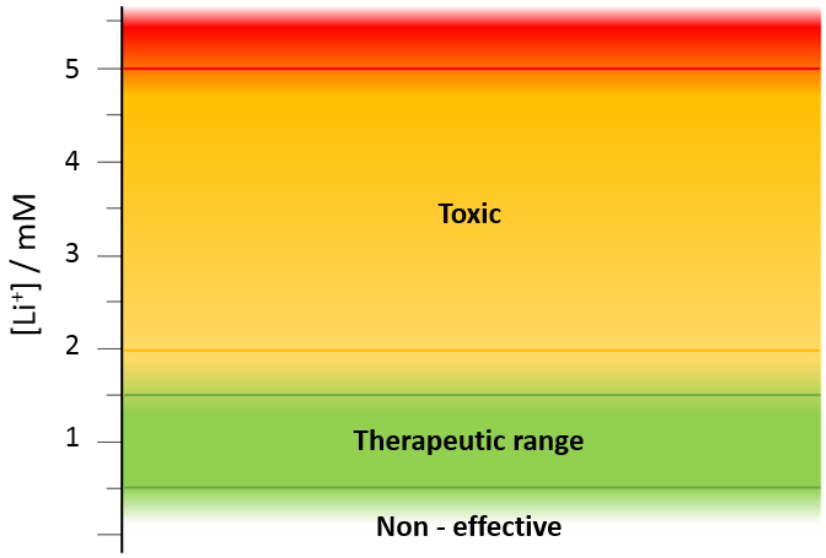

Figure 6.1. Effects of lithium levels in blood.

Reaching and sustaining the right therapeutic level while avoiding risks is not a simple task, since there are many factors that affect the lithium uptake and retention. It is well known that individual variability, as well as changes in salt intake, caffeine, drug interaction, etc.[4] may have a significant effect on the blood levels of Li. To find the right dosage, doctors must administer the drug and then check actual Li levels in blood, adjusting the dose until the right value is reached[5]. Blood samples must be taken at least 12 h after the last administration, and the whole analytical process may take variable lag time (usually from a few days to weeks). Furthermore, Li levels in blood must be then monitored during the whole treatment. This whole approach is troublesome for both, the healthcare professional and the patient. The need to have frequent blood tests is a nuisance for the patient, while the delay between the sample extraction and the evaluation of the results limits the possibility of early detection and correction of problems. Alternative approaches to alleviate this issue –such as monitoring the levels in urine or saliva- have been proposed[6], but the results obtained are not yet reliable. Thus, blood testing still remains as the gold standard. Evidently, approaches that

could provide results in real time with minimal disruption for the patient will be highly desired.

Although several methods for the measurement of lithium in blood, such as colorimetry[7], or photometry[8–10] have been reported, routine analysis are usually performed by flame emission photometry, atomic absorption spectroscopy or ion-selective electrodes[2,11]. Evidently, all these determinations must be performed in a laboratory, with suitable expertise and instrumentation. The need to have quicker and simpler ways to determine the levels of Li in blood has motivated the development of several decentralized approaches, such as those used in point of care[12]. Glazer *et al*.[10] have reported an instant test that allows the quantification of lithium in plasma by means of photometry. The test is composed by a blood-cell separator membrane linked to a micro-cuvette prefilled with a colorimetric reagent. Van den Berg *et al*.[13–16] have developed a point-of-care hand-held analyser that uses prefilled disposable chips with integrated microfluidics where the blood components are separated by capillary electrophoresis and lithium is detected conductimetrically. All these devices show promise, although problems associated to cost and simplicity of the instrumentation need still to be tackled.

As it has been extensively discussed, paper is a low-cost and highly versatile substrate to build analytical platforms. In the previous chapter it has been shown that it is possible to build paper-based ion-selective potentiometric sensors whose performance is similar to that obtained with the conventional lab-based sensors. Potentiometric sensors are nowadays widely used for the determination of ions in biological fluids[18], including lithium. One of the main limitations of ion-selective electrodes (ISE) for the detection of lithium in blood has traditionally been the interference of sodium, which is present at much higher concentrations. However, significant progress improving the selectivity for lithium has been achieved during the last few years. Several groups have reported the detection of lithium in serum samples with conventional ISE[18–22]. Coldur *et al*.[19] demonstrated that the addition

of trioctylphosphine oxide into the lithium ion-selective membrane allows the accurate determination of lithium in presence of sodium at the levels normally present in blood. This opens a clear opportunity to develop paper-based potentiometric sensors for Li in blood. Evidently, to develop a truly useful diagnostic device, a whole potentiometric cell is required.

This chapter introduces for the first time the development of disposable paper-based micro-potentiometric cell for the fast and accurate determination of Li in whole blood. First, a novel paper-based solid-state reference electrode is developed. Thereafter, a new paper ISE for Li is built and characterised. Last, these two electrodes are combined to create a potentiometric cell with a total approximate volume of 50 µL.

6.3 Experimental part

6.3.1 Paper ISEs and cell construction.

The detailed procedure to make the paper-ISEs has been described in the previous chapter. To refresh, 15 µl of the lithium ion-selective membrane and 25 µl of the reference membrane are deposited on the respective electrodes in successively amounts of 5 µl. Once the electrodes are built independently (see Figure 6.2 A), to arrange the miniaturized cell, paper electrodes are sandwiched leaving a cavity of approximately 50 µl volume, as shown in Figure 6.2 B. This cavity is open in the top for the sample introduction. Both, paper-ISE and reference electrode are connected to the potentiometer by their conductive ends.

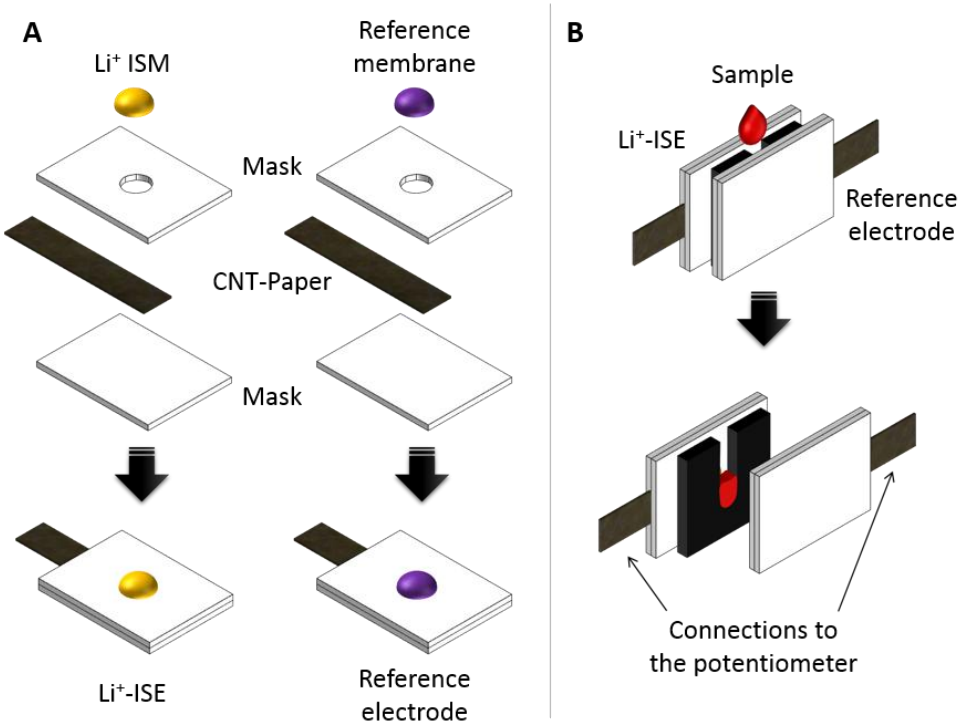

Figure 6.2. A) Scheme of the independent construction of the two paper-electrodes. B) Scheme of the complete paper-cell, the two electrodes are placed with the membranes facing the inside and leaving a cavity –using a rubber with a specific shape- for the sample introduction (measuring setup).

6.3.2 Instrumentation and measurements

Atomic emission spectrometry (AES) (Unicam Solar 969) was used to obtain reference values to compare with the lithium levels determined by potentiometry. The measurements were performed using a mildly oxidizing air/acetylene flame, with a single slot burner head. The slide width was 160 µm and the band pass 0.5 nm. Lithium emission was measured at 670.8 nm. Linear regression between 0.1 – 0.5 mg/ml was used to calculate the lithium concentration of the tested samples.

6.4 Results and discussion

6.4.1 Development of the paper-based Li^+- ISE

For optimization and comparison purposes, Li^+-ISEs using glassy carbon (GC-ISE) as support were initially built and their results compared with the paper-based electrodes. The Li^+-GC-ISEs show a sensitivity of 58.4 ± 0.4 mV/dec (water), very similar to the value obtained for Li^+-paper-ISEs (59.8 ± 1.4 mV/dec). A plot comparing the EMF values obtained for a calibration curve of both electrodes simultaneously does not show significant differences (Figure 6.3). This shows that, as it was mentioned in the previous chapter, no significant differences are found between paper and conventional solid-state ISEs in terms of sensitivity and linear range.

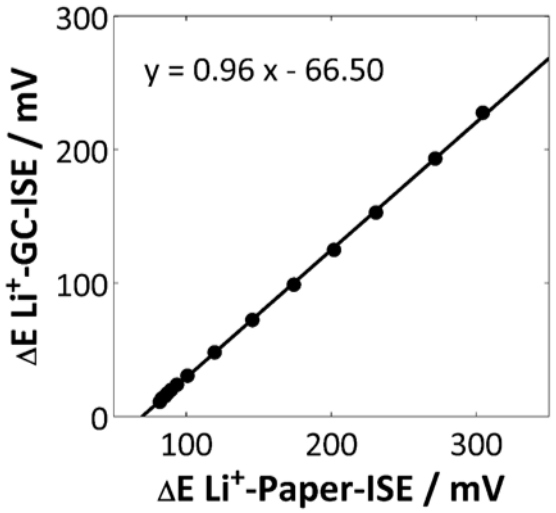

Figure 6.3. Comparison of the potential values obtained for Li^+-Paper-ISE and Li^+-GC-ISE for different lithium concentrations.

Details of the time-trace response of a Li^+-paper electrode and the corresponding calibration plot are shown in Figure 6.4. The electrodes show a Nernstian response between $3.6 \cdot 10^{-5}$ and $1 \cdot 10^{-1}$ M. The standard deviation between three measurements of the same concentration is in all cases below 2 mV and therefore

error bars cannot be appreciated in the plot. The most relevant analytical parameters are summarized and compared with values already reported[19] for the same type of membrane (see Table 6.1). Interestingly, the results show that the paper-based electrode shows slightly better sensitivity. It should be noted that the system reported in the literature uses a coated wire approach without ion-to-electron transducer. In general, in the absence of transducer, these electrodes show a poorer performance. Previous work from our group[23] has shown that carbon nanotubes improve the transduction of the potentiometric signal and in the previous chapter it was also demonstrated the great adherence of polymeric membranes over the CNT-paper. The high hydrophobicity of the carbon nanotubes is also a crucial factor to avoid the formation of a water layer[24], improving long term stability of the signal.

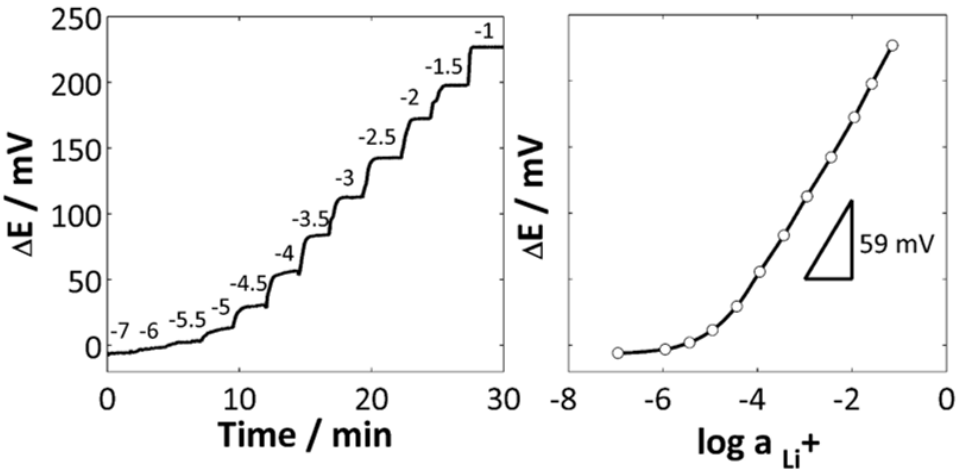

Figure 6.4. Potentiometric response for the Li^+-paper-ISE. Time trace (left) and corresponding calibration plot (right) upon increasing lithium concentration.

Table 6.1. Analytical performance of the Li^+-paper-ISE (n=3).

	Paper	**Reported**[19]
Sensitivity (mV/dec)	59.8 ± 1.4	47.6
Linear range (M)	$3.6\cdot10^{-5} – 1\cdot10^{-1}$	$2.7\cdot10^{-6} – 1\cdot10^{-1}$
Limit of detection (M)	$1.1\cdot10^{-5}$	$5\cdot10^{-6}$
pH stability	From 4 to 12	From 4 to 12
Membrane bulk resistance (MΩ)	3	
Response time (s)	40	20
Medium term stability, 16h (mV/h)	0.4	

To be fair, paper-based electrodes show slightly worse limit of detection (LOD). This has been already observed in the paper potentiometric platform[25]. Even so, this LOD is sufficient for the purpose of this work, regarding the clinically relevant analytical range ($5\cdot10^{-4} – 1.5\cdot10^{-3}$ M). The response time of about 40 seconds for a 10^{-4} M solution is excellent for the use of those sensors in decentralized analysis. A medium term stability test shows a drift of about 0.4 mV/h (16 hrs), which is also satisfactory, considering that the electrode is intended for a single, short reading. The stability of the electrode at different pH values has also been evaluated. It has been found that the electrodes are stable in a range of pH from 4 to 12. The experiment was carried out by measuring the potential change of the electrode when changing the pH values by adding HCl acid to a universal buffer solution at initial pH of 14. Experiments were also conducted to evaluate the presence of a water layer, which may affect the long term stability of the sensor, but no evidence of water layer was found. In any case, in a routine procedure, the sensor should be calibrated and the measurement performed soon after. Therefore, in this type of short-term measurements, these factors regarding the long-term stability should not be extremely relevant.

Although it has been observed that most of the surfactant from the carbon nanotubes ink is eliminated during the washing[25] (see chapter 4), there had been some concern on whether some surfactant remaining on the system might be affecting the sensor performance. To explore this possibility, conductive papers were subject to a very rigorous washing that involves overnight leaching in water during several days. This "extreme" washing leads to highly hydrophobic CNT-papers, already presented in chapter 4. A comparison of the analytical parameters of electrodes made with both types of paper (normal and hard washing) do not show significant differences in terms of sensitivity, LODs and linear ranges (see Figure 6.5). These electrodes did not show any evidence of a water layer either. Interestingly, the only parameter that has been improved by the hard washing conditions is the long term stability, which was reduced down to 0.04 mV/h. Evidently, the elimination of traces of surfactants may be improving the role of the CNTs as transducers of the potentiometric signal. All in all, this hard washing does not seem to add much when considering the analytical parameters, although it could be an option if better long term stability is required.

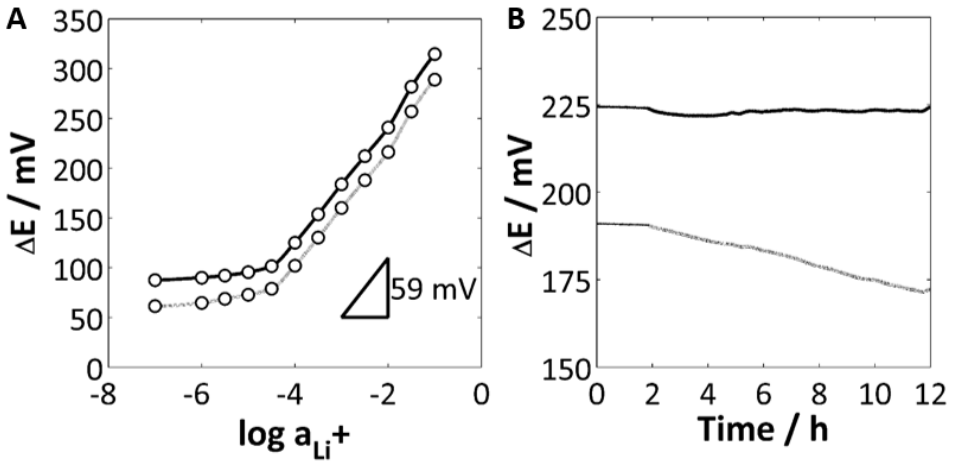

Figure 6.5. Comparison of a normal Li^+-paper-ISE (---) and a highly hydrophobic Li^+-paper-ISE (–). A) Calibration curve and B) Stability at 10^{-2} M LiCl.

Selectivity is a crucial factor when developing systems for the analysis in blood or serum. Selectivity coefficients of the Li^+-paper-ISEs towards the most abundant ions and organic compounds in blood were evaluated. Table 6.2 displays the values ($logK_{Lij}^{pot}$ ± standard deviation (n=3)) obtained for the Li^+-paper-ISE with Fixed Interference Method (FIM) and Separate Solution Method (SSM) compared to the reported ones with Matched Potential Method (MPM). I this work, this method was not used due to its high dependence of experimental conditions[26]. It should be stressed that selectivity coefficients depend on the method used for calculation, so comparisons need to be made with caution. Considering a range of Li^+ between 0.5 to 1.5 mM, one of the major interferences in blood or serum is Na^+, usually present in the range 135 to 145 mM. From the selectivity coefficients obtained, it could be expected that the determination of Li^+ could be carried out in serum or blood without major interferences (see concentration of ions in blood in Table 6.3).

Table 6.2. Selectivity coefficients of the Li^+-paper-ISE obtained with Fixed Interference Method (FIM) and Separate Solution Method (SSM) compared to the ones reported with the Matched Potential Method (MPM).

	log K_{Lij}^{pot}						
	NH_4^+	**K^+**	**Na^+**	**Mg^{2+}**	**Ca^{2+}**	**Urea**	**Glucose**
Li^+-paper-ISE							
FIM	-2.58	-2.69	-2.66	-2.78	-2.75	-2.89	-2.8
SSM	-3.29	-3.34	-3.11	-2.54	-2.93	-5.56	-3.66
Reported							
MPM	-3.14	-2.75	-3.01	-3.69	-3.13	---	---

Table 6.3. Normal values of ions in blood.

Analyte	Concentration (mM)
Na^+	135-145
K^+	3.5-5
Ca^{2+}	2.2-2.6
Mg^{2+}	0.62-0.99
Cl^-	98-106
HCO_3^-	23-28
HPO_4^{2-}	0.87-1.45
Urea	2.1-7.1
Glucose	3.5-5.3

To prove this point, the analytical performance of the Li^+-paper-ISEs in artificial serum media was studied. The results show that there is not significant differences of the parameters of interest when comparing the calibration in water and in artificial serum (see Figure 6.6 and Table 6.4). Indeed, a Nernstian response (57.3 ± 0.8 mV/dec) is still obtained. As it could be expected, due to the interference of Na^+ the LOD obtained is slightly worse ($5.7 \cdot 10^{-5}$ M), but this value is still under the lower limit of the lithium therapeutic range.

6.4.2 Development of the paper-based reference electrode

After the optimization of the paper-ISE, the construction of the potentiometric cell requires the development of a paper reference electrode (RE). This RE is built in a similar way to the working electrode, *i.e.* by drop-casting a membrane (in this case, the reference membrane) on the conductive paper substrate. The use of this solid-state reference membrane on a glassy carbon support has been previously described[27], and no variation of the potential with a large number of inorganic ions and organic substances over a wide range of concentrations was found. It should be pointed out, however, that the paper RE does not show the same performance.

For example, a variation of about 6 mV/dec was obtained when changing the concentration of Li in water. These values, however, were reduced down to 1 mV/dec when working in a constant ionic strength solution (*i.e.* artificial serum). In other words this paper RE is actually working as a pseudo reference electrode. Nevertheless, since the measurement of Li will be performed in serum (or blood) samples, with a fairly constant ionic strength, this pseudo reference electrode will work fine. In a typical routine, calibration should be performed in each individual disposable cell using standards in artificial serum. Figure 6.6 shows the response of the reference-paper electrode upon changes on lithium concentration on artificial serum sample. Clearly, no significant changes are observed. The same is true for small variations in the ion concentration of other serum components, in particular sodium. As the concentration of all the components in serum is really similar for each person -in the same order of magnitude (see Table 6.3)- the performance of the reference electrode will not be affected for these small changes. Later, it is proved that this reference electrode exhibit a good prediction for samples coming from different people, therefore not being affected for the changes coming from different ions concentration in serum.

6.4.3 Potentiometric paper cell

Finally, a paper potentiometric cell was assembled as shown in Figure 6.2 B, and the system was used to measure lithium in artificial serum samples. First, a calibration plot was performed on this cell and compared to the previously obtained plots. The results for this whole paper potentiometric cell (Li^+-paper-ISE *vs.* Reference-paper) show a Nernstian response (56.3 ± 0.7 mV/dec) and similar linear ranges and response times than the conventional cell. The LOD is slightly higher ($8.9 \cdot 10^{-5}$ M), but still adequate for the scope of this work.

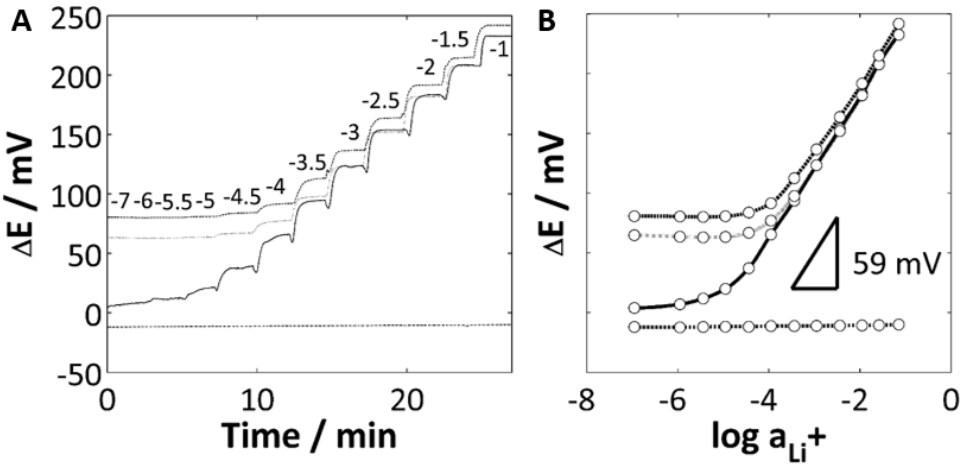

Figure 6.6. Instrumental response of the different Li^+ potentiometric cells. Time trace (A) and corresponding calibration plot (B) upon increasing lithium concentration. (–) Commercial reference vs. Li^+-paper-ISE in aqueous solution; (···) Commercial reference vs. Li^+-paper-ISE in artificial serum solution; (-·-) Commercial reference vs. reference paper in artificial serum solution; and (---) reference paper vs. Li^+-paper-ISE in artificial serum solution.

Table 6.4. Analytical performance of the different Li^+ potentiometric cells. Commercial reference (R_{Com}), Li^+-paper-ISE (Li), reference paper (R_{Paper}), aqueous solution (H_2O) and artificial serum solution (Serum).

	R_{Com} *vs.* Li (H_2O)	**R_{Com} *vs.* Li (Serum)**	**R_{Com} *vs.* R_{Paper} (Serum)**	**R_{Paper} *vs.* Li (Serum)**
Sensitivity (mV/dec)	59.8 ± 1.4	57.3 ± 0.8	0.9 ± 0.6	56.3 ± 0.7
Linear range (M)	$3.6\cdot10^{-5} – 10^{-1}$	$10^{-4} – 10^{-1}$	$10^{-9} – 10^{-1}$	$10^{-4} – 10^{-1}$
Limit of detection (M)	$1.1\cdot10^{-5}$	$5.7\cdot10^{-5}$	---	$8.9\cdot10^{-5}$

6.4.4 Prediction of lithium in artificial serum

After the calibration, artificial serum samples with lithium concentration on the therapeutic range were placed on the cell and its concentration was predicted using the calibration plot obtained. Following this procedure, seven samples were evaluated. The same samples were measured with a reference method –Atomic Emission Spectroscopy (AES)- that is normally used in routine analysis of Li in blood and serum. A comparison of the results obtained for both methods are shown in Figure 6.7. Error bars show the standard deviation of each value for both techniques. Also, a similar determination with paper electrodes in a conventional (large volume) cell was performed, to evaluate whether the small volume cell was affecting the analytical performance. The results show that the miniaturised cell has the same performance of a conventional (larger volume) cell. In both cases, the prediction of lithium was accurate when comparing the potentiometric results with those obtained by AES. Join confidence region test show no significant difference between the values at 95 % confidence ($F_{calculated}$=4.78; $F_{tabulated}$=5.79).

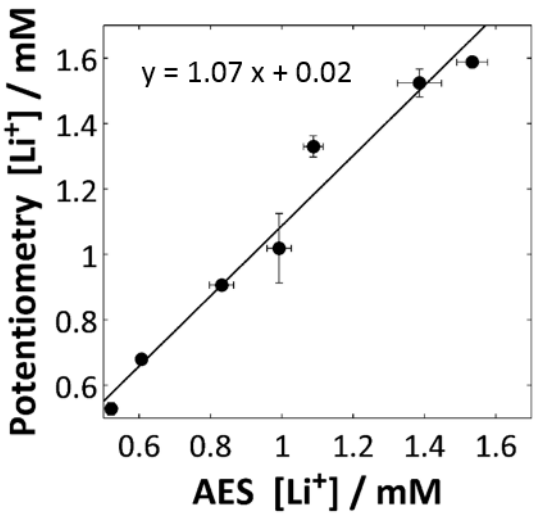

Figure 6.7. Prediction of Li^+ concentrations (mM) in artificial serum samples determined by the Li^+-paper-ISE and Ref-paper and AES.

6.4.5 Prediction of lithium in real samples

With this same type of cell, blood and serum samples provided by a local hospital of people undergoing Li treatment were directly measured. Before measuring each sample with the paper potentiometric cell, two lithium standards of 0.3 and 3 mM were placed on the cell to obtain the calibration curve. These two standards were chosen as they are outside the therapeutic range, but close enough so they give a more precise prediction. After measuring the standards, the cell is washed and then the sample is measured. 9 whole blood and 2 serum samples were measured following this procedure, and the concentration of Li was predicted using the two-point calibration. Samples were also measured by AES to check these results. By using just these two standards, it was possible to obtain the lithium concentration in the sample in less than 5 minutes, as it just requires the measurement of three solutions altogether. The results can be seen in Table 6.5. The two samples that where placed outside the range, where predicted with a low standard of 0.1 mM for a better prediction. It should be mentioned that the same electrodes have been used repeatedly for at least 10 predictions without decreasing their performance. While this is possible with a meticulous work, a tedious cleaning in between each different sample is required. However, the prospective and applicability of the system is thought to be used with new electrodes for each sample, to avoid contamination, and make the procedure simpler. In this work the two manners were combined, the same cell was used for different samples –with the proper cleaning- and different disposable cells were used for other samples, all the cells giving an accurate prediction.

Table 6.5. Concentration of lithium predicted by potentiometry and AES.

Type	Potentiometry [Li] (mM)	AES [Li] (mM)	Recovery Potentiometry /AES (%)
Blood	0.49 ± 0.06	0.52 ± 0.01	94
Blood	0.26 ± 0.06	0.30 ± 0.01	87
Blood	0.43 ± 0.01	0.47 ± 0.01	92
Serum	0.69 ± 0.02	0.72 ± 0.01	96
Blood	0.61 ± 0.06	0.53 ± 0.01	115
Serum	0.63 ± 0.05	0.68 ± 0.01	93
Blood	<0.1	<0.1	
Blood	0.63 ± 0.06	0.60 ± 0.01	105
Blood	1.16 ± 0.13	1.10 ± 0.01	105
Blood	0.50 ± 0.04	0.50 ± 0.01	100
Blood	0.43 ± 0.01	0.45 ± 0.01	96

Regarding the results, a recovery higher than 90 % (except for one sample) was obtained in all cases. A very interesting result is that no difference was found for the prediction of Li in serum or blood. This is certainly a huge advantage, because it means that the blood matrix components are not interfering and the analysis can be performed without a preliminary separation. It should be also considered that, although we do not have actual data, Li is often administered with other drugs, none of which seem to have interfered in the determination. More studies are necessary to fully assess possible interferences from drugs. Figure 6.8 shows the comparison between the values obtained for both methods, paper potentiometry and AES. The correlation with the joint confidence region test shows no significant difference between the values at a confidence level of 95 % ($F_{calculated}$=3.03; $F_{tabulated}$=4.46).

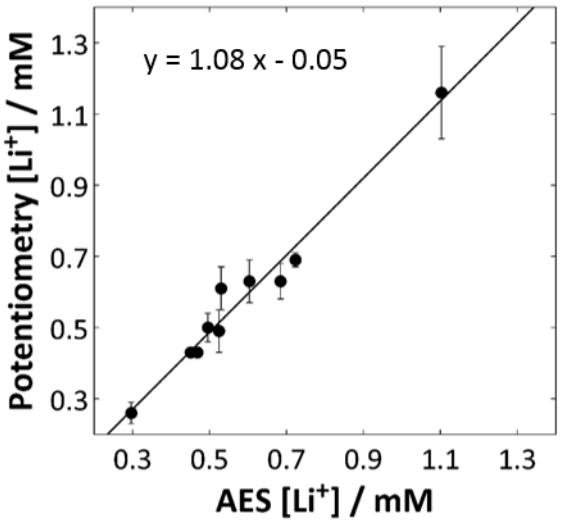

Figure 6.8. Prediction of Li^+ concentrations (mM) in real samples determined by the miniaturised paper cell and AES. AES error bars cannot be seen due to its magnitude (<0.01 mM).

Several features of this cell can be further improved. This device was presented as a proof of principle, but further optimization on the cell volume and miniaturization of the electrodes can still be achieved. Regarding the operation, it has been already shown that disposable potentiometric sensors can work reliably with a 1 point calibration solution. In this case, the manufacturing of the electrodes is not yet ready to achieve so much reproducibility, and the minimization of risks may imply that a 2 point strategy is still preferred. Last, but not least, the simplicity of the potentiometric technique is another very interesting feature of this approach. In the following chapter, the use of a miniaturized (credit-card sized) wireless potentiometer in combination with ISEs is presented[28]. This device would be certainly a perfect addition for a point-of-care Li determination system.

6.5 Conclusions

This work has presented the successful development of a paper potentiometric cell for the determination of lithium in whole blood and serum samples. The method is extremely simple and low cost, and the results obtained can be compared with those obtained with more sophisticated lab-based approaches, such as AES. Among the most attractive features, the system works with only one drop (50 µL), it can work on whole blood (so no complicated separation steps are required) and it is relatively fast. Therefore, it can be an ideal addition to the growing field of paper-based analytical platforms.

Above all, the work is a proof of concept of the approach suggested at the beginning of this work. Indeed, while scientific research is necessary to detect rare diseases, it is also true that new tools for the management of conventional, well-established conditions are increasingly required. Therefore, although potentiometry cannot compete in terms of limits of detection with many other electroanalytical tools, this work clearly shows that there is still enough room for it to become a powerful tool for the emergent trends of telemedicine and remote healthcare management.

6.6 References

(1) Licht, R. W. *CNS Neurosci. Ther.* **2012**, *18*, 219–226.

(2) Christian, G. D. *J. Pharm. Biomed. Anal.* **1996**, *14*, 899–908.

(3) Christian, G. D. *Sensors* **2002**, *2*, 432–435.

(4) Hopkins, S.; Gelenberg, J. *Bipolar Disord.* **2000**, *2*, 174–179.

(5) Parker, G. *Clin. Rev.* **2008**, 37.

(6) Shetty, S. J.; Desai, P. B.; Patil, N. M.; Nayak, R. B. *Biol. Trace Elem. Res.* **2012**, *147*, 59–62.

(7) Gruson, D.; Lallali, A.; Furlan, V.; Taburet, A. M.; Legrand, A.; Conti, M. *Clin. Chem. Lab. Med.* **2004**, *42*, 1066–1068.

(8) Christenson, R. H.; Mandichak, J. J.; Duh, S. H.; Augustyn, J. M.; Thompson, J. C. *Clin. Chim. Acta* **2003**, *327*, 157–164.

(9) Thompson, J. C. *Clin. Chim. Acta* **2003**, *327*, 149–156.

(10) Glazer, W. M.; Sonnenberg, J. G.; Reinstein, M. J.; Akers, R. F. *J. Clin Psychiatry* **2004**, *65*, 652–655.

(11) Rumbelow, B.; Peake, M. *Ann. Clin. Biochem.* **2001**, *38*, 684–686.

(12) Price, C. P. *Clin. Rev.* **2001**, *322*, 1285–1288.

(13) Vrouwe, E. X.; Luttge, R.; Olthuis, W.; van den Berg, A. *Electrophoresis* **2005**, *26*, 3032–3042.

(14) Vrouwe, E. X.; Luttge, R.; van den Berg, A. *Electrophoresis* **2004**, *25*, 1660–1667.

(15) Vrouwe, E. X.; Luttge, R.; Vermes, I.; van den Berg, A. *Clin. Chem.* **2007**, *53*, 117–123.

(16) Floris, A.; Staal, S.; Lenk, S.; Staijen, E.; Kohlheyer, D.; Eijkel, J.; van den Berg, A. *Lab Chip* **2010**, *10*, 1799–1806.

(17) Bakker, E.; Pretsch, E. *Angew. Chem. Int. Ed.* **2007**, *46*, 5660–5668.

(18) Wang, J. *TrAC, Trends Anal. Chem.* **2002**, *21*, 226–232.

(19) Coldur, F.; Andac, M. *Sens. Lett.* **2011**, *9*, 1738–1744.

(20) Coldur, F.; Andac, M.; Isildak, I.; Saka, T. *J. Electroanal. Chem.* **2009**, *626*, 30–35.

(21) Gupta, V. K.; Chandra, S.; Agarwal, S.; Lang, H. *Sens. Actuators, B* **2005**, *107*, 762–767.

(22) Kimura, K.; Oishi, H.; Miura, T.; Shono, T. *Anal. Chem.* **1987**, *59*, 2331–2334.

(23) Crespo, G. A.; Macho, S.; Bobacka, J.; Rius, F. X. *Anal. Chem.* **2009**, *81*, 676–681.

(24) Crespo, G. A.; Macho, S.; Rius, F. X. *Anal. Chem.* **2008**, *80*, 1316–1322.

(25) Novell, M.; Parrilla, M.; Crespo, G. A.; Rius, F. X.; Andrade, F. J. *Anal. Chem.* **2012**, *84*, 4695–4702.

(26) Bakker, E.; Pretsch, E.; Bühlmann, P. *Anal. Chem.* **2000**, *72*, 1127–1133.

(27) Guinovart, T.; Crespo, G. A.; Rius, F. X.; Andrade, F. J. *Anal. Chim. Acta* **2014**, *821*, 72–80.

(28) Novell, M.; Guinovart, T.; Murkovic Steinberg, I.; Steinberg, M.; Rius, F. X.; Andrade, F. *Analyst* **2013**, *138*, 5250–5257.

UNIVERSITAT ROVIRA I VIRGILI
PAPER-BASED POTENTIOMETRIC PLATAFORMS FOR ESCENTRALISED CHEMICAL ANALYSIS.
Marta Novell Recasens
Dipòsit Legal: T 1462-2015

CHAPTER

7

INTEGRATION OF THE POTENTIOMETRIC PAPER CELL WITH A RFID POTENTIOMETER

UNIVERSITAT ROVIRA I VIRGILI
PAPER-BASED POTENTIOMETRIC PLATAFORMS FOR ESCENTRALISED CHEMICAL ANALYSIS.
Marta Novell Recasens
Dipòsit Legal: T 1462-2015

7.1 Summary

The previous chapters have dealt with the development of sensors that can adapt to the challenges of the decentralised chemical analysis. The line of thinking of this thesis unfolds with an increasing level of integration: first the conductive paper, then the paper-based ISE, thereafter the whole paper-based potentiometric cell. Therefore, it is unavoidable to discuss the problem of signal detection and transmission. This chapter presents a novel radio frequency identification (RFID) potentiometer that can be used in combination with ISEs. Clearly, as with sensors, detection instruments must also adapt to those new scenarios. The combination of both areas is presented and discussed in this chapter, as a proof of principle of what a whole integrated device may look like in the future.

7.2 Introduction

As explained in the introduction, the explosive growth of mobile communication technologies over the last two decades created an increased social need for real-time access to (bio)chemical information. This need to generate data from vast and usually widespread points is creating a growing demand for robust, fast, simple and low-cost analytical devices. Two major and growing trends in healthcare -such as telehealth or point of care - require diagnostics tools that can be applied in a remote, decentralized fashion[1,2]. Similarly, environmental analysis, food production, homeland security, etc.[3,4] are also increasingly relying on this type of decentralized measurements. As disposable, low-cost sensors are quickly gaining terrain[5,6], efforts to develop instrumental approaches that can match simplicity and cost are needed. Additionally, as the world of smart objects –such as intelligent textiles- evolves[7], and sensors become embedded into objects, analytical instruments that can adapt to different environments and generate chemical data *in situ* will be required. All in all, to respond to these needs, the analytical sciences

must adapt and develop new detection strategies as well as new ways in which data is acquired, processed and transmitted[8].

From a detection point of view, potentiometric sensors have several advantages compared to other sensing approaches because of their simplicity of operation, low power consumption, wide linear dynamic range and robustness. The "*silent revolution*"[9] initiated almost two decades ago by solid-state technology, which led to massive improvements in the construction, operation and analytical performance of potentiometric sensors, has recently been enhanced by the use of nanomaterials[10], such as carbon nanotubes[11], gold nanoparticles[12] and graphene[13] as ion-to-electron transducers. Today, solid-contact (SC) ion-selective electrodes (ISE) are one of the preferred approaches to monitor the levels of different ions outside of the laboratory[14].

Developing effective solutions to monitor chemical substances outside the lab is a multifaceted challenge that requires looking at the whole analytical process, *i.e.* the performance, the cost and the simplicity of the whole procedure –from the measurement step to transmission and interpretation of the data- must be equally considered. Indeed, in a typical lab-based routine, samples are properly conditioned to be analysed by an instrument. This instrument-centred approach is not valid anymore for remote monitoring. Instead of the "one size fits all" instrument, outside the lab, it is the tool that must be adapted to fit the analytical problem. Therefore, as the demand for out-of-the-lab chemical sensing tools grows, a proliferation of different types of analytical devices that could monitor similar chemical parameters but show different contextual advantages are needed. In general, these "adaptive analytical tools" must follow some basic rules, such as reduced human intervention (particularly minimal skills required to operate the devices), reduced cost and small footprint. Evidently, traditional performance parameters that guarantee the reliability of these measurements are also of utmost importance.

Diamond *et al*. (WCSN)[15–19] have pioneered the development of autonomous devices in the form of wireless chemical sensing networks (WCSN). Ideally, in this approach a fully autonomous device can generate and wirelessly transmit the analytical data, creating a vast, widespread monitoring network. The concept is extremely attractive, since it should allow the gathering of real-time chemical data in a remote fashion, but it is not free from problems. Beyond certain technical issues –such as power requirements-, which are rapidly being addressed, the results show that chemical sensors for monitoring ions in solution need frequent re-calibration. This "chemical paradox"[18] is a major barrier when attempting to create truly autonomous analytical devices. Thus, semi-autonomous tools, where human intervention is minimized but still required, remain still a viable and necessary solution.

A key idea of the WCSN is to exploit the already existing vast data transmission networks, such as mobile phones (3G), WiFi, etc. A technology that has not been yet fully used, but that shows promise in the area of mobile analytics, is radio-frequency identification (RFID), an approach where data between two devices can be exchanged using a radio-frequency beacon signal. The technology is already widely used in transport logistics and has become the global standard for the tracking and unique identification of assets and items. In its most basic form, an RFID system comprises a base unit, or reader, and one or more transponder units (sometimes called RFID tags). The reader emits a radio-frequency beacon signal, which is absorbed by the tags and partially reflected back to the reader. This back-scattered signal contains the identification information (usually a unique number) stored on the tag in digital form. The reflected signal may also be used to geographically locate a tag's position by triangulation. Importantly, RFID tags can harvest the energy absorbed from the RF beacon field of the reader to energise themselves, and therefore do not need an independent power source, such as a battery, in order to operate (these are known as *passive* tags). Therefore, unlike some other wireless technologies, RFID tags are ultra-low-power devices which

may be miniaturized to dimensions smaller than a coin. They can provide digital data on demand and may be scaled-up to create star networks comprising up to 255 tags per one reader. The technology is low-cost, and tags can be manufactured on a mass scale. Although is less familiar than mobile or WiFi networks, radio-frequency identification is nowadays widely used to track items and people (*e.g.* hospital patients), and to grant access to buildings, etc. usually with tags in the form of smart cards or swipe cards[20]. Since high-frequency passive tags can only be read from a few centimetres distance, the technology has also been adopted for use in Near Field Communication (NFC). Very interestingly, NFC is being implemented on most new generation smart phones, and is being rolled out for a number of applications, including identification (*e.g.* in passports), and to perform cash-less payments (the e-wallet), etc. Thus, an RFID analytical tool could be easily read by a new generation smart phone. During the last few years, there have been some attempts to use RFID tags as analytical platforms through the chemical modification of the tag's radio antenna. This approach has been demonstrated for the detection of gaseous compounds, and water vapour, etc.[21–23].

A different way to exploit RFID technology is by conceiving the radiofrequency receiver (tag) as a miniaturized, low-power consumption radio transponder that can be coupled to an analytical instrument or sensor. In this way, by incorporating an analytical device into a RIFD tag, the instrument output can be remotely read. An RFID-enabled analytical device can be wirelessly access to program and set measuring parameters as well as to read the output signal. Recently, such an RFID (NFC) analytical electrochemical sensing platform has been developed[25]. This device is a credit card sized instrument that can perform autonomous electrochemical measurements (potentiometry, conductimetry, amperometry, etc.) and store the data into an internal memory. The device can be wirelessly accessed to read at any time with an RFID reader. This approach has also been demonstrated through the development of a radio-frequency tag with an optoelectronic interface[26], which has been applied to the colorimetric

determination of pH. The device can be either passive (batteryless) or battery-assisted when autonomous data logging to memory is needed. This type of device will be ideally suited for potentiometric detection, a technique where minimal external power is required to generate an analytical signal at the electrode. This platform thus opens the way to explore the advantages of combining modern solid contact-ion-selective electrode (SC-ISE) technology with radio-frequency potentiometers to generate miniaturized, autonomous and wireless analytical devices.

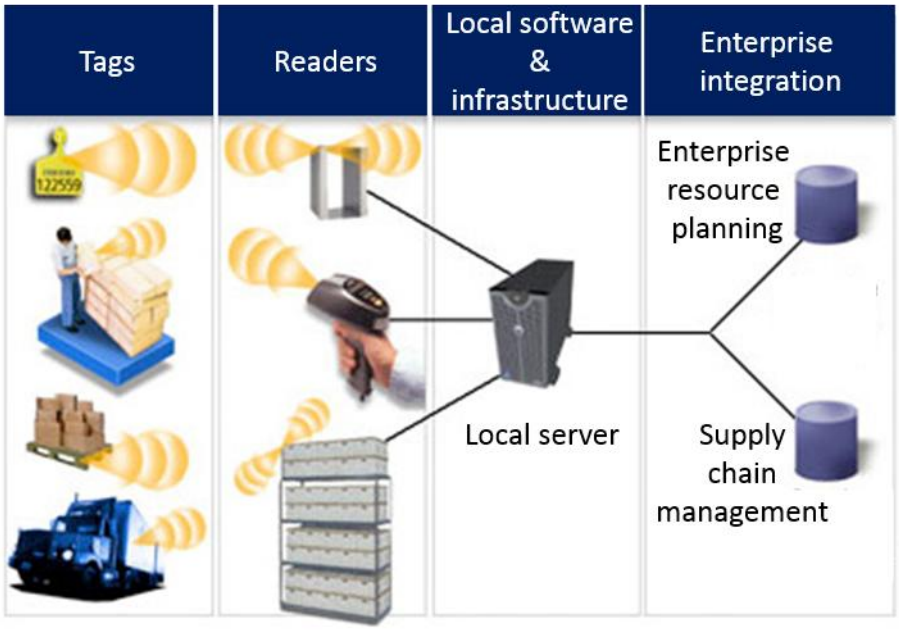

Figure 7.1. General RFID system[24]. RFID tags filled with information can be incorporated in any object. When these objects are inside the reader field, the information of its tag can be read and send to a local server, which at the same time can feed other areas such as the resource planning or the supply chain management.

This work explores the use of SC-ISEs in combination with an RFID potentiometer. Results of this novel combination are compared to measurements made with conventional potentiometers. The analytical performance for the determination of ions in liquid samples is compared with traditional approaches. Instrumental

performance in terms of noise, and short and long term stabilities are compared. Potential uses and applications, as well as future implementations, are discussed.

7.3 Experimental part

7.3.1 Electrode preparation

In this chapter GC electrodes were used, therefore, ion-selective electrodes were built with PVC membrane cocktails containing MWCNTs as described in the experimental part. Mirror-polished glassy carbon (GC) rod (3mm diameter, 50 mm length) were inserted in a Teflon body as described elsewhere[11] and 50 µL of the membrane cocktail were drop-casted onto the GC and let them dry for about two hours.

7.3.2 RFID potentiometer

The RFID potentiometer is a high frequency (HF) RFID contactless/wireless sensor node, model GoSense π-StatID™ (see Figure 7.2). The device works at an operating frequency of 13.56 MHz, has a data logger with a real time clock, 8 Kbit EEPROM (*Electrically Erasable Programmable Read-Only Memory)* memory (256 x 32-bit) and a programmable out-of-limits alarm function. It has an internal temperature sensor and an operating temperature ranging from -20 °C to 60 °C. The potentiometer has an input impedance of 100 GΩ, and a potential measurement range of ± 300 mV. An internal battery (3 V lithium coin cell, type CR1216) works as a power supply for the electronic components.

The potentiometer RFID-tag is the size of a credit card (8 cm x 5 cm x 0.1 cm) and has an approximate weight of 10 g. In the current design, the 10-bit ADC converter has a maximum resolution of 0.5865 mV, and a maximum sampling rate of 1.25 samples/s. The internal EEPROM memory allows for storage of up to 750 data points.

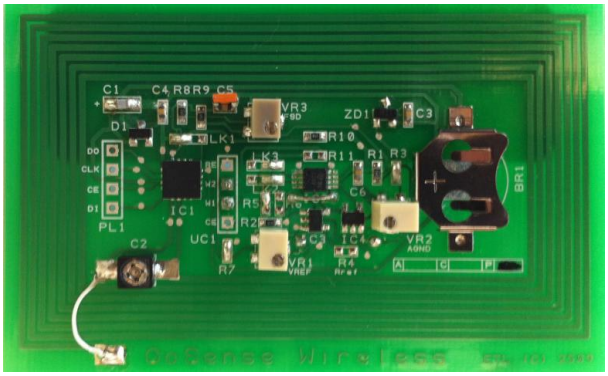

Figure 7.2. RFID potentiometer. Tag dimensions are 5.0 cm x 8.0 cm x 0.1 cm.

The working principle of this wireless potentiometer is illustrated in Figure 7.3. The potential difference (electromotive force) between the two electrodes is measured, converted to digital form, and then stored in the tag's internal memory. The stored data can be wirelessly retrieved at any time by bringing the reader and the tag within reading distance (a few centimetres in the case of this NFC device). This reading distance depends upon the power of the RFID reader, a low-power USB desktop reader can reach up to 5 to 7 cm while an industrial 7 Watt reader can read upon 100 cm. The RFID tag comprises several important components; a digital RFID chip with data logger and analogue input, an instrumentation amplifier potentiostat, and an RF antenna. The antenna receives the RF beacon signals from the reader and sends them to the digital RFID chip, which subsequently handles all of the RFID wireless protocol and data exchange. An instrumentation amplifier provides a high input impedance buffer between the ion-selective electrode and the analogue to digital converter (ADC) in the RFID chip. This ADC is one of the most crucial component of the potentiometer, since it must allow the work under nearly zero current conditions. Sequential potential measurements acquired and stored in the RFID chip's memory are read out through the antenna back to the RFID reader. Finally, the RFID reader decodes the digital measurement data received back from the tags and sends it to a computer via USB for display on a voltage-time chart.

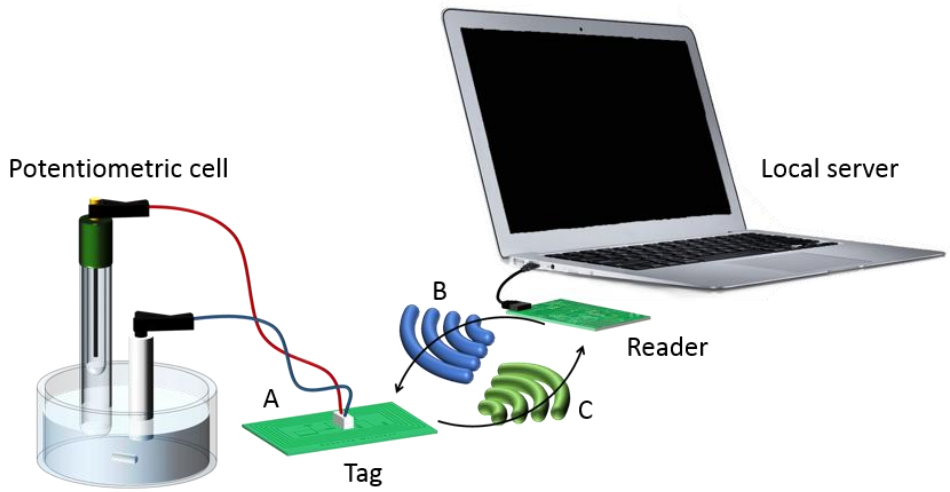

Figure 7.3. Illustration of the working principle of the RFID potentiometer. A: The potentiometric tag reads and store the data; B: while in proximity, the reader sends a radiofrequency signal to the tag; C: The backscattered radiofrequency signal contains information about the tag identification and the stored chemical data.

7.3.3 Measurement procedure

In order to evaluate the analytical performance of this new device, three different potentiometers (see Table 7.1) were used to record the electromotive force (EMF): a high input impedance (10^{15} Ω) EMF16 multichannel data acquisition device (Lawson Laboratories, Inc. Malvern); a Keithley 6514 electrometer (input impedance 10^{14} Ω) and the GoSense π-StatID™ potentiometer (input impedance 10^{11} Ω, as described in the previous section). The potential readings were simultaneously recorded for all the devices. Preliminary tests were performed by sequentially disconnecting devices, to verify that they did not interfere each other with the measurements. No cross-talk or interference between devices was found.

Atomic emission spectrometry (AES) (Unicam Solar 969,) was used as a reference method to which the potentiometric measurements were compared. Six standard solutions between 0.05 and 0.5 mg/ml have been used to establish a regression line and calculate the Mg^{2+} concentration of the tested samples by AES. Five

commercial water samples and three local tap waters were used for the determination of magnesium and potassium.

Table 7.1. Potentiometer specifications.

	Lawson	**Keithley**	**GoSense RFID**
Size (cm)	20 x 23 x 6	35 x 22 x 10	5 x 8 x 0.1
Channels	16	1	1
Input impedance (Ω)	10^{15}	10^{14}	10^{11}

7.4 Results and discussion

7.4.1 Wireless sensor platform

As shown in Figure 7.3, the measurement platform consists of the RFID reader, which is connected to a computer via USB cable, and the credit card sized RFID potentiometer, where the reference and ion-selective electrodes are connected. Software control (see Figure A 7.1 in the additional information of this chapter) allows programming of certain tag parameters, such as the sampling frequency, the logging interval and the delay time before the tag starts reading and recording.

The potentiometer settings can be wirelessly accessed through the reader. Once programmed, the potentiometer can easily be moved around or positioned anywhere as needed, and data recording will start at the pre-programmed time. In this way, this small unit can act autonomously, collecting and storing electrode data, which can later be uploaded to the computer once the reader and the potentiometer are within read range of one another. Once the tag data has been read, the memory can be cleared to free up storage space for subsequent experiments.

7.4.2 Instrumental performance: noise levels, short and long term stability and accuracy of potential measurements

First trials were performed to evaluate the instrument noise levels, short and long term stability, and robustness. The instrument was located in different places, inside and outside the lab, in order to verify the sensitivity of the electronic components to movement or external sources of noise. Trials were first made without electrodes –in order to identify sources of noise that may affect the instrument alone-, and then with the electrodes connected and immersed in water. In some experiments, the instrument was set to read potential every one second while being carried in a pocket. Interestingly, some measurements were also performed while the RFID potentiometer was inside a closed vessel, and the reading was wirelessly performed through walls of plastic, glass or cardboard container.

In all cases, the short term noise level registered for the potentiometer was in the 0.59 mV range, *i.e.* the bit noise limited by the ADC resolution. This value is higher than that obtained for the conventional potentiometers, but is acceptable for some remote field or mobile applications. It can be expected that further improvements to the detection electronics of the device should address these features. The values obtained for the long term stability of the device with and without electrodes are not significantly different from the values obtained for the short term stability, indicating that there is no drift or long term fluctuation. The readings show that the instrumental response is not affected by movement and by exposure to different environments, which is important when dealing with industrial, domestic and other out-of-lab applications or scenarios.

The accuracy of the voltage reading was evaluated by connecting a regulated power supply, which was measured with both a Keithley electrometer and the RFID potentiometer. Figure A 7.2 in the additional information of this chapter shows that the RFID potentiometer can trace the voltage changes in an accurate way. It is

important to stress that the potentiometer was originally calibrated in the factory and arrived at the lab in an envelope sent through conventional mail. No additional calibration of the tag potentiostat was performed.

Noise levels, short and long term stability of the device do not significantly differ from conventional instruments, and are so far appropriate for performing field-based measurements.

7.4.3 Chemical sensors response

As a proof of principle, solid contact ISE for potassium and magnesium ions were used. The work was focused on assessing the analytical performance of the RFID device under different experimental conditions, by comparing the results obtained with three different potentiometers and, in the case of real samples, also against a referee method. First, electrodes were immersed in water and data was recorded until stable readings were obtained (usually within a few seconds). No significant differences in the stabilization time were obtained between devices. Baseline readings are offset a few mV between potentiometers, but this is not relevant for these experiments. After stable readings were obtained, the EMF variation with the increasing additions of the primary analyte for the two target ions (K^+ and Mg^{+2}) was recorded (see Figure 7.4), and analytical parameters were evaluated (see Table 7.2). Evidently, as this first generation RFID potentiometer is a single-channel device, experiments were performed sequentially for each ion.

The inset of Figure 7.4 shows a detail of the superimposed time trace signals for the different potentiometers. Despite the better time and voltage resolution obtained with the conventional devices, it can be clearly seen that the RFID potentiometer accurately tracks the variations of potential as a function of time. No additional time-constants –and more importantly- no significant bias in the potential readings are introduced by the use of the RFID device. Analytical responses for K^+ and Mg^{2+} show in all cases a Nernstian slope of around 56 mV/dec in the first case, and 28 mV/dec in the second case. The linear ranges obtained were between 10^{-5} M to 10^{-1}

M. Standard deviations of the values obtained for repetitions of 3 measurements of each concentration ion are usually well below 5 mV (thus error bars cannot be seen in the graph).

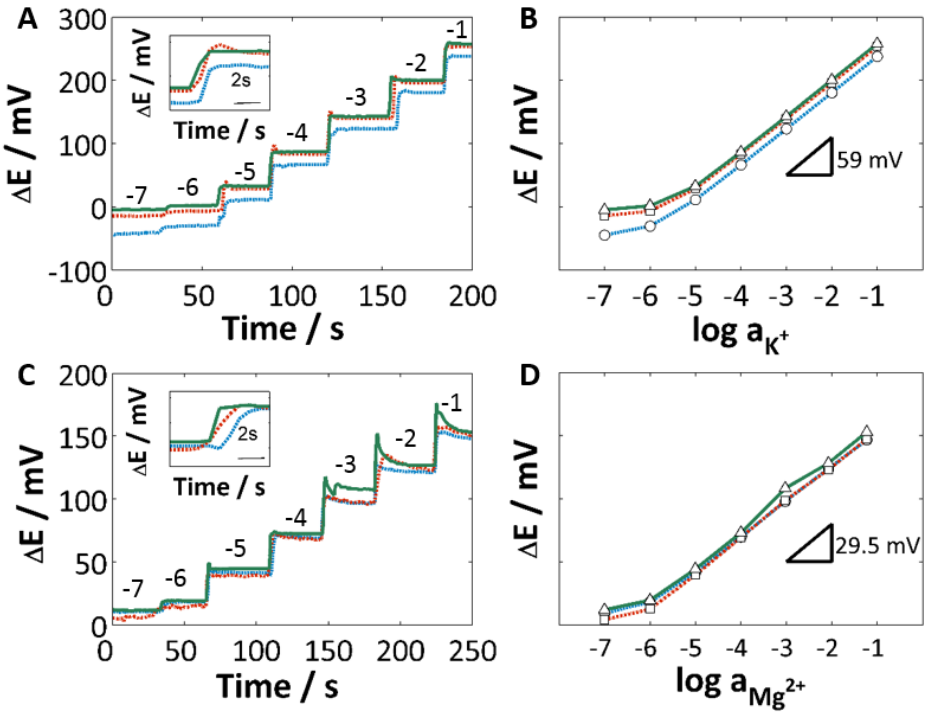

Figure 7.4. Potentiometric response for three different potentiometers (--, blue) Keithley, (-·-, red) Lawson and (-, green) GoSense RFID. Plots show the EMF response over time with increasing concentrations of the primary analyte (left) and the corresponding calibration plots (right) for (A, B) K^+-SC-ISE and (C, D) Mg^{2+}-SC-ISE. On the plots A and C, the inset shows a detail of the superimposed trace signals, and the numbers represent the logarithm of the primary analyte concentration at each step. The triangles on the plots B and D show the magnitude of the Nernstian slope.

Table 7.2. Analytical parameters of K^+-SC-ISE and Mg^{2+}-SC-ISE obtained with the three potentiometers. Stability values have been calculated in a 10^{-4} M solution of the primary analyte for 12h.

Potassium	**Lawson**	**Keithley**	**GoSense RFID**
Sensitivity (mV/dec)	56.70 ± 0.35	56.32 ± 0.38	56.05 ± 0.53
Linear range (M)	10^{-5} – 10^{-1}	10^{-5} – 10^{-1}	10^{-5} – 10^{-1}
Limit of detection (M)	1.32 x 10^{-6}	1.81 x 10^{-6}	2.76 x 10^{-6}
Stability (mV/h)	0.42	0.95	0.25

Magnesium	**Lawson**	**Keithley**	**GoSense RFID**
Sensitivity (mV/dec)	28.16 ± 0.56	28.04 ± 0.16	28.39 ± 0.48
Linear range (M)	10^{-5} – 10^{-1}	10^{-5} – 10^{-1}	10^{-5} – 10^{-1}
Limit of detection (M)	9.49 x 10^{-7}	8.59 x 10^{-7}	9.58 x 10^{-7}
Stability (mV/h)	0.37	0.21	-0.29

Slopes of the regression lines obtained with the three potentiometers have been compared using a t-test, in pairs (Keithley *vs.* Lawson; Keithley *vs.* RFID; and Lawson *vs.* RFID). Residual variances between the potentiometers for potassium measurements were found to be equal using an F-test, so the appropriate t-Test was then used. In all cases, no statistically significant differences between the slopes were found. Regarding the magnesium measurements, residual variances between potentiometers were also equal except for the pair Keithley-RFID, where an approach similar to the Cochran test[27] was employed to obtain the t value. The results also indicate non-statistically significant differences between potentiometers (see statistical tests in the additional information of this chapter).

One of the “litmus tests” of a good potentiometer is to have the input impedance high enough to work under virtually zero current conditions. As shown by the Nernstian response obtained in the calibration plots, and the lack of drift of the measurements, this requirement is fulfilled by the RFID potentiometer. All in all,

the results clearly show that the RFID device can be used for potentiometric measurements without significantly affecting the analytical performance. Although small and portable potentiometric devices already exist, three interdependent factors make this approach unique: a) reduced size, b) low power consumption and c) wireless radio-frequency data transmission. The reduced size of the device is in part due to the fact the instrument has been stripped-down of all non-essential components. The ability to wirelessly access through a computer makes that the instrument lacks of electronic components to program and setting parameters (keyboards, controls, etc). Also displays have been eliminated. This reduces the footprint and also the power requirements of the device. A small battery is used for powering the operational amplifier, electronic circuits and data storage during autonomous sampling. This is not a minor feature, since the problem of energy consumption in portable or autonomous devices is a major issue. For this reason, RFID/NFC is an ideal approach. Alternative wireless data transmission systems –such as the cell phone network (3G) or Wi-Fi transmitter- require much higher powers. Since the RFID tag uses energy harvested from the radio-frequency signal from the reader, no additional power is required for data transmission. All in all, the combination of size, ultra-low-power consumption and NFC becomes an ideal marriage for mobile, field-based, semi-autonomous devices. It should only be added that potentiometry is the ideal analytical technique to further compliment all these features.

In all the experiments performed, the device does not show any sort of compromise in the analytical parameters –beyond the limitations of the electronic components in terms of time or signal resolution-. Sensitivity, linear ranges, limits of detection (LODs) and reproducibility are comparable in all the devices tested, and therefore seem to be essentially limited by the electrode's performance and not by the detection unit. It is true that potentiometric sensors can reach better LODs with careful control of the experimental conditions, but these experiments have served as proof of principle.

An alternative test was performed to evaluate the ability of the RFID potentiometer to respond to changes in concentration and whether the signal will return to baseline. To do so, solutions of 10^{-2} M and 10^{-7} M of $MgCl_2$ were alternatively measured for ten times (see Figure 7.5).

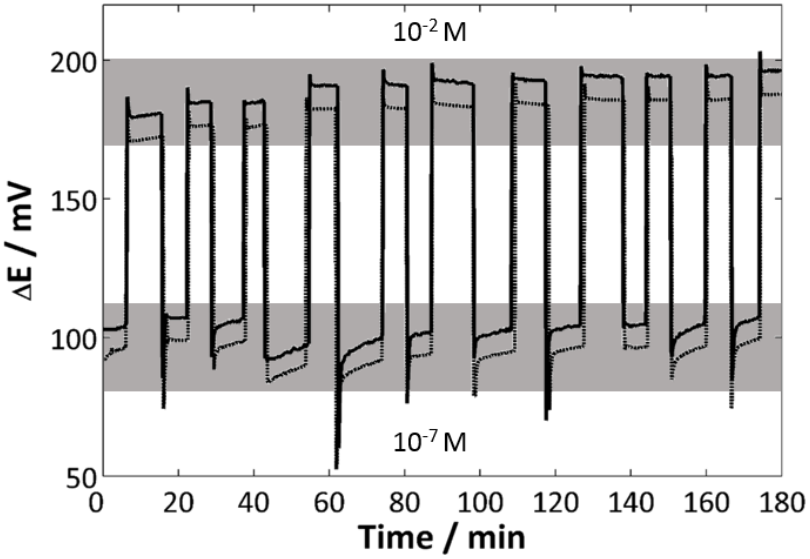

Figure 7.5. Time evolution of the potentiometric response in consecutive solutions of 10^{-7} M and 10^{-2} M of $MgCl_2$ with (-) RFID and (--) Keithley.

The sequence of values obtained for the RFID potentiometer do not show any significant different, indicating the absence of drift. Furthermore, baseline-subtracted values for both potentiometers (RFID and Keithley) were subject to a one-way ANOVA test and non-significant differences were found (see statistical tests in the in the additional information of this chapter).

A further evaluation of the dynamic response of the RFID potentiometer and the ability to track changes in concentration as a function of time was performed by immersing the electrodes in a 20 ml well stirred flow cell. This cell was continuously fed with a 10^{-2} M solution of $MgCl_2$ (Figure 7.6) and, at a given time, this feeding solution of $MgCl_2$ was replaced by water. Under these conditions, the cell is washed

in an exponential fashion, so the potentiometric response as function of the time should be almost linear. The responses obtained by the RFID and Keithley potentiometer were compared in terms of response time. No statistically significant differences were detected between the two voltage-time curves (see statistical tests in the in the additional information of this chapter).

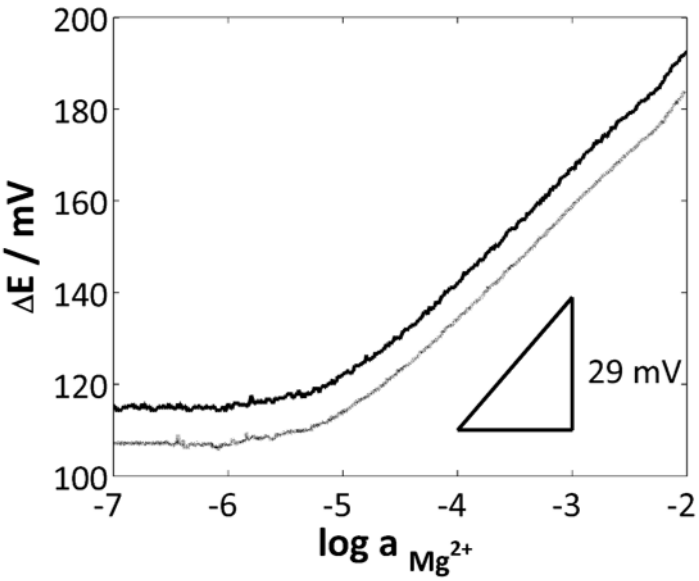

Figure 7.6. Dynamic response of (-) Keithley and (-) GoSense RFID potentiometers starting from 10^{-2}M of $MgCl_2$.

Time evolution of the electrodes has also been tested; medium term (12 h) drifts obtained are less than 1 mV/h in all the cases being the electrode immersed in a solution of 10^{-4} M of the primary analyte concentration. These stability values improve with higher concentrations of the primary analyte. In a long term test, sensitivity values of the calibration curve of the electrodes remain with a standard deviation less than 1 mV, which is acceptable for this type of electrode in field applications.

Time-based characteristics of the RFID potentiometer itself have also shown no limitations. The device has not shown any particular drift due to capacitive

coupling, and the response to rapid changes in concentration was comparable to that shown by the other conventional devices. It must be stressed that the potentiometric sensors usually show a response time in the order of several seconds, thus the rate-limited sampling frequency of the RFID device of 1 sample/s is not a serious limitation. Also, the combination of this device with the SC-ISE using carbon nanotubes as transducers seems an ideal option, taking into account that these sensors display great stability and robustness (light and redox insensitivity, etc), which is ideal for field measurements[28].

7.4.4 Measurements of real samples

The magnesium content of eight different drinking waters was determined with atomic absorption spectroscopy and potentiometry (with both, Keithley and RFID potentiometers). Values obtained with AAS were taken as reference values and compared to the ones obtained by potentiometry (see Figure 7.7 and Table 7.3).

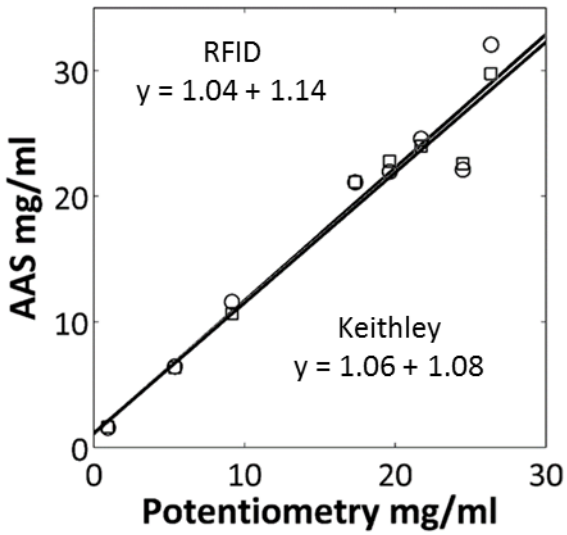

Figure 7.7. Concentration of Magnesium (mg/ml) in water samples obtained by AAS and Potentiometry: (○) Keithley and (□) GoSense RFID tag. The plot also shows the regression lines of the values found against the AAS approach for both devices.

The relative percentage error between values obtained by AAS and each one of the potentiometers were usually less than 20 % (except for Bezoya water, which was around 75%). Whereas the relative percentage error between the potentiometers was less than 10 % in all samples, and in most cases less than 5 %.

Table 7.3. Values of Magnesium concentration in mg/ml obtained with AAS, RFID and Keithley potentiometers.

Sample	AAS	Keithley	GoSense RFID
Font Vella	9.17	11.59	10.66
Bezoya	0.94	1.57	1.64
Fuen Mayor	17.35	21.11	21.13
Viladrau	5.37	6.44	6.32
Solan de Cabras	24.48	22.11	22.60
Reus	21.70	24.58	23.97
Tarragona	19.63	21.95	22.78
El Catllar	26.36	32.07	29.74

Regarding the applications of the device in real scenarios, the determination of magnesium in drinking waters has demonstrated that the RFID potentiometer can be a good addition to classical, lab-based approaches, since in all cases, no significant bias has been observed between any of the potentiometric measurements. The concept of “vanguard” analytical approaches -coined by Valcárcel *et al.*[29]- fits very well with this RFID potentiometer. For these tools that can act as a “first line of attack” of a given problem, speed, simplicity and cost are key components of the analytical performance. The differences found between AAS and potentiometric measurements seem more a characteristic of the technique rather than the device. Indeed, independently of the instrument used, similar bias between potentiometric methods and AAS was found. It is well known that the potentiometric measurement responds to the activity of the target species, and therefore it will be affected by matrix composition. This apparent disadvantage

could be turned into a powerful advantage when dealing with speciation problems[30].

7.4.5 Future applications

This device opens a plethora of possibilities and future applications as a tool for decentralized analytical measurements. The reduced size, autonomy and the wireless access to data provides significant flexibility in adapting to different analytical scenarios. For example, it can be used as a highly portable chemical data logger for tracking changes in chemical properties of food in transport. Also, an area of growing interest is the development of smart objects, in particular smart textiles. As wearable chemical sensors are quickly being developed[7,31,32], instruments that can be worn while minimizing the disruptions to the end user are crucial. The RFID potentiometer will be an ideal tool for these kinds of situations.

Last, but not least, a unique –and very attractive- feature of this device is the ability to communicate wirelessly through a container wall or packaging that can be made from glass, plastic, wood, paper, textile, etc. Figure 7.8 A shows a schematic view of an experiment in which the RFID potentiometer fitted with an ISE and a reference electrode were placed inside a large vessel containing a 10^{-3} M solution of a target ion. The vessel was closed and the concentration of the solution was smoothly raised to a final value of 10^{-2} M of the target species. The reader of the potentiometric RFID tag was from time to time approached to the walls of the container. The results can be seen in Figure 7.8 B, where the curve of potential as a function of time shows a total increment in the signal of about 55 mV, which correspond to the change of one order of magnitude in concentration. The spikes observed in the graph correspond to the moment in which the reader approaches and connects to the tag (just phantom spikes). This plots shows clearly that the measurement obtained does not correspond to a single point (when the potentiometer is read), but to all the time series stored in the device. This ability to

be read in a simple and robust fashion through textiles, cardboard, etc., opens a very interesting avenue for future applications.

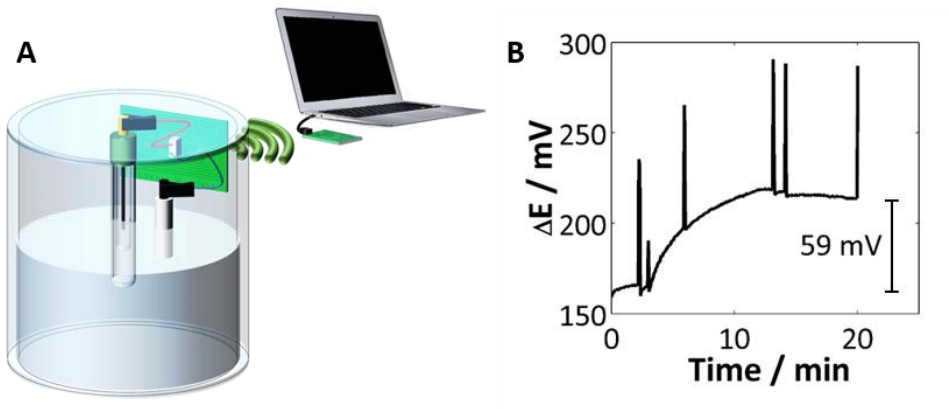

Figure 7.8. Reading the RIFD tags through the glass walls of a vessel. A: illustration of the experimental setup where the tag and sensors are floating inside the closed vessel with a 10^{-3} M solution of the target ion. B: time traces of the signal as a function of the time for a change of one order of magnitude in the concentration. The spikes in the signal indicates the time the reader connects with the tag.

It should be stressed that most of the practical and analytical limitations of this device found in this work are mostly due to the architecture of the electronics, such as resolution of the ADC, memory size, sampling rate, etc. All of these features are easily scalable and can be changed and improved so as to allow next generation RFID tags to achieve further reductions in size, increased number of measuring channels, wider measuring range, higher resolution and faster sampling rates. Furthermore, as NFC is fast becoming the global standard for non-contact device communication (e-wallet, identification, etc.), all smart phones are quickly moving towards incorporating RFID/NFC reading capabilities. This will further enhance the applicability and usefulness of this RFID-potentiometric tag in a broader social context, especially as the internet-of-things develops.

7.5 Conclusions

As once stated by Sir Humphry Davy, *"Nothing begets good science like the development of a good instrument"*[33]. In a time when the need for the generation of chemical information on site on time is quickly rising, novel analytical tools that can cope with speed and simplicity are required. This work has demonstrated the analytical features of an RFID potentiometer using solid-contact ion-selective electrodes. It has been shown that this device works in a comparable way to classical potentiometers, opening new possibilities for potentiometric measurements. Several practical advantages –such as small size, low weight, non-contact reading and programming capabilities and insensitivity to external sources of noise– make this device ideal for use in out-of-the-lab and mobile applications. Furthermore, as the near field communication technology becomes more and more common, the ability to read the potentiometer directly from a mobile phone will increase its range of applications. On the other hand, some drawbacks of the approach should be also mentioned. First, the need to read the instrument from a close (few cm) distance may be an obstacle for some applications. Second, the potentiometric system requires periodical recalibration –thus needing human intervention- and the device shows a limited autonomy due to small internal battery. All in all, some of the main characteristics of this RFID-potentiometer have been illustrated through the determination of magnesium ions in real samples, which clearly show the reliability of the system. Evidently, these determinations were used as a proof of principle, but the evidence suggests that similar results should be obtained with other membrane-based SC-ISE. The way in which this device could be integrated into other platforms, such as large-scale wireless sensor networks, is still open to exploration. Evidently, there are still several challenges to face regarding the widespread on-site use of this device. The robustness of the data generated by the systems is –from an analytical perspective- one of the most important ones. The combination of this RFID potentiometer with other types of

SC-ISEs (such as disposable paper electrodes) has also lead to satisfactory results. Also, these new platforms could find potential use in wearable sensing devices, medical diagnostics, intelligent packaging, food and environmental monitoring, just to name a few examples.

7.6 Additional information

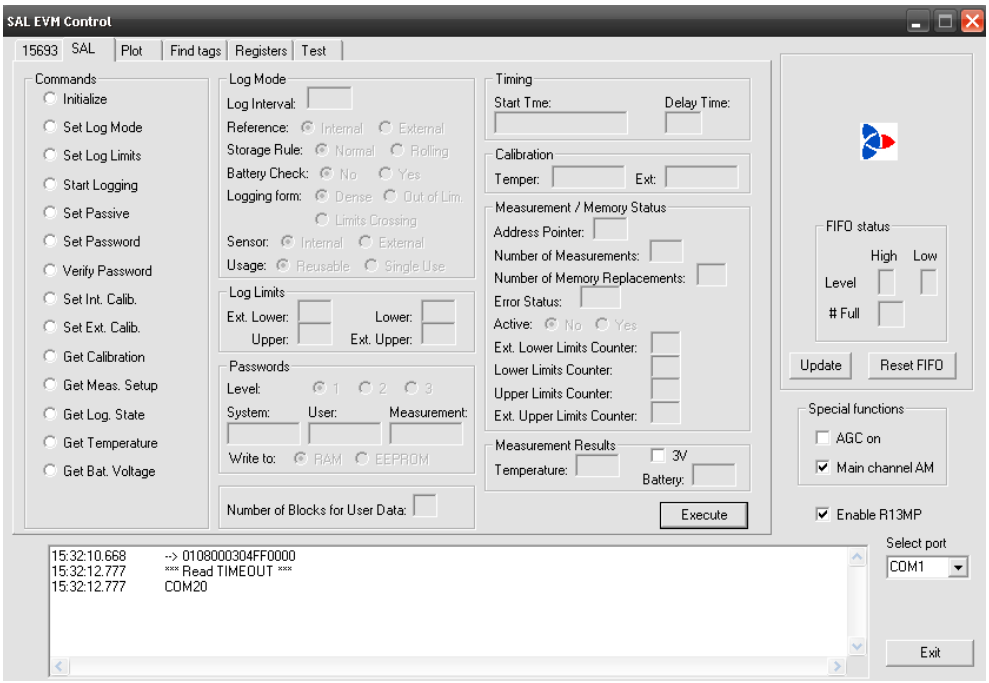

Figure A 7.1. Software control window. It allows the control of many variables, such as the logging interval, the sampling frequency (delay time in the software), the starting time of the measurement, limits outside which no data is recorder, etc.

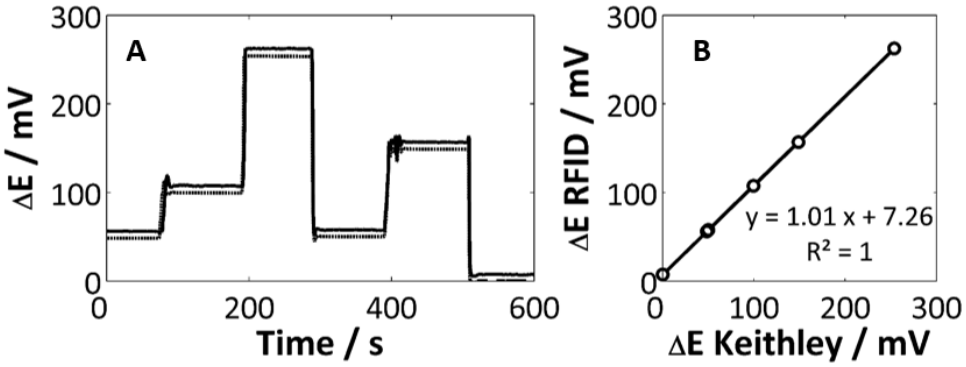

Figure A 7.2. A) Potential trace of (--) Keithley and (-) GoSense RFID read from a regulated power supply. B) Comparison between both potentiometers.

Statistical tests:

1. T-test for slopes of Figure 7.4 (B and D).

K: $t_{(Keithley\ vs.\ Lawson)}$ =0.59 ; $t_{(Keithley\ vs.\ RFID)}$ = 0.31; and $t_{(Lawson\ vs.\ RFID)}$ = 0.92; with $t_{(0.025,6)}$ = 2.45.

Mg: $t_{(Keithley\ vs.\ Lawson)}$ =0.35 ; $t_{(Keithley\ vs.\ RFID)}$ = 0.61; and $t_{(Lawson\ vs.\ RFID)}$ = 0.35; with $t_{(0.025,6)}$ = 2.45.

2. ANOVA for values in Figure 7.5.

$F_{(10^{-7}M)}$=0.007 and $F_{(10^{-1}M)}$=0.024; with $F_{(0.05,9)}$=4.414.

3. T-test for slopes of Figure 7.6.Figure 7.6

$t_{(Keithley\ vs.\ RFID)}$ = 0.64; with $t_{(0.025,\infty)}$ =1.96.

7.7 References

(1) Price, C. P. *Clin. Rev.* **2001**, *322*, 1285–1288.

(2) Yager, P.; Domingo, G. J.; Gerdes, J. *Annu. Rev. Biomed. Eng.* **2008**, *10*, 107–144.

(3) Culler, D.; Deborah, E.; Srivastava, M. *IEEE Comput. Soc.* **2004**, *37*, 41–49.

(4) Murray, R. *Anal. Chem.* **2010**, *82*, 1569.

(5) Rius-Ruiz, F. X.; Crespo, A.; Bejarano-Nosas, D.; Blondeau, P.; Riu, J.; Rius, F. X. *Anal. Chem.* **2011**, *83*, 8810–8815.

(6) Jaworska, E.; Lewandowski, W.; Mieczkowski, J.; Maksymiuk, K.; Michalska, A. *Analyst* **2013**, *138*, 2363–2371.

(7) Windmiller, J. R.; Wang, J. *Electroanalysis* **2013**, *25*, 29–46.

(8) Valcárcel, M.; Lucena, R. *TrAC, Trends Anal. Chem.* **2012**, *31*, 1–7.

(9) Bakker, E.; Pretsch, E. *Angew. Chem. Int. Ed.* **2007**, *46*, 5660–5668.

(10) Aragay, G.; Merkoçi, A. *Electrochim. Acta* **2012**, *84*, 49–61.

(11) Crespo, G. A.; Macho, S.; Bobacka, J.; Rius, F. X. *Anal. Chem.* **2009**, *81*, 676–681.

(12) Woźnica, E.; Wójcik, M. M.; Mieczkowski, J.; Maksymiuk, K.; Michalska, A. *Electroanalysis* **2013**, *25*, 141–146.

(13) Hernández, R.; Riu, J.; Bobacka, J.; Vallés, C.; Jiménez, P.; Benito, A. M.; Maser, W. K.; Rius, F. X. *J. Phys. Chem. C* **2012**, *116*, 22570–22578.

(14) Zhuiykov, S. *Sens. Actuators, B* **2012**, *161*, 1–20.

(15) Diamond, D. *Anal. Chem.* **2004**, *76*, 279–286.

(16) Diamond, D.; Coyle, S.; Scarmagnani, S.; Hayes, J. *Chem. Rev.* **2008**, *108*, 652–679.

(17) Diamond, D.; Lau, K. T.; Brady, S.; Cleary, J. *Talanta* **2008**, *75*, 606–612.

(18) Byrne, R.; Diamond, D. *Nat. Mater.* **2006**, *5*, 421–424.

(19) Vincenzini, P.; Diamond, D. *Wearable/Wireless Body Sensor Networks for Healthcare Applications*; Ltd., Trans Tech Publications: Switzerland, 2013.

(20) Xiao, Y.; Yu, S.; Wu, K.; Ni, Q.; Janecek, C.; Nordstad, J. *Wirel. Commun. Mob. Comput.* **2007**, *7*, 457–472.

(21) Ong, K. G.; Zeng, K.; Grimes, C. A. *IEEE Sens. J.* **2002**, *2*, 82–88.

(22) Potyrailo, R. A.; Morris, W. G. *Anal. Chem.* **2007**, *79*, 45–51.

(23) Potyrailo, R. A.; Mouquin, H.; Morris, W. G. *Talanta* **2008**, *75*, 624–628.

(24) www.rigzone.com/.

(25) Kassal, P.; Steinberg, I. M.; Steinberg, M. D. *Sens. Actuators, B* **2013**, *184*, 254–259.

(26) Steinberg, I. M.; Steinberg, M. D. *Sens. Actuators, B* **2009**, *138*, 120–125.

(27) Massart, D. L.; Vamndeginste, B. G. M.; Buydens, L. M. C.; De Jong, S.; Lewi, P. J.; Smeyers-Verbeke, J. *Handbook of chemometrics and qualimetrics*; Elsevier: Amsterdam, 1997.

(28) Crespo, G. A.; Macho, S.; Rius, F. X. *Anal. Chem.* **2008**, *80*, 1316–1322.

(29) Valcárcel, M.; Cárdenas, S. *TrAC, Trends Anal. Chem.* **2005**, *24*, 67–74.

(30) Bakker, E.; Pretsch, E. *TrAC, Trends Anal. Chem.* **2001**, *20*, 11–19.

(31) Yang, Y.-L.; Chuang, M.-C.; Lou, S.-L.; Wang, J. *Analyst* **2010**, *135*, 1230–1234.

(32) Malzahn, K.; Windmiller, J. R.; Valdes-Ramirez, G.; Schoning, M. J.; Wang, J. *Analyst* **2011**, *136*, 2912–2917.

(33) Hieftje, G. *Anal. Chem.* **2000**, *72*, 309A.

UNIVERSITAT ROVIRA I VIRGILI
PAPER-BASED POTENTIOMETRIC PLATAFORMS FOR ESCENTRALISED CHEMICAL ANALYSIS.
Marta Novell Recasens
Dipòsit Legal: T 1462-2015

CHAPTER

8

LIMITATIONS AND IMPROVEMENTS OF THE SENSORS

UNIVERSITAT ROVIRA I VIRGILI
PAPER-BASED POTENTIOMETRIC PLATAFORMS FOR ESCENTRALISED CHEMICAL ANALYSIS.
Marta Novell Recasens
Dipòsit Legal: T 1462-2015

8.1 Summary

From the substrate (conductive paper), to a whole instrumental approach, this work has increased the degree of integration of the analytical tools. In this chapter a general discussion about the reach and limitations of the work performed and the progress achieved so far -together with some proposals to overcome some of the drawbacks found- are proposed. Improvements on the electrode's performance -specially the LOD- is carried out. Also, an in-depth study of the reproducibility of the standard potential between electrodes is performed. The results show promise in terms of the possibilities to take paper-based sensors to perform field-based measurements.

8.2 Introduction

The work performed up to this point has shown the possibility of building a complete paper-based potentiometric cell, *i.e.* reference and working electrodes. This system, which has been proved to work for the most common cations, has been applied to real samples –such as water or blood- showing a performance similar to conventional ion-selective electrodes. However, there are still some problems to tackle with the paper electrodes in order to optimize their work as autonomous, out-of-the-lab analytical tools.

As mentioned in chapter 5, the LODs of the ISE-paper electrodes are slightly worse than other SC electrodes. Although the LODs obtained with paper ISEs are good enough for the applications in mind –disposable, cheap, decentralised sensors-, the improvement of this parameter must not be forgotten. For example, measuring traces of metals in drinking waters or blood requires submicromolar limits of detection[1]. Also, lower detection limits allow for sample dilution, which is an effective way to overcome some interference, particularly when dealing with electrode fouling. For this reason, soon after we first reported the paper-based

potentiometric sensors, many approaches to improve the LOD of ISEs (and paper ISEs) have been proposed. The use of strict conditioning protocols, sophisticated configurations[2] or modifications of the sensor inner solution[3] falls outside the concept of simple, cheap and disposable electrodes and therefore these solutions have not been investigated. However, the use of alternative substrates[4] or inks[5] to make the conductive papers, or different kinds of membranes[6] have resulted in some cases in a better LOD. One of the most promising systems is the one described by Menash *et al.*[6], where a gold layer and conducting polymer have been added over the CNT-paper described here. Moreover, they use an acrylate membrane instead of the conventional PVC membrane. With all these modification they reported a LOD of $1.1 \cdot 10^{-8}$ M for potassium ion in aqueous solution –more than one order of magnitude better than the obtained for the same ion paper-ISEs developed in this work-.

The improvement of the LOD is just one of the challenges that paper-ISEs must face to be really useful for "real world" applications. The biggest problem of potentiometric sensors –regardless their nature- is that they require calibration and re-calibrations. Calibrations are time-consuming and could be difficult to perform by non-trained users. In the envisioned applications where these paper-ISEs –POC and telemedicine- are considered to be used, the end user will not have enough training (or willingness) to perform such operations.

The two parameters needed for predicting the concentration of a species in a sample using potentiometric sensors are the sensitivity and the standard potential of the electrode. The scope of the calibration curve is to provide a robust estimation of these parameters. Usually, the sensitivity of the electrodes is very reproducible for a given batch. However, this is not the case for the standard potential, thus requiring individual calibration of each electrode. The "standard potential" is in fact a phenomenological coefficient that depends on many factors, that involves all potentials generated at the inner interfaces. Since these potentials

are unknown and change with time for a given electrode, a calibration before the measurement is required. If the standard potential could be controlled, either by fixing it to a known value or making it reproducible for each batch of electrodes, no calibration or one-electrode calibration per batch will be enough.

Several approaches to address this problem have been proposed. One of the most recent and nowadays popular is the control of the potential at the interface by introducing species with redox buffer capacity. The redox buffer will help to maintain a stable and reproducible potential in the presence of oxidizing or reducing impurities or when a small electrical current passes through the cell. The use of systems containing Ag^+/Ag^0 in epoxy resines[7,8] and mixtures of gold nanoclusters with different charge states[9] has shown to improve the reproducibility of the standard potential. However, the most promising system up to date is the one proposed by Zou *et al.*[10] which consists on the incorporation of a Co(II)/Co(III) redox couple inside the ISM and which has led to standard deviations of the E^0 between electrodes as low as 0.7 mV.

Other approaches take advantage of the use of conducting polymers as ion-to-electron transducers to control their redox state while controlling the interface potential and thus the E^0. Two recent and successful strategies proposed by Vanamo *et al.* use PEDOT(PSS) in the interface. One strategy consists on applying a current or a potential[11] to tune the conducting polymer redox state and the other one, short circuit the electrodes[12] to let them to reach an equilibrium between them.

The most promising ones for our paper system are those using the membrane modification with a redox buffer[10,13,14], the application of a potential to control the redox state of the interface[11] or the short circuiting of the electrodes[12] so they can equilibrate themselves.

In any case, eliminating the calibration or reducing it to its minimum –one electrode per batch- is a very important feature, since for real applications

calibration-free electrodes will be an important step forward. Just imagining a real scenario where an elder person is monitoring some ion blood levels –similarly to measuring sugar blood levels-, clearly shows that a previous calibration of the sensor -with all the steps involved- does not fall within the ideal expectations. Therefore if a batch of electrodes has a constant E^0, they can be factory calibrated and tagged somehow to allow the reader to know the calibration parameters.

For this reason, the next sections describe the exploration of improvements on the LOD, as well as approaches towards the development of calibration-free paper sensors.

8.3 Experimental part

8.3.1 Construction of different K^+-ISEs for improving the LOD

Modifications in the construction of the paper sensors -the nature of the conductive paper, the transducers and the membrane- have been carried out in order to explore their influence on the analytical response. Figure 8.1 shows the different modifications applied at each part of the sensor. The modifications have been tested individually but also combinations between them have been evaluated.

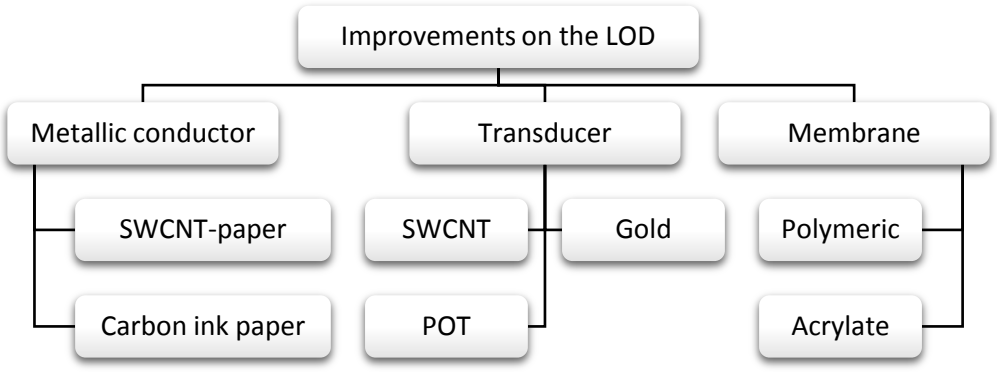

Figure 8.1. Scheme of the different parts of the sensor that have been modified to improve the LOD, and modifications used in each one.

Two different procedures to make conductive papers have been used:

1) painting a filter paper with SWCNT-ink (largely used during the thesis). In all cases “normal” conductive papers have been used. In some particular cases (clearly mentioned in the text) hydrophobic papers are employed.
2) using a commercial carbon ink. This procedure is as simple as spreading the ink with a squeegee over the paper.

Regarding the first procedure, two further modifications have been explored:

a) sputtering a layer of 50 nm of gold

b) depositing a layer of poly(3-octylthiophene) (POT) -12 µl of a solution of 25 mM POT in chloroform-.

Regarding the second procedure (modified with carbon ink) a layer of SWCNTs was also deposited by dropping 30 µl –3 drops of 10 µl- of a suspension containing 3.5 mg of SWCNT per 1 ml of THF.

Regarding the ion-selective membrane, three different ones have been used, which composition is shown in Table 8.1. As usual, 100 mg of each cocktail are dissolved in 1ml of THF. 15 µl of the membrane are drop casted onto the electrode following the usual procedure -3 drops of 5 µl-. Table 8.2 describes the electrode manufacturing approach, electrodes will be referred with their respective capital letter from now on.

Table 8.1. Composition of the membranes in wt %. KTClPB stands for potassium tetrakis (4-chlorophenyl) borate, NaTFPB for sodium tetrakis[3,5-bis(trifluoromethyl)phenyl]borate, PVC for poly(vinylchloride), DOS for bis(2-ethylhexyl) sebacate, ETH 500 for tetradodecylammonium tetrakis(4-chlorophenyl) borate and MMA-DMA is the copolymer methyl methacrylate and n-decyl methacrylate.

	Polymeric K^+-ISM	**Polymeric K^+-ISM with ETH 500**	**Acrylate K^+-ISM with ETH 500**
Valinomycin	2	1.7	1.7
KTClPB	0.5	0.4	0.4
NaTFPB			
PVC	32.8	32.2	
DOS	64.7	64.5	
MMA - DMA			96.7
ETH		1.2	1.2

Table 8.2. Composition of the electrodes tested.

	Paper modification			**Membrane**	
A	SWCNTs ink			Polymeric K^+-ISM	
B	SWCNTs ink superhydrophobic			Polymeric K^+-ISM	
C	Carbon ink			Polymeric K^+-ISM	
D	Carbon ink	SWCNTs		Polymeric K^+-ISM	
E	SWCNTs ink	Gold		Polymeric K^+-ISM	
F	SWCNTs ink	Gold	POT	Polymeric K^+-ISM	
G	SWCNTs ink	Gold	POT	Polymeric K^+-ISM	ETH 500
H	SWCNTs ink			Acrylate K^+-ISM	ETH 500
I	SWCNTs ink	Gold	POT	Acrylate K^+-ISM	ETH 500

8.3.2 Improving the reproducibility of the standard potential

Three different methodologies have been tested in order to improve the reproducibility of the standard potential between electrodes (Figure 8.2). All of them are based on the control of the potential generated at the interface between the membrane and the underlying electronic conductor –in our case the CNT-paper-. The first strategy -proposed by Bühlmann and co-workers[10,14]- consists on introducing a redox couple at the interface; the second one –proposed by Vanamo *et al*.[11]- consists on introducing a layer of a conducting polymer –PEDOT- on the interface and controlling its oxidation state by applying a potential; and the third one –also proposed by Vanamo *et al*.[12]- consists on short-circuiting the electrodes in order to reach a natural equilibrium between all the potentials.

K^+-ISEs were used for all the studies. Electrodes were built as described in previous chapters, with a standard experimental arrangement of filter paper with SWCNT-ink sandwiched between two plastic masks.

For the strategy that relies on using a redox buffer, 30 µl of a K^+-ISM were drop cast over the conductive paper. The membrane composition is shown in Table 8.3. 233 mg of the mixture were dissolved in 1 ml of THF.

Table 8.3. Composition of the membrane with redox buffer. Units are expressed in wt %. LiTPFPB stands for lithium tetrakis(pentafluorophenyl)borate ethyl etherate, PVC for poly(vinylchloride) and NPOE for 2-nitrophenyl octyl ether.

	Polymeric K^+-ISM
Valinomycin	0.9
LiTPFPB	0.3
$Co(phen)_3(TPFPB)_2$	5.8
$Co(phen)_3(TPFPB)_3$	7.9
PVC	28.3
NPOE	56.7

On the other hand, for the strategy based on the equilibration of potentials between electrodes, two types of electrodes were compared. First, the conventional electrodes, and then, a modification using a PEDOT layer deposited between the paper and the electrode. A solution of 0.01 M 3,4-Ethylenedioxythiophene (EDOT) and 0.1 M poly(sodium 4-styrenesulfonate) (NaPSS) was used for the polymerization. The solution was stirred overnight in dark conditions and bubbled with N_2 for 30 min before polymerization. A galvanostatic method was used for the polymerization by applying 14 µA for 714 s. A three-electrode electrochemical cell was used with a Ag/AgCl/NaPSS 0.1 M as reference electrode, GC as a counter electrode and CNT-paper as working electrode. The electrodes were rinsed with deionized water and let dry overnight. In order to control the E^0, two methods were tested and compared. Both approaches are similar, but trying to control the potential on the CNT layer or on the PEDOT.

In order to control the potential at the interface, an external power supply was used to apply 0.2 V on the electrodes for 300 sec in a KCl 0.1 M solution. In this case, the working electrode of the electrochemical cell is either the CNT-paper or CNT-paper-PEDOT electrode (depending on the layer where the potential has to be controlled, either the CNT or the PEDOT, respectively). The rest of the cell has a conventional arrangement, with a Ag/AgCl/KCl 3 M reference electrode and a GC as a counter electrode. After the CNT-papers or CNT-PEDOT-papers were subject to the application of electrical potential and let dry, a conventional K^+-ISM was drop cast over them.

Finally, the common K^+-ISE and the reference membrane presented in chapter 5 were used for the experiments where electrodes are short-circuited. Electrodes were built together and stored with 0.01 M KCl solution for 24 h. Thereafter, they were separated and measured independently.

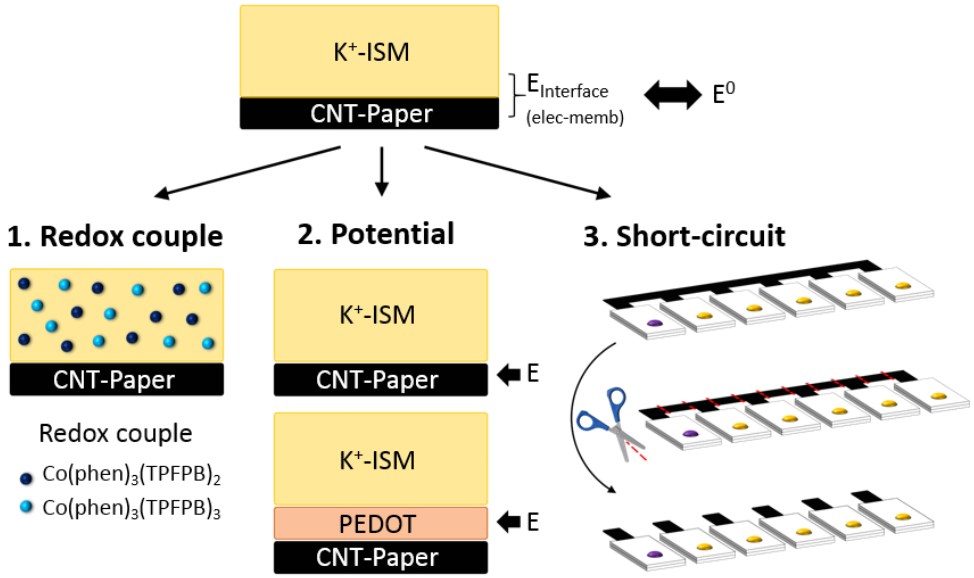

Figure 8.2. Methodologies used to control the E^0: 1. Addition of a redox buffer in the K^+-ISM; 2. Application of a potential in the CNT-paper or in the PEDOT layer and 3. Short circuiting of the electrodes.

8.4 Results and discussion

8.4.1 Improvement of the LOD of the potentiometric paper sensors

Typical K^+-ISEs presented in chapter 5 have a LOD in the range of $4 \cdot 10^{-6}$ M, slightly worse than the conventional SC glassy carbon electrodes. Interestingly, since the first works, improvements on the paper used for the electrodes and increased expertise acquired with time has allowed to reduce this LOD has down to $4 \cdot 10^{-7}$ M, order of magnitude lower. Some of the modifications recently reported were adapted to our paper sensors configuration to test potential improvements on the LOD. In order to assess which modification of the system presented by Menash *et al.*[6] (to refresh, a Au layer and conducting polymer were added over the CNT-paper developed in this thesis and an acrylate membrane was cast) leads to such an improvement in the LOD, different systems were built. The systems tested are shown in Table 8.1 and all have been assembled following the typical arrangement

–a conductive paper sandwiched in between two plastic masks and the ISM-. All the sensors have been characterised following the conditioning protocol described in the experimental chapter and the results obtained are shown in Figure 8.3 and Table 8.4.

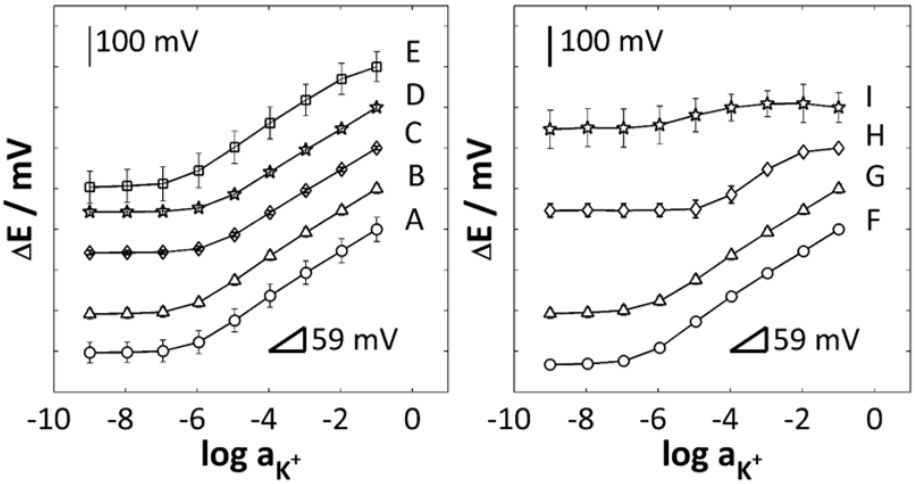

Figure 8.3. Calibration plots for the different systems, some error bars cannot be seen due to its small magnitude. The potential values have been shifted for a clearer understanding of the figure.

Table 8.4. Analytical parameters of the different K^+-ISEs.

	A	B	C	D	E
Sensitivity (mV/dec)	56.2 ± 0.3	56.7 ± 0.2	53.58 ± 0.1	53.61 ± 0.1	56.8 ± 1.0
Limit of detection (M)	$4.6 \cdot 10^{-7}$	$4.3 \cdot 10^{-7}$	$1.7 \cdot 10^{-6}$	$1.7 \cdot 10^{-6}$	$6.2 \cdot 10^{-7}$
Linear range (M)	10^{-6} - 10^{-1}	10^{-6} - 10^{-1}	10^{-5} - 10^{-1}	10^{-5} - 10^{-1}	10^{-6} - 10^{-2}

	F	G	H	I
Sensitivity (mV/dec)	58.3 ± 0.1	56.0 ± 0.1	53.2 ± 2.3	22.9 ± 1.0
Limit of detection (M)	$2.0 \cdot 10^{-7}$	$3.8 \cdot 10^{-7}$	$8.5 \cdot 10^{-6}$	$1.3 \cdot 10^{-7}$
Linear range (M)	10^{-6} - 10^{-1}	10^{-6} - 10^{-1}	10^{-5} - 10^{-2}	10^{-5} - 10^{-2}

The results show that some of these approaches have given some degree of improvement regarding the LOD. In particular, for the sensors incorporating the layers of gold and POT (F and G), it can be seen that the layer of gold will further increase the hydrophobicity of the paper, thus, reducing the possible formation of a water layer and providing better stability to the sensors. It also seems that the LOD can be slightly improved. This improvement, however, is barely half an order of magnitude when comparing with a paper without gold (A and B). Therefore, although there is some improvement, it could be argued that also adds complexity to the system. Sputtering a layer of gold is not a simple step –it requires big and expensive instrumentation– and adds cost to the sensor.

In a previous chapter it was also mentioned some degree of controversy regarding the effect of the SDBS that may remain in the normal CNT-papers (A). The results seem to put an end to this controversy by proving that they both display very similar sensitivity and LOD in comparison with the superhydrophobic ones (B). Moreover, the advantage of the CNT-ink that provides a 3-D conductive network in the paper has been reaffirmed by comparing the CNT-papers (A and B) with carbon ink papers (C and D) –which just have an electrical conductive carbon layer-; papers with CNTs have better sensitivity and limits of detection. The last parameter to evaluate is the nature of the membrane, in this case acrylate membranes (H) perform worse than polymeric ones (A), probably due to their higher resistance. Altogether, simplicity and costs from one side and better performance from the other must be balanced and taking into account each different situation one or another system can be used.

8.4.2 Attempts to improve the reproducibility of the E^0 of the paper sensors

The typical standard deviation values of E^0 between different K^+-paper-ISEs ranges from 10 to 50 mV for the E^0. These values do not come from the paper substrate, as similar values have been reported for GC or gold electrodes[14]. However, this high

standard deviation makes impossible the construction of a calibration-free system. For this reason, the following sections will explore the three main approaches already reported for other systems to decrease this standard deviation in order to evaluate how they can be used in the paper-based potentiometric sensors.

8.4.2.1 Addition of a redox couple in the membrane

Electrodes with the redox couple $Co(phen)_3(TPFPB)_2$ / $Co(phen)_3(TPFPB)_3$ inside a polymeric potassium membrane show a standard deviation of the E^0 of 1.6 mV (see Figure 8.4). The amount of the redox buffer at the membrane is 30 mmols/kg, higher than the one reported by Zou e*t al.*[14] (which was about 7 mmols/kg). The optimal value for this parameter in our system was 30 mmols/kg, which transforms to 280 nmols/electrode after drop casting 30 µl of the membrane at each electrode. For a lower concentration of the redox buffer in the membrane, higher volume of the cocktail was needed to be drop casted on the papers, and the standard deviation obtained were higher –around 5 to 8 mV-. Furthermore, since the higher the volume cast the thicker membranes formed, and the thicker the membrane the larger the impedance, a decrease on the general performance was achieved.

According to what was later reported by Zou *et al.*[10] the introduction of this salt in the membrane slightly decreases the sensitivity, giving a value of 54.8 ± 0.5 mV/dec. The authors attribute this reduction of sensitivity to the loss of redox-active cations into the aqueous solution, caused by primary cation transfer from the sample into the ISM due to the highly energy-favoured binding of the primary cations to the ionophore. Introducing a more lipophilic redox couple has been proposed as a solution, however this approach has not yet been examined over the K^+-paper-ISEs. Taking into account the differences between both systems (our K^+-ISM is doped with a less lipophilic redox couple and drop casted over a CNT-paper, and the reported system has a more lipophilic redox couple on the K^+-ISM, which is

drop casted over a gold electrode modified with a self-assembled monolayer of 1-hexanethiol), the analytical performance of them is compared in Table 8.5.

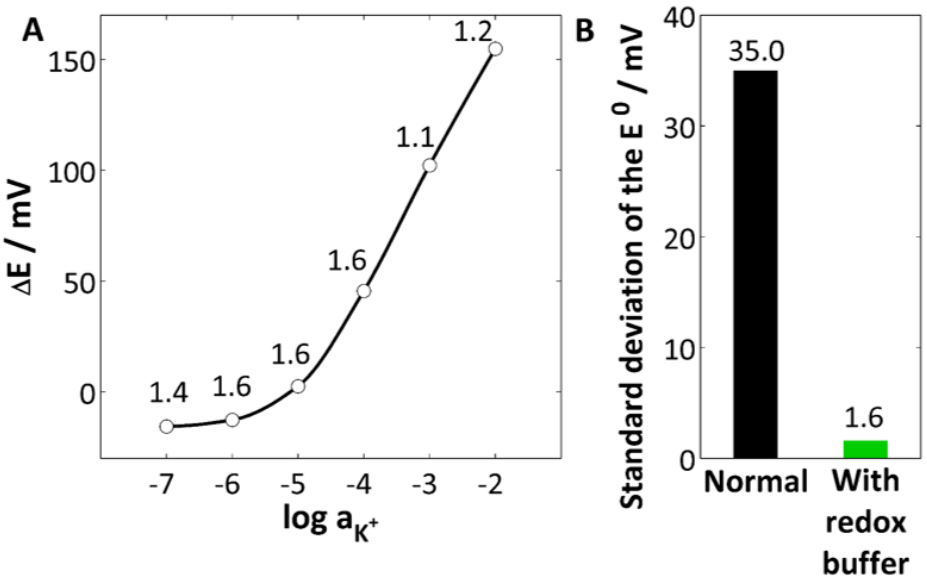

Figure 8.4. A) Average calibration curve for 5 K^+-ISEs with redox buffer. Numbers at the top of the bars show the standard deviation –in mV- at each concentration level. B) Comparison between the E^0 standard deviation of the normal K^+-paper-ISEs and the redox modified.

Table 8.5. Analytical parameters of the K^+-paper-ISE with redox buffer compared to the reported[10].

	K^+-paper-ISE with redox buffer	**Zou *et al.*[10]**
Sensitivity (mV/dec)	54.8 ± 0.5	60.0 ± 0.8
Limit of detection (M)	$7.9 \cdot 10^{-6}$	-
Linear range (M)	$10^{-4} – 10^{-2}$	-
E^0 (mV)	263.3 ± 1.6	731.3 ± 2.6

The reproducibility of the E^0 of the K^+-paper-ISEs is still better than the proposed by Zou *et al.*[10], however the sensitivity is slightly worse. The exploration of other

alternatives –such as the introduction of the more lipophilic redox couple- could be a potential route to improve this area.

Some other attempts to introduce the redox buffer, such as drop casting the salt dispersed in THF in between the CNT-paper and the membrane, or drop casting a 5 µl solution of the membrane doped with the salt and then membrane without over it, did not show such a reduction of the standard deviation of the E^0.

8.4.2.2 Application of a potential at the interface membrane-electrode

Applying a potential on a PEDOT layer over the CNT-paper can tune the redox state of the conducting polymer and thus help to control the final E^0 of the electrode[11]. It could be argued whether the application of a potential over the CNT-paper could have a similar effect and also help to tune the standard potential. Results for the application of a potential in the PEDOT layer show satisfactory results with an improvement of the E^0 standard deviation, however the application of the potential over the CNT-paper did not show significant improvement of this parameter (see Figure 8.5 and Table 8.6). As it is well known, the E^0 depends on the potential generated at each interface. Thus, controlling one of these potentials should improve the difference of the E^0 between electrodes. The results show that this is what happens –up to certain degree- in both systems that have been pre-treated with an applied potential. However, when the potential is applied to the PEDOT layer, the standard deviation of the E^0 between electrodes is better than when applying it over the CNTs. That could be attributed to the redox sensitivity of the conducting polymers, which can exist in different redox states, while CNTs are redox insensitive. Evidence for this it that systems where the potential have been applied to the PEDOT have a standard potential (200.1 ± 5.6 mV) equal to the potential applied (200 mV). This is a great approach as ideally, it should not be necessary to calibrate one electrode in a batch since they will all have a well-known standard potential that matches the applied one. However, the introduction of a PEDOT layer in the K^+-paper-ISEs adds one layer of complexity to the system and

goes one step backwards reintroducing conducting polymers. Since they show several drawbacks in practical applications[15,16].

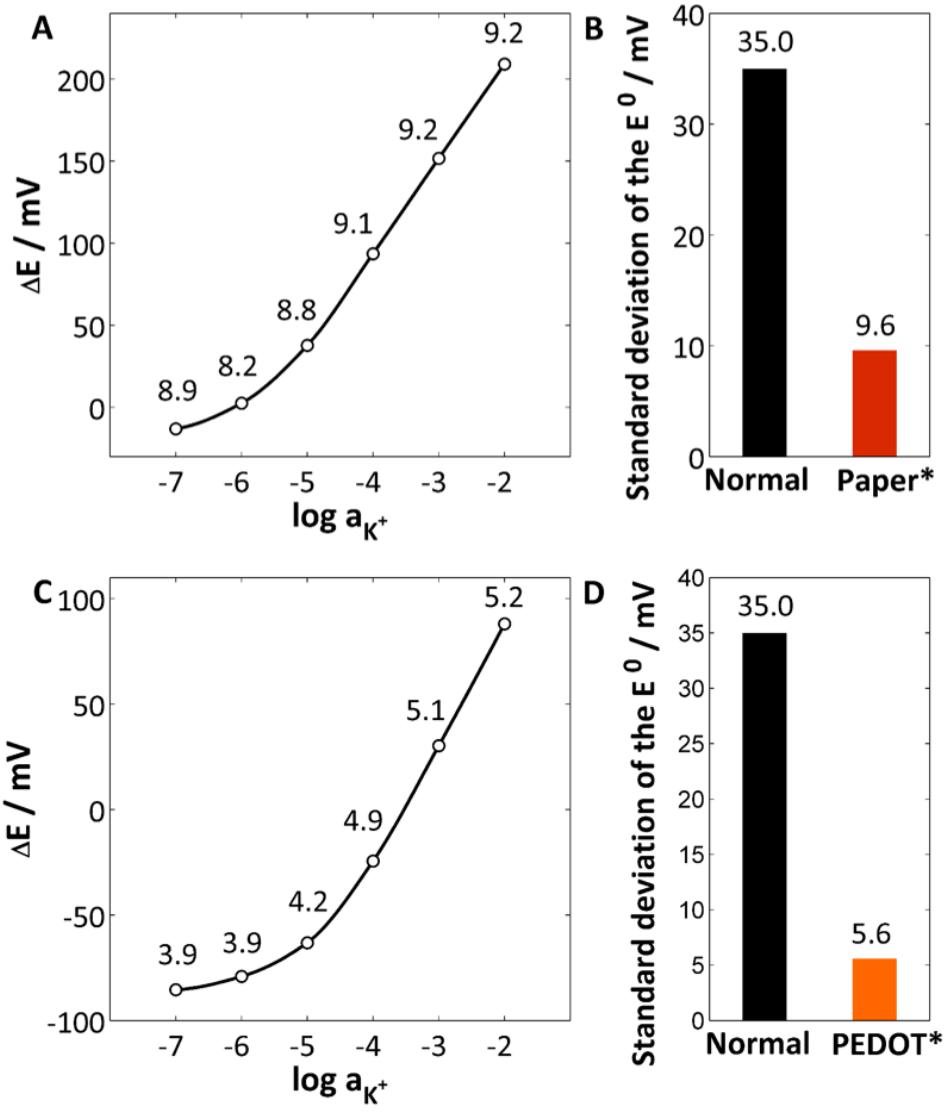

Figure 8.5. A) Average calibration curve for 4 K^+-ISEs with 0.2 V applied on the CNT-paper and C) on the PEDOT layer. Numbers at the top of the bars show the standard deviation –in mV- at each concentration level. B) Comparison between the E^0 standard deviation of the normal K^+-paper-ISEs and K^+-paper*-ISEs and D) K^+-paper-PEDOT*-ISEs. The (*) indicates the layer subjected to the potential.

Table 8.6. Analytical performance of electrodes subjected to an application of potential. The (*) indicates the layer subjected to the potential.

	K^+-paper*-ISE	**K^+-paper-PEDOT*-ISE**
Sensitivity (mV/dec)	57.2 ± 0.2	56.3 ± 0.4
Limit of detection (M)	$1.3 \cdot 10^{-6}$	$7.9 \cdot 10^{-6}$
Linear range (M)	$10^{-5} – 10^{-2}$	$10^{-4} – 10^{-2}$
E^0 (mV)	323.3 ± 9.6	200.1 ± 5.6

8.4.2.3 Short circuiting of the electrodes for potential equilibration

A novel approach to control the E^0 of the electrodes introduced by Vanamo *et al.*[12], consists on short-circuiting the electrodes, *i.e.* setting a direct connection between the working and the reference electrode avoiding the measuring device. The concept is the same that when a potential is applied, however in this case, there is no potential applied and the short-circuit of the electrodes produces a self-equilibration of the electrodes until the difference of potential between them is close to zero. When 5 K^+-paper-ISEs are short circuited with a paper reference electrode, even without a conducting polymer, this equilibration is also produced, and the resulting electrodes –after removing the short-circuit- measured, display a high reproducibility of the E^0 –with a standard deviation of 2.7 mV- (see Figure 8.6).

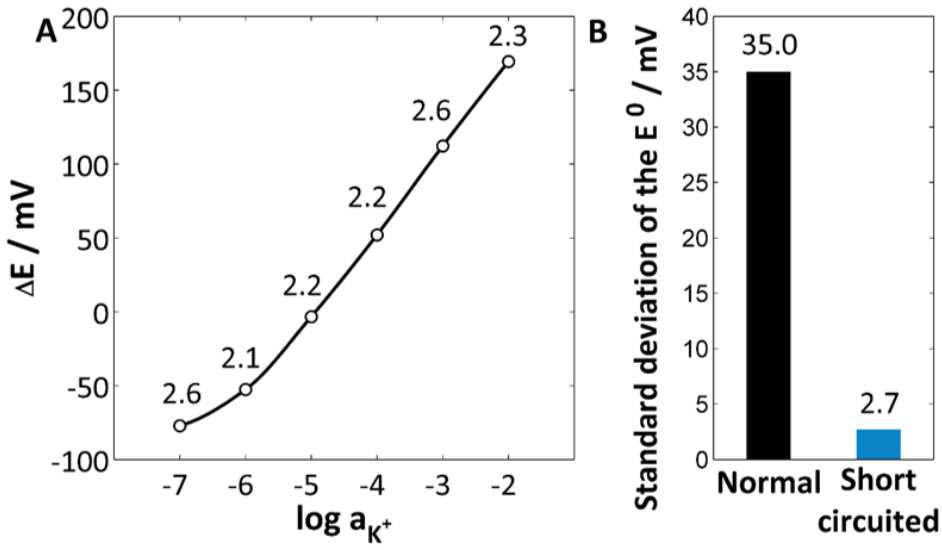

Figure 8.6. A) Average calibration curve for 5 K^+-ISEs which have been short circuited. Numbers at the top of the bars show the standard deviation –in mV- at each concentration level. B) Comparison between the E^0 standard deviation of the normal K^+-paper-ISEs and K^+-paper-ISEs short circuited.

8.4.2.4 Comparison of all the approaches

All the three approaches dramatically improves the standard deviation of the E^0, however the incorporation of the redox buffer is the one that gave better results (see Figure 8.7 and Table 8.7).

From a practical point of view, the application of a potential is the "trickiest" one as it involves multiple steps. It requires the electropolymerization of a conducting polymer –as directly controlling the potential in the CNT did not show good results-, thus the typical construction process is extended, as two extra steps are required. The short-circuiting of the electrodes is a good approach as it gives low E^0 standard deviation and is simple if working with paper electrodes. Electrodes could be stored short circuited and cut when they need to be used. Of course, significant work still needs to be done, as aspects regarding the paper reference electrode and how different potentiometric cells will be separated maintaining the same standard

potential need to be explored. The doping of the membrane with a redox buffer is a straightforward step and the resulting electrodes are those with the most reproducible E^0, thus being the approach with the highest potential for real applications of paper electrodes. Also, this approach requires reference electrodes with the same standard potential. Doping the reference electrode with a redox buffer could also help to maintain a stable potential, however, this area has not yet been explored. Future work on this problem is necessary for the development of whole paper cells with a fixed standard potential.

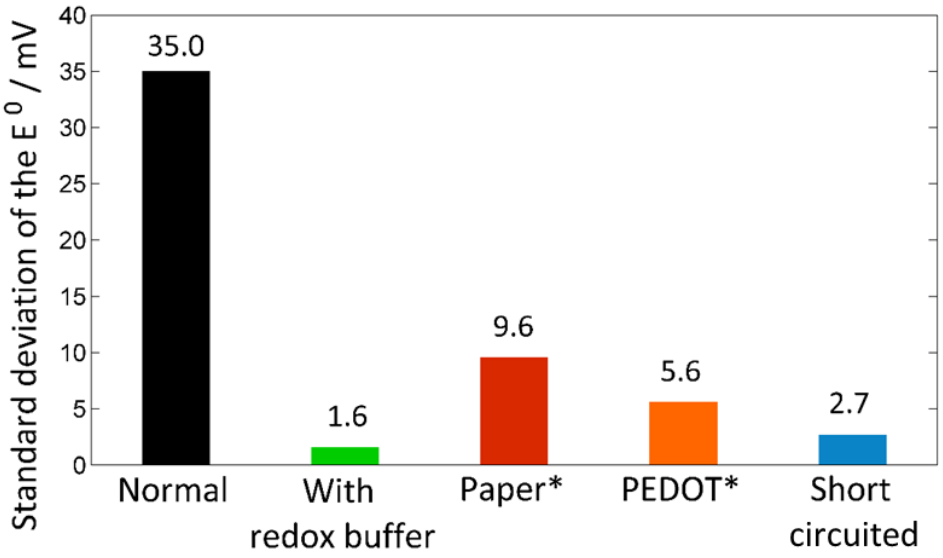

Figure 8.7. Comparison of the standard deviation of the E^0 for the different systems.

Table 8.7. Comparison of the analytical parameters for all the K^+-ISEs tested. The (*) indicates the layer subjected to 0.2 V.

	Normal	With redox buffer	Paper*	PEDOT*	Short circuited
Sensitivity (mV/dec)	57.2 ± 0.3	54.8 ± 0.5	57.2 ± 0.2	56.3 ± 0.4	57.8 ± 0.2
Limit of detection (M)	$5.0 \cdot 10^{-7}$	$7.9 \cdot 10^{-6}$	$1.3 \cdot 10^{-6}$	$7.9 \cdot 10^{-6}$	$5.0 \cdot 10^{-6}$
Linear range (M)	10^{-6} - 10^{-1}	10^{-4} – 10^{-2}	10^{-5} – 10^{-2}	10^{-4} – 10^{-2}	10^{-5} – 10^{-2}
E^0 (mV)	415.2 ± 12.3	263.3 ± 1.6	323.3 ± 9.6	200.1 ± 5.6	285.1 ± 2.7

In order to test the real applicability of the best approach with paper –the redox buffer introduction-, 15 K^+-ISEs were constructed. The response of all of them was measured in seven different concentration levels that fall inside the linear range -10^{-4}, $10^{-3.8}$, $10^{-3.6}$, 10^{-3}, $10^{-2.4}$, $10^{-2.2}$ and 10^{-2} M-. The average slope was 54.0 ± 0.7 mV/dec and the standard potential 261.8 ± 1.5 mV. A Grubbs tests was performed for the potential values obtained at each level and no outliers were found, thus confirming the excellent reproducibility of the electrodes. Then, three random electrodes were selected and the calibration curve, together with confidence and prediction intervals was calculated just taking into account the levels 10^{-4}, 10^{-3}, and 10^{-2} M. This calibration curve is used to predict the concentration of the other electrodes (not used for the calibration) at the other levels -$10^{-3.8}$, $10^{-3.6}$, $10^{-2.4}$, $10^{-2.2}$ M-. The values obtained fall all inside the prediction intervals, thus demonstrating the ability of the method to accurately predict concentrations with non-calibrated electrodes, and being a step forward to free-calibration potentiometric electrodes (see Figure 8.8).

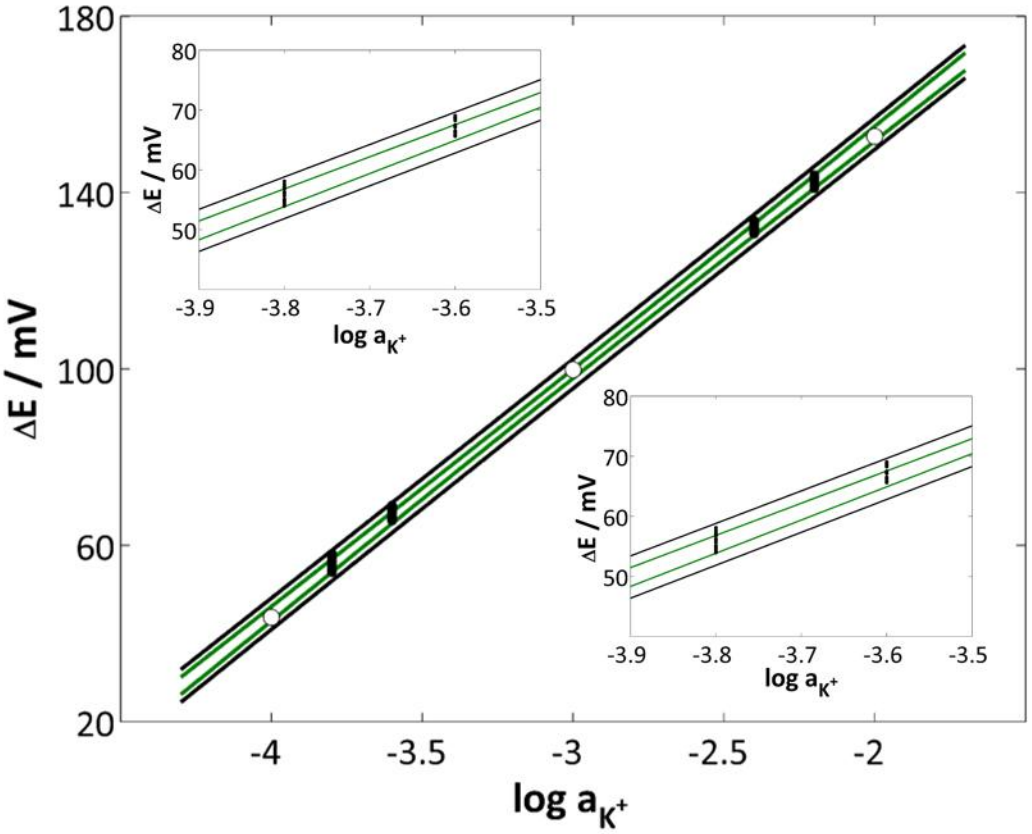

Figure 8.8. Calibration plot showing the calibration points (○) used with their respective confidence (in green) and prediction (in black) intervals, and the potential values obtained for predicted points (●). The two magnifications of the predicted points clearly show that they fall inside the prediction intervals.

With 15 electrodes there are 455 possible combinations that can result from taking three random electrodes. All these combinations have been evaluated and from all the predicted values obtained 98.2 % fall inside the prediction interval. Thus confirming the excellent performance of the methodology.

8.5 Conclusions

This chapter has explored several recent trends for the improvement of the ion-selective potentiometric sensors applied to the paper-based sensors. In general terms, it can be said that regarding the LODs, the pain does not match the gain: the efforts to improve LODs do not yield significant improvements. The introduction of a gold and a POT layers over the CNT-paper can slightly improve the LOD of the paper-ISEs, however, this little improvement could not be worst in many of the application of the paper-ISEs. Adding complexity and price to the electrode goes against the natural characteristics of disposable electrodes. In any case, other approaches to improve the LOD of ISEs will appear and research to improve this parameter if the application demands it is a future work to keep in mind.

On the other hand, it is encouraging to see that approaches to decrease the standard deviation of the E^0 have been really successful. This chapter has demonstrated that K^+-paper-ISEs with a standard deviation of the E^0 of 1.6 mV have been developed, which may have significant practical applications. Moreover, a first test of a real situation of calibration and prediction has led to promising results towards free calibration electrodes. In that area there is still work to do, the control of the paper reference E^0 is a must if calibration-free sensors are desired. This control could be done in a similar way –by introducing a redox couple in the membrane[13]-.

8.6 References

(1) Pretsch, E. *TrAC, Trends Anal. Chem.* **2007**, *26*, 46–51.

(2) Malon, A.; Vigassy, T.; Bakker, E.; Pretsch, E. *J. Am. Chem. Soc.* **2006**, *128*, 8154–8155.

(3) Radu, A.; Peper, S.; Bakker, E.; Diamond, D. *Electroanalysis* **2007**, *19*, 144–154.

(4) Jaworska, E.; Lewandowski, W.; Mieczkowski, J.; Maksymiuk, K.; Michalska, A. *Analyst* **2013**, *138*, 2363–2371.

(5) Ping, J.; Wang, Y.; Fan, K.; Tang, W.; Wu, J.; Ying, Y. *J. Mater. Chem. B* **2013**, *1*, 4781–4791.

(6) Mensah, S. T.; Gonzalez, Y.; Calvo-Marzal, P.; Chumbimuni-Torres, K. Y. *Anal. Chem.* **2014**, *86*, 7269–7273.

(7) Liu, D.; Meruva, R. K.; Brown, R. B.; Meyerhoff, M. E. *Anal. Chim. Acta* **1996**, *321*, 173–183.

(8) Lutze, O.; Meruva, R. K.; Frielich, A.; Ramamurthy, N.; Brown, R. B.; Hower, R.; Meyerhoff, M. E. *Fresenius. J. Anal. Chem.* **1999**, *364*, 41–47.

(9) Zhou, M.; Gan, S.; Cai, B.; Li, F.; Ma, W.; Han, D.; Niu, L. *Anal. Chem.* **2012**, *84*, 3480–3483.

(10) Zou, X. U.; Zhen, X. V; Cheong, J. H.; Bühlmann, P. *Anal. Chem.* **2014**, *86*, 8687–8692.

(11) Vanamo, U.; Bobacka, J. *Electrochim. Acta* **2014**, *122*, 316–321.

(12) Vanamo, U.; Bobacka, J. *Anal .Chem.* **2014**, *86*, 10540–10545.

(13) Zou, X. U.; Chen, L. D.; Lai, C.-Z.; Bühlmann, P. *Electroanalysis* **2015**, *27*, 602–608.

(14) Zou, X. U.; Cheong, J. H.; Taitt, B. J.; Bühlmann, P. *Anal .Chem.* **2013**, *85*, 9350–9355.

(15) Lindfors, T. *J. Solid State Electrochem.* **2009**, *13*, 77–89.

(16) Düzgün, A.; Zelada-Guillén, G. A.; Crespo, G. A.; Macho, S.; Riu, J.; Rius, F. X. *Anal. Bioanal. Chem.* **2011**, *399*, 171–181.

UNIVERSITAT ROVIRA I VIRGILI
PAPER-BASED POTENTIOMETRIC PLATAFORMS FOR ESCENTRALISED CHEMICAL ANALYSIS.
Marta Novell Recasens
Dipòsit Legal: T 1462-2015

UNIVERSITAT ROVIRA I VIRGILI
PAPER-BASED POTENTIOMETRIC PLATAFORMS FOR ESCENTRALISED CHEMICAL ANALYSIS.
Marta Novell Recasens
Dipòsit Legal: T 1462-2015

CHAPTER

9

NEW DIRECTIONS IN PAPER-BASED ELECTROCHEMICAL SENSORS

UNIVERSITAT ROVIRA I VIRGILI
PAPER-BASED POTENTIOMETRIC PLATAFORMS FOR ESCENTRALISED CHEMICAL ANALYSIS.
Marta Novell Recasens
Dipòsit Legal: T 1462-2015

9.1 Summary

Despite of all their attractive features, ion-selective potentiometric sensors have inherent limitations. As analytical chemists, it is clear that tools have the scope to solve some types of problems, and while their use can be stretched, there is a point where new tools based on new principles are required. This chapter describes some alternative applications for the conductive paper platform. First, a chemiresistor built over this paper for the detection of human immunoglobulin G (HIgG) is presented as a proof of concept that the platform can be used with other techniques different than potentiometry. Second, a potentiometric sensor for the detection of glucose over platinized paper is presented as a proof of principle for the extension of the disposable potentiometric papers for analytes other than ions.

9.2 Introduction

Paper ISEs will allow the determination of many ions usually checked in routine analysis, ranging from water monitoring to blood analysis. However, more and more, the determination of other type of analytes is required. In a typical blood analysis, for example, the levels of many proteins and organic molecules have to be evaluated. Those types of analytes cannot be quantified with ISEs, therefore other type of sensors are needed.

Affinity-based biosensors are one type of sensors with most promising potential applications in several fields: healthcare, food contamination, environmental safety and homeland security, among others. For instance, detecting a human disease or infection in its early stage would represent a considerable advantage for the medical treatment to be effective. Constructing these sensors over the paper platform previously developed will result in simple, portable and low-cost biosensors[1]. Making possible their extension to diagnosis for non-developed countries[2,3].

Resistance-based biosensors (chemiresistors) emerge as an attractive complement to other electrochemical methods of detection. These label-free devices can measure small changes of the target analyte concentration with high precision and low power consumption[4,5]. Typical chemiresistors based on nanostructured materials are composed of interdigitated microelectrodes containing one-dimensional nanostructures as transducer elements, and are often applied to gas sensing[6]. In addition to these nanostructured materials, the incorporation of molecular recognition elements –such as aptamers, artificial receptors or antibodies-, which confer selectivity to the system, considerably broaden the available sensing analytes from typical volatile organic compounds (VOC) to different chemicals[7], biomolecules[8] or bacteria[9]. Although the detection technique (*i.e.* measurement of electrical resistance or intensity of electrical current) displays simplicity of operation, the conventional construction of device still limits the real applications the sensors can address. These chemiresistors are commonly built on SiO_2/Si surfaces with manufacturing approaches that involve specialized equipment such as lithography techniques and trained personnel so that both -the substrate and the construction strategy- considerably raise the final cost of production. Among other drawbacks, these devices have been often reported with a lack of estimation of some essential performance parameters; furthermore, the need to obtain better reproducibility, both in the measurement and the construction stages, hinders the ultimate goal of these sensing devices: the measurement of real samples[10].

Another type of sensors for the detection of non-ionic species are enzyme-based sensors. As explained in chapter 2, this group of sensors englobes a wide range of sensors whose signal is the result of the reaction of an enzyme –usually immobilized in its recognition layer- with the analyte of interest. Many amperometric enzyme sensors have been reported[11–14], even some of them over paper substrate[15,16]. However, the area of potentiometric enzyme sensors has not been too dynamic and only recently -with the introduction of nanomaterials- the

area has been revisited. The group of Willander has reported many works immobilizing different enzymes over nanostructures of ZnO for the detection of glucose[17], cholesterol[18–20], lactate[21] and uric acid[22,23]. Glucose has also been detected using iron ferrite magnetic nanoparticles[24] and cholesterol with the use of cobalt oxide nanoparticles[25]. Other groups have also reported potentiometric determinations with enzymes[26–28]. Amongst all these sensors, the use of chitosan to immobilize enzymes has been widely used[29–31] due to its excellent biological compatibility, which allows the retention of the enzyme activity.

The possible integration of both kind of sensors –chemiresistors and enzyme-based- in daily materials such as yarns, rubber or paper materials[32–34] emerged as an attempt to solve the cost-related and adoption issues. For instance, Shim *et al.*[32] have taken advantage of cotton yarns to build a SWCNT based chemiresistor for protein detection, and Ammu *et al.*[35] reported flexible chemiresistor vapour sensors based on cellulosic substrates and plastics. The 3D paper structure is an excellent material that allows the easy immobilization of the biomolecules needed for the recognition layer –either antibodies or enzymes-.

This chapter is divided in two sections, in order to present two lines of development. First, in part 1, a novel paper-based chemiresistor for rapid, direct and sensitive detection of proteins is introduced. SWCNTs have been used as efficient transducers and HIgG has been used as a proof-of-concept for immunoreaction. The analytical performances of the resulting biosensors afford-picomolar detection of HIgG. Second, in part 2, a new approach for the development of an enzyme-based potentiometric paper sensor is also described. The detection of glucose is presented as a proof-of-principle for the extension of such sensors to other analytes.

Thereafter, general conclusions regarding the benefits, limitations and horizons of the conductive papers as analytical platform are provided.

9.3 Part 1: Chemiresistor

9.3.1 Experimental part

The base of the chemiresistor is a CNT conductive-paper. Nevertheless, unlike the substrate used in potentiometry –where the value of the resistance was minimized down to 500 ohms- the optimal resistance of the paper for this application was found to be around 200 kΩ, and therefore only three painting cycles –painting, drying, washing and drying- are usually applied. The resistance obtained after these three layers ranges from 150 to 250 kΩ. For optimization of theses parameters, papers with different resistances –obtained by applying different number of painting cycles- were tested.

The conductive paper was cut into strips of 2 mm width and 10 cm long. Each strip was further trimmed so that at inner part of 1 mm width and 5 mm long was left in the centre of the strip (see Figure 9.1). Then, each strip was coated with glue at 1.5 cm from the ends in both sides keeping free the ending parts of the CNT-paper where the connections to the measuring device were done. Finally, an adhesive mask was incorporated onto the upper side of the chemiresistor –leaving a circular window of 6.2 mm^2- to avoid any direct contact with the solution.

The SWCNTs in the centre of the strip that are not protected by the mask were functionalized by adsorption of anti-HIgG (1 μg/ml) over the SWCNTs: the papers were incubated with 400 μl of anti-HIgG during 3 hours (a vial was placed upside down on top of the paper). Then 400 μl of 0.3 % Tween 20 were added during one hour to block the SWCNTs not coated with anti-HIgG –in order to prevent any non-specific adsorption-. Eventually, the biosensors were washed with 2 mM PBS and were stored in PBS. In this way, the masked SWCNTs work as electric conductor whereas the unmasked SWCNTs functionalized with antibodies work both as the sensing and transducing layer (see Figure 9.1).

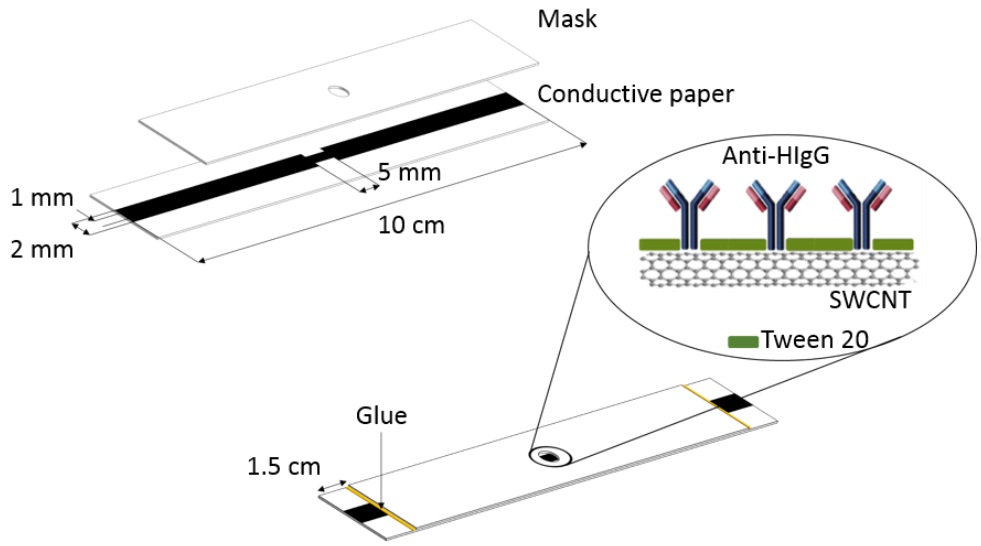

Figure 9.1. Schematic representation of the chemiresistor with the ideal attachment of the anti-HIgG onto the SWCNTs.

9.3.2 Results and discussion

The chemiresistor was electrochemically characterised after each functionalization step. The current vs. voltage (*I*–*V*) curves for SWCNT immobilization onto the paper, anti-HIgG physisorption onto the SWCNT, Tween 20 blockage of the SWCNTs gaps and 62 pM HIgG addition were recorded (Figure 9.2). The current decreased after each functionalization step (from bare SWCNT to Tween 20) accounting for suitable functionalization of the paper-based biosensor. The immobilized molecules over the SWCNTs act as electron donators providing negative charges to the p-type SWCNT in presence of air, which lead to a reduction of the charge carriers so that the current value decreases[7,36–38]. The change in the addition of 62 pM concentration of HIgG corresponds to a change of about 18 nA in the response signal from the Tween 20 curve, which cannot be appreciated in Figure 9.2 due to the scale. This change in intensity, however, can be clearly differentiated from other additions of HIgG (see Figure 9.4 A and further discussion below).

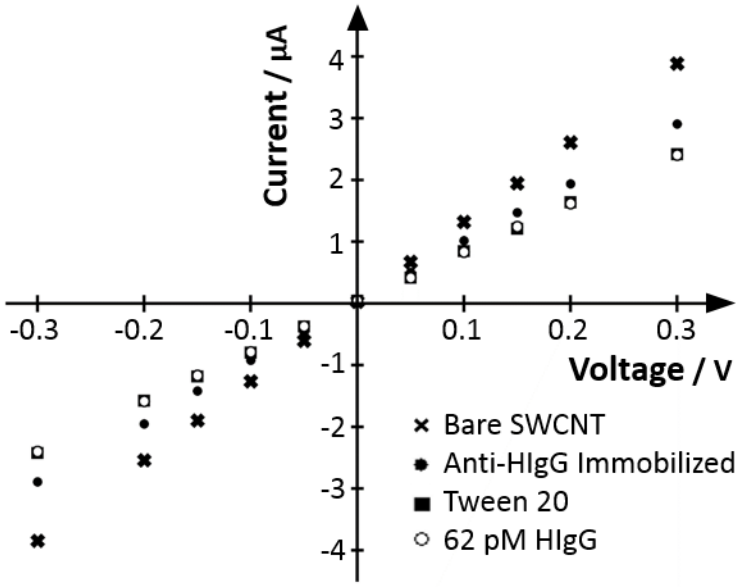

Figure 9.2. I-V characterisation curves of the paper-based chemiresistor for the different construction steps and HIgG sensing.

The instrumental response of chemiresistors depends on the change of the recorded resistance upon the addition of the target molecule. Therefore, among other factors, the sensitivity depends on the SWCNTs density (which is tuned by increasing or decreasing the number of painting cycles). Therefore, this factor was selected to optimize the biosensor performance. A batch of four biosensors with decreasing amounts of deposited SWCNTs, and therefore with increased resistances from 4 kΩ to 360 kΩ, was tested to select the optimal sensitivity. Figure 9.3 shows the instrumental response (in terms of normalized resistance of the four biosensors $100\cdot(R-R_0)/R_0$, where R and R_0 are the resistances of the biosensor after the exposure to 6.3 pM of HIgG and to buffer, respectively) as a function of the measured resistance (related to the density of the immobilized SWCNT). A resistance around 200 kΩ yields the optimal response. This value of resistance was selected for the next experiments. This behaviour agrees with previous

chemiresistors based on SWCNTs (although using different substrates than paper) where an intermediate resistance yields the optimum sensitivity[7]. Noteworthy, the paper-based chemiresistor requires a denser network of SWCNTs compared to the perfectly flat SiO_2/Si surfaces where higher resistances have been reported (1 – 10 MΩ)[38]. In our case, the formation of the network of SWCNTs is clearly altered by the 3 D structure of the paper while in a flat surface –such as SiO_2/Si – the SWCNTs are easier to locate and interweave. This reason may explain the fact that the optimal resistance values for SiO_2/Si surfaces correspond to less dense networks of SWCNTs and hence to higher resistance values.

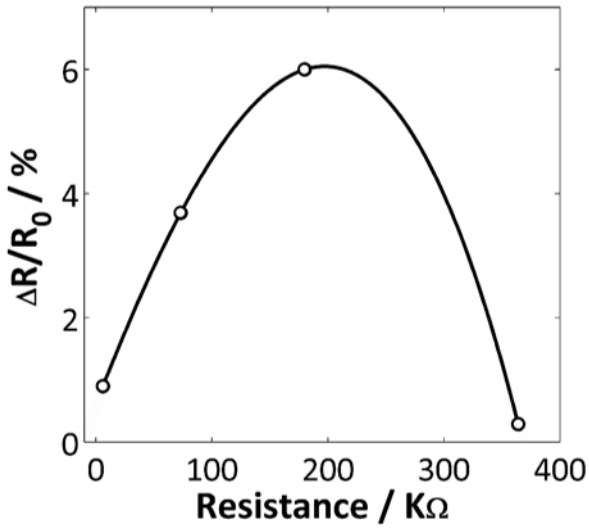

Figure 9.3. Dependence of the instrumental response on the resistance of the paper-based chemiresistor for 6.3 pM of HIgG.

The intensity of current of a single biosensor was measured upon addition of different concentrations of HIgG (see Figure 9.4 A). Here, two distinct phenomena can be discriminated: the sensitivity for the range 0–6.3 pM is −1.73 ± 0.85 nA/(pmols/L), which may correspond to the detection of the HIgG, and the sensitivity in the range 6.3 – 62 pM is −70.8 ± 58.7 pA/(pmols/L). This second range may correspond to the increasing saturation of the recognition site availability[5].

Besides, the measurements were achieved at different times (15 and 25 min and afford similar results). Interestingly, the paper substrate did not alter the required incubation time for protein sensing since the latter characteristics was comparable to conventional systems[38].

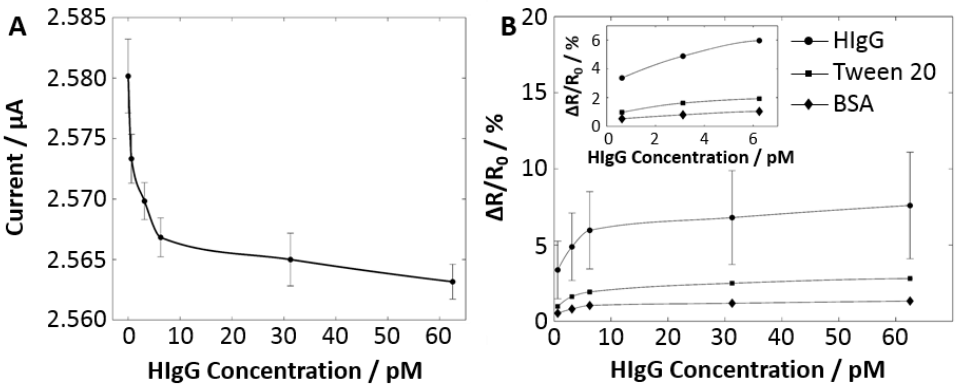

Figure 9.4. (A) Response of one biosensor in 2 mM PBS. Each data point is an average of three measurements with the same sensor. The error bars correspond to the standard deviations of the three measurements. (B) Biosensor calibration for HIgG in 2 mM PBS (●; upper curve), negative control with BSA (♦; bottom curve), and the Tween 20 control experiment where no antibody was immobilized onto SWCNTs control (■; middle curve). Data points of HIgG calibration are averages of three different biosensors with the corresponding standard deviation. The inset shows a magnification (without error bars) of the low concentration range.

The calibration curve corresponding to three different biosensors is shown in Figure 9.4 B. For the sake of clarity, Figure 9.4 B shows the normalized response of the three biosensors. Despite the comparable initial resistance of the biosensors, a significant standard deviation was observed when monitoring the target HIgG. This fact could be attributed to several factors. First, these biosensors were hand-made, which decreases the reproducibility of the construction between different biosensors in parameters such as the area over the layer of SWCNTs where the functionalization was done, or the uniformity of the 3D network of SWCNTs. Nevertheless, the biosensor construction was based on a painting process which is

one of the simplest and low-cost methodologies so that mass manufacturing could be easily achieved. Second, the functionalization process was achieved by adsorption of anti-HIgG onto SWCNTs. Ideally the recognition domain should be accessible to the antigen but it should be noted that due to random adsorption of anti-HIgG over SWCNTs, a fraction of anti-HIgG might not be accessible for the bio-recognition event, thus affecting the detection[39].

These results show that further work is indeed required to improve the reproducibility of the paper-based biosensor: the generation of conductive paper, the SWCNT-ink density, the surfactant and its concentration are some of the parameters that could improve the biosensor construction as well as its performance. Ideally, an easy and simple mechanical process should be incorporated in the biosensor construction in order to ensure a constant and exact value of the biosensor size, particularly in the sensing part where the anti-HIgG is placed. Here, we were able to detect concentrations at the picomolar range in less than 15 min. These values in liquid samples are significantly lower than those reported for other chemiresistors based on SiO_2/Si, whose limits of detection of 98 nM of salivary α-amylase have been reached[40]. Currently, HIgG levels are usually measured in blood tests through nephelometry, which is based on light diffraction. Although this technique could be easily automated, this new chemiresistor may become an attractive alternative that represents a considerable progress for decentralized tools.

To assess the selectivity of the biosensor the response was measured for increasing concentrations of bovine serum albumin, BSA, the most abundant protein in human serum (Figure 9.4 B). Several works in the literature claim that proteins are strongly and non-specifically adsorbed onto carbon nanotubes[41,42]. The use of BSA allows determining the effect of nonspecific binding of proteins in this new paper-based device. Interestingly, the additions of BSA did not yield significant response: 1.0 % at 6.6 pM BSA vs. 6.0 % at 6.6 pM HIgG. In addition, the response was

measured for increasing concentrations of HIgG without previous functionalization with anti-HIgG. Again, a reduced response was given in comparison with the one from the functionalized sensor (1.9 % vs. 6.0 % at 6.6 pM HIgG, respectively). This may correspond to unspecific HIgG/SWCNTs interactions due to a non-totally homogeneous coating of the SWCNTs by Tween 20.

9.4 Part 2: Enzymatic glucose electrode

9.4.1 Experimental part

In this case, paper was made conductive by using Pt instead of CNT. To do this, conventional filter papers were sputtered with platinum up to a final platinum layer of 50 nm. Thereafter, the construction of the sensor is similar to the process used along all the work for CNT-papers.

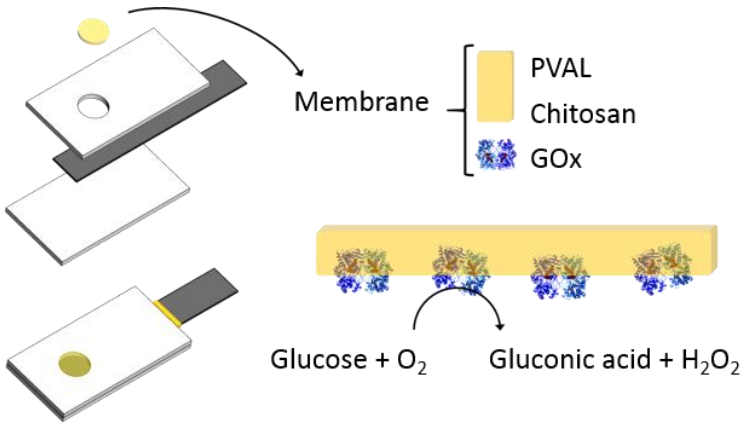

Figure 9.5. Schematic representation of the glucose sensor including the reaction between the glucose and the GOx produced in the membrane.

Solutions of 1 wt. % of chitosan in acetic acid 1 wt. % and 1 wt. % of poly vinyl alcohol (PVAL) in water are prepared and stored in the fridge when not in use. A cocktail of chitosan and PVAL in a 2.5 ratio with 1mg/ml of glucose oxidase (GOx) is used for the electropolymerization. The electropolymerization of the membrane on the platinum electrode is performed by applying 25 µA for 300 s. After the

electropolymerization of the membrane, the electrodes are rinsed with water and let it dry for 10 minutes, after which are stored in a dry chamber at the fridge.

9.4.2 Results and discussion

The response of the enzymatic paper-based glucose electrodes were tested in PBS 100 mM at pH=7.4. Figure 9.6 show the time trace of a typical glucose calibration curve. The electrode shows a negative response upon increasing glucose concentrations, thus indicating that the electrode surface is being somehow negatively charged (a deeper discussion about the mechanism is attempted in the following paragraphs). The shape of the response resembles the typical enzyme kinetic reaction time-trace. The response time depends on the concentration added: the higher the concentration, the faster the response. As it can be seen the response is not instantaneous and can vary from 1 to 5 minutes depending on the concentration added.

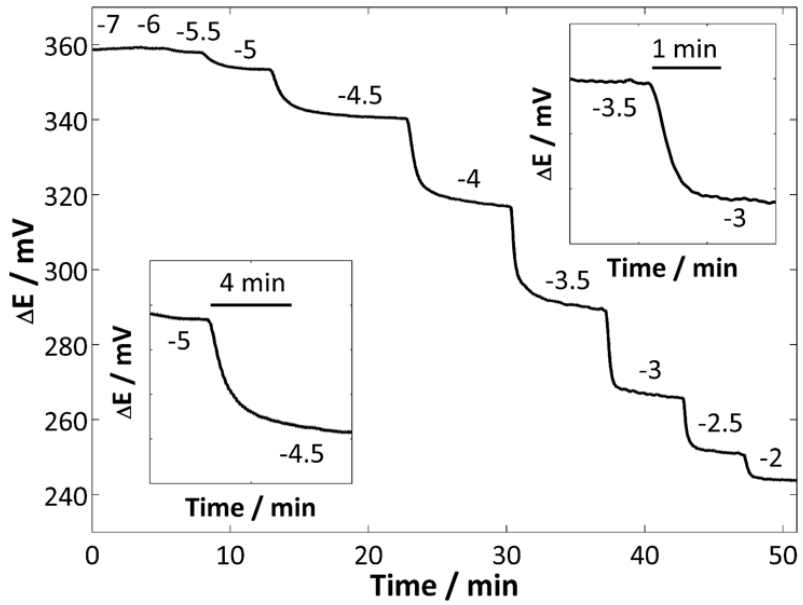

Figure 9.6. Time trance of a glucose sensor upon increasing glucose concentration. Numbers at each step represent the log [Glucose]. The two insets show a magnification of the response at different concentrations.

The glucose electrode has a sensitivity of -44.1 ± 0.8 mV/dec in the range from 10^{-5} M to $10^{-2.5}$ M. Blank controls have been performed in order to assess the selectivity of the electrode response on the enzymatic reaction. Thus, the potentiometric response of electrodes without enzyme –only chitosan and PVAL over the platinum (Blank1)- and platinum electrode alone (Blank 2) has been also evaluated. The blanks show a response towards glucose of -1.9 ± 1.3 mV/dec and -3.2 ± 1.0 mV/dec respectively in the working linear rage of the glucose electrode (see Figure 9.7 and Table 9.1). It is also noteworthy the high reproducibility of the standard potential between glucose electrodes with a value of 138.1 ± 6.5 mV. This could be probably attributed to the methodology used for building the sensor and the high reproducibility of all the steps, the sputtering of the platinum and the electrodeposition of the membrane.

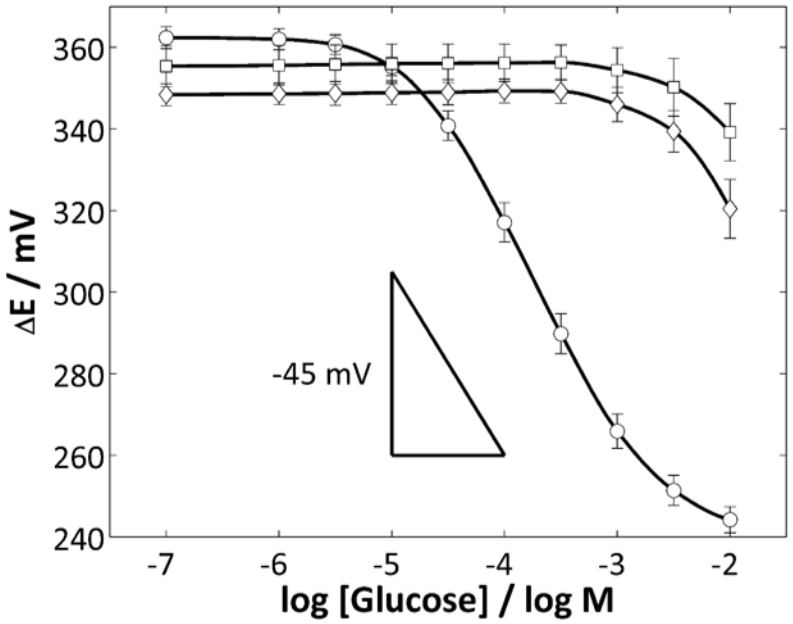

Figure 9.7. Glucose calibration curves for (○) glucose electrode, (□) Blank 1 and (◊) Blank 2.

Table 9.1. Analytical parameters obtained for the glucose electrode.

	Glucose electrode
Sensitivity (mV/dec)	-44.1 ± 0.8
Linear range (M)	10^{-5} – $10^{-2.5}$
Lower LOD (M)	$7.9 \cdot 10^{-6}$
Upper LOD (M)	$4.0 \cdot 10^{-3}$
E^0 (mV)	138.1 ± 6.5

The glucose electrode is composed of a chitosan and polyvinyl alcohol matrix that entraps the glucose oxidase enzyme. Tests to evaluate the composition of the matrix have shown that both components are needed in order to have optimum sensor parameters in terms of reproducibility and linear range, the sensitivity does not experiment significant changes with just one of the components or both. Electrodes with chitosan alone in the matrix were less reproducible and electrodes with only PVAL showed a reduced linear range. The role of both components is to provide stability to the membrane formed and a good chemical environment for the enzyme; however, to the best of our knowledge, they are not involved in the response mechanism.

Normal levels of glucose in blood are between 3.5 to 5.9 mM –which converts to $10^{-2.5}$ and $10^{-2.2}$ M– thus falling outside the linear range of the electrode. However, a simple dilution of 1 to 10 will place the sample inside the linear range, and more, will help to reduce the interferences from the sample (particularly potential electrode fouling and presence of redox-active substances).

The interferences might be considered one of the main drawbacks of this electrode. The glucose electrode is insensitive to common substances such as L-glutamine, L-alanine and urea. However, as it is common in the vast majority of electrochemical sensors, L-ascorbate interference may be a serious drawback. The levels of ascorbic acid in blood range between 23 to 85 µM. At the highest level of

ascorbate, the sensor cannot sense glucose, making impossible the measurement of glucose in the presence of ascorbate. However, the dilution needed for the prediction of glucose will also reduce the ascorbate levels one order of magnitude, thus making possible the glucose detection.

In any case, real samples may contain other reducing agents similar to ascorbate and the selectivity of the glucose electrode towards them must be increased. Current work is being conducted in order to minimize the interference caused by reducing agents by attaching an oxidizing membrane over the sensor. The membrane contains MnO, which oxidizes the substances prior to their arrival to the sensing layer.

An important feature of the enzymatic-paper glucose electrode is its stability over time. The electrode is thought to be disposable, therefore its reusability is not an important parameter. In contrast, the stability upon storage is essential, as sensors cannot be built at the moment they are needed. Figure 9.8 A and Table 9.2 show the calibration curves and analytical performance of the same three electrodes reused over time, after 1, 5 and 12 days of the construction. It is clear that the electrodes suffer a drop of performance as they are reused, since both the sensitivity and the linear range are decreasing. This could probably be due to the reduction of activity of the enzyme or to a damage of the electrode due to a bad cleaning before storage. On the other hand, Figure 9.8 B and Table 9.3 show the calibration curves and analytical performance of different electrodes that were all build at the same time but have been stored different over different periods. Some of them were measured just the day after construction (day 1), while others were stored in the fridge and measured two days after (day 2). Finally, some electrodes were stored and measured three days after they had been constructed (day 3). The results show that the electrodes keep a similar linear range and sensitivity independently of the storage time. Even more, it seems that the sensitivity is slightly increased with the storage. This could be due to a better curing of the

membrane or internal membrane processes that need time to stabilize. Further studies are needed to see if there is a tendency and the sensitivity can be further increased.

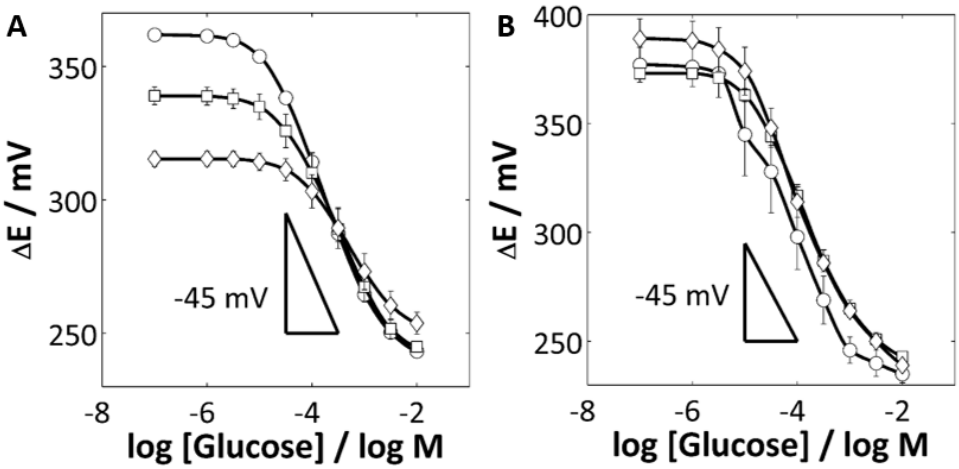

Figure 9.8. Changes of the calibration curves of glucose electrodes over time. (A) Calibration curves at day 1 of construction, after 5 days and after 12 days with the same electrodes (reusability). (B) Calibration curves at day 1, day 2 and day 3 after construction with new electrodes every day (storage).

Table 9.2. Analytical performance of the electrodes upon reusability (n=3).

	Day 1	**Day 5**	**Day 12**
Sensitivity (mV/dec)	-43.7 ± 0.7	-39.4 ± 2.6	-28.9 ± 0.7
Linear range (M)	$10^{-5} – 10^{-2.5}$	$10^{-4} – 10^{-2.5}$	$10^{-4} – 10^{-2.5}$
Lower LOD (M)	$7.7 \cdot 10^{-6}$	$1.8 \cdot 10^{-5}$	$3.7 \cdot 10^{-5}$
Upper LOD (M)	$3.8 \cdot 10^{-3}$	$4.2 \cdot 10^{-3}$	$5.1 \cdot 10^{-3}$

Table 9.3. Analytical performance of the electrodes upon storage days (n=3).

	Day 1	**Day 2**	**Day 3**
Sensitivity (mV/dec)	-45.9 ± 6.3	-47.2 ± 0.1	-51.5 ± 5.0
Linear range (M)	$10^{-5.5} – 10^{-2.5}$	$10^{-5} – 10^{-2.5}$	$10^{-5} – 10^{-2.5}$
Lower LOD (M)	$1.6 \cdot 10^{-6}$	$6.3 \cdot 10^{-6}$	$4.6 \cdot 10^{-6}$
Upper LOD (M)	$3.1 \cdot 10^{-3}$	$3.5 \cdot 10^{-3}$	$3.5 \cdot 10^{-3}$

Regardless the problem of the interferences –which is currently being addressed-, this enzymatic-based glucose electrode may have a large impact if it can be used for determinations of glucose and -what is also important- to become a general approach for other analytes. For the extension of the platform to other analytes – by employing other enzymes- the knowledge of the sensing mechanism would be an important step.

While there is some controversy in the literature, our initial proposition contemplates that that the electrode is sensing the hydrogen peroxide generated upon the glucose oxidation (see Equation 9.1), as it happens in the amperometric sensors.

$$\text{glucose} + O_2 \xrightarrow{\text{GOx}} \text{gluconic acid} + H_2O_2 \qquad \textit{Equation 9.1}$$

To test this assumption, calibration curves for the glucose electrode and their blanks when hydrogen peroxide is added were performed. Figure 9.9 and Table 9.4 display the important analytical parameters for the three systems. The sensitivity and linear range of the three systems is very similar, thus suggesting that the platinum is the sensing element. Moreover, the sensitivity towards hydrogen peroxide is pretty similar to the one obtained for glucose, which may suggest that the electrode is actually responding to hydrogen peroxide. Other tests have shown that the electrode is totally insensitive to gluconic acid in a buffered media.

However, it is sensitive to redox changes on solution, hence explaining its sensitivity to ascorbic acid.

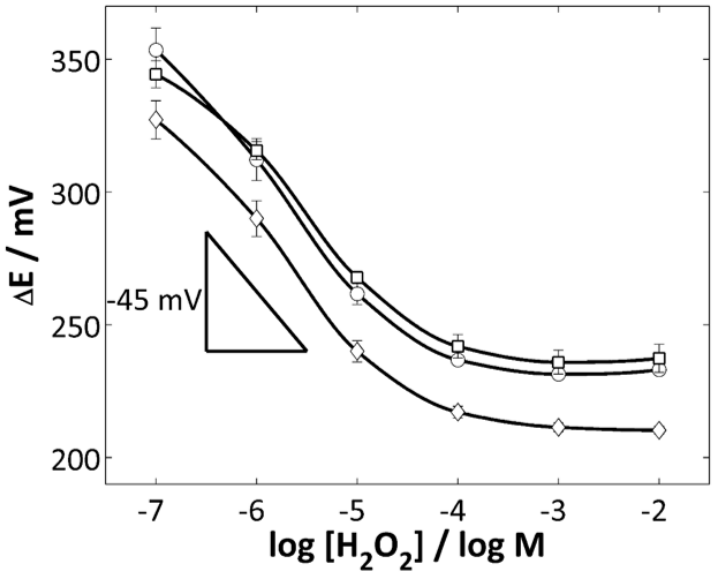

Figure 9.9. Hydrogen peroxide calibration curves for (○) glucose electrode, (□) Blank 1 and (◊) Blank 2.

Table 9.4. Analytical parameters obtained for the glucose electrode and their respective blanks for hydrogen peroxide calibrations (n=3).

	Glucose electrode	**Blank 1 (without enzyme)**	**Blank 2 (platinum paper)**
Sensitivity (mV/dec)	-45.9 ± 2.1	-38.2 ± 1.5	-43.6 ± 1.8
Linear range (M)	$10^{-7} – 10^{-5}$	$10^{-7} – 10^{-5}$	$10^{-7} – 10^{-5}$
Upper LOD (M)	$5.4 \cdot 10^{-5}$	$9.1 \cdot 10^{-5}$	$4.7 \cdot 10^{-5}$

The mechanism that makes platinum sensitive to hydrogen peroxide is complex[43-46]. In phenomenological terms, it is well known that Pt is highly sensitive to the redox potential of the solution. In this particular case, the signal can be seen as an exchange of electrons when hydrogen peroxide gets oxidized (Equation 9.2) or reduced (Equation 9.3) in contact with the platinum.

$$H_2O_2 \xrightarrow{Pt} O_2 + 2H^+ + 2e^- \qquad \textit{Equation 9.2}$$

$$H_2O_2 + 2e^- + 2H^+ \xrightarrow{Pt} 2H_2O \qquad \textit{Equation 9.3}$$

Either one or the other reaction -or a mix of both can- occur at the surface of the platinum electrode, depending on the pH of the solution and the platinum oxidation state[46]. As the pH at the glucose electrode surface might not be stable due to the generation of gluconic acid, a mixture of both reactions might be happening, thus having a sensitivity around -44 mV/dec that corresponds to the exchange of 1.34 electrons. It is also reported that above a concentration of hydrogen peroxide of 1 mM, there is a depression of the platinum response due to electrode surface saturation by hydrogen peroxide and oxygen[44]. This might be explaining the fact that the electrodes have a higher limit of detection. This higher limit of detection has been repeatedly observed in all the sensors build and has been hardly tried to improve without any success. The oxidation of hydrogen peroxide is favoured on oxidized platinum surfaces, which suggests that modifying the platinum surface one can favour the oxidation or reduction of hydrogen peroxide[45], therefore controlling the sensitivity of the electrode.

Current work is being carried out to improve the selectivity of the electrode, test it in real samples and extend its application to other analytes.

9.5 Conclusions

In this work it has been shown for the first time the development of a disposable and low-cost chemiresistor for HIgG detection. Compared to conventional systems built over silicon oxide, the biosensor construction was significantly simplified and the cost was dramatically reduced[47]. Even though the sensitivity of the sensor was not maintained as high as for conventional systems, this paper-based biosensor allowed picomolar detection of proteins in a selective manner and with a significantly reduced cost. Further optimization should be required to improve the

reproducibility of the biosensor construction. Point-of-care applications with integration of this paper-based biosensor come as the next step in the elaboration of out of the laboratory early diagnosis.

The enzyme-based glucose electrode also represents a step beyond current state of the art on conventional paper-based electrochemical sensors, since it allows the direct determination of glucose in diluted artificial serum. The sensor exhibits a reproducible sensitivity if stored in proper conditions. The detection of glucose is a proof of principle for the possibility to use an enzymatic reaction to monitor uncharged biomolecules at clinically relevant levels using potentiometric tools. This paves the way to use other enzymes to detect other species. Moreover, the low-cost and simplicity of these kinds of sensors will make them an ideal tool for the POC applications in mind.

All in all, the use of conductive papers has been successfully extended to other techniques and to the detection of other type of analytes. After demonstrating the good performance of potentiometric ion-selective and enzyme electrodes and protein chemiresistors, the paper confirms its great potential to be a universal platform for the construction of sensors that can be used with different techniques and for the detection of different kind of analytes.

9.6 References

(1) Wang, J. *Biosens. Bioelectron.* **2006**, *21*, 1887–1892.

(2) Mabey, D.; Peeling, R. W.; Ustianowski, A.; Perkins, M. D. *Nat. Rev. Microbiol.* **2004**, *2*, 231–240.

(3) Peeling, R. W.; Mabey, D. *Clin. Microbiol. Infect.* **2010**, *16*, 1062–1069.

(4) Esser, B.; Schnorr, J. M.; Swager, T. M. *Angew. Chemie Int. Ed.* **2012**, *51*, 5752–5756.

(5) Das, B. K.; Tlili, C.; Badhulika, S.; Cella, L. N.; Chen, W.; Mulchandani, A. *Chem. Commun.* **2011**, *47*, 3793–3795.

(6) Li, J.; Lu, Y.; Ye, Q.; Cinke, M.; Han, J.; Meyyappn, M. *Nano Lett.* **2003**, *3*, 929–933.

(7) Wang, F.; Yang, Y.; Swager, T. M. *Angew. Chemie Int. Ed.* **2008**, *47*, 8394–8396.

(8) Cella, L. N.; Chen, W.; Myung, N. V.; Mulchandani, A. *J. Am. Chem. Soc.* **2010**, *132*, 5024–5026.

(9) García-Aljaro, C.; Cella, L. N.; Shirale, D. J.; Park, M.; Muñoz, F. J.; Yates, M. V.; Mulchandani, A. *Biosens. Bioelectron.* **2010**, *26*, 1437–1441.

(10) Yáñez-Sedeño, P.; Pingarrón, J. M.; Riu, J.; Rius, F. X. *TrAC, Trends Anal. Chem.* **2010**, *29*, 939–953.

(11) Umar, A.; Ahmad, R.; Hwang, S. W.; Kim, S. H.; Al-Hajry, A.; Hahn, Y. B. *Electrochim. Acta* **2014**, *135*, 396–403.

(12) Batra, N.; Tomar, M.; Gupta, V. *Analyst* **2012**, *137*, 5854–5859.

(13) Bandodkar, A. J.; Jia, W.; Yard, C.; Wang, X.; Ramirez, J.; Wang, J. *Anal .Chem.* **2015**, *87*, 394–398.

(14) Umar, A.; Rahman, M. M.; Al-Hajry, A.; Hahn, Y.-B. *Talanta* **2009**, *78*, 284–289.

(15) Kong, F. Y.; Gu, S. X.; Li, W. W.; Chen, T. T.; Xu, Q.; Wang, W. *Biosens. Bioelectron.* **2014**, *56*, 77–82.

(16) Yang, J.; Nam, Y. G.; Lee, S. K.; Kim, C. S.; Koo, Y. M.; Chang, W. J.; Gunasekaran, S. *Sens. Actuators, B* **2014**, *203*, 44–53.

(17) Ali, S. M. U.; Nur, O.; Willander, M.; Danielsson, B. *Sens. Actuators, B* **2010**, *145*, 869–874.

(18) Psychoyios, V. N.; Nikoleli, G.-P.; Tzamtzis, N.; Nikolelis, D. P.; Psaroudakis, N.; Danielsson, B.; Israr, M. Q.; Willander, M. *Electroanalysis* **2013**, *25*, 367–372.

(19) Israr, M. Q.; Sadaf, J. R.; Nur, O.; Willander, M.; Salman, S.; Danielsson, B. *Appl. Phys. Lett.* **2011**, *98*, 253705.

(20) Israr, M. Q.; Sadaf, J. R.; Asif, M. H.; Nur, O.; Willander, M.; Danielsson, B. *Thin Solid Films* **2010**, *519*, 1106–1109.

(21) Ibupoto, Z. H.; Shah, S. M. U. A.; Khun, K.; Willander, M. *Sensors* **2012**, *12*, 2456–2466.

(22) Ali, S. M. U.; Alvi, N. H.; Ibupoto, Z.; Nur, O.; Willander, M.; Danielsson, B. *Sens. Actuators, B* **2011**, *152*, 241–247.

(23) Ali, S. M. U.; Ibupoto, Z. H.; Kashif, M.; Hashim, U.; Willander, M. *Sensors* **2012**, *12*, 2787–2797.

(24) Khun, K.; Ibupoto, Z. H.; Lu, J.; AlSalhi, M. S.; Atif, M.; Ansari, A. A.; Willander, M. *Sens. Actuators, B* **2012**, *173*, 698–703.

(25) Ibupoto, Z. H.; Elhag, S.; Nur, O.; Willander, M. *Electroanalysis* **2014**, *26*, 1928–1934.

(26) Shukla, S. K.; Deshpande, S. R.; Shukla, S. K.; Tiwari, A. *Talanta* **2012**, *99*, 283–287.

(27) Ramesh, R.; Puhazhendi, P.; Kumar, J.; Gowthaman, M. K.; D'Souza, S. F.; Kamini, N. R. *Mater. Sci. Eng. C* **2015**, *49*, 786–792.

(28) Yang, Z.; Zhang, C.; Zhang, J.; Bai, W. *Biosens. Bioelectron.* **2014**, *51*, 268–273.

(29) Luo, X.-L.; Xu, J.-J.; Du, Y.; Chen, H.-Y. *Anal. Biochem.* **2004**, *334*, 284–289.

(30) Anusha, J. R.; Kim, H. J.; Fleming, A. T.; Das, S. J.; Yu, K. H.; Kim, B. C.; Raj, C. J. *Sens. Actuators, B* **2014**, *202*, 827–833.

(31) Kaushik, A.; Khan, R.; Solanki, P. R.; Pandey, P.; Alam, J.; Ahmad, S.; Malhotra, B. D. *Biosens. Bioelectron.* **2008**, *24*, 676–683.

(32) Shim, B. S.; Chen, W.; Doty, C.; Xu, C.; Kotov, N. A. *Nano Lett.* **2008**, *8*, 4151–4157.

(33) Wang, L.; Chen, W.; Xu, D.; Shim, B. S.; Zhu, Y.; Sun, F.; Liu, L.; Peng, C.; Jin, Z.; Xu, C.; Kotov, N. a. *Nano Lett.* **2009**, *9*, 4147–4152.

(34) Sekitani, T.; Noguchi, Y.; Hata, K.; Fukushima, T.; Aida, T.; Someya, T. *Science* **2008**, *321*, 1468–1472.

(35) Ammu, S.; Dua, V.; Agnihotra, S. R.; Surwade, S. P.; Phulgirkar, A.; Patel, S.; Manohar, S. K. *J. Am. Chem. Soc.* **2012**, *134*, 4553–4556.

(36) Star, A.; Gabriel, J. P.; Bradley, K.; Gruner, G. *Nano Lett.* **2003**, *3*, 459–463.

(37) Heller, I.; Janssens, A. M.; Mnnik, J.; Minot, E. D.; Lemay, S. G.; Dekker, C.; Ma, J. *Nano Lett* **2008**, *8*, 591–595.

(38) Salehi-Khojin, A.; Khalili-Araghi, F.; Kuroda, M. A.; Lin, K. Y.; Leburton, J. P.; Masel, R. I. *ACS Nano* **2011**, *5*, 153–158.

(39) Chevalier, S.; Cuestas-Ayllon, C.; Grazu, V.; Luna, M.; Feracci, H.; de la Fuente, J. M. *Langmuir* **2010**, *26*, 14707–14715.

(40) Tlili, C.; Cella, L. N.; Myung, N. V; Shetty, V.; Mulchandani, A. *Analyst* **2010**, *135*, 2637–2642.

(41) Byon, H. R.; Choi, H. C. *J. Am. Chem. Soc.* **2006**, *128*, 2188–2189.

(42) So, H. M.; Won, K.; Kim, Y. H.; Kim, B. K.; Ryu, B. H.; Na, P. S.; Kim, H.; Lee, J. O. *J. Am. Chem. Soc.* **2005**, *127*, 11906–11907.

(43) Hall, S. B.; Khudaish, E. A.; Hart, A. L. *Electrochim. Acta* **1998**, *43*, 2015–2024.

(44) Hall, S. B.; Khudaish, E. A.; Hart, A. L. *Electrochim. Acta* **1997**, *43*, 579–588.

(45) Katsounaros, I.; Schneider, W. B.; Meier, J. C.; Benedikt, U.; Biedermann, P. U.; Auer, A. A.; Mayrhofer, K. J. J. *Phys. Chem. Chem. Phys.* **2012**, *14*, 7384–7791.

(46) Strbac, S. *Electrochim. Acta* **2011**, *56*, 1597–1604.

(47) Han, J. W.; Kim, B.; Li, J.; Meyyappan, M. *J. Phys. Chem. C* **2012**, *116*, 22094–22097.

UNIVERSITAT ROVIRA I VIRGILI
PAPER-BASED POTENTIOMETRIC PLATAFORMS FOR ESCENTRALISED CHEMICAL ANALYSIS.
Marta Novell Recasens
Dipòsit Legal: T 1462-2015

UNIVERSITAT ROVIRA I VIRGILI
PAPER-BASED POTENTIOMETRIC PLATAFORMS FOR ESCENTRALISED CHEMICAL ANALYSIS.
Marta Novell Recasens
Dipòsit Legal: T 1462-2015

CHAPTER

10

CONCLUSIONS

UNIVERSITAT ROVIRA I VIRGILI
PAPER-BASED POTENTIOMETRIC PLATAFORMS FOR ESCENTRALISED CHEMICAL ANALYSIS.
Marta Novell Recasens
Dipòsit Legal: T 1462-2015

10.1 Conclusions

This thesis has demonstrated –through various achievements- the possibility to build a low-cost paper-based potentiometric platform for its use in decentralised analysis. The reduction of cost has been possible due to the combination of paper, carbon nanotubes (CNTs) and potentiometry, which has allowed the possibility to substitute conventional electrodes for a paper impregnated with CNTs. The paper also allows the miniaturization and disposability of the sensors.

The demonstration that paper-based potentiometric sensors exhibited an analytical performance that is comparable to conventional electrodes was the first "proof-of-concept" for this platform. On the other hand, the successful combination of these sensors with an RFID potentiometer and the reliable measurement of lithium in real samples were crucial steps to demonstrate the feasibility of substituting conventional systems for paper-based sensors. These last trials have been truly "litmus tests" for this platforms, since they have shown the ability to solve real analytical problems. Initial studies have also demonstrated the possibility to build with this platform alternative -other than ion-selective electrodes- potentiometric sensors, such as enzyme electrodes. The successful development of a chemiresistor with the CNT-paper also shows the versatility of the paper-CNTs platform. Therefore, this opens the possibility of measuring a wide range of analytes and providing –up to the date- two different techniques to choose the most appropriate one for each specific analyte.

Evidently, there is still a long way to go with this platform. From one side, some limitations of the system still need to be overcome. The calibration of the electrodes is maybe the most significant. Solutions such automatic calibration of the electrodes or calibration-free electrodes need to be tested and implemented. Other issues regarding the electrodes storage, data treatment and the integration

of the whole system in a portable device where the final user just need to press a button to obtain the desired result are also points to tackle.

The platform developed here opens the possibility to substitute conventional sensors for these low-cost paper sensors, thus unlocking a whole new range of possibilities. The feasibility of performing real-time chemical analysis will allow a completely different system where decentralised modes can provide instantaneous information that can be accessed for anyone at any time. This will have a huge impact for example in the medical field. This platform together with other existing devices can be used for point-of-care tests and telehealth.

A good example of the power of these devices was shown through the determination of Lithium in blood. Patients undergoing Li therapy require periodical check-ups, which imply several visits to the healthcare centre and days -sometimes weeks- waiting for the results. The paper potentiometric cell showed the possibility to perform the analysis *in-situ*, in real time, with a very low cost, thus competing with techniques such as atomic emission spectroscopy, which requires expensive and complex equipment, laboratory facilities and expert operation.

Evidently, the goal of this work is not the simple competition with existing analytical techniques, but the development of tools that can give people effective tools to take care of their own help. While this empowers people and communities to be more connected and responsible in their healthcare, it helps society to make more efficient and effective use of resources. Therefore, these tools should be effective ways to change the culture.

10.2 Future prospects

This thesis has demonstrated the possibility to substitute conventional sensors for paper-based sensors, with all the advantages already discussed. However, the detection event is just a part of the whole analytical process, which includes sampling, sample treatment, detection and data treatment[1]. Therefore the next big challenge is to integrate the whole analytical process in a cheap and portable instrument. Sampling will not be a huge difficulty if the main idea is to work with biological samples, as the idea is to have a portable instrument, the sample can be directly placed on the system –thus avoiding transport and storage-. Other kind of samples can also be directly applied on the system immediately after being collected. The sample treatment may be one of the biggest challenges, this steps involves a huge variety of processes such as dilution, filtration, separation or change of pH, just to name a few. There are many options being developed that face some of these issues, one possibility is to use microfluidic channels and chambers to store and transport liquids. Channels can have integrated filters or dilution systems to process the sample. Another possibility is to perform all these actions in "microfluidic paper-based analytical devices" (µPADs) which are thought to emulate all the analytical process[2–4]. The detection step is what has been developed and optimized along this thesis. Even though the sensors still require a minimal calibration, this could be performed with –some modifications in- the same fluidic system used for the sample treatment. Portable potentiometers that fulfil the requirements for decentralised analysis –such as the RFID tested in chapter 7- are already in the market, but some interface that automatically converts the reading –in mV- to a valuable information for the user –concentration, risk levels, etc.- should be developed and integrated with the detection.

An ideal system will have such optimized sensors for each application that the sample treatment and sensors calibration will not be needed anymore, and the direct contact of the sensor with the sample will provide the desired result. In that

fashion, chemical analysis of biological samples, water, food, etc. could be done at any time for anyone, thus creating a network of chemical information useful for personal health care management, disease and environmental control, etc. However, this does not seem still feasible in the near future, and small but robust steps are required in order to build this ideal system. The development of the paper-based potentiometric sensors presented here is certainly one of these crucial steps towards these systems.

10.3 References

(1) de Castro, M. D. L. *Pure Appl. Chem.* **2002**, *74*, 2293–2298.

(2) Vella, S. J.; Beattie, P.; Cademartiri, R.; Laromaine, A.; Martinez, A. W.; Phillips, S. T.; Mirica, K. A.; Whitesides, G. M. *Anal. Chem.* **2012**, *84*, 2883–2891.

(3) Martinez, A. W.; Phillips, S. T.; Whitesides, G. M.; Carrilho, E. *Anal. Chem.* **2010**, *82*, 3–10.

(4) Martinez, A. W.; Phillips, S. T.; Whitesides, G. M. *PNAS* **2008**, *105*, 19606–19611.

UNIVERSITAT ROVIRA I VIRGILI
PAPER-BASED POTENTIOMETRIC PLATAFORMS FOR ESCENTRALISED CHEMICAL ANALYSIS.
Marta Novell Recasens
Dipòsit Legal: T 1462-2015

UNIVERSITAT ROVIRA I VIRGILI
PAPER-BASED POTENTIOMETRIC PLATAFORMS FOR ESCENTRALISED CHEMICAL ANALYSIS.
Marta Novell Recasens
Dipòsit Legal: T 1462-2015

APPENDICES

UNIVERSITAT ROVIRA I VIRGILI
PAPER-BASED POTENTIOMETRIC PLATAFORMS FOR ESCENTRALISED CHEMICAL ANALYSIS.
Marta Novell Recasens
Dipòsit Legal: T 1462-2015

Appendix 1. Abbreviations

Φ – Phase shift

$\mu_I^0(aq)$ – Chemical standard potentials of the ion I^{z_I+} in the aqueous phase

$\mu_I^0(org)$ – Chemical standard potentials of the ion I^{z_I+} in the organic phase

β_{iL} – Formation constant between the analyte and the ionophore

$|i_{pa}/i_{pc}|$ – Ratio of the peak currents

µPAD – microfluidic paper-based analytical device

ΔE – Peak separation

ω – Radial frequency

A - Electrode area

ADC – Analogue to digital converter

AES – Atomic emission spectroscopy

a_I (aq) – Activity of the primary ion in the aqueous sample

a_I (DL) – Activity of the primary ion in the limit of detection

a_I (org) – Activity of the primary analyte in contact with the organic phase boundary

a_J (BG) – Activity of the interfering ion in the background solution

ANOVA – Analysis of variance

ASSURED – Affordable, sensitive, selective, user-friendly, rapid and robust, equipment free and deliverable to end users

BSA – Bovine serum albumin

C – Capacitance

c – Concentration of analyte in solution

C_D – Bulk capacitance

CCD – Charge-coupled device

CHI – Chitosan

CNT – Carbon nanotube

CP – Conductive polymer

CV – Cyclic voltammetry

D – Diffusion coefficient

DMA – N-decyl methacrylate

DNA – Deoxyribonucleic acid

DOS – Bis(2-ethylhexyl)sebacate

E_I^0 – Potential of the primary ion at 1M concentration, also known as standard potential

E_J^0 – Potential of the interfering ion at 1M concentration

E_0 – Amplitude of the signal

E^0 – Standard potential

$E^{0\prime}$ – Formal reduction potential

E_{Const} – Constant potential generated at the internal interfaces

E_D – Diffusion potential inside the membrane

EDOT – 3,4-Ethylenedioxythiophene

EEPROM – Electrically erasable programmable read-only memory

EIS – Electrochemical impedance spectroscopy

E_j – Interface potentials

ELISA – Enzyme-linked immunosorbent assay

EMF – Electromotive force

E_{pa} – Anodic peak potential

E_{PB} – Phase boundary potential between the sample-membrane interface

E_{pc} – Cathodic peak potential

ESEM – Environmental scanning electron microscopy

E_t – Potential at time t

ETH 500 – Tetradodecylammonium tetrakis(4-chlorophenyl) borate

ETH 5234 – Calcium ionophore (IV)

ETH 5506 – Magnesium ionophore (VI)

ETH 8045 – [12-(4-ethylphenyl)dodecyl] 2-nitrophenyl ether

F – Faraday constant (96485 C/mol)

FIM – Fixed interference method

GC – Glassy carbon

GOx – Glucose oxidase

HF – High frequency

HigG – Human immunoglobulin G

I – Current

I – Primary ion

I_0 – Amplitude

IoT – Internet of things

I_p – Peak current

i_{pa} – Anodic peak current

i_{pc} – Cathodic peak current

ISE – Ion-selective electrode

ISM – Ion-selective membrane

I_t – Current at time t

J – Interfering ion

K_{IJ}^{pot} – Selectivity coefficient of the *I*-ISE towards the ion *J*

k_I – Constant function of the relative free energies of solvation in both the sample and the membrane phase

KTClPB – Potassium tetrakis (4-chlorophenyl) borate

L – Ionophore concentration

LOD – Limit of detection

MMA – Methyl methacrylate

MPM – Matched potential method

MWCNT – Multi-walled carbon nanotube

n – Number of electrons transferred per molecule diffusing to the electrode surface

NaPSS – Poly(sodium 4-styrenesulfonate)

NaTFPB – Sodium tetrakis[3,5-bis(trifluoromethyl)phenyl]borate

NFC – Near field communication

NPOE – 2-nitrophenyl octyl ether

PEAA – Poly(ethylene-co-acrylic acid)

PEDOT – Poly(3,4-Ethylenedioxythiophene)

POC – Point-of-care

POCT – Point-of-care tests

POT – Poly(3-octylthiphene)

PSS – Poly(sodium 4-stryrene sulfonate)

PVAL – Poly(vinyl alcohol)

PVB – Butvar B-98

PVC – Polyvinyl chloride

R – Resistance

R"– Universal gas constant (8.314 J/K·mol)

R_0 – Initial resistance

RE – Reference electrode

RFID – Radio frequency identification

R_S – Solution resistance

R_T – Ionic sites

SC – Solid contact

SDBS – Sodium dodecylbenzenesulfonate

SEM – Scanning electron microscopy

SSM – Separate solution method

SWCNT – Single-walled carbon nanotube

T – Absolute temperature (K)

THF – Tetrahydrofuran

TOPO – Trioctylphosphine oxide

v - Scan rate

V – Voltage

VOC – Volatile organic compounds

W – Warburg impedance

WBSN – Wireless body sensing networks

WCSN – Wireless chemical sensing networks

WE – Working electrode

WSN – Wireless sensing networks

wt % – Weight percentage

Z_0 – Impedance magnitude

Z_D – Finite-length Warburg diffusion

z_I – Charge of the primary ion

z_J – Charge of the interfering ion

Appendix 2. Relation of figures and tables

Figures

Figures in the Appendices

Tables

Tables in the Appendices

Appendix 3. Short CV

Papers directly resulting from the doctoral thesis

Novell, M.; Parrilla, P.; Crespo, G.A.; Rius, F.X.: Andrade, F.J. Paper-based ion-selective potentiometric sensors. *Anal. Chem.* **2012**, *84*, 4695-4702.

Novell, M.; Guinovart, T.; Murkovic Steinberg, I.; Steinberg, M.; Rius, F.X.; Andrade, F.J. A novel miniaturized radiofrequency potentiometer tag using ion-selective electrodes for wireless ion sensing. *Analyst* **2013**, *138*, 15–19.

Pozuelo, M.; Blondeau, P.; Novell, M.; Andrade, F.J.; Rius, F.X.; Riu, J. Paper-based chemiresistor for detection of ultralow concentration of protein. *Biosens. Bioelectron.* **2013**, *49C*, 462–465.

Novell, M.; Guinovart, T.; Blondeau, P.; Rius, F.X.; Andrade, F.J. A paper-based potentiometric cell for decentralized monitoring of Li levels in whole blood. *Lab Chip* **2014**, *14*, 1308–1314.

Collaborations

Cuartero, M.; Blondeau, P.; Novell, M.; Steinberg, M.; Rius, F.X.; Andrade, F.J. A simple and versatile approach to generate conducting and stretchable rubbers: Modification, performance and wireless strain sensor application. *In preparation.*

Sjörbeg, P.; Määttänen, A.; Vanamo, U.; Novell, M.; Ihalainen, P.; Andrade, F.J.; Bobacka, J.; Peltonen, J. Paper-based potentiometric ion sensors with ink-jet ptinted gold electrodes. *In preparation.*

Montiel, L.; Novell, M; Andrade, F.J.; Claver, C.; Blondeau, P.; Godard, C. A paper-based nanocatalyst. *In preparation.*

Oral communications

Novell, M.; Parrilla, P.; Crespo, G.A.; Rius, F.X.; Andrade, F.J. Paper-based ion-selective potentiometric sensors. *V Workshop on Nanoscience and Nanotechnology.* **2011**, Toledo (Spain).

Novell, M.; Guinovart, T.; Blondeau, P.; Rius, F. X.; Andrade, F. J. Paper-based ion-selective electrodes for the determination of lithium in blood. *VI Workshop on Nanoscience and Nanotechnology.* **2013**, Alcalá de Henares (Spain).

Posters

Novell, M.; Parrilla, P.; Crespo, G.A.; Rius, F.X.; Andrade, F.J. Paper-based potentiometric sensors. *Mátrafüred 2011 – International Conference on Electrochemical Sensors.* **2011**, Budapest (Hungary).

Novell, M.; Parrilla, P.; Crespo, G.A.; Rius, F.X.; Andrade, F.J. Paper-based potentiometric sensors. *V Workshop on Nanoscience and Nanotechnology.* **2011**, Toledo (Spain).

Novell, M.; Parrilla, P.; Crespo, G.A.; Rius, F.X.; Andrade, F.J. Paper-based potentiometric sensors. *XVII Transfrontier Meeting of Sensors and Biosensors.* **2012**, Tarragona (Spain).

Novell, M.; Guinovart, T.; Blondeau, P.; Rius, F. X.; Andrade, F. J. Paper-based ion-selective electrodes for the determination of lithium in blood. *VI Workshop on Nanoscience and Nanotechnology.* **2013**, Alcalá de Henares (Spain).

UNIVERSITAT ROVIRA I VIRGILI
PAPER-BASED POTENTIOMETRIC PLATAFORMS FOR ESCENTRALISED CHEMICAL ANALYSIS.
Marta Novell Recasens
Dipòsit Legal: T 1462-2015

UNIVERSITAT ROVIRA I VIRGILI
PAPER-BASED POTENTIOMETRIC PLATAFORMS FOR ESCENTRALISED CHEMICAL ANALYSIS.
Marta Novell Recasens
Dipòsit Legal: T 1462-2015

UNIVERSITAT ROVIRA I VIRGILI
PAPER-BASED POTENTIOMETRIC PLATAFORMS FOR ESCENTRALISED CHEMICAL ANALYSIS.
Marta Novell Recasens
Dipòsit Legal: T 1462-2015

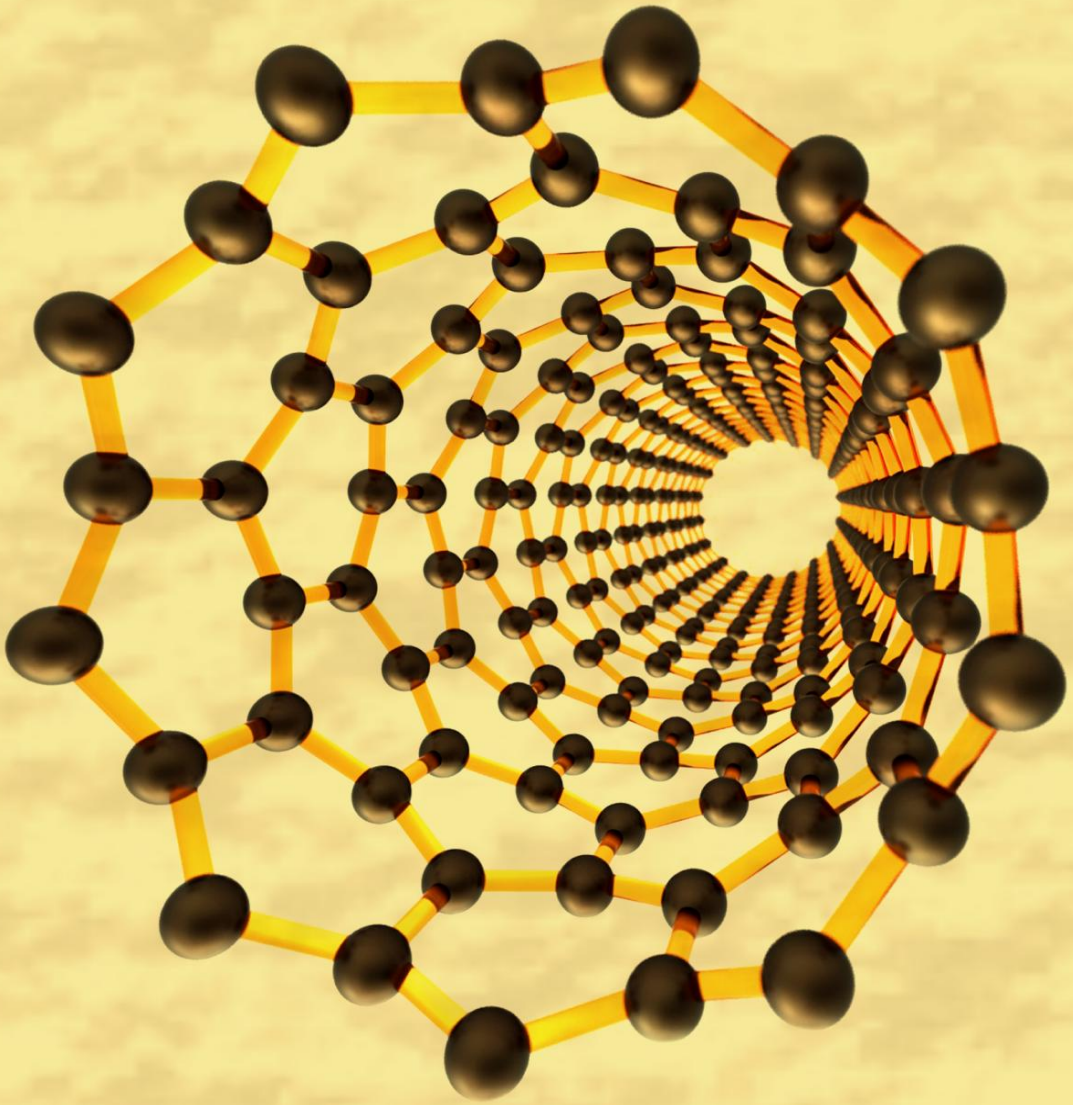

UNIVERSITAT ROVIRA I VIRGILI